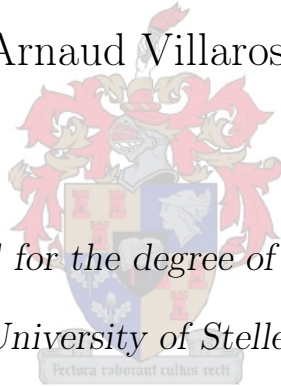


Petrogenesis of S-type Granite with Particular
Emphasis on Source Processes: The Example of the
S-type Granite of the Cape Granite Suite

by

Arnaud Villaros



*Dissertation presented for the degree of Doctor of Philosophy
at the University of Stellenbosch*

Department of Geology
Private Bag X1
University of Stellenbosch
South Africa

Promoters:

Pr. G. Stevens Pr. I.S Buick

2010

Forewords

The entirety of the work done during my PhD is contained therein. It has to be noted that 3 chapters of this work are the result of collaboration with co-authors and have been object of publications (details for each publication are stated at the beginning of the relevant chapters).

Declaration

I, the undersigned, hereby declare that the work contained in this dissertation is my own original work and that I have not previously in its entirety or in part submitted it at any university for a degree.

Signature:

A. Villaros

Date: 20th December 2009

Copyright © 2010 University of Stellenbosch

All rights reserved.

Abstract

S-type granite intrusions are extremely common in the continental crust and form from the partial melting of metasediments. Compositions of S-type granite range from leucogranite to granodiorite and have trace element contents that globally increase with increasing maficity ($Fe + Mg$). Models proposed for the formation of S-type granite do not answer satisfactorily all petrological and compositional requirements. In this study, S-type granite of the Cape Granite Suite (CGS), South Africa is used to discriminate between potential sources of compositional variation. Experimental studies show that melt produced from the partial melting of sediment is exclusively leucocratic. On this basis, the entrainment of up to 20 wt.% of peritectic garnet within S-type melt can be established to produce the observed major element variations. S-type CGS locally contains garnet. This garnet is in equilibrium with granite composition at P-T conditions (5kb and 750°C for the core of the garnet and 3kb and 720°C for the rim) well below conditions recorded by xenoliths from the same granite (10 kb and 850°C from a metabasite). From this result it seems that the originally entrained garnet no longer exists in the S-type CGS and it have been replaced by newly formed minerals (garnet, cordierite and biotite). Considering the short time necessary to emplace granites (about 100 000 years), it appears that garnet has been compositionally re-equilibrated

through a dissolution-precipitation process. The study of trace element variations in S-type CGS shows that most leucocratic compositions are undersaturated in Zr and Ce compared to predictions from experimental models for dissolution of accessory zircon and monazite in their source regions. Thus, S-type melts are likely to be formed in disequilibrium with respect to accessory phase stability. As a result the observed increase in trace element content with increasing maficity indicates that accessory minerals such as zircon and monazite are co-entrained with peritectic garnet in melt to produce the observed trace element variation in S-type granite. Trace element disequilibrium in the CGS S-type granitoids requires particularly short times of residence of melt within the source region. Together, these results provide for the first time, a fully comprehensive model for major and trace elements variations. Compositional variation in CGS S-type granite results from source processes by a selective entrainment of peritectic and accessory minerals. After entrainment, these minerals are likely to be re-equilibrated within the magma, through a dissolution-reprecipitation process. In addition, it appears that the construction of large S-type granitic bodies occurs through successive addition of magma batches of different composition that originates directly from the source region.

Abstrak

S-tipe granietinstrusies is baie algemeen in die kontinentale kors en vorm deur die gedeeltelike smelting van metasedimente. Samestellings van S-tipe graniete strek vanaf leukograniet tot granodioriet en het spoorelementsamstellings wat global toeneem met 'n toenemende mafiese component ($Fe + Mg$). Modelle wat voorgestel is vir die formasie van S-tipe graniete beantwoord nie bevredigend al die petrologiese en komposisionele benodigdhede nie. In hierdie studie word S-tipe graniete van die Kaapse Graniet Suite (CGS), Suid Afrika, gebruik om te diskrimineer tussen potensiele bronne van komposisionele variasie. Eksperimentele studies wys dat smelt, geproduseer van die gedeeltelike smelting van sedimente, uitsluitlik leukokraties is. Op hierdie basis kan bewys word, dat die optel-en-meevoering van tot 20 wt% van peritektiese granaat in S-tipe smelt, die waargeneemde hoofelement variasies kan produseer. S-tipe CGS bevat lokale granaat. Hierdie granaat is in ekwilibrium met die graniet samestelling by P-T kondisies (5kb en $750^{circ}C$ vir die kern van die granaat en 3kb en $720^{circ}C$ vir die rand) ver onder kondisies waargeneem by xenoliete van dieselfde granite (10kb en $850^{circ}C$ van 'n metabasiet). Van hierdie resultaat kan afgelei word dat die oorspronklike opgetel-en-meegevoerde graniet bestaan nie meer in die S-tipe CGS en dat dit vervang is deur nuutgevormde minerale (granaat, kordieriet en biotiet). As in ag geneem word die kort tyd

wat nodig is om graniete in te plaas (omtrent 100 000 jaar), wil dit voorkom dat granaat se samestelling geherekwilibreer word deur 'n oplossings-presipitasie proses. Die studie van spoorelement variasies in S-tipe CGS wys dat meeste leukokratiese samestellings is onderversadig in Zr en Ce in vergelyking met voorspellings deur eksperimentele modelle vir die oplossing van bykomstige zircon en monasiet in hulle brongebiede. Dus is S-tipe smelte meer geneig om gevorm te word in disekwilibrium in verhouding tot bykomstige mineraalstabiliteit. Met die gevolg is dat die waargenome toename in spoorelementinhoud met toename in mafiese component wys dat bykomstige minerale, soos zirkoon en monasiet, word saam opgetel-en-meegevoer met peritektiese granaat in smelt om die waargenome spoorelement variasie in S-tipe graniete te verklaar. Spoorelement disekwilibrium in die CGS S-tipe granitoide benodig veral kort tye van residensie van die smelt binne die brongebied. Saam gee hierdie resultate vir die eerste keer 'n algehele antwoord vir hoof- en spoorelement variasies. Variasie in samestelling in CGS S-tipe graniete is die resultaat van bronprosesse deur 'n selektiewe optel-en-meevoer van peritektiese en bykomstige minerale. Na die optel-en-meevoer van hierdie minerale word hulle geherekwilibreer binne die magma deur 'n oplossings-presipitasie proses. Addisioneel wil dit voorkom of die konstruksie van groot S-tipe granietliggame plaasvind deur opeenvolgende toevoegings van magma lotte van verskillende samestellings wat direk uit die brongebied kom.

Résumé

Les granites de type S sont communs dans la croûte continentale et sont formés à partir de la fusion partielle de sédiments. Les compositions de ces granites varient de leucogranitique à granodioritique, avec des concentrations en éléments traces augmentant selon la maficité (Fe+Mg molaire). Les modèles proposés jusqu'à présent pour la formation de ces granites ne répondent pas de manière satisfaisante à tous les problèmes pétrologiques et compositionnels soulevés par la pétrogenèse des granites de type S. Dans cette étude, le granite de type S de la série granitique du Cap (CGS), Afrique du Sud, est utilisé pour discriminer les sources potentielles des variations de composition des granites de type S. Des travaux expérimentaux montrent que le liquide produit lors de la fusion partielle de sédiments est exclusivement leucocratique. Nous avons pu établir que jusqu'à 20 wt.% de grenats peritectics sont entraînés dans le liquide de type S pour produire les variations en éléments majeurs observés dans le granite. Les granites de type S de la CGS contiennent localement des grenats. Nous avons pu démontrer que ces grenats étaient à l'équilibre avec la composition du granite qui les entoure à des conditions P-T (5kb et 750°C pour le coeur du grenat et 3kb et 720°C pour la couronne) bien inférieures aux conditions enregistrés par les xenoliths contenu dans le même granite (10kb and 850°C pour un metabasalte). A partir de ce résultat il semble que le grenat entraîné dans le

liquide hors de la source n'existe plus dans le granite et qu'il est remplacé par une nouvelle génération de grenat ou d'autres minéraux ferromagnésiens (cordierite, biotite). Si l'on considère qu'un granite est formé dans un temps géologiquement court (environ 100 000 ans) le grenat est totalement rééquilibré avec son environnement par dissolution-précipitation. L'étude des éléments en trace dans les types S de la CGS montre que les concentrations de saturation en Zr et Ce pour des compositions de liquides expérimentaux sont largement supérieures aux concentrations en Zr et Ce mesurées dans les granites les plus leucocratiques. Donc les liquides de type S semble être formé en déséquilibre par rapport à la stabilité des phases accessoires riche en Zr et Ce (zircon et monazite respectivement). En accord avec cette observation, l'augmentation de la concentration avec la maficité du magma indique que les minéraux accessoires tels que le zircon et la monazite sont co-entraînés dans le liquide avec le grenat péritectique, produisant les variations de concentration observée dans le granite de type S. Le déséquilibre en éléments traces observé témoigne d'un temps de résidence du liquide dans la source particulièrement court (<100 ans). Ces résultats permettent d'établir pour la première fois un modèle expliquant à la fois les variations en éléments majeurs et traces dans les granites de type S. Ces variations sont obtenues à partir de processus de source par l'entraînement sélectif de grenat et de minéraux accessoires dans le liquide issu de la fusion partielle. Après leur entraînement, ces minéraux sont rééquilibrés par dissolution précipitation en fonction de la composition du magma environnant et des conditions pression et température. De plus il apparaît que la construction de large corps granitique se fasse par l'accumulation de petites intrusions magmatiques successives et de composition variables fonction de la quantité de minéraux entraînés depuis la source.

Acknowledgements

I'd like to particularly thank my supervisors, Gary Stevens and Ian Buick who offered me the opportunity to undertake this work under their supervision, to discover Stellenbosch, the Western Cape and South African lifestyle and a bit of Australia. I thank them for their patience and their advices which have been of great help. I particularly want to thank Jean-françois "Jeff" Moyen for presenting me Stellenbosch University and for the thousand (at least) cups of coffee. I also thank all the people from the department, the staff: John JC Clemens, Loxie Conradie, Jodie Miller, Abraham Rozendaal, Reyno Scheepers, Riana Van der Berg, Hayley De Wet Swartz, Riana Rossouw, Madelaine Frazenburg, but also all the postgrad students and postdoctorates: Rob Ward, Cristiano Lana, Jeanne Taylor, Cynthia Sanchez-Garrido, Cecilia Mukosi, Mafusi Rapopo, Amandine Prelat, Esme Spicer, and many other people. And of course, I want to thank all my family and friends in France who supported during all my studies, which are finally over. And all the people I know and who are not listed above.

Contents

Forewords	ii
Declaration	iii
Abstract	iv
Abstrak	vi
Résumé	viii
Acknowledgements	x
Contents	xi
List of Figures	xiii
List of Tables	xv
1 Introduction	1
2 What are S-type granites?	7
2.1 Composition of S-type Granite	8
2.2 melting reaction and melt composition	8
2.2.1 Conditions of melting and melting reaction	10
2.2.2 Melt composition	12
2.2.3 Extraction from the source region	16
2.3 Controls on S-type granitoids	18
2.3.1 Magma mixing	18
2.3.2 Fractional Crystallisation	20
2.3.3 Crustal assimilation	21
2.3.4 Entrainment of source material	22

3	The S-type CGS	32
3.1	The Saldanian Orogenic Belt	33
3.1.1	Introduction	33
3.1.2	Stratigraphy of the Saldania Orogen	34
3.1.3	Tectonic context	38
3.1.4	The Cape Granite Suite	40
3.2	The S-type CGS	42
3.2.1	The Peninsula Pluton and the Darling Batholith	42
3.2.2	Different facies and compositional variations	44
3.2.3	Enclave Material in the S-type CGS	51
4	Selective peritectic garnet entrainment	59
5	Tracking S-type granite	65
6	The trace element compositions of S-type granites	86
7	Synthesis and general conclusions	107
7.1	A comprehensive model	108
7.1.1	Peritectic phase entrainment in the petrogenesis of S-type granites	108
7.1.2	The fate of the entrained peritectic phase	112
7.1.3	Entrainment and the fate of accessory minerals	115
7.2	Time of residence	117
7.3	General Conclusions	118
	General references	123
	Appendices	144
.1	Compilation S-type granite composition	145
.2	Compilations of experimental melt compositions	160
.3	Mineral compositions and Structural Formulaes	182
.4	Relative standard deviation obtained using Stellenbosch ICP-MS . .	199
.5	Partition coefficient used for modelling	201
	Abstract to international Conferences	203
.6	Goldschmidt conference - Melbourne - 2006	203
.7	Hutton conference - Stellenbosch - 2007	205
.8	Abstract: AGU - Fall meeting - San Francisco - 2007	208

List of Figures

2.1	Compositional variations in S-type granite	9
2.2	Phase diagram of common partial melting reaction in metasediments	11
2.3	Ternary diagrams showing compositional variations in experimental melt in relation to the composition of the source.	15
2.4	Ternary diagrams showing differences between S-type granites of the Cape Granite Suite composition and experimental melt.	17
3.1	Palaeogeographic reconstruction of the Panafrican orogenies at 550 Ma.	34
3.2	Simplified geological map of the Saldanian Orogenic Belt	35
3.3	Simplified geological map of the Cape Granite Suite	36
3.4	stratigraphy of the western part of the Saldania belt.	39
3.5	Geological Sketch of the Cape Peninsula, and the Peninsular pluton. .	43
3.6	Geological Sketch of the Darling batholith	45
3.7	Examples of facies in the S-type CGS and their relationships.	47
3.8	Examples of occurrences of garnet and cordierite in S-type CGS. . . .	49
3.9	Magmatic Enclaves in the S-type CGS (Boulders beach).	50
3.10	Interactions between magmatic enclaves and the Cape Granite.	52
3.11	Xenolithic enclaves (Darling Batholith).	54
3.12	Example of the complexity of relation between metasedimentary xenoliths and different granitic facies. The Size of the enclave is about 10cm.	55
4.1	A comparison of the compositions of experimental glasses and the compositions of Cape Granite Suite S-type rocks.	63
4.2	The model for the petrogenesis of S-type granite proposed in this study.	64
5.1	A comparison of the compositions of experimental glasses and the compositions of Cape Granite Suite S-type rocks	69
5.2	Geological context	70
5.3	Relevant field relationships from the Peninsular Pluton	71
5.4	Thin section image illustrating the textures of the garnet-bearing assemblages in the granites and in the metasedimentary xenoliths. . . .	72

5.5	Garnet in S-type CGS granitoids.	75
5.6	Typical X-ray element maps of garnet from the granites and xenoliths.	76
5.7	Garnet in metasedimentary xenoliths.	77
5.8	Pseudosection calculated for granodiorite.	79
5.9	Pseudosections calculated for granitoids	81
5.10	Mineral proportions extracted from pseudosections	82
5.11	Log (time) vs. Log (radius) diagram showing diffusion rates in garnet	83
5.12	P T diagram summarizing the thermobarometry information from the metamafic xenolith.	83
6.1	Atomic Fe /Mg versus trace element concentration diagram.	90
6.2	Geological Settings.	92
6.3	Field relationships in the Peninsular Pluton.	93
6.4	Harker diagrams displaying compositional variation within the S-type CGS rocks	94
6.5	Trace element versus Fe /Mg variation diagrams for the Peninsular Pluton.	97
6.6	A diagrammatic illustration of the principles underpinning the trace element modelling in this study	100
6.7	Results of modelling compared to compositions of the S-type CGS . .	101
6.8	concentration versus time in a melt.	104
7.1	Fe+Mg vs. A/CNK diagrams showing the modelling of magma mixing.	109
7.2	Fe+Mg vs. A/CNK diagrams showing the Modelling for contamina- tion processes (restite, pelite).	113

List of Tables

2.1	Summary of requirements, field and compositionnal expression and limits of models proposed for S-type granite petrogenesis	19
5.1	Average garnet major and trace elements compositions from garnet-bearing granites, as well as metamorphic mineral compositions from the xenoliths	74
5.2	Results of the average P–T estimate calculations from the metamafic xenolith using THERMOCALC.	78
5.3	Garnet self-diffusion modelling using Fe, Mg, Ca and Mn diffusivities	82
6.1	Trace element composition of monazite (mnz) and zircon (zrc); major and trace element of the source and the calculated zircon-and-monazite free source	98
6.2	Phase proportions determine at conditions of partial melting and partition coefficients	99
6.3	Results of calculation	103

Chapter 1

Introduction

The differentiation of the continental crust is one of the unique features of the Earth. Granitic rocks (granitoids) make up approximately 70% of the continental crust. Granitoid are felsic plutonic rocks and are commonly derived from the partial melting of crustal material at relatively low temperature ($< 1000^{\circ}\text{C}$). The presence of water, in excess in the source rock or trapped in hydrous minerals, is an absolute necessity to produce such magma. This definition of granitoid is very broad and corresponds to an extremely wide range of composition. Composition of granitoids can be affected in many ways. The earliest granitoids of Archean age are mostly characterised by Tonalite-Trondheimite-Granodiorite (TTG) compositions. The subsequent waning of the Earth's thermal regime from Archean to Phanerozoic has considerably changed the dynamics of continental crust formation (e.g. Martin and Moyen 2002). This secular change in thermal regime was accompanied by changes in the type of granitoids towards post-Archean compositions that mostly range from leucogranite to granodiorite (using Debon and Le Fort 1982). Different sources also produce granitoids with different petrological and geochemical characteristics. For instance, granitoids produced from partial melting of clastic metasediments (S-type) are geochemically and petrologically distinct from granitoids produced from partial melting of meta-igneous source (I-type)(Chappell and White 1974). The production of granitoids from the partial melting of clastic metasediment is particularly interesting. Indeed, clastic sediments are formed from the deposition of material coming from eroded continental crust. From here, the making of a granite from clastic sediment constitutes a mechanism to recycle continental crust, making new continental crust from a pre-existing continental crust. Interestingly, observations made on such granites reveal a particularly large scatter of composition (from leucogranite to granodiorite). This observation raises several

questions: How is this variation do possible? What processes could generate such a variation? To what extend these processes might affect the composition of the granite? Answering these questions would help understanding the processes of recycling of the continental crust and at the same time understanding a bit more about its formation.

This study aims to determinate the mechanisms that control the origin of compositional variations recorded in S-type granite and to propose a comprehensive petrogenetic model for S-type granite in regard to source processes. The composition of the melt produced from the partial melting of clastic metasediments appears to be a key to determine the importance of each process determined above. Some authors claim that melt produced from metasediment is leucocratic (e.g. Sawyer 1991, Brown 2001, Clemens 2003). If melt is indeed leucocratic, then several questions need to be answered: what material has been added to this magma to produce the observed compositional variations? Why is not there petrological evidence of this addition? It appears that answers to these questions can be found by focusing on source processes: discussing the composition of melt produced from metasediments, identifying which material can be added to melt and if they can affect magma composition significantly to produce the variations observed in S-type granite. I have tried to answer these questions on the basis of major and trace elements compositions and petrological observations of typical S-type granitoids: the S-type granite of the Cape Granite Suite (CGS). The study will be presented as follows:

1. A general definition of S-type granite (chapter ??). This chapter describes the compositional variation of S-type granites in relation with the composition of experimental melt derived from clastic metasediments. It also presents the processes that can potentially affect S-type granite composition.

2. The description and petrology and geochemistry of S-type granitoids from the Cape Granite Suite, their tectonic setting and geodynamical context (chapter 3).
3. Selective peritectic garnet entrainment as the origin of geochemical diversity in S-type granites (Publication in the journal *Geology*). On the basis of experimental work on partial melting of metasediment, chapter 4 aims to discuss the major element composition of S-type melt and to determine which additional material within the source region can be added to melt to produce major element variations in S-type CGS.
4. Tracking S-type granite from source to emplacement: Clues from garnet in the Cape Granite Suite (Publication to *Lithos*). This section aims to determine the fate of additional material in S-type CGS by looking for petrological evidence of the presence of such material. To do so, chapter 5 is based on the petrological description of S-type CGS and thermobarometrical calculation on mineral assemblages in xenoliths in order to determinate conditions of formation of S-type CGS. Pseudosection calculations are used to establish the condition of stability of garnet within S-type CGS compositions. Altogether this results provide an overview of the evolution of S-type CGS from the source towards crystallisation site.
5. The trace element compositions of S-type granites: Evidence for disequilibrium melting and accessory phase entrainment in the source (Publication to *Contributions to Mineralogy and Petrology*). This section aims to determine the process that could explain the observed trace element variations in S-type CGS, in agreement with the process responsible of major element variations.

In order to achieve this, chapter 6 establishes the trace element composition of S-type melt using experimental melt major element composition. By determining the Zr and LREE saturation level for experimental melt it is possible to model the behaviour of zircon and monazite within S-type melt. Then, the results of this modelling can be compared to the actual trace element composition of the S-type CGS to establish the role of accessory minerals in the composition of S-type granite.

6. All of these results are then synthesized to establish a comprehensive model (petrology, major and trace element variations) for S-type granite compositional variations and to discuss the relative importance of source material entrainment, magma mixing and fractional crystallisation in the petrogenesis of S-type Granites.

References

- Brown M., 2001. Crustal melting and granite magmatism: Key issues. *Phys. Chem. Earth Part A - Sol. Earth and Geod.* 26:201-212.
- Chappell B. W. and White A. J. R., 1974. Two contracting granite types. *Pac. Geol.* 8:173-174.
- Clemens J. D., 2003. S-type granitic magmas - petrogenetic issues, models and evidence. *Earth-Sci. Rev.* 61:1-18.
- Debon F., and Lefort P., 1982. A chemical-mineralogical classification of common plutonic rocks and associations. *Trans. Royal Soc. Edinburgh: Earth Sci.*, 73:135-139
- Martin H. and Moyen J.-F., 2002. Secular changes in tonalite-trondhjemite-granodiorite composition as markers of the progressive cooling of Earth. *Geology* 30:319-322.
- Petford N., A. R. Cruden, McCaffrey K. J. W. and Vigneresse J.-L., 2000. Granite magma formation, transport and emplacement in the Earth's crust. *Nature* 408:669-673.
- Sawyer E. W., 1991. Disequilibrium melting and the rate of melt residuum separation during migmatization of mafic rocks from the Grenville Front, Quebec. *J. Pet.* 32:701-738.

Chapter 2

What are S-type granites?

2.1 Composition of S-type Granite

Strongly peraluminous granitoids formed from the partial melting of peraluminous clastic sediments (S-type) are extremely common in the continental crust. They are characterised by an Aluminium Saturation Index ($ASI = 2 \times Al / (Ca + 2 \times Na + 2.K)$) in excess of 1.1 Na_2O contents of less than 3.2wt.% (White and Chappell 1988; Chappell and White 1992; Chappell and White 2001; Collins and Hobbs 2001; Clemens 2003; Johannes *et al.* 2003) and extremely variable FeO_{tot} and MgO contents. Typically, S-type granitoid compositions vary from leucogranitic to granodioritic with $Fe + Mg$ contents from 2 up to 12 mol% (Figure 2.1). This variation is strongly correlated with TiO_2 and CaO variations, but anti-correlated with K_2O and SiO_2 (Figure 1.1). As suggested by their chemical composition, highly peraluminous minerals such as muscovite, cordierite or garnet are common in S-type granitoids. Additionally, accessory minerals such as zircon, monazite and ilmenite are common (Bea 1996; Watson 1996; Villaseca *et al.* 2007). Accessory minerals in S-type granites concentrate most trace elements and the content of elements such as Y, Zr or Hf increases with increasing maficity of the granites (White and Chappell 1988; Clemens 2003).

2.2 Melting reaction, melt composition and extraction from the metasedimentary source

Granitic magma is generally considered as a mixture of liquid and crystals (e.g. Petford 2003). The formation of high-level S-type granite can be summarized in four main stages (Clemens 1992; Clemens 2003; Petford 2003):

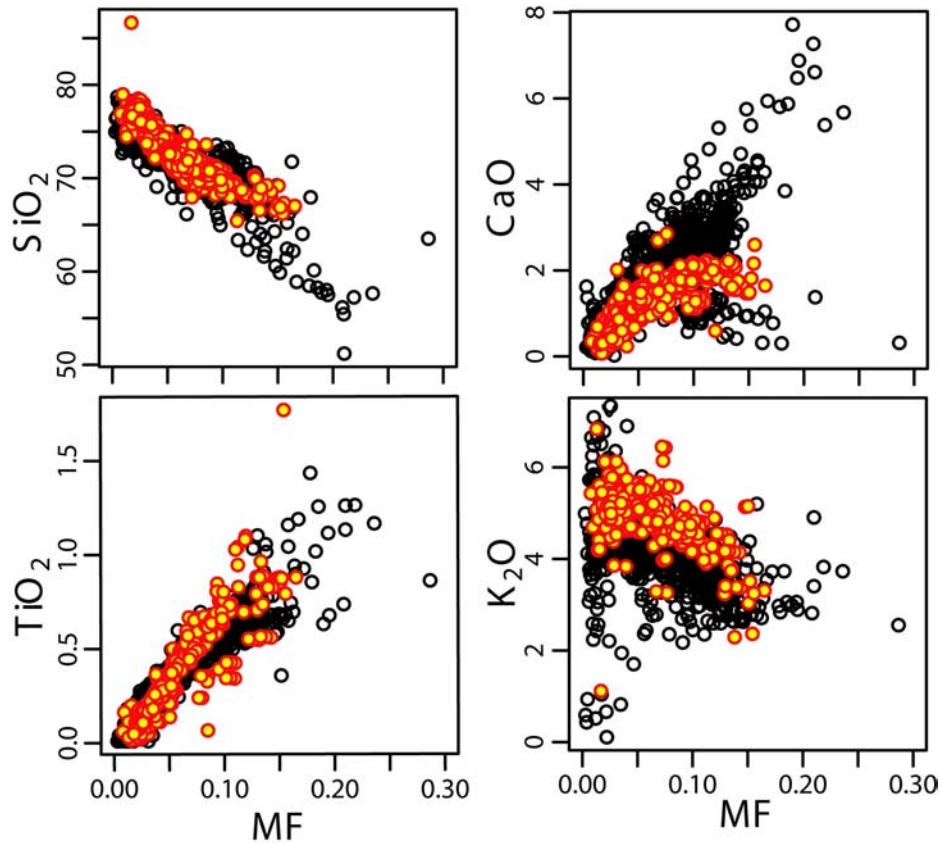


Figure 2.1: Compositional variations in S-type granite, Comparison between a dataset of S-type granite from (1200 analysis) (Goad and Cerny 1981; Day and Weiblen 1986; Georget *et al.* 1986; Bourne and Danis 1987; Downes and Duthou 1988; Downes *et al.* 1990; Scaillet *et al.* 1990; Chappell and White 1992; Nabelek *et al.* 1992; Inger and Harris 1993; Bea *et al.* 1994; Williamson *et al.* 1996; Ayres and Harris 1997; Williamson *et al.* 1997; Solgadi *et al.* 2007) and composition from S-type Cape Granite Suite (Scheepers 1990; Scheepers 1995; Scheepers and Nortje 2000; Scheepers and Poujol 2002 and this study).

1. **Melting** of a clastic metasedimentary source through a fluid-absent partial melting reaction.
2. The **segregation** of the magma from the residuum of its source.
3. The **transport** of the magma towards the future emplacement of granite.
4. The **crystallisation** and emplacement of the granite .

During each of these 4 stages the composition of the magma can be altered (e.g. entrainment of source material or fractionnal crystallisation) or changed by the addition of material (e.g. magma mixing or crustal contamination). The resulting granite is the consequence of events taking places during these four stages.

2.2.1 Conditions of melting and melting reaction

Conditions of formation for S-type melt depend on the composition of its source and the conditions of partial melting ($P-T-a_{(H_2O)}$). Clastic aluminous sediments, from which S-type granite originate, have a relatively large range of composition from psammite (or greywacke) to metapelite (Vielzeuf and Montel 1994; Gardien *et al.* 1995; Montel and Vielzeuf 1997; Stevens *et al.* 1997; Patiño-Douce and Harris 1998). Water has a preponderant role in melting. Depending on its availability two types of melting reactions have been identified (Figure 2.2): fluid-present and fluid-absent reactions. In the case of fluid-present melting water is in excess in the metasediment, and melting results in the coexistence of water-saturated silicate liquid with a free fluid phase. In contrast, fluid-absent reactions require the breakdown of hydrous minerals, mainly white mica and biotite in typical clastic metasediments, and result in the production of a water undersaturated melt.

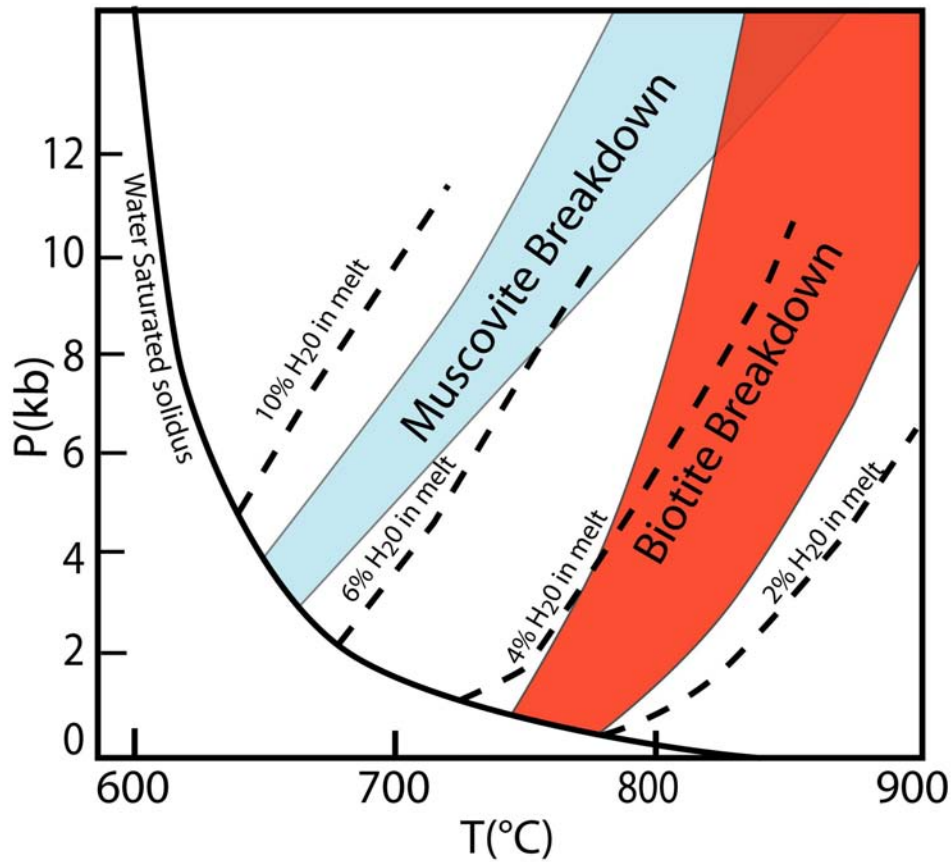


Figure 2.2: Phase diagram of common partial melting reaction in metasediments (from Vielzeuf and Montel 1994).

Fluid-present melting (i.e. $a_{H_2O} = 1$) occurs at considerably lower temperature (from $\sim 670^\circ C$) than fluid-absent melting (from $750^\circ C$) (Vielzeuf and Schmidt 2001). The breakdown of a hydrous phase is commonly accompanied by the formation of solid peritectic mineral phases (incongruent melting). The nature of the peritectic phase depends on the hydrous mineral that is breaking down. In the case of biotite melting the peritectic phases are typically ferromagnesian minerals (garnet, orthopyroxene and/or cordierite) (Vielzeuf and Montel 1994). Melting reactions in the source region of high-level S-type granite are still subject to discus-

sion, Some authors claim that melting occurs at temperatures significantly below 800°C (Chappell 1984; White and Chappell 1988; Chappell and White 1992), but most of the studies seem to indicate that partial melting occur at higher temperature above 800°C and likely to be around 850°C (Vielzeuf and Montel 1994; Clemens and Watkins 2001; Johnson *et al.* 2001). At these conditions the partial melting reaction corresponds to fluid-absent biotite melting. During such reactions melt production is commonly accompanied by the production of peritectic garnet. e.g. $Bt + Qtz + Pl + Sil \leftrightarrow melt + Grt + Ilm \pm Ksp$ for a metapelite and $Bt + Qtz + Plg \leftrightarrow melt + Grt + Opx \pm Ksp$ for a metapsammite are typical melting reactions from temperatures around 800°C and above.

2.2.2 Melt composition

The direct observation of melt in natural rocks is extremely rare and difficult to achieve as there are only rare examples of quenched peraluminous melt and these occur as inclusions in mineral particularly difficult to analyse (e.g. Maas *et al.* 2001). In order to determine the composition of melt produced through partial melting of sediments, experimental studies have been shown to be particularly efficient, and the consistency between the different studies give experimental results a considerable reliability (Johannes 1985; Holtz and Johannes 1991; Stevens and Clemens 1993; Vielzeuf and Montel 1994; Carrington and Harley 1995; Gardien *et al.* 1995; Patino-Douce and Beard 1995; Icenhower and London 1996; Clemens *et al.* 1997; Stevens *et al.* 1997; Patiño-Douce and Harris 1998; Kriegsman 2001; Scaillet and MacDonald 2001; Acosta-Vigil *et al.* 2006). Experimental melting of natural and synthetic metasediment compositions shows that the melt produced from any

sediment composition is always leucocratic with $FeO+MgO$ contents below 4 wt.% (e.g. Montel and Vielzeuf 1997). Melt composition varies substantially in regard with composition of the source in particular Na_2O and K_2O contents (Figure 2.3). For a given source composition, the resulting melt composition is particularly homogeneous and very leucocratic a relatively high SiO_2 (72 wt.% in average) and high Al_2O_3 (12 wt.% in average). Figure 2.4 shows that the relative homogeneity of experimental melt compositions contrasts strongly with the variation of maficity observed in S-type granite. Indeed, S-type granite compositional variations cannot be explained by variation in melt composition and some additional chemical processes must occur in order to produce S-type magma. This figure also illustrates that the composition of the least mafic granitoids corresponds nicely with that of experimental melt, thus showing the genetic relationship between S-type magma and melt, and that process generating S-type granite variation allow the preservation of melt major element composition. Concerning the trace element composition of melt it is rather difficult to determine from experimental work, mainly because of problems of obtaining "clean" analyses (i.e. unaffected by contamination by peritectic minerals) from small glass films in experimental charges (Icenhower and London 1996; Rubatto and Hermann 2007). However, a few studies that have focused on trace element partitioning in natural rocks, determine a difference of behaviour between high field strength elements (HFSE) such as Zr and LREE and large ion lithophile elements (LILE) such as Rb, Sr or Ba. These studies suggest that HFSE melt composition is mostly controlled by the dissolution/precipitation kinetics of accessory phases and that melt is probably undersaturated in HFSE with respect to equilibrium saturation with accessory minerals (Watt and Harley 1993; Bea *et al.*, 1994; Bea 1996) while LILE are likely to be concentrated in the

melt (e.g. Watt and Harley 1993 or Junget *al.* 1998)

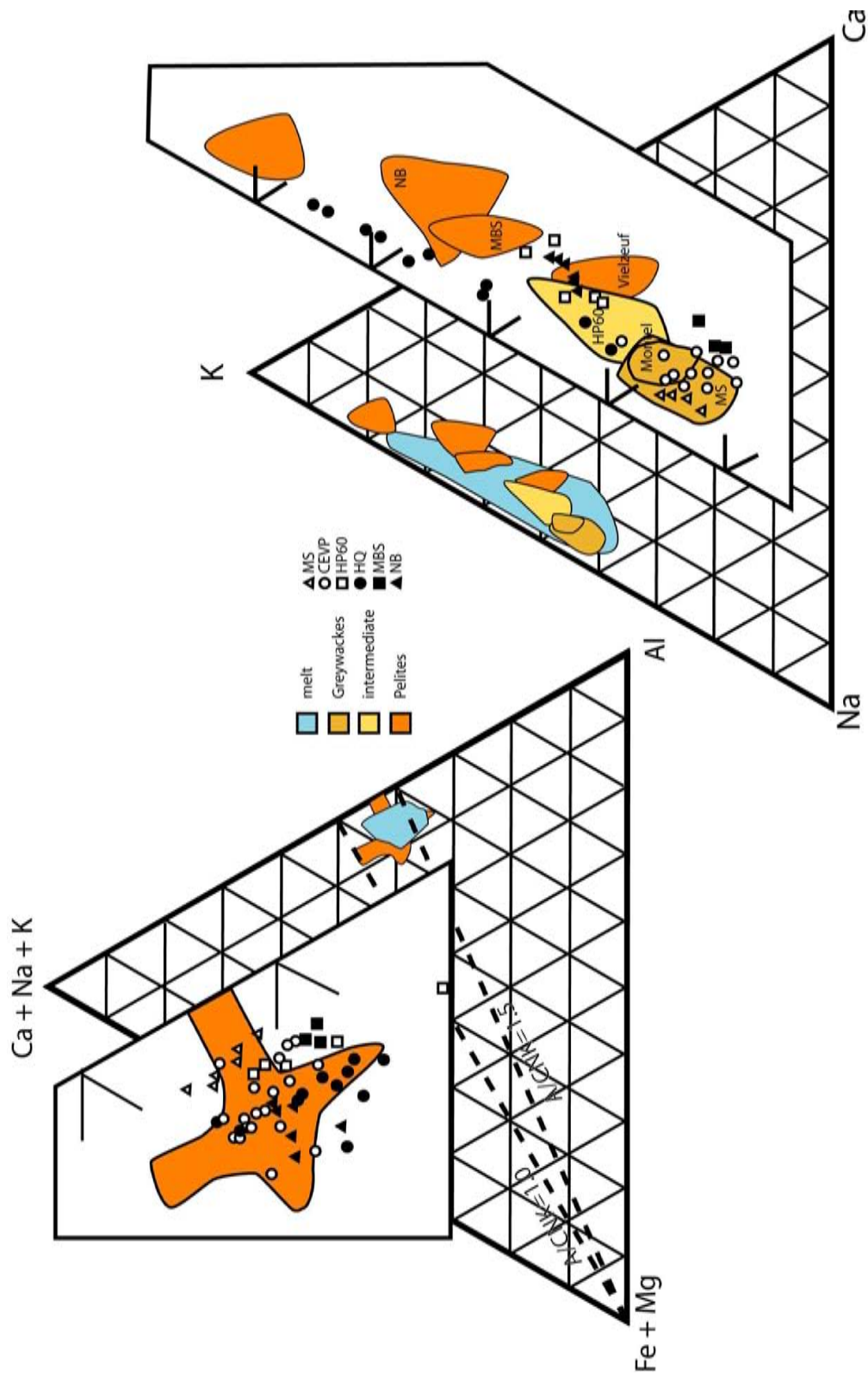


Figure 2.3: Ternary diagrams showing compositional variations in experimental melt in relation to the composition of the source. MS and MBS (Patino-Douce and Harris 1998); CEVP (Montel and Vielzeuf 1997), HQ (Patino-Douce and Johnston 1991) HP (Pickering and Johnston 1998) NB (Stevens *et al.* 1997). Courtesy of J.-F. Moyen

2.2.3 Extraction from the source region

Migmatitic terranes are commonly considered as the source region of S-type granite. Direct observations have been made for the connection of migmatite and S-type granite at lower to mid-crustal levels (Inger and Harris 1993; Ayres and Harris 1997; Sawyer 1998; Solar and Brown 2001; Vigneresse and Burg 2002). This connection is particularly difficult to build in the case of large high level S-type plutons, as the source region remains generally at much lower crustal level than that of granite emplacement. Observations in migmatitic terranes have helped in understanding melt production and melt extraction (Johannes 1988; Ellis and Obata 1992; Sawyer 2001; Droop *et al.* 2003; Brown 2005). As a result of such studies, a commonly accepted idea is that melt extraction is deformation-controlled in the source region and that efficiency of melt extraction depends on the deformation of the source area (Ellis and Obata 1992; Brown 1994; Sawyer 1994; Brown *et al.* 1995; Holtzman and Kohlstedt 2007). Studies that focus on melt extraction in migmatitic terranes put in relief a particularly short time of residence of melt in the source (Sawyer 1991; Nabelek and Glascock 1995; Bea 1996; Ayres and Harris 1997; Davies and Tommasini 2000). Additionally, a number of studies have described the occurrence of garnet in very leucocratic granitic dykes (Sawyer 1991; Bea *et al.* 1994; Jung *et al.* 1999; Kriegsman 2001) suggesting that potentially peritectic phases can be entrained along with melt out of the source. Sawyer (1996) suggested that the entrainment of peritectic phases can be the origin of the variation of maficity in S-type granites.

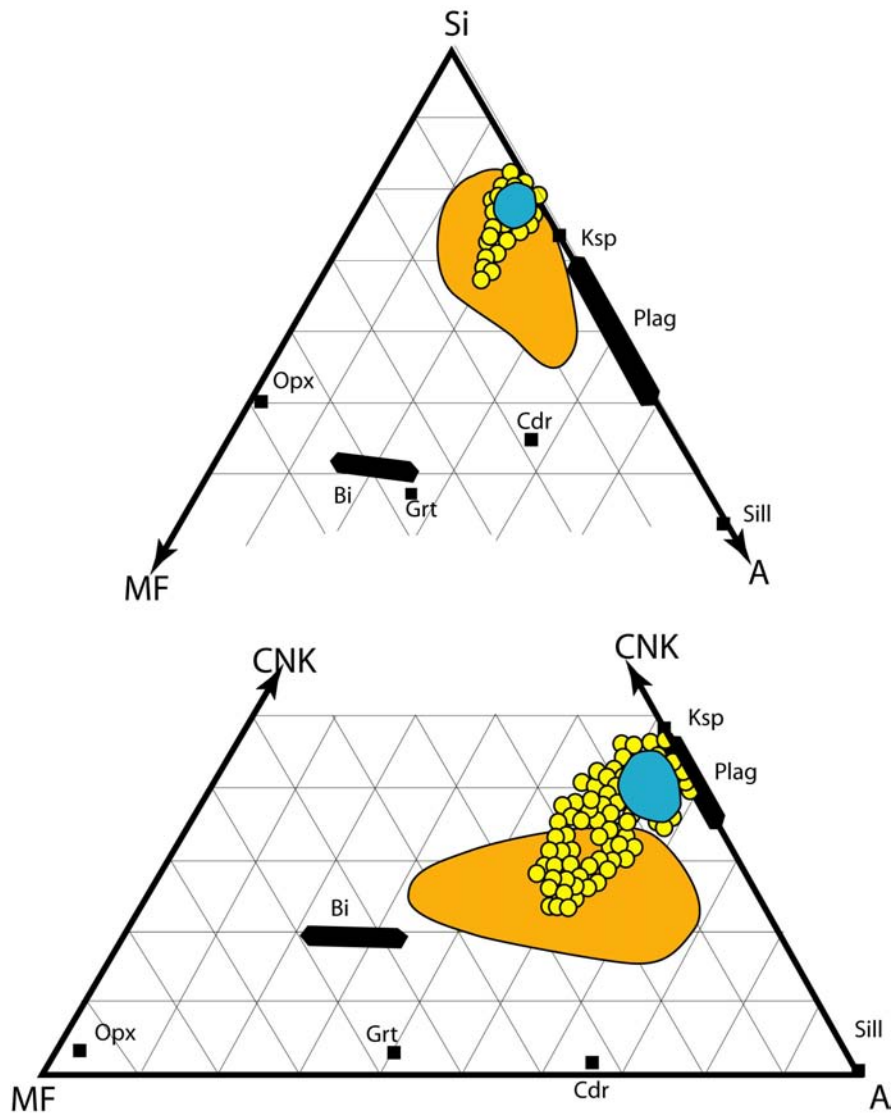


Figure 2.4: Ternary diagrams showing differences between S-type granites of the Cape Granite Suite composition and experimental melt. (experimental melt compositions similar to Figure 2.3; Composition of S-type Cape Granite Suite from Scheepers (1990; 1995; 2000; 2002) and this study. Courtesy of G. Stevens.

The Blue area is the composition of Experimental melt, the orange area the composition of the source, Yellow circles are S-type Granite compositions

2.3 What controls compositional variations in S-type granitoids?

Several models have been proposed to explain compositional variation in granites namely:

- Magma mixing
- Fractional crystallisation
- Entrainment of source material
- Crustal contamination

All of these models are based on strong evidence but none of them answers satisfactorily the problems raised by petrological and compositional variations. The requirements, expressions and limits of each of the processes stated above are summarized in Table 2.1 .

2.3.1 Magma mixing

Compositional change due to magma mixing implies the existence of at least two magmas of different compositions. Variations observed in S-type granite suggest mixing between very leucocratic magma, and a more mafic component. According to some authors (Didier 1982; Reid *et al.* 1983; Didier 1984; DiVincenzo *et al.* 1996; Keay *et al.* 1999; Collins and Hobbs 2001; Healy *et al.* 2004) magmas involved in magma mixing originate from different sources generally of metasedimentary and mantellic origin respectively providing a felsic and a mafic component for mixing.

	Magma mixing	Fractional crystallisation	Source material entrainment	Assimilation of Crustal Rocks
Requirements	two magmas of different compositions	a mafic original magma	extraction of melt and solid material	entrainment of crustal rocks in the magma
Expression	local field evidence for magma interactions	layering and cumulates of mafic minerals	compositional trend tends toward source composition	presence of xenoliths very common
Limits	melt from metasediment is only leucocratic - lack of evidence for extensive presence magma of different source - mixing homogenize composition	S-type melt are leucocratic	source material not preserved - lack of field evidence	problem for the assimilation of large body of crustal rocks in a cooling magma

Table 2.1: Summary of requirements, field and compositionnal expression and limits of models proposed for S-type granite petrogenesis

Field evidence for a close relationship between juvenile mafic magma and the formation of S-type granite is extremely rare, and the mixing of magmas of different composition and temperatures faces is particularly difficult (McKenzie and Onions 1991; Bogaerts and Schmidt 2006). Furthermore, the trace element composition of juvenile mafic material is likely to have low concentration of trace elements (mainly LILE). Thus the addition of juvenile mafic magma to a leucogranitic S-type melt are unlikely to produce an increase of trace element contents correlated to the increas-

ing maficity of the resulting magma. Thus the mixing of magma produced from different sources as a source of extended compositional variation is rather dubious (Brown and Pressley 1999; Clemens 2003). Other studies suggest that magmas are produced from only one source type (i.e. metasedimentary) (Ayres and Harris 1997). This requires an additional process to create the compositional variation between magma involved prior of mixing. In that case magma mixing tends to homogenise variation and thus it is not the source of compositional variation in S-type granite.

2.3.2 Fractional Crystallisation

Fractional crystallisation is commonly proposed in granite petrogenesis models and is generally suggested by the presence of layered structure e.g. concentrically compositionally zoned plutons. The differentiation of magma through fractional crystallisation typically produces more felsic residual magma (Wager and Brown 1968; Cawthorn 1996; Couch 2003). Thus, considering the observed compositional variation in S-type granites (Figure 2.1), in order for fractional crystallisation to be the origin of such variation implies that the magma at the origin of the granite corresponds to a rather ferromagnesian endmember of the range. The fractional crystallisation of such magma would be expressed by formation of ferromagnesian cumulates and layered structures formed in the magma chamber as a consequence of gravity driven segregation. However, as shown earlier, S-type melt are exclusively leucogranitic, thus it is unlikely that S-type melt produces mafic minerals cumulates. In the same way, fractional crystallisation would imply that the less mafic (more evolved) magmas are the most rich in trace elements (mainly HFSE),

it is sometimes the case, but it is not systematic.

2.3.3 Crustal assimilation

Another model commonly proposed for S-type granite compositional variation suggests the contamination of the magma with crustal rock (Jung *et al.* 1999; Clarke and Carruzo 2007). In S-type granite, the entrainment of crustal material is supported by the common presence of commonly metasedimentary xenoliths of various metamorphic grades (Chappell 1984; White and Chappell 1988). The time necessary for the assimilation of a relatively large material (few cm of diameter) in a cooling magma (Temperature below 850°C) can be achieved in a very short time (100 hours, in an andesitic composition) (McLeod *et al.* 1998). Assimilation of country rocks is often associated with fractional crystallisation (e.g. De Paolo 1981; Foden *et al.* 2002) suggesting that magma composition has been changed by the addition of material before fractional crystallisation is effective, and thus that the original magma is leucocratic. This assimilation fractional crystallisation (AFC) model (De Paolo 1981) suggests that the energy released during fractional crystallisation increases the efficiency of xenolith assimilation in a magma (Bohrson and Spera 2001; Spera and Bohrson 2001). However, the preservation of large number of relatively large metasedimentary xenoliths in S-type granites indicates that assimilation of metasedimentary xenoliths in S-type magmas is only limited (Clemens 2003; Vernon 2007). According to compositional variations observed in S-type granite (Figure 2.1 and 2.4) the large Fe+Mg variations are only possible through AFC if an extremely large amount ($\gg 50\%$) of metasedimentary material is assimilated to obtain the more mafic S-type granite compositions (Clemens and Mawer 1992;

Clemens 1998). The preservation of a large quantity of metasedimentary xenolith indicates that, on the contrary, assimilation is not particularly efficient. Thus it is unlikely that crustal material assimilation is the origin of compositional variation in S-type granites.

2.3.4 Entrainment of source material

The entrainment of source material is commonly invoked as an origin for compositional variations of S-type granites. This material is generally identified as *restite* which corresponds to the solid residuum of partial melting (peritectic phases and reactant minerals left over due to incomplete reaction) (Chappell and White 1974; Chappell *et al.* 1987; White and Chappell 1988). The entrainment of restite as the origin of compositional variations of the S-type granite implies that granite composition varies between a leucocratic magma composition and the composition of the source. This suggests that the mafic character is inherited from the source and thus that compositional variations are inherited from the source. However, among the different studies suggesting restite entrainment (Williamson *et al.* 1997; Chappell 1999; Jung *et al.* 1999), the lack of strong field evidence in favour of the preservation of entrained source material is particularly problematic. In addition, the composition of restite remains unclear and thus difficult to track during magma evolution.

The Panafrican Cape Granite Suite (CGS, South Africa) is an ideal example in order to study S-type Granite compositional variation. The different plutons of the S-type CGS offer a large scatter in composition representative of the variation observed in S-type Granite from different localities across the world (Figure 2.1). Using plutons of the CGS as example it would be possible to answer the different question asked above in the Introduction (Chapter 1).

References

- Acosta-Vigil, A., London D. and Morgan G., 2006. Experiments on the kinetics of partial melting of a leucogranite at 200 MPa H_2O and 690 – 800°C: compositional variability of melts during the onset of H₂O-saturated crustal anatexis. *Contrib. Mineral. Petrol.* 151:539-557.
- Ayres, M. and Harris N., 1997. REE fractionation and Nd-isotope disequilibrium during crustal anatexis: constraints from himalayan leucogranites. *Chem. Geol.* 139:249-269.
- Bea, F., 1996. Controls on the trace element composition of crustal melts. *Trans. Royal Soc. Edinburgh-Earth Sci.* 87:33-41.
- Bea F., Pereira M. D. Corretge L. G. and Fershtater G. B., 1994. Differentiation of Strongly Peraluminous, Perphosphorus Granites - the Pedrobernardo Pluton, Central Spain. *Geochim. Cosmochim. Acta* 58:2609-2627.
- Bea F., Pereira M. D. and Stroh A., 1994. Mineral leucosome trace-element partitioning in a peraluminous migmatite (a Laser Ablation-ICP-MS Study). *Chem. Geol.* 117:291-312.
- Bogaerts M. and Schmidt M. W., 2006. Experiments on silicate melt immiscibility in the system Fe₂SiO₄-KAlSi₃O₈-SiO₂-CaO-MgO-TiO₂-P₂O₅. *Contrib. Mineral. Petrol.* 152:257-274.
- Bohrson W. A. and Spera F. J., 2001. "Energy-Constrained Open-System Magmatic Processes II: Application of Energy-Constrained Assimilation-Fractional Crystallization (EC-AFC) Model to Magmatic systems." *J. Petrol.* 42:1019-1041.
- Bourne J. and Danis D., 1987. A proposed model for the formation of reversely zoned plutons based on study of the Lacorne Complex, Superior Province, Quebec. *Can. J. Earth Sci.* 24:2506-2520.
- Brown M., 1994. The generation, segregation, ascent and emplacement of granite magma - the migmatite-to-crustally-derived-granite connection in thickened orogens. *Earth Sci. Rev.* 36:83-130.
- Brown M., 2005. The mechanism of melt extraction from lower continental crust of orogens. *Trans. Royal Soc. Edinburgh, Earth Sci.* 95:35-48.
- Brown M., Averkin Y. A., McLellan E. L. and Sawyer E. W., 1995. Melt segregation in migmatites. *J. Geophys. Res. Sol. Earth* 100:15655-15679.
- Brown M. and Pressley R. A., 1999. Crustal melting in nature: prosecuting source processes. *Phys. Chem. Earth Part A-Solid Earth Geod.* 24: 305-316.

- Carrington D. P. and Harley S. L., 1995. partial melting and phase-relations in high-grade metapelites - an experimental petrogenetic grid in the KFMASH system. *Contrib. Mineral. Petrol.* 120:270-291.
- Cawthorn R. G., 1996. *Layered Intrusions*. Amsterdam, Elsevier. 531p.
- Chappell B. W., 1984. Source rocks of I- and S-type granites in the Lachlan Fold Belt, southeastern Australia. *Phil. Trans. Royal Soc. London Series a-Mathem. Phys. Eng. Sci.* 310: 693-707.
- Chappell B. W., 1999. Aluminium saturation in I- and S-type granites and the characterization of fractionated haplogranites. *Lithos* 46:535-551.
- Chappell B. W. and White A. J. R., 1974. Two contrasting granite types. *Pac. Geol.* 8:173-174.
- Chappell B. W. and White A. J. R., 1992. I-Type and S-Type granites in the Lachlan Fold Belt. *Trans. Royal Soc. of Edinburgh-Earth Sci.* 83:1-26.
- Chappell B. W. and White A. J. R., 2001. Two contrasting granite types: 25 years later. *Austr. J. Earth Sci.* 48:489-499.
- Chappell B. W., White A. J. R. and Wyborn D., 1987. The importance of residual source material (Restite). *J. Petrol.* 28:1111-1138.
- Clarke D. B. and Carruzo S., 2007. Assimilation of country-rock ilmenite and rutile in the south mountain batholith, Nova Scotia, Canada. *Can. Mineral.* 45:31-42.
- Clemens J. D., 1992. Partial melting and granulite genesis - a partisan overview. *Pre-camb. Res.* 55:297-301.
- Clemens J. D., 2003. S-type granitic magmas - petrogenetic issues, models and evidence. *Earth-Sci. Rev.* 61(1-2): 1-18.
- Clemens J. D., Droop G. T. R., and Stevens G., 1997. High-grade metamorphism, dehydrations and crustal melting: a reinvestigation based on new experiments in the silica-saturated portion of the system $KAlO_2 - MgO - SiO_2 - H_2O - CO_2$ at $P \leq 1.5GPa$. *Contrib. Mineral. Petrol.* 129:308-325.
- Clemens, J. D. and Watkins J. M., 2001. The fluid regime of high-temperature metamorphism during granitoid magma genesis. *Contrib. Mineral. Petrol.* 140:600-606.
- Collins W. J. and Hobbs B. E., 2001. What caused the Early Silurian change from mafic to silicic (S-type) magmatism in the eastern Lachlan Fold Belt? *Austr. J. Earth Sci.* 48:25-41.
- Couch S., 2003. Experimental investigation of crystallization kinetics in a haplogranite system. *Amer. Mineral.* 88:1471-1485.

- Davies G. R. and Tommasini S., 2000. Isotopic disequilibrium during rapid crustal anatexis: implications for petrogenetic studies of magmatic processes. *Chem. Geol.* 162:169-191.
- Day W. C. and Weiblen P. W., 1986. Origin of late Archean granite: geochemical evidence from the Vermilion Granitic Complex of northern Minnesota. *Contrib. Mineral. Petrol.* 93:283-296.
- De Paolo D.J., 1981. Trace element and isotopes effects of combined wallrock assimilation and fractional crystallization. *Earth Planet. Sci.lett.* 53:189-202.
- Di Vincenzo G., Andriessen P. A. M., and Ghezzo C., 1996. Evidence of two different components in a Hercynian peraluminous cordierite-bearing granite: The San Basilio intrusion (Central Sardinia, Italy). *J. Petrol.* 37:1175-1206.
- Didier J., 1982. Mantle and crustal granites: Genetic classification of orogenic granites and the nature of their enclaves. *J. Volc. Geoth. Res.* 14:125-132.
- Didier J., 1984. The problem of enclaves in granitic rocks, a review of recent ideas on their origin. In, *Geology of Granites and Their Metallogenic Relations*. K. T. Xu, G. Beijing, Science Press: 137-144.
- Downes H., Dupuy C. and Leyreloup A., 1990. Crustal evolution of the Hercynian belt of Western Europe: evidence from lower crustal xenoliths (French Massif Central). *Chem. Geol.* 83:209-231.
- Downes H. and Duthou J.-L., 1988. Isotopic and trace-element arguments for the lower-crustal origin of Hercynian granitoids and pre-Hercynian orthogneisses, Massif Central (France). *Chem. Geol.* 68:291-308.
- Droop G. T. R., Clemens J. D. and Dalrymple D. J., 2003. Processes and conditions during contact anatexis, melt escape and restite formation: the Huntly Gabbro Complex, NE Scotland. *J. Pet.* 44:995-1029.
- Ellis D. J. and Obata M., 1992. Migmatite and melt segregation at Cooma, New South Wales. *Trans. Royal Soc. Edinburgh, Earth Sci.* 83:95-106.
- Foden J. D., Elburg M. A., Turner S. P., Sandiford M., O'Callaghan J., and Mitchell S., 2002. Granite production in the Delamerian Orogen, South Australia. *J. Geol. Soc.* 159:557-575.
- Gardien V., Thompson A. B., Grujic D. and Ulmer P., 1995. Experimental melting of biotite + plagioclase + quartz \pm muscovite assemblages and implications for crustal melting. *J. Geophys. Res.-Sol. Earth* 100:15581-15591.

- Georget Y., Martineau F. and Capdevilla R., 1986. Age tardi-hercynien et origine crustale du granite de Brignogan (Finistère, France). Conséquences sur l'interprétation des granites Nord-armoricains = Late-Hercynian radiometric age and crustal origin of Brignogan granite (Finistere, France). Consequences on the interpretation of the North-Armorican granites. *C.-R. Acad. Sci Série 2, Méca., Phys. Chim. Sci. Univ. Sci. Terre* 302:237-242.
- Goad B. E. and Cerny P., 1981. Peraluminous pegmatitic granites and their pegmatite aureoles in the Winnipeg River District, southeastern Manitoba *Can. Mineral.* 19:177-194.
- Healy B., Collins W. J. and Richard S.W., 2004. A hybrid origin for Lachlan S-type granites: the Murrumbidgee Batholith example. *Lithos* 78:197-216.
- Holtz F. and Johannes W., 1991. Genesis of Peraluminous Granites .1. experimental investigation of melt compositions at 3 and 5 Kb and various H_2O activities. *J. Petrol.* 32:935-958.
- Holtzman B. K. and Kohlstedt D. L., 2007. Stress-driven melt segregation and strain partitioning in partially molten rocks: effects of stress and strain. *J. Petrol.* 48:2379-2406.
- Icenhower J. and London D., 1996. Experimental partitioning of Rb, Cs, Sr, and Ba between alkali feldspar and peraluminous melt. *Amer. Mineral.* 81:719-734.
- Inger S. and Harris N., 1993. Geochemical constraints on leukogranite magmatism in the Langtang Valley, Nepal Himalaya. *J. Petrol.* 34:345-368.
- Johannes W., 1985. The significance of experimental studies for the formation of migmatites. In Ashworth J. R. (Ed) *Migmatites*, Blackie, Glasgow, p 36-85
- Johannes W., 1988. What controls partial melting in migmatites? *J. Metam. Geol.* 6:451-465.
- Johannes W., Ehlers C. , Kriegsman L. M. and Mengel K., 2003. The link between migmatites and S-type granites in the Turku area, southern Finland. *lithos* 68:69-90.
- Johnson T. E., Hudson N. F. C. and Droop G., 2001. Partial melting of the Inzie Head gneisses: The role of water and a petrogenetic grid in KFMASH applicable to anatectic pelitic migmatites. *J. Metam. Geol.* 19:99-118.
- Jung S., Mezger K. , Masberg P., Hoffer E. and Hoernes S., 1998. Petrology of an intrusion-related high-grade migmatite: implications for partial melting of metasedimentary rocks and leucosome forming processes. *J. Metam. Geol.* 16:425-445.

- Jung S., Hoernes S., Masberg P. and Hoffer E., 1999. The petrogenesis of some migmatites and granites (central Damara Orogen, Namibia): Evidence for disequilibrium melting, wall-rock contamination and crystal fractionation. *J. Petrol.* 40:1241-1269.
- Keay S., Steele D. and Compston W., 1999. Identifying granite sources by SHRIMP U-Pb zircon geochronology: an application to the Lachlan fold belt. *Contrib. Mineral. Petrol.* 137:323-341.
- Kriegsman L. M., 2001. Partial melting, partial melt extraction and partial back reaction in anatectic migmatites. *Lithos* 56:75-96.
- Kriegsman L. M., 2001. Quantitative field methods for estimating melt production and melt loss. *Phys. Chem. Earth, Part A: Sol. Earth and Geod.* 26:247-253.
- Maas R., Nicholls I. A., Greig A. and Nemchin A., 2001. U-Pb zircon studies of mid-crustal metasedimentary enclaves from the S-type Deddick Granodiorite, Lachlan Fold Belt, SE Australia. *J. Petrol.* 42:1429-1448.
- McKenzie D. and Onions R. K., 1991. Partial Melt Distributions from Inversion of Rare-Earth Element Concentrations. *J. Petrol.* 32: 1021-1091.
- McLeod P., Stephen R., 1998. The dynamics of xenolith assimilation. *Contrib. Mineral. Petrol.* 132:21-33.
- Montel J. M. and Vielzeuf D., 1997. Partial melting of metagreywackes .2. compositions of minerals and melts. *Contrib. Mineral. Petrol.* 128:176-196.
- Nabelek P. I. and Glascock M. D., 1995. Rare earth element-depleted leucogranites Black Hills, South Dakota: A consequence of disequilibrium melting of monazite-bearing schists. *J. Petrol.* 36:1055-1071.
- Nabelek P. I., Russ-Nabelek C. and Haeussler G. T., 1992. Stable isotope evidence for the petrogenesis and fluid evolution in the Proterozoic, Harney Peak leucogranite, Black Hills, South Dakota. *Geochim. Cosmochim. Acta* 56:403-417.
- Patiño-Douce A. E. and Beard J. S., 1995. Dehydration-melting of biotite gneiss and quartz amphibolite from 3 to 15 Kbar. *J. Petrol.* 36:707-738.
- Patiño-Douce, A. E. and Harris N., 1998. Experimental constrains on himalayan Anatexis. *J. Petrol.* 39:689-710.
- Patiño-Douce A. E. and Johnston A. D., 1991. Phase equilibria and melt productivity in the pelitic system: implications for the origin of peraluminous granitoids and aluminous granulites. *Contrib. Mineral. Petrol.* 107:202-218.
- Petford N., 2003. Rheology of granitic magmas during ascent and emplacement. *Ann. Rev. Earth Planet. Sci.* 31:399-427.

- Pickering J. M. and Johnston A. D., 1998. Fluid-absent melting behavior of a two-mica metapelite: Experimental constraints on the origin of black hills granite. *J. Petrol.* 39:1787-1804.
- Reid J. B., Evans O. C. And Fates O. C., 1983. Magma mixing in granitic rocks of the central Sierra Nevada, California. *Earth Planet. Sci. Lett.* 66:243-261.
- Rubatto D. and Hermann J., 2007. Experimental zircon/melt and zircon/garnet trace element partitioning and implications for the geochronology of crustal rocks. *Chem. Geol.* 241: 38-61.
- Sawyer E. W., 1991. Disequilibrium melting and the rate of melt residuum separation during migmatization of mafic rocks from the Grenville Front, Quebec. *J. Petrol.* 32:701-738.
- Sawyer E. W., 1994. Melt segregation in the continental crust. *Geology* 22:1019-1022.
- Sawyer E. W., 1996. Melt segregation and magma flow in migmatites: Implications for the generation of granite magmas. *Trans. Royal Soc. Edinburgh-Earth Sci.* 87:85-94.
- Sawyer E. W., 1998. Formation and evolution of granite magmas during crustal reworking: the significance of diatexites. *J. Petrol.* 39:1147-1167.
- Sawyer E. W., 2001. Melt segregation in the continental crust: distribution and movement of melt in anatectic rocks. *J. Metam. Geol.* 19:291-309.
- Scaillet B., France-Lanord C. and Le Fort P., 1990. Badrinath-Gangotri plutons (Garhwal, India): Petrological and geochemical evidence for fractionation process in a high himalayan leucogranite. *J. Volc. Geotherm. Res.* 44:163-188.
- Scaillet B. and MacDonald R., 2001. Phase relations of peralkaline silicic magmas and petrogenetic implications. *J. Petrol.* 42:825-845.
- Scheepers R., 1990. Magmatic association and radioelement geochemistry of selected Cape Granites with special reference to subalkaline and leucogranitic phases (In Afrikaans). Stellenbosch, South Africa, University of Stellenbosch. Unpubl. Ph.D. dissertation.
- Scheepers R., 1995. Geology, Geochemistry and petrogenesis of Late Precambrian S-, I- and A-type granitoids in the saldania belt, Western Cape Province South Africa. *J. Afr. Earth Sci.* 21:35-58.
- Scheepers R. and Nortje A. N., 2000. Rhyolitic ignimbrites of the Cape Granite Suite, southwestern Cape Province, South Africa. *J. Afr. Earth Sci.* 31: 647-656.

- Scheepers R. and Poujol M., 2002. U-Pb zircon age of Cape Granite Suite ignimbrites: characteristics of the last phases of the Saldanian magmatism. *S. Afr. J. Geol.* 105:163-178.
- Solar G. S. and Brown M., 2001. Petrogenesis of migmatites in Maine, USA: Possible source of peraluminous leucogranite in plutons? *J. Petrol.* 42:789-823.
- Solgadi F., Moyen J.-F., Vanderhaeghe O., Sawyer E. W. and Reisberg L., 2007. The role of crustal anatexis and mantle derived magmas in the genesis of syn-orogenic Hercynian granites of the Livradois Area, French Massif Central. *Can. Mineral.* 45:581-606.
- Spera F. J. and Bohron W. A., 2001. Energy-constrained open-system magmatic processes I: general model and energy-constrained assimilation and fractional crystallization (EC-AFC) formulation. *J. Petrol.* 42:999-1018.
- Stevens G. and Clemens J. D., 1993. Fluid-absent melting and the roles of fluids in the lithosphere - a slanted summary. *Chem. Geol.* 108:1-17.
- Stevens G., Clemens J. D., and Droops G. T. R., 1997. Melt production during granulite-facies anatexis: experimental data from primitive metasedimentary protoliths. *Contrib. Mineral. Petrol.* 128:352-370.
- Vernon R. H., 2007. Problems in identifying restite in S-type granites of southeastern Australia, with speculations on sources of magma and enclaves. *Can. Mineral.* 45:147-178.
- Vielzeuf D. and Montel J.-M., 1994. Partial melting of metagreywackes .1. fluid-absent experiments and phase-relationships. *Contrib. Mineral. Petrol.* 117:375-393.
- Vielzeuf D. and Schmidt M. W., 2001. Melting relations in hydrous systems revisited: application to metapelites, metagreywackes and metabasalts. *Contrib. Mineral. Petrol.* 141:251-267.
- Vigneresse J.-L. and Burg J.-P., 2002. The paradoxical aspect of the Himalayan granites. *J. Virt. Expl.* 9:1-13.
- Villaseca C., Orejana D. and Paterson B. A., 2007, Zr LREE rich minerals in residual peraluminous granulites, another factor in the origin of low Zr LREE granitic melts? *Lithos* 96:375-386.
- Wager, L. and Brown G., 1968. *Layered Igneous Rocks*, Edinburgh, Oliver and Boyd (Eds). P588.
- Watson E. B., 1996. Dissolution, growth and survival of zircons during crustal fusion: kinetic principles, geological models and implications for isotopic inheritance. *Trans. Royal Soc. Edinburgh: Earth Sci.* 87:43-56.

- Watt G.R. and Harley S.L., 1993. Accessory mineral phase controls on the geochemistry of crustal melts and restites produced during water-undersaturated partial melting. *Contrib. Mineral. Petrol.* 114:550-566
- White A. J. R. and Chappell B. W., 1988. Some supracrustal (S-type) granites of the Lachlan Fold Belt. *Trans. Royal Soc. Edinburgh, Earth Sci.* 79:169-181.
- Williamson B. J., Shaw A. Downes H. and Thirlwall M. F., 1996. Geochemical constraints on the genesis of hercynian two-mica leucogranites from the Massif Central, France. *Chem. Geol.* 127:25-42.
- Williamson B. J., Downes H., Thirlwall M. F. and Beard A., 1997. Geochemical constraints on restite composition and unmixing in the Velay anatectic granite, French Massif Central. *Lithos* 40:295-319.

Chapter 3

A Case Study: The S-type Cape Granite Suite

3.1 The Saldanian Orogenic Belt

3.1.1 Introduction

The Saldania Orogenic Belt is one of the Panafrican age orogenic belts located on the southwestern part of the African continent along with the Damara belt, the Kaoko belt or the Gariiep belt on the African continent facing their South American counterpart the Dom Feliciano Belt. These Panafrican belts are the consequence of the Gondwana assembly and the closure of the Adamastor Ocean. Located on the southern and south eastern margin of the Kalahari craton(Figure 3.1) The Saldania Belt results from the convergence of Paraña and Kalahari Cratons. It is only poorly exposed, locally unroofed in mega-anticlinal hinges of the Permo-Triassic Cape Fold Belt (figure 3.2 and 3.3). The westernmost part of the Saldania Belt host most the intrusions that compose the Cape Granite Suite. In this area, the Saldania Belt is divided into three distinct tectonic domains:

- the Boland domain (or North Eastern domain)
- the Swartland domain (or central domain)
- the Tygerberg domain (or South Western domain)

The meta-volcano-sedimentary sequence of the Malmesbury Group which compose most of the Saldania Belt stratigraphical sequence is defined through out these 3 domains.

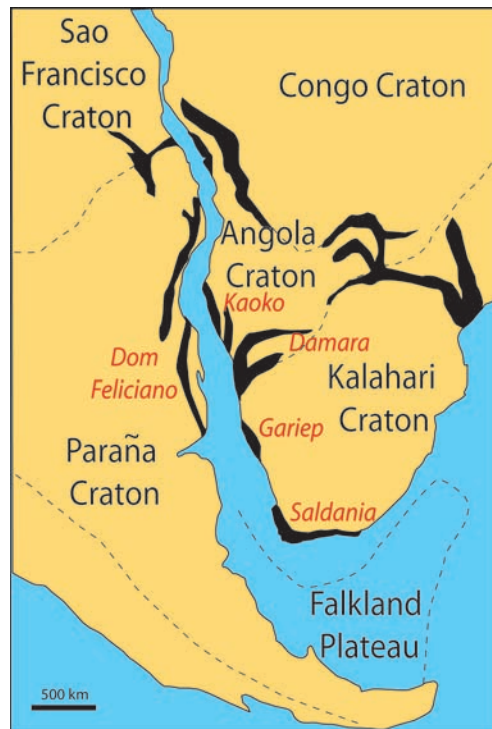


Figure 3.1: Palaeogeographic reconstruction of the Panafrican orogenies at 550 Ma from Rozendaal *et al.* 1999

3.1.2 Stratigraphy of the Saldania Orogen

The Tygerberg domain (southwest) is the host of the of S-type granite of the CGS. It consists mainly in an alternation of greywacke, shale and siltstone called the Tygerberg formation (figure 3.4). The Tygerberg formation is largely exposed along the 3 km of Atlantic coast between Sea Point and Cape Town displaying sedimentary structures (cross-bedding and ripple mark) (Von Veh 1983). The Blou-berstrand memeber (15 km north from Cape Town) constitutes an extremely local volcanic succession of tuff agglomerates and andesite.

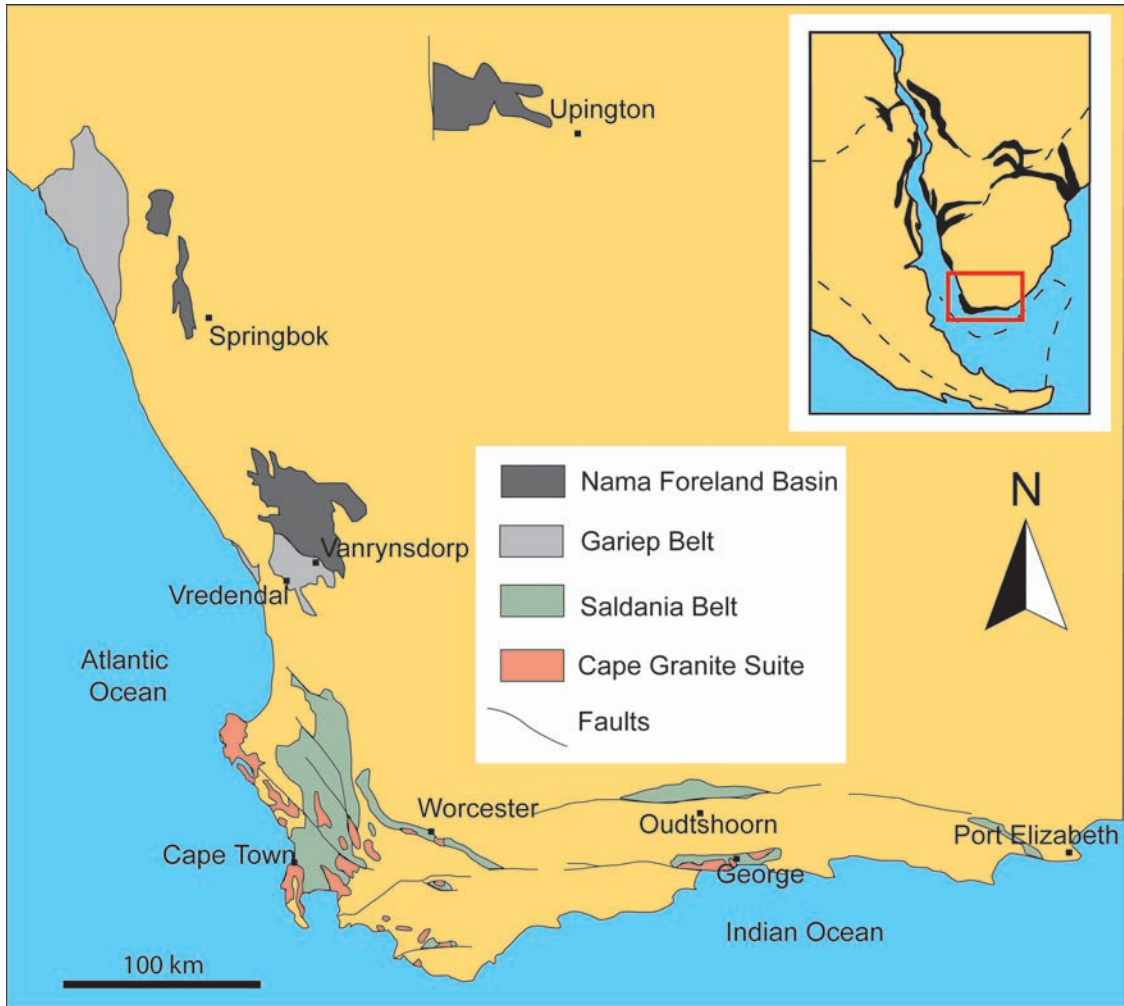


Figure 3.2: Simplified geological map of the Saldanian Orogenic Belt (after, Gresse *et al.* 2006).

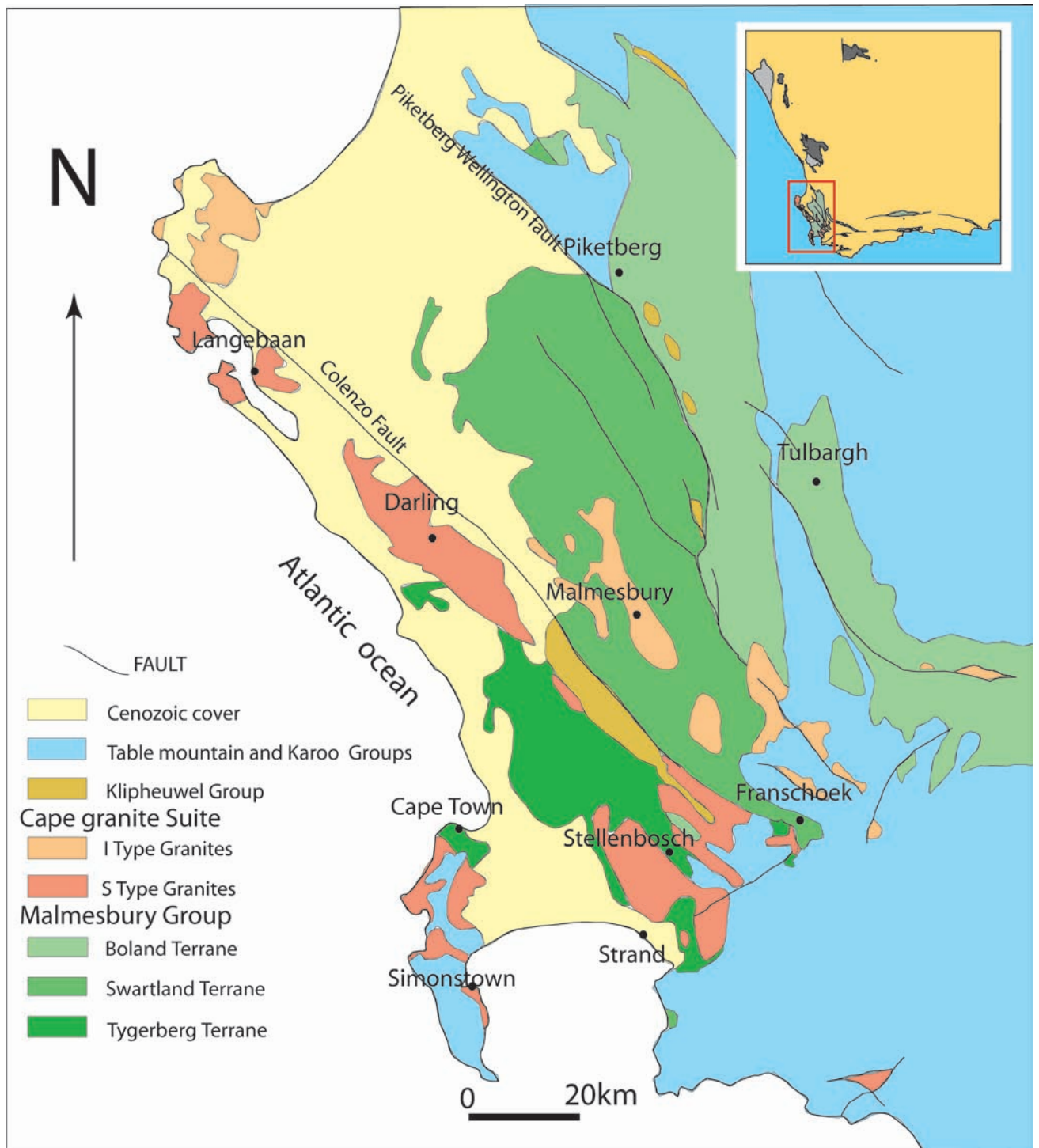


Figure 3.3: Simplified geological map of the Cape Granite Suite in the western part of the Saldania Belt (Theron *et al.* 1992, and Belcher *et al.* 2003)

The Swartland domain (central) is more complex than the Tygerberg Domain. The Malmesbury Group is essentially represented by the association the Swartland Subgroup: the association of the Berg River Formation (chlorite schists and greywacke); the Kliplaat Formation (quartz sericite and chlorite schist) and finally, the Mooresburg Formation (interlayered greywacke and phyllites) that compose most of the Central Domain (figure 3.4). Locally two distinct formations have been described in the swartland domain. The Franschoek Formation a succession of feldspathic conglomerate and quartzite; and the Bridgetown Formation essentially metavolcanic located at the boundary between the central and northeastern domain, and composed of tholeiitic metabasalts and serpentinitised ultramafic and metavolcanic rocks (Slabber 1995), dolomites, cherts and graphite schist. The within plate signature and metasedimentary association suggests an ophiolitic succession where the large dolomitic bodies would be seamount cappings (Slabber 1995; Gresse *et al.* 2006)

In the Boland domain the malmesbury group is represented by the Boland Subgroup composed by 4 formations: the Piketberg, Norree, Porterville and Brandwacht Formations. The Piketberg formation comprises highly foliated feldspathic quartzite, greywacke, sericite schist and conglomerate and some impure feldspathic limestone (Rozendaal 1994). The Piketberg formation seems to be interfingered with the Porterville Formation and might have links with the Franschoek Formation (Hartnady *et al.* 1974; Gresse and Theron 1992). The Porterville Formation is mainly composed of phyllitic shale and greywacke with quartzite limestone and cherts. The Noree Formation consists of greywacke, feldspathic and sericitic quartzite and dolomite. Finally, the Brandwacht Formation comprises a greywacke and pelite

association with interbedded conglomerate and metavolcanic rocks (figure 3.4).

The Klipheuwel Group is composed principally of conglomerate and coarse-grained sandstone (figure 3.4). The Klipheuwel Group unconformably overlies the Malmesbury Group ¹ (and is unconformably overlain by the Table Mountain Group) mark the end of the Malmesbury and thye end of the formation of the Saldania Belt.

3.1.3 Tectonic context

The Malmesbury Group belongs to a complex structural and tectonostratigraphic framework. The Boland domain has been described as a rifted margin succession of sediments on the Kalahari Craton, while the Swartland and Tygerberg domain can be considered as subsequently accreted allochthonous terranes. Hartnady (1985) and Stump (1976) suggested that the Boland Domain sedimentary succession was similar to a shallow marine to shelf deposit. According to Hartnady (1985) the Swartland Subgroup may represent sediment accretion and intensed localised polyphase deformation. In that case, the boundary between the three different domain of the eastern Saldania Belt could be geosuture while the Bridgetown Formation can be interpreted as a relict of oceanic crust. The flysch-like deposits of the Tygerberg formation are clearly of turbiditic origin accumulated on the continental rise in an oceanic trench or as submarine fans at the foot of the continental slope in a tectonically active environment (Hartnady *et al.* 1974 and Tankard *et al.* 1982). The

¹Former stratigraphical sequence of the Saldania Belt suggested that both Malmesbury Group and Klipheuwel Group belong to the Malmesbury Supergroup. Although this former stratigraphy is used in articles presented in this thesis, this chapter describe the latest stratigraphical sequence slightly difference from the one used in Chapter 5 and 6

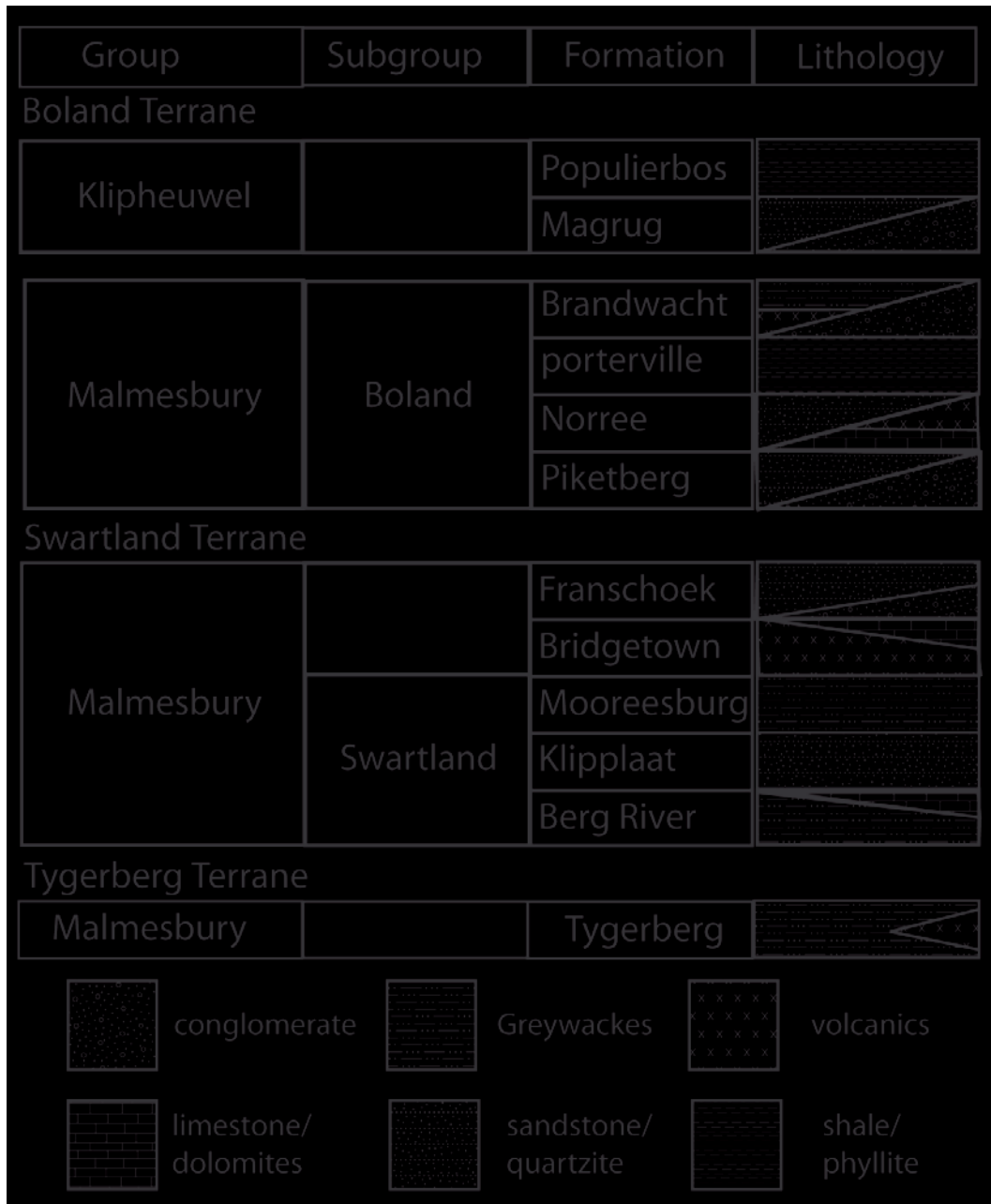


Figure 3.4: stratigraphy of the western part of the Saldania belt. (after, Gresse *et al.* 2006)

detrital zircon ages obtained from these rocks by Armstrong *et al.* 1998 are mostly older than the age of the CGS placing the Tygerberg Formation in the same time bracket as the Nama foreland basin. This may indicate that the tygerberg domain is a part of an accreted southern foreland of the Saldania Orogen.

3.1.4 The Cape Granite Suite

The CGS granitoids were emplaced during the Saldanian Orogeny. The CGS is principally composed of S- and I- type granites as well rare A-type intrusions. S-type granite is the oldest (560 to 530 Ma) and the most volumetrically important intrusive component in the CGS. S-type granitoids are followed in time (and volume) by I-type (540 to 520 Ma) and finally A-type (~ 520 Ma). The northwest-southeast Colenzo Fault physically separates S- and I-types intrusions respectively southward and northward from the fault (Figure 3.2). S-type intrusions form 4 main plutons: the Peninsula Pluton, the Darling Batholith, the Saldania Pluton and the Stellenbosch Pluton, while I-type intrusions form 2 main plutons: the Paarl and Malmesbury Plutons (Dunlevey 1988; Kisters *et al.* 2002). S-type granitoids intrude the sediments of the Malmesbury Group at a relatively shallow level, as shown by Malmesbury Group metasedimentary country rocks that occur outside of the contact aureoles, reached (at most) upper greenschist facies conditions. In association with the S-type granites, S-type volcanic rocks (ignimbrites) occur as a late phase that post-dates emplacement of the I- and A-type granites (515 ± 3 Ma) (Postberg Peninsula) (Figure 3.2) (Scheepers and Poujol 2002). Except for the Peninsula Pluton, S-type plutons are located along the Colenzo Fault recording a more or less important deformation. The Darling Batholith appears to be the

closest to the fault and the most affected by the deformation, while the Peninsular Pluton remains remarkably undeformed (Walker and Mathias 1946; Schoch *et al.* 1977; Scheepers 1990).

I-type granites are syn- to post-tectonic (Scheepers 1995) and are found only in the Swartland and Boland Terranes, north of the Colenso Fault (Figure 3.3). I-types are metaluminous and sometimes contain amphiboles in addition to biotite. The dominant association (Paarl, Malmesbury and Vredenburg plutons) is totally undeformed and can be either fine or coarse grained. Its composition ranges from quartz monzonite to granite and alkali feldspar granite. meta-igneous enclaves are common and generally more mafic material than host granite medium-grained, intermediate in composition and fairly well rounded (Scheepers 1995).

A-type granite and mafic intrusions are the last plutonic phase in the CGS and are clearly post tectonic. A-type granite is only represented by very few intrusions of small size (the Klipberg and Riviera Granites), they are metaluminous in composition, and locally evolving towards peralkali compositions. They can contain amphibole in addition to biotite; they also typically contain subhedral quartz. Typical composition ranges from amphibole-bearing quartz syenite to alkali granite and biotite quartz syenite. A-type bodies intrude mostly in the Tygerberg terrane (Klipberg pluton). The Yzerfontein Suite, dated at $519 \pm 7Ma$ (Jordaan 1990; Jordaan *et al.* 1995), is a high-K calc-alkaline series and defined by olivine-gabbro, gabbro, monzogabbro, monzonite and syenite. It is intrusive into the Tygerberg Terrane.

Rhyolites and ignimbrites on the Postberg Peninsula are peraluminous S-type volcanic and sub-volcanic magmas and the last intrusions of the CGS (515 ± 3 Ma, Scheepers and Poujol 2002) (Figure 3.3). The time gap (35Ma) between S-type plutons and S-type volcanics is interpreted as the expression of progressive magma accumulation in the magmatic chamber before its final extraction (Scheepers and Nortje 2000).

3.2 The S-type CGS

3.2.1 The Peninsula Pluton and the Darling Batholith

The Peninsula Pluton and the Darling Batholith provide a good overview of the diversity of composition and structure of the S-type CGS. Indeed, the Darling Batholith, located next to the Colenzo Fault is quite deformed, while the Peninsula Pluton located about 40 km south of the Colenzo Fault is undeformed. Both show a large scatter of composition.

The Peninsula Pluton's exposure follows the coast line (Atlantic Ocean and False Bay) of the Cape Peninsula (Figure 3.5) from Cape Point in the south to Cape Town in the north. The Pluton is overlain by Palaeozoic sandstones of the Table Mountain Group (TMG), and Palaeocene shales. Only at Sea Point does the contact with the sediment of the Malmesbury Group offers the possibility of observing an extremely local (on a few metres wide band from the contact) ductile deformation in the Peninsula Pluton. It is characterized by a horizontal northward shortening. Beside this contact, the Peninsula Pluton is only affected by late extensional faulting affecting the TMG in the same way. From a petrological

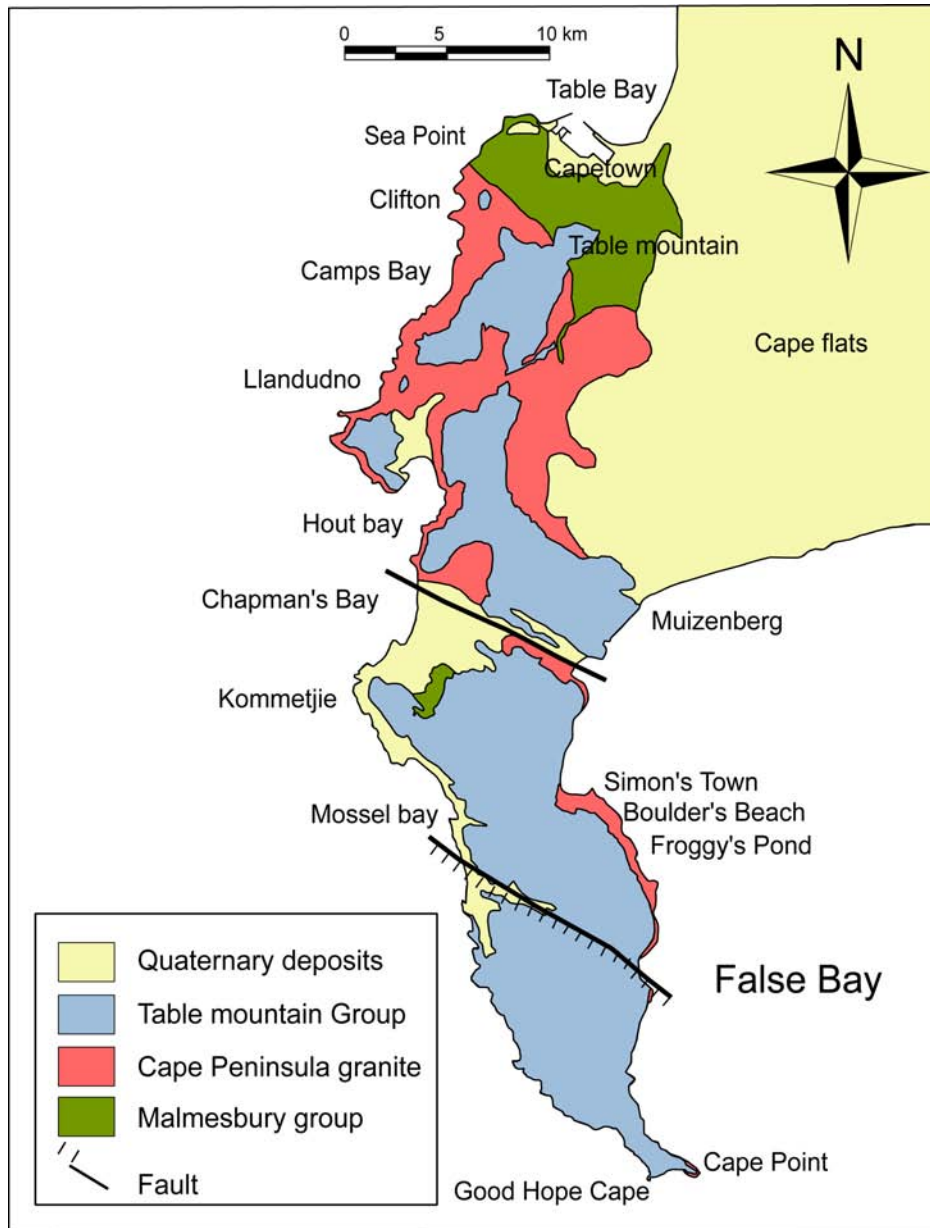


Figure 3.5: Geological Sketch of the Cape Peninsula, and the Peninsular pluton (after, Hartnady *et al.* 1974)

point of view, the granitoids of the Peninsula Pluton do not show large-scale (mappable) heterogeneities. However the pluton does show meterscale zones of varying composition from granodioritic to leucogranitic (Scheepers 1995; Scheepers 2000).

The Darling Batholith is located inland along the Colenso Fault. It is a batholith of 40 km length and 15 km width and is oriented NE to NNE, sub-parallel to the strike of the Colenso fault (Figure 3.6). The Darling Batholith directly intrudes the Malmesbury Group, although there is no remarkable contact such as the Sea Point Contact. One of the particular features of the Darling Batholith is its close proximity to the Colenso fault. The Darling Batholith has been widely deformed by the action of the fault and records an early reverse sinistral movement (Kisters *et al.* 2002). Another feature of the Darling Batholith is its composite character (Schoch 1975; Schoch *et al.* 1977) as it contains mappable units varying in composition from granodiorite to leucogranite. These rocks are identical to meter scale compositional variation within the Peninsula Pluton. Relationships of those various granitoids has been nicely described by Schoch (1975). These relationships are described in the following section and few examples are shown in figure 3.7.

3.2.2 Different facies and compositional variations

Different facies of S-type CGS have been described in previous studies (Schoch 1975; Schoch *et al.* 1977; Scheepers 1995; Scheepers and Nortje 2000; Scheepers and Armstrong 2002; Scheepers and Poujol 2002). They offer an excellent overview and descriptions of field relationships. Compositional variations within the S-type CGS, can be divided in 4 main facies, characterised predominantly by variations in the modal abundances of ferromagnesian phases, but also in grain size and the presence

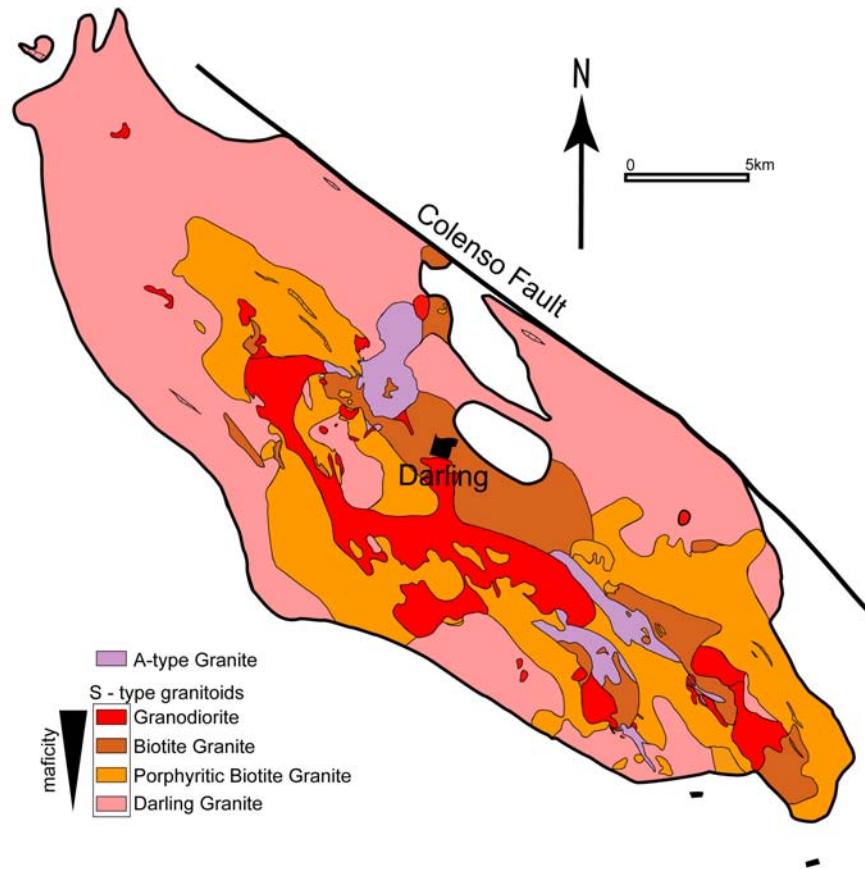


Figure 3.6: Geological Sketch of the Darling batholith (after, Schoch 1975)

or absence of K feldspar phenocrysts. These main facies are: (1) Cape Granodiorite; (2) Porphyritic Biotite Granite; (3) Non-Porphyritic Biotite Granite; (4) Common Cape Granite. Common Cape Granite: occurs in the Darling Batholith and the Peninsula Pluton as the most typical and volumetrically most important S-type CGS facies (Schoch, 1975). Common Cape Granite is characterised by abundant K-feldspar phenocrysts, plagioclase and quartz, and by sub-equal amounts of biotite and cordierite. (Figure 3.7 B, E, F). Porphyritic Biotite Granite is similar to the Common Cape Granite in the sense that it contains abundant quartz, pla-

gioclase and K-feldspar phenocryst, but it contains a higher content of biotite and cordierite, as well as some occurrences of garnet, which is generally absent in the Common Cape Granite (Figure 3.7 C, D, E). The Biotite Cape Granite contains a similar content of ferromagnesian phases (biotite, cordierite and garnet) (Figure 3.7 D) as the Porphyritic Biotite Granite but it contains only limited number of K-feldspar phenocryst with on average a smaller size than in either the Porphyritic Biotite Granite or the Common Cape Granite. Finally, the Cape Granodiorite is the most ferromagnesian facies. Phenocrystic K-feldspars are largely absent and the grain size is generally smaller than in other facies (Figure 3.7 B and G).

Field relationships illustrate the S-type CGS compositional variation. The rocks contain many enclave materials of different origins, metasediment xenoliths, or magmatic enclave, or, rarely, metabasite xenolith. The relationships between the different facies of S-type CGS are slightly different between the Peninsula Pluton and Darling Batholith. The Darling Batholith has been the subject of largescale mapping (Schoch and Burger 1976) which revealed a complex history made up of at least 18 different intrusions of the four different facies types. In contrast, the Peninsula Pluton does not show largescale compositional variations. Instead, the transition between different facies is more local, on the outcrop scale. Both intrusions offer complementary information about the relationship between each facies (Figure 3.7). Both granitic bodies are characterised by the presence of a zone of accumulation of mafic minerals, generally biotite and cordierite but interestingly, also garnet (Figure 3.8). Detailed field descriptions of relationships in the Darling Batholith has been provided by the study of Schoch (1975) which resulted in a particularly accurate map of the batholith. Spatial relationships between the different

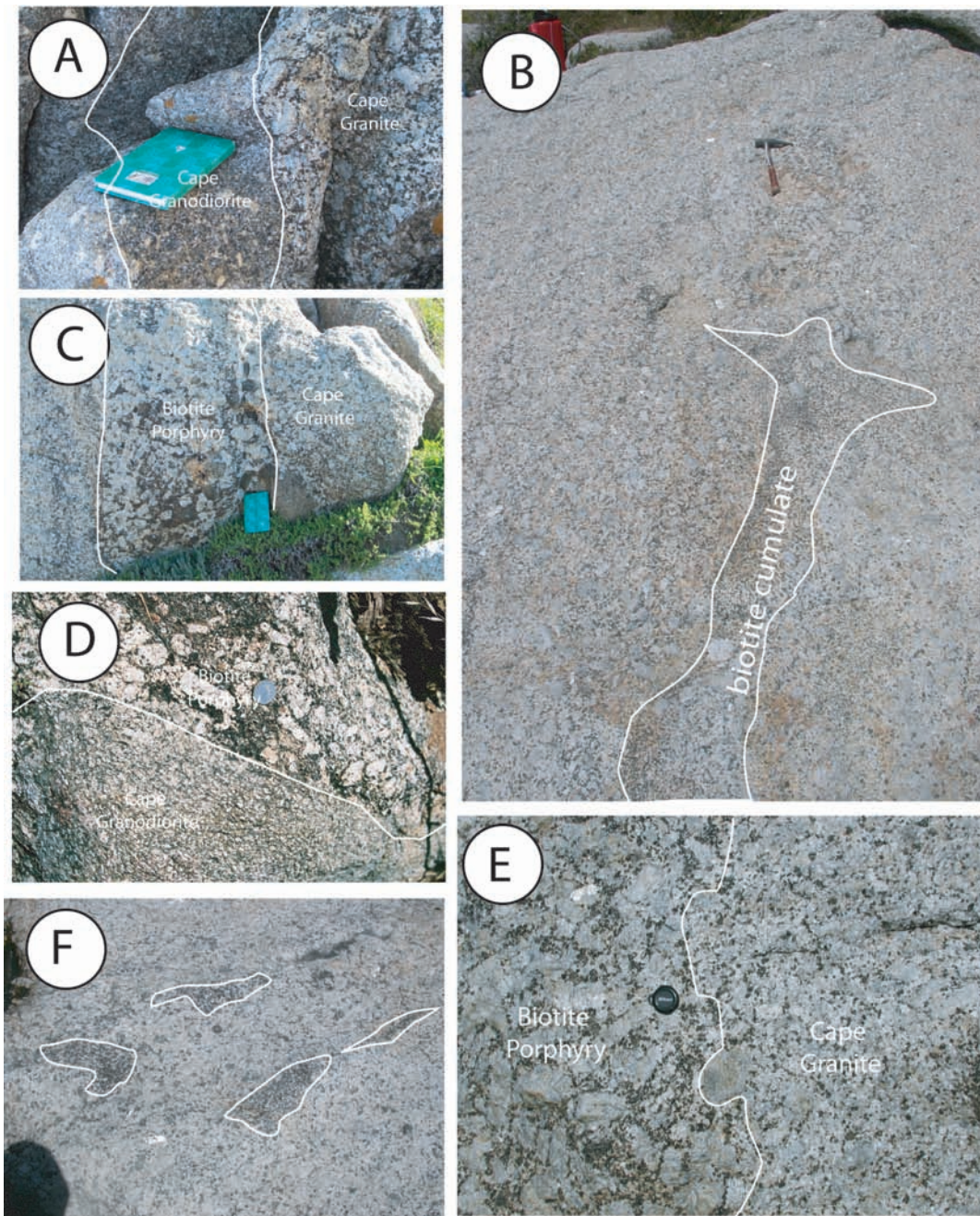


Figure 3.7: Examples of facies in the S-type CGS and their relation. A: small dyke of Cape Granodiorite in Cape Granite. B: Biotite cumulate in the Cape Granite (cumulate is oriented sub-vertically). C: large dyke of biotite porphyry in the Cape Granite. D: Contact between biotite porphyry and Darling granodiorite (contact is parallel to foliation). E: contact between biotite porphyry and Cape Granite (plan is horizontal). F: Biotite and cordierite cumulate bounding a dike in the Cape Granite.

phases is complex, and no clear chronology appears between them. Contacts suggest that the different phases are commonly mutually interpenetrative. The map (Figure 3.6) shows that the most ferromagnesian phases occupy a central position in the Batholith while the most leucocratic, the Darling Granite, is everywhere located on the rim of the batholith.

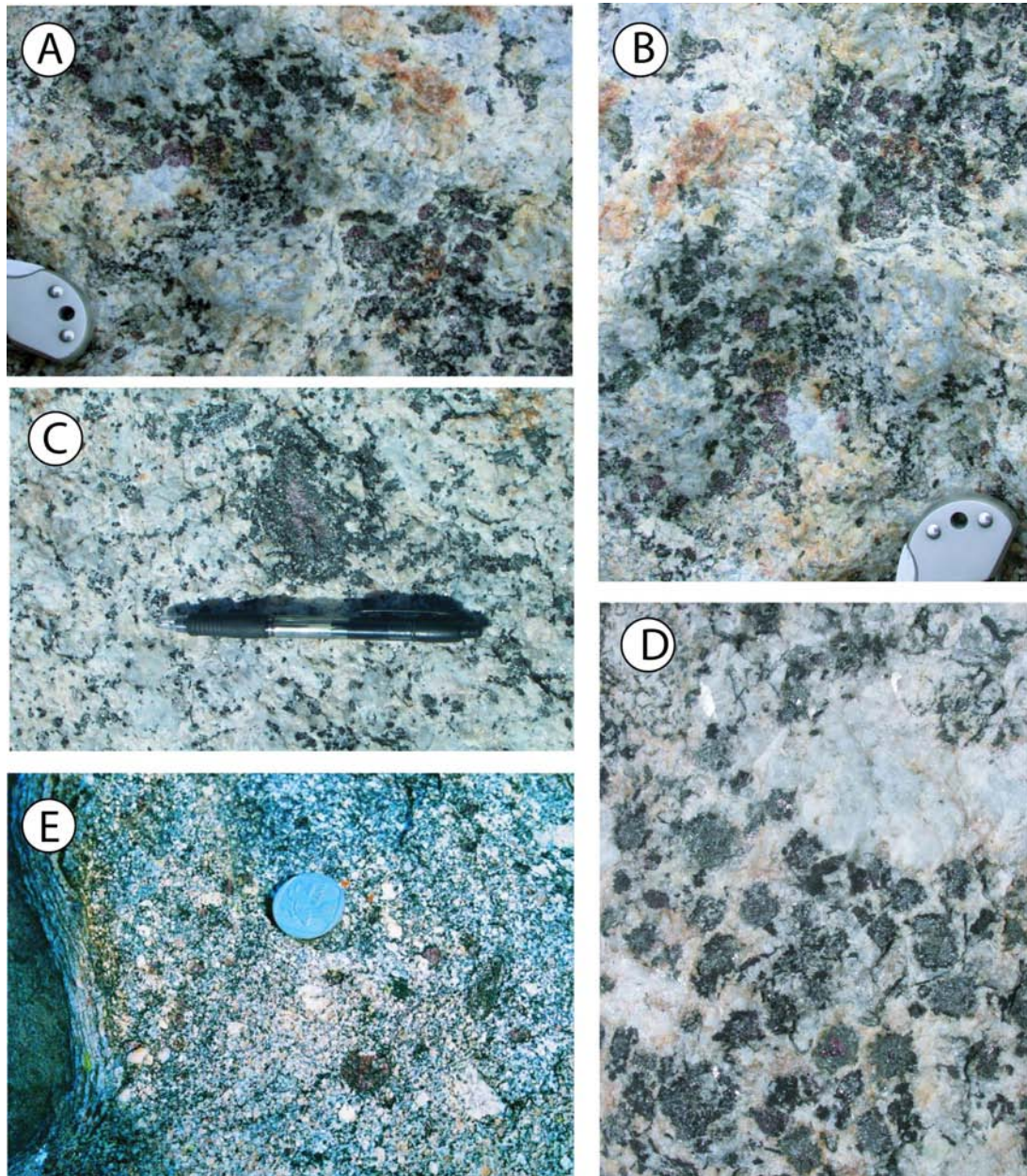


Figure 3.8: Examples of occurrences of garnet and cordierite in the S-type CGS. A and B: garnet-biotite cumulate. C: Garnet replaced by cordierite and biotite. D: Cordierite cumulates showing cordierite replacing garnet (size of cordierite 5mm). E: Garnet in the granodiorite (Darling Batholith).

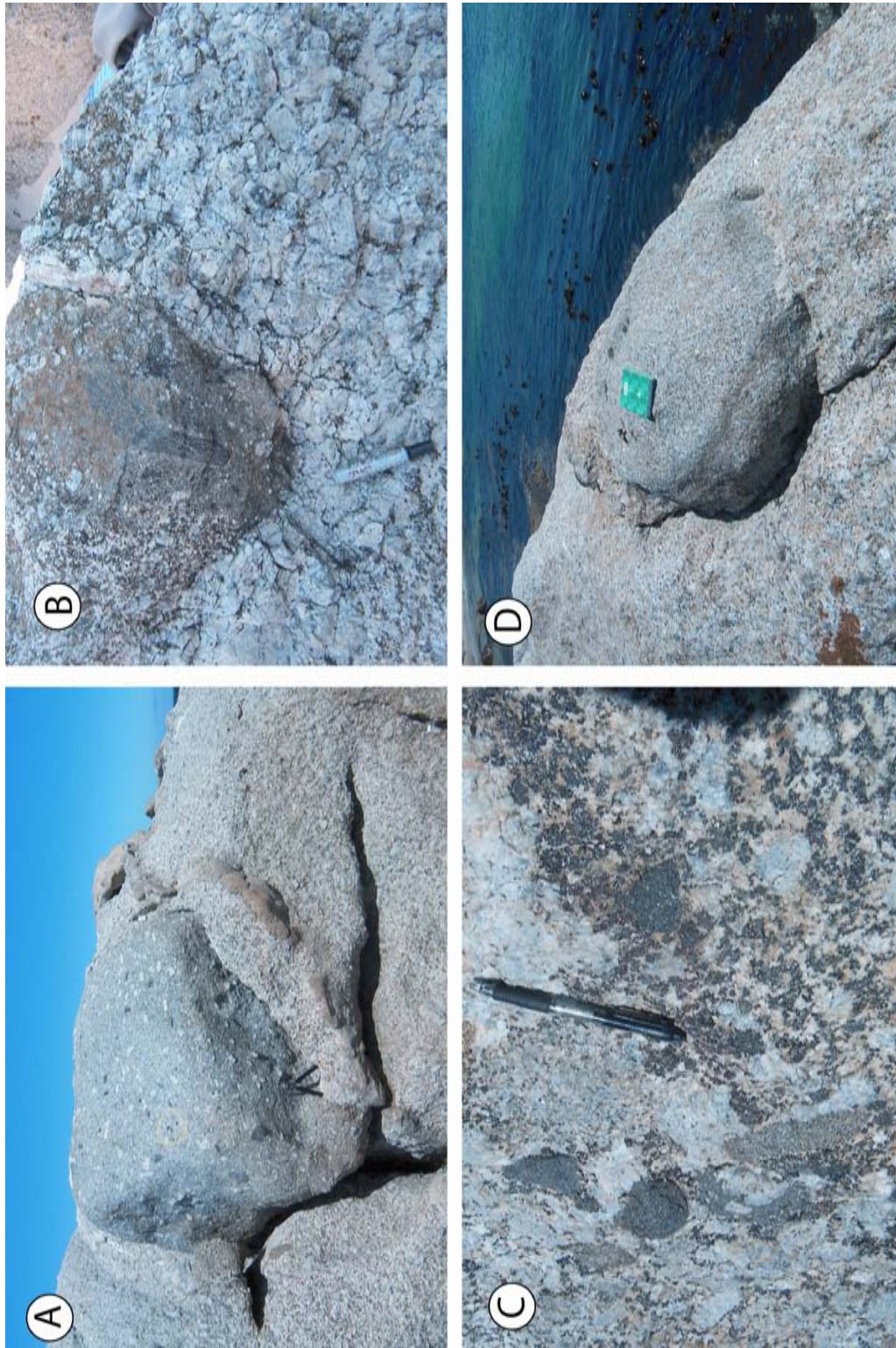


Figure 3.9: Magmatic Enclaves in the S-type CGS (Boulders beach). A. magmatic enclave of granodiorite in the peninsular granite. B. granodioritic enclave containing a metasedimentary xenolith. The magmatic enclave is surrounded by biotite porphyry granite (left) and typical Cape Granite (Peninsular granite). C: example of cumulate of metasedimentary xenolith and magmatic enclave in biotite porphyry granite. D: Granodioritic enclave in Cape Granite.

Even though the Peninsula Pluton is homogeneous on the map scale, at the outcrop scale many localities in the Cape Peninsula show facies variation identical to those observed in the Darling Batholith. As the scale is consequently smaller than in the Darling Batholith, the Peninsula Pluton offers different information about S-type petrogenesis in the CGS. The most voluminous facies, the Peninsula Granite is very similar to the Darling Granite. It contains large K-feldspars phenocrysts, and minor biotite and cordierite, but unlike the Darling Granite, is nearly undeformed. Facies boundaries generally occur as vertical structures (Figure 3.7 A, B, C) either as large dykes, up to several metres wide or tubular structures of 1 to 2 metres diameter. These dykes and tubes commonly contain more mafic phases intruding or cross-cutting the Peninsular Granite and the contact between the different facies is generally very diffuse.

3.2.3 Enclave Material in the S-type CGS

Magmatic enclaves (Figure 3.9) shows identical mineral assemblages, but finer grain sizes, than the host granite (< 2mm). However, garnet is particularly rare in the magmatic enclaves. The clear and sharp transition from enclave to host granite confirms that enclave was already crystallised when it has been collected by the magma (Figure 3.9 A, B, D). In rare cases, magmatic enclaves show particular interaction with granite giving evidence for local contamination (Figure 3.10).

Metasediment xenoliths vary in size from few cm up to 30 or 40 cm long (Figure 3.11 and 3.12). They can be isolated or accumulated in xenolith-rich zones in the granite. The metamorphic grade recorded by the xenoliths varies from lower greenschist facies to garnet-bearing amphibolite facies. Greenschist-facies metased-

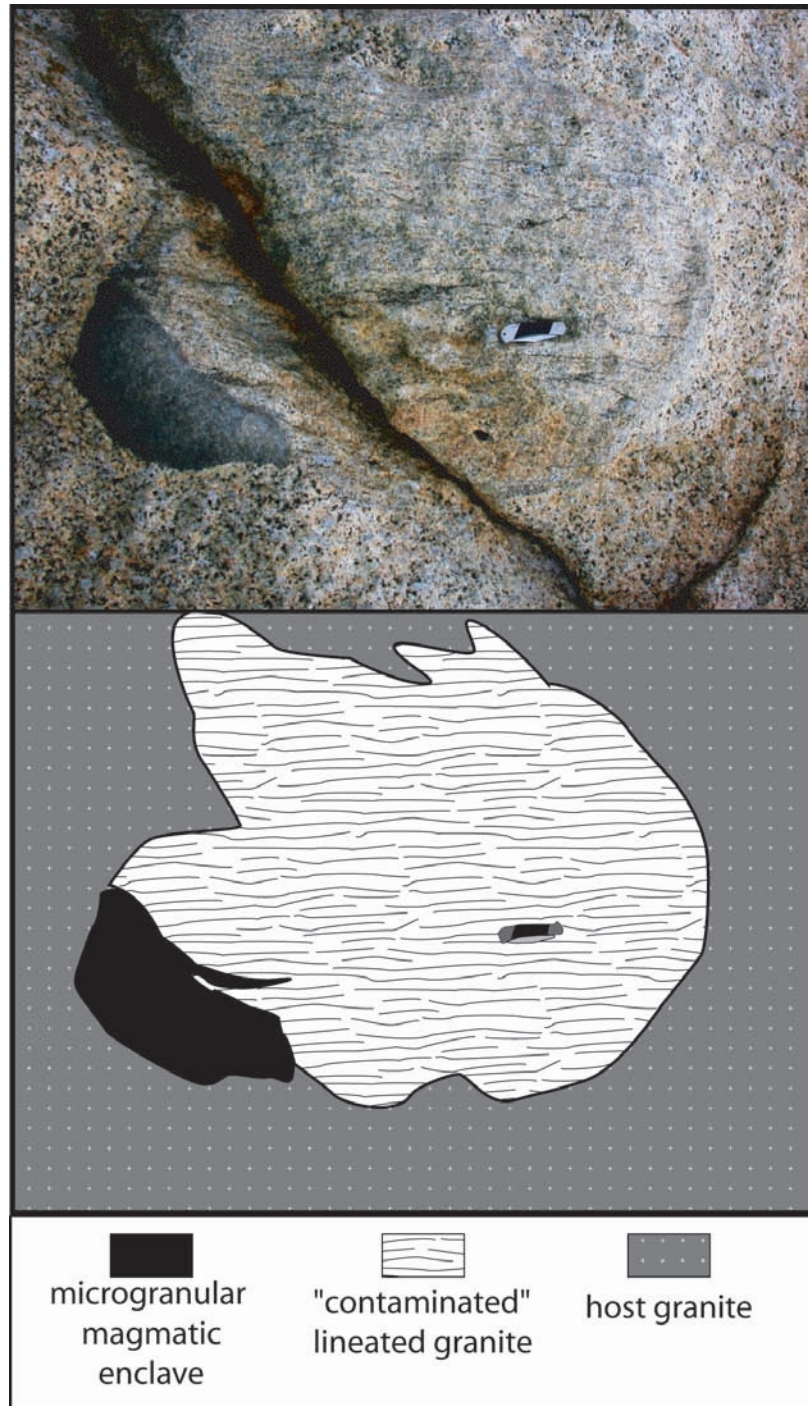


Figure 3.10: Interactions between magmatic enclaves and the Cape Granite.

iment additionally contains quartz veins associated with chlorite, similar to those described in parts of the Malmesbury Group (Hartnady *et al.* 1974; Belcher and Kisters 2003). As with magmatic enclaves, metasedimentary xenoliths can show very local interaction with the granite (Figure 3.12). As illustrated by figures 3.11 and 3.12 metasedimentary xenoliths only show little evidence for magma penetration in the xenolith and the extent of a potential contamination of magma from xenoliths is generally extremely local. Both figures show a few cm area surrounding the xenolith of a more leucocratic halo surrounding the xenolith, which can be considered as an effect of the depletion of ferromagnesian mineral from local granite which precipitate on the surface of the xenolith. As those features do not correspond to the general case, they must be considered to be of secondary importance.

Metabasite xenoliths are extremely rare and essentially found only in the Darling Batholith, where they are found as small rounded bodies of 10 cm maximum diameter (Schoch 1975). As for the metasediments, the metabasite xenoliths are foliated, suggesting a metamorphic origin.

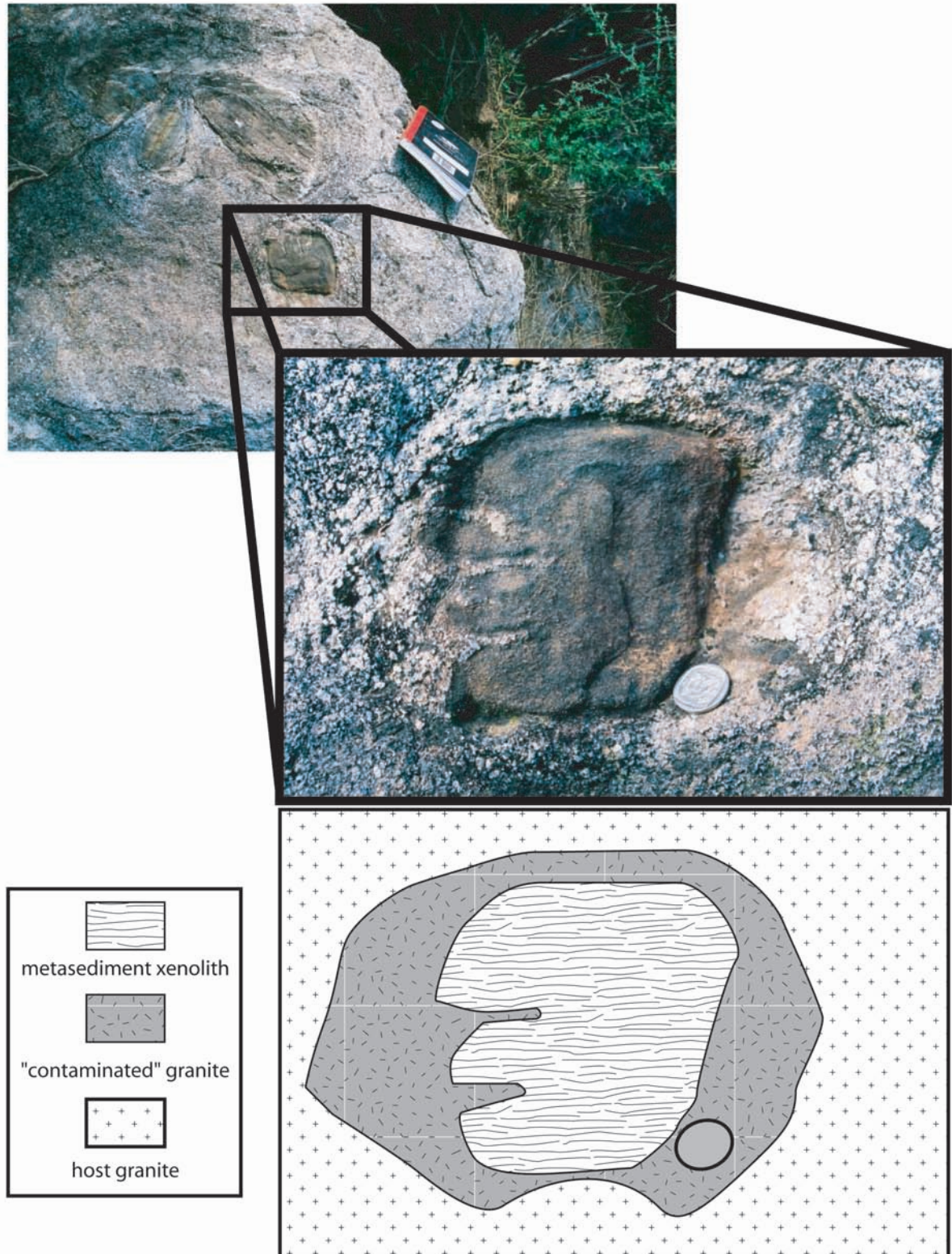


Figure 3.11: Xenolithic enclaves (Darling Batholith). Top picture general view of xenolith cumulate, middle picture: close up on one of the metasedimentary xenoliths represented above. Bottom pictures: sketch showing the extend of the interaction between xenolith and surrounding granite

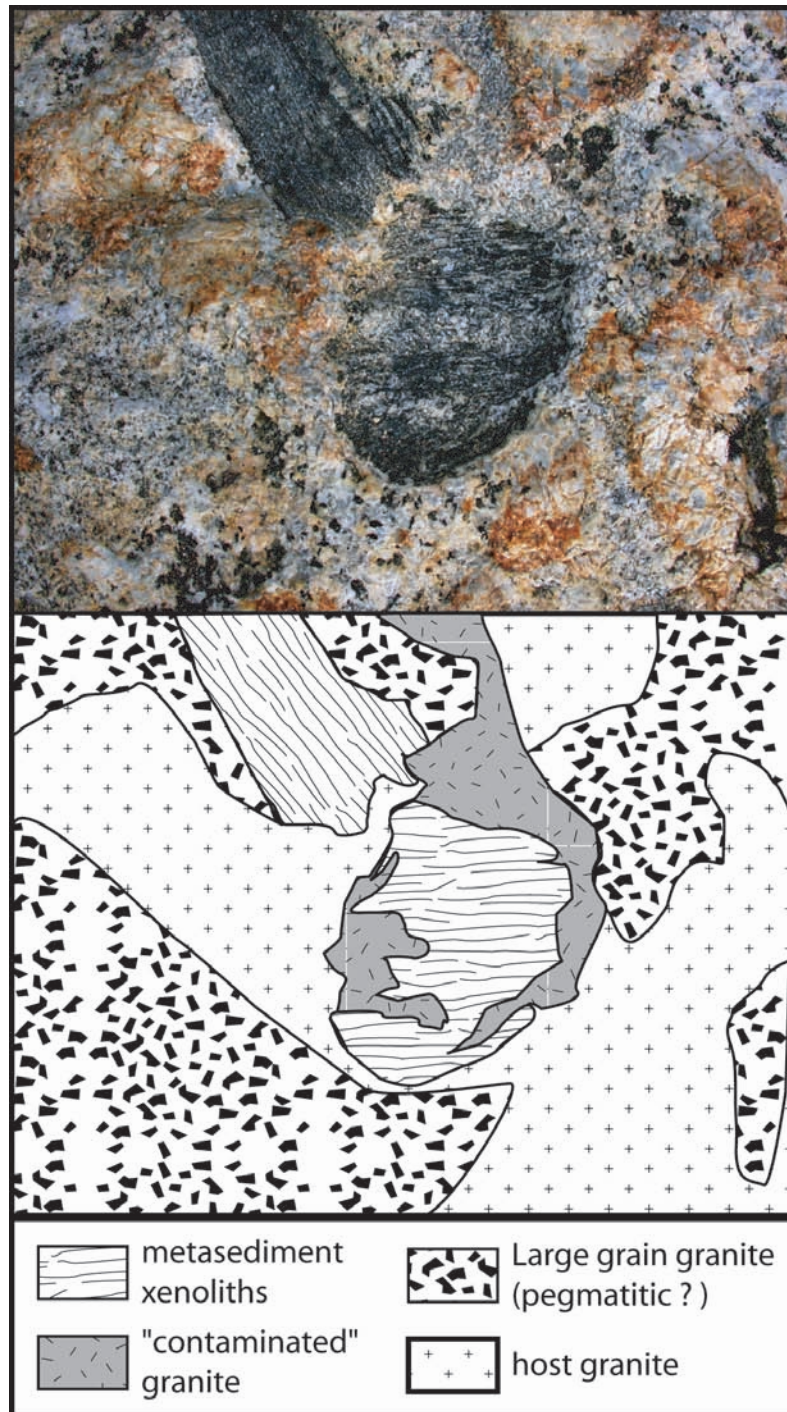


Figure 3.12: Example of the complexity of relation between metasedimentary xenoliths and different granitic facies. The Size of the enclave is about 10cm.

References

- Belcher R.W. and Kisters A.F.M., 2003. Lithostratigraphic correlations in the western branch of the Pan-African Saldania Belt, South Africa: the Malmesbury Group revisited. *S. Afr. J. Geol.* 106:327-342.
- Dunlevey J.N., 1988. Evolution of the Saldanian Orogeny and development of the Cape Granite Suite. *S. Afr. J. Sci.* 84:565-568.
- Gresse P.G., Theron J.N., Fitch F.J. and Miller J.A., 1992. Tectonic inversion and radiometric resetting of the basement in the Cape Fold Belt. In: De Wit M.J. and Ransome I.G.D. (Eds), *Inversion tectonics in the Cape Fold Belt, Karoo and Cretaceous basins of Southern Africa*. A.A. Balkema, Rotterdam, 217-228.
- Gresse P.G., Von Veh M.W. and Frimmel H.E., 2006. Namibian (Neoproterozoic) to early Cambrian successions. In Johnson M.R., Anhaeuser C.R. and Thomas R.J. (Eds) *The geology of South Africa*, Geological society of South Africa, Johannesburg and Council for Geoscience, Pretoria.
- Hartnady C.J.H., Newton A.R., and Theron J.N., 1974. The stratigraphy and structure of the Malmesbury Group in the southwestern Cape. *Bull. Precamb. Res. Unit* 15: 193-213.
- Hartnady C.J.H., Joubert P. and Stowe C.W., 1985. Proterozoic crustal evolution of southwestern Africa. *Episodes*, 8:236-244.
- Jordaan L.J., 1990. The Geology and geochemistry of mafic and intermediate igneous rocks associated with the Cape Granites. Department of Geology. Stellenbosch, University of Stellenbosch. M.Sc.: 243.
- Jordaan L.J., Scheepers R., and Barton E.S., 1995. Geochemistry and isotopic composition of the mafic and intermediate igneous components of the Cape Granite Suite, South Africa. *J. Afr. Earth Sci.* 21:59-70.
- Kisters A.F.M., Belcher R.W., Scheepers R., Rozendaal A., Jordaan L.S. and Armstrong R.A., 2002. Timing and kinematics of the Colenso Fault: The Early Paleozoic shift from collisional to extensional tectonics in the Pan-African Saldania Belt, South Africa. *S. Afr. J. Geol.* 105:257-270.
- Rozendaal A., Gresse P.G., Scheepers R. and De Beer C.H., 1994. Structural setting of the Riviera W-Mo deposit, Western Cape, South Africa. *Explor. Mining Geol.* 3:1747-1770
- Rozendaal A., Gresse P.G., Scheepers R. and Le Roux J.-P., 1999. Neoproterozoic to early cambrian Crustal Evolution of the Pan-African Saldania Belt, South Africa. *Precamb. Res.* 97:303-323.

- Scheepers R., 1990. Magmatic association and radioelement geochemistry of selected Cape Granites with special reference to subalkaline and leucogranitic phases (In Afrikaans). (Unpubl.) Ph.D. dissertation., Stellenbosch, South Africa, Stellenbosch Univ.
- Scheepers R., 1995. Geology, geochemistry and petrogenesis of late Precambrian S-, I- and A-type granitoids in the Saldania belt, Western Cape Province South Africa. *J. Afr. Earth Sci.* 21:35-58.
- Scheepers R., 2000. Granites of the Saldania mobile belt, South Africa: radioelements and P as discriminators applied to metallogeny. *J. Geochem. Expl.* 68: 69-86.
- Scheepers R., and Armstrong R.A., 2002. New U-Pb SHRIMP zircon ages of the Cape Granite Suite: implications for the magmatic evolution of the Saldania Belt. *S. Afr. J. Geol.* 105:241-256.
- Scheepers, R. and Nortje A. N., 2000. Rhyolitic ignimbrites of the Cape Granite Suite, southwestern Cape Province, South Africa. *J. Afr. Earth Sci.* 31:647-656.
- Scheepers R. and Poujol M., 2002. U-Pb zircon age of Cape Granite Suite ignimbrites: characteristics of the last phases of the Saldaniaan magmatism. *S. Afr. J. Geol.* 105:163-178.
- Schoch, A.E., 1975. The Darling granite batholith. *Ann. Univ. Stellenbosch* A1:1-104.
- Schoch, A.E. and Burger A.J., 1976. U-Pb ages of the Saldanha quartz porphyry. *Trans. Geol. Soc. S. Afr.* 79:239-241.
- Schoch, A.E., Leterrier J. and De La Roche H., 1977. Major element geochemical trends in the Cape granites. *Trans. Geol. Soc. S. Afr.* 80:197-209.
- Slabber N., 1995. *The geology and geochemistry of the Bridgetown Formation of the Malmesbury Group, Western Cape Province.* M.Sc thesis (unpubl.), Univ. Stellenbosch.
- Stump E., 1976. On the late Precambrian-early Palaeozoic metavolcanic and metasedimentary rocks of the Queen Maud Mountains, Antarctica and a comparison with rocks of a similar age of southern Africa. *Rep Inst. Polar Studies, Ohio State Univ.*, 62:212.
- Tankard A.J., Jackson M.P.A., Eriksson K.A., Hobday D. K., Hunter D.R. and Winter W. E. L., 1982. *Crustal evolution of Southern Africa: 3.8 billion years of Earth history.* Springer-Verlag, New York, 523p.
- Theron J.N., Gresse P.G., siegfried H.P. and Rogers J., 1992. The Geology of the Cape Town area. Explan. Sheet 3318 Cape Town, Geol. Surv. S. Afr., 140p.

- Von Veh, M.W., 1983. Aspects of sedimentation, structure and tectonic evolution in the Tygerberg terrane, southwestern Cape Province. *Bull. Precamb. Res. Unit, Univ. Cape Town* 32:88.
- Walker, F. and Mathias M., 1946. The petrology of two granite-slate contacts at Cape Town, South Africa. *Quart. J. Geol. Soc.* 102:499-521.

Chapter 4

Selective peritectic garnet
entrainment as the origin of
geochemical diversity in S-type
granites

Presentation of the publication

This Paper ¹ submitted to *Geology* by Gary Stevens constitutes the basis of this PhD. Looking at experimental partial melting of sediments to constrain S-type granite major element composition. This paper brings new insight to S-type petrogenesis. Geochemical modelling has been lead by Jean-Francois Moyen in collaboration with the two other authors, while PerpleX calculation has been made by myself, in collaboration with the two other authors. The dataset used for modelling corresponds to previous publications mainly by Dr. Reyno Scheepers (published and unpublished data, see appendix).

Gary Stevens

Arnaud Villaros

Jean-François Moyen

Department of Geology

Stellenbosch University Private Bag X1

Stellenbosch 7602 South Africa

¹Refer as: Stevens G., Villaros A., Moyen J.-F., 2007 Selective peritectic garnet entrainment as the origin of geochemical diversity in S-type granites. *Geology* 35:9-12 10.1130/G22959A.1

Selective peritectic garnet entrainment as the origin of geochemical diversity in S-type granites

Gary Stevens
Arnaud Villarros
Jean-François Moyen

Department of Geology, Stellenbosch University, Private Bag X1, Stellenbosch 7602, South Africa

ABSTRACT

Experimental melt (glass) compositions indicate that most of the S-type granites of the Cape Granite Suite in South Africa have ferromagnesian contents too high to represent melts. Consequently, the composition of the more mafic granites demands the addition of an Fe- and Mg-rich component to the magma. The compositions of the granites evolve along well-defined trends away from the likely melt composition for many components plotted against Mg + Fe. An increase in A/CNK, Mg#, Ca, and HREEs, as well as a decrease in K and Si, as a function of increasing Mg + Fe appears to limit the contaminant to garnet (up to 20 wt%). The rate of Ti increase, as a function of Mg + Fe increase in the granites, matches that defined by the stoichiometry of high-temperature biotite, but cannot be the product of accumulation of biotite (\pm other phases) in the magma because the chemical trends are inconsistent with this, particularly those portrayed by K and Ti as a function of Mg + Fe. This, in conjunction with the fact that no large, counterbalancing population of very leucocratic material exists in the Cape Granite Suite, suggests that the relatively mafic granites are not the products of garnet fractional crystallization. Rather, these appear to be the result of selective entrainment of peritectic garnet and ilmenite. Thus, this work indicates that much of the compositional variation in the granites is primary, reflecting the magma composition that ascended from the source, and is controlled by the proportion of peritectic products entrained into the melt. There is no indication of entrainment of a mineralogically diverse residuum (restite).

Keywords: S-type granite, granite geochemistry, granite petrogenesis, garnet.

INTRODUCTION

Partial melting (anatexis) of the crust can give rise to granite (s.l.) bodies that range in scale from centimeter-wide leucosomes in migmatites, to intrusive plutons and felsic volcanic sequences that crop out over thousands of km². Anatexis can occur in a number of different ways that largely depend on source mineralogy and the fluid regime during high-temperature metamorphism (see summaries by Stevens and Clemens, 1993, and Clemens and Droop, 1998). However, the important anatexis processes here are those that have generated voluminous and hot granitic magmas, capable of migration to high crustal levels, as this has produced the buoyant and chemically differentiated continental crust. A fundamental aspect of these high-level granites that remains temporally poorly understood is the origin of the major- and trace-element geochemical diversity that these rocks exhibit. Typically, large plutons or groups of temporarily and chemically related plutons (suites) show substantial major- and trace-element geochemical variability, without the clear and obvious field evidence for how this may have arisen that is typical for mafic intrusive bodies. Consequently, despite broad acceptance that source chemistry controls the genesis of fundamentally different chemical varieties of granitic magmas, little consensus exists on the dominant processes controlling the observed geochemical variations. In

many cases, several alternative processes appear to be viable, resulting in nonunique models. A possible reason for this is that the starting point from which compositional evolution must proceed is poorly constrained. This is despite the fact that experimental studies of partial melting have produced information that would seem to be useful in determining the major-element composition of the melts involved in granite genesis. This paper explores the use of experimental melt compositions in the specific case of the petrogenesis of granites derived through the partial melting of metasediments, using the example of the S-type granitic rocks of the Cape Granite Suite of South Africa.

S-TYPE GRANITE PETROGENESIS

Strongly peraluminous granites are believed to arise through the partial melting of aluminous clastic sediments (metapelites and metapsammities) (e.g., Chappell and White, 1974). The nature of the anatexis reactions involved in the genesis of such granites is well known, through theoretical considerations (e.g., Clemens and Watkins, 2001), experimental studies (e.g., Vielzeuf and Montel, 1994), and studies of migmatites (e.g., Johnson et al., 2001). The dominant melting reactions typically have the form $Bt + Qtz + Pl + Sil = Grt + melt + Ilm \pm Kfs$ and $Bt + Qtz + Pl = Grt + Opx + melt + Ilm \pm Kfs$, in metapelites and metapsammities, respec-

tively. Melting of biotite by these reactions typically begins at temperatures of 780 and 820 °C respectively (at 500 MPa), and progresses over a further 40–80 °C, within which biotite of changing composition coexists with granitic melt, a garnet-dominated solid peritectic mineral assemblage, and an assemblage of reactant restitic minerals.

S-type granites are characterized by significant major-element geochemical variation, from tonalitic to leucogranitic compositions, within suites of rocks that are temporally and genetically related. Typically, SiO₂ can vary from 65 to 79 wt%, Al₂O₃ from 11 to 17 wt%, FeO from near 0 to 8 wt%, MgO from near 0 to 3.5 wt%, CaO from near 0 to 3 wt%, Na₂O from 1 to 4 wt%, and K₂O from 2.2 to 6 wt%. In general, Mg + Fe values are strongly positively correlated and also correlate positively with the important ratios Mg# and Ca/Na. These variables usually correlate negatively with Si. Many different processes have been proposed to account for this geochemical variation. Among these, source-induced variation in initial melt composition (e.g., Brown and Pressley, 1999), fractional crystallization (e.g., Foden et al., 2002; Breaks and Moore, 1992), magma mixing (Gray, 1990; Collins, 1996), and restite unmixing (e.g., White and Chappell, 1977; Chappell, 1996) feature most prominently. Relatively few studies have considered the likely composition of the initial melt as a constraint. Notable exceptions are (1) Sawyer (1996), who proposed that the component of source residuum that combined with the melt to form peraluminous leucosomes was not simply a random sample of unmelted material, but rather the solid peritectic products of the melting reaction, and (2) the observation by Miller et al. (1985) and Montel and Vielzeuf (1997) that the increase in ferromagnesian component in the melts produced in high-temperature melting experiments was insufficient to account for the range of compositions observed in natural granites.

EXPERIMENTAL MELT COMPOSITIONS AND S-TYPE GRANITE PETROGENESIS

As the specific composition of the source of the Cape Granite Suite is unknown, this study has considered the melt produced from a wide range of metasedimentary protolith compositions and conditions of melting (Stevens et al.,

1997; Pickering and Johnston, 1998; Patiño Douce and Harris, 1998; Patiño Douce and Beard, 1996; Vielzeuf and Montel, 1994; Patiño Douce and Johnston, 1991; Spicer et al., 2004). As reactions identified through phase changes in the experimental charges are the biotite incongruent melting reactions discussed above, the experimental glass compositions should reflect the compositions of the melts that existed in the anatectic sources of a wide variety of S-type granites. All the experimental glasses are silicic (Fig. 1), even those from experiments at 1000 °C, where melt proportions were >60 vol% of the products. Total FeO + MgO values for the 100 wt% normalized glass compositions vary between 0.9 and 3.9 wt%, with a general increase in this parameter with temperature. A/CNK [0.5Al/(Ca + 0.5Na + 0.5K)] values for the glasses vary from 1.0 to 2.0. K is not correlated with Mg + Fe values; A/CNK, Ca, Mg#, and Ti are positively correlated with Mg + Fe; and Si is negatively correlated with Mg + Fe (Fig. 1).

The S-type granites of the Cape Granite Suite occur as part of an extensive belt of S- and I-type granites developed as a consequence of the Pan-African Saldanian orogeny along the southwestern margin of Africa (Scheepers and Pujol, 2002). These rocks form a suite of strongly peraluminous ($1 < A/CNK < 2$), K-rich granites with a substantial range in total FeO + MgO values (between 0.8 and 9 wt%) (Fig. 1). The suite contains both volcanic and plutonic rocks, and the presence of garnet, cordierite, and tourmaline confirms the inference of an aluminous metasedimentary source. As is typical for such granites, Si decreases as a fairly tightly constrained function of Mg + Fe; A/CNK, Ti, Mg#, and Ca correlate positively with Mg + Fe; and K decreases as a function of Mg + Fe (Fig. 1; GSA Data Repository¹).

When compared to the experimental melt compositions, a significant proportion of the Cape Granite Suite rocks plots outside of the compositional range of the experimental glasses (Fig. 1). Typically, the glasses coincide only with the more leucocratic Cape Granite Suite compositions ($Mg + Fe < \sim 0.06$), and even the 1000 °C experimental melts contain less than half the Mg + Fe component of common S-type granites. This suggests that within the compositions defined by both the source rocks and the mafic granites, suitably mafic melts do not appear to be able to exist at reasonably attainable conditions. Thus, the mafic granites cannot represent mafic granitoid melts that evolved

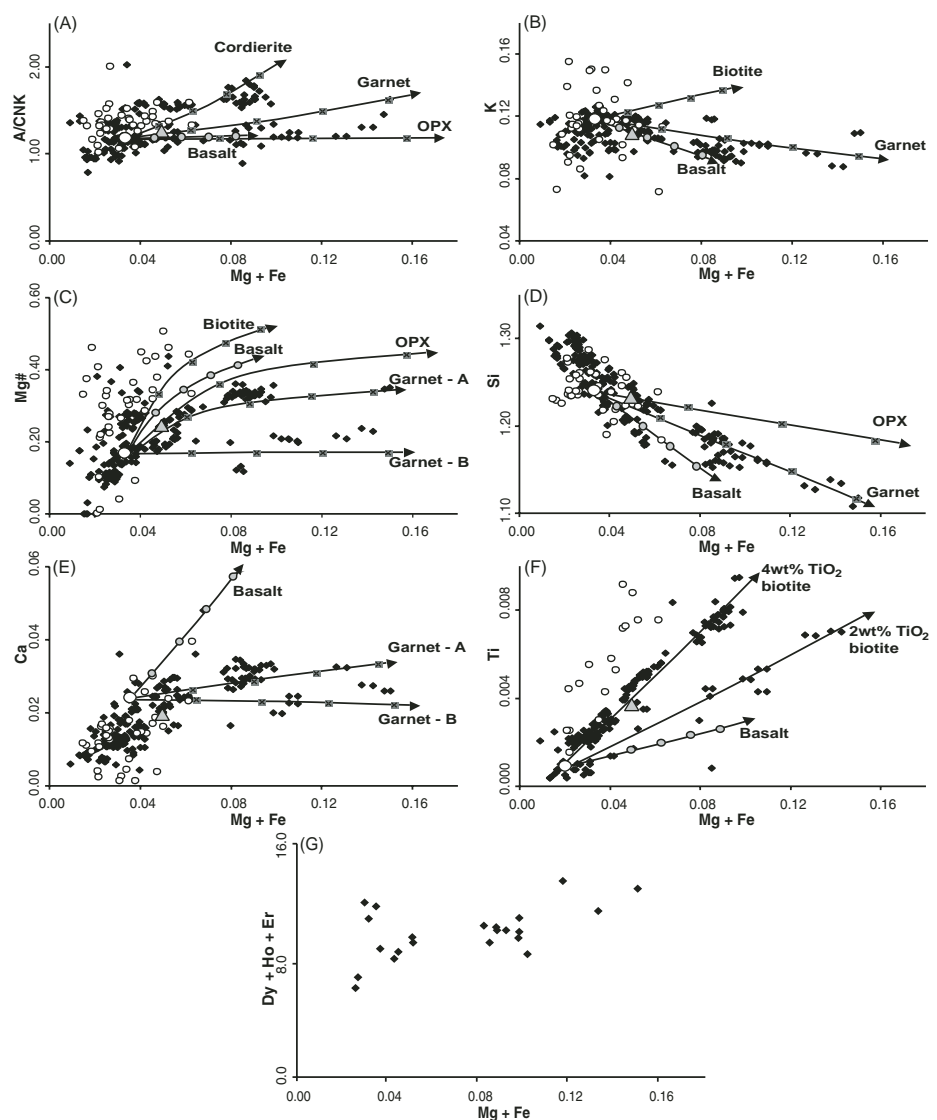


Figure 1. A comparison of the compositions of experimental glasses (small white circles) and the compositions of Cape Granite Suite S-type rocks (black diamonds) from Scheepers (1990), Scheepers and Pujol (2002), and Scheepers and Armstrong (2002). The suite of Cape Granite Suite rocks includes a small subset of rocks that have $A/CNK < 1.1$, considered to be genetically related to the more aluminous granites (Scheepers, 1990). The gray triangle represents the average of the Cape Granite Suite compositions. The large white dot represents a leucocratic S-type subvolcanic composition (sample B16) from the Cape Granite Suite, considered to be a nearly pure-liquid composition. The evolution of this composition, as a function of the addition of the labeled mineral and basalt components in 5 wt% increments, is shown by the evolution of the gray crossed squares away from this proposed melt composition. Garnet A (4 wt% CaO and $Mg\# = 38$) and garnet B (0.5 wt% CaO and $Mg\# = 17$) represent two different garnet compositions from granulite facies metasediments.

via fractionation toward the more silicic compositions. Rather, these compositions must be achieved by the inclusion of an Fe- and Mg-rich component in the silicic melt.

Two possible mechanisms proposed to account for the compositional range exhibited by the S-type granites of the well-studied Lachlan Fold Belt, i.e., magma mixing (e.g., Collins, 1996) and restite unmixing (Chappell, 1984; Chappell et al., 2000), have been evaluated for the Cape Granite Suite compositions. Addition of a basaltic magma to granitic melt in a pro-

portion sufficient to produce the observed Mg + Fe values results in both a decrease in A/CNK to below 1 and an increase in Ca values to 0.12 (0.05 is the maximum value in the Cape Granite Suite S-types). Furthermore, the addition of some 40 wt% basaltic melt is required to drive the granitoid magma to suitably mafic compositions. These factors appear to rule out the involvement of a mafic magma of this composition in Cape Granite Suite S-type petrogenesis. The effects of residuum (restite) entrainment are complicated by the fact that the nature of the

¹GSA Data Repository item 2007012, experimental melt and mineral compositions used in the geochemical modeling presented in this paper, is available online at www.geosociety.org/pubs/ft2007.htm, or on request from editing@geosociety.org or Documents Secretary, GSA, P.O. Box 9140, Boulder, CO 80301, USA.

residuum changes as a function of source composition, as well as the P - T conditions and fluid regime of melting. The restite unmixing model argues that variation in chemical composition within suites of granites results from varying degrees of entrainment and subsequent segregation of restite (unmelted source material) in the melt (White and Chappell, 1977; Chappell et al., 1987). It further proposes that the temperatures of melt generation are typically toward the low end of the magmatic range (750 °C or less) (Chappell et al., 2000) and that melt ascent occurred following the attainment of a critical melt fraction (Chappell et al., 2000). Collectively, these conditions imply fluid-present melting, that significant biotite incongruent melting is unlikely, and that the upper amphibolite facies xenoliths commonly contained within S-type plutons represent an entrained source component. This melting scenario differs from the high-temperature, fluid-absent process under discussion here. However, the effects of entrainment of a residual mineral assemblage appropriate to the granulite facies conditions of melting can most simply be evaluated by considering the effects of entrainment of a mineral in addition to garnet, which will generally always be present in metapelitic sources under these conditions. Other likely major residual phases include orthopyroxene, sillimanite, quartz, Ca-plagioclase, and cordierite. Addition of significant mixtures between garnet and any of these minerals to the melt produces magma evolution trends that differ from those defined by the Cape Granite Suite in Figure 1. For example, residua consisting primarily of garnet + sillimanite mixtures (as would be common for metapelitic sources) results in trends of A/CNK evolution with Mg + Fe values that plot above the garnet line on Figure 1A. Garnet + Ca-plagioclase mixtures (common for metapsammites) results in vectors on Figure 1E that are more Ca-rich than the natural rocks. Garnet + quartz (possible in some metapsammites and metapelites) addition produces compositions on Figure 1D that lie above the garnet trend. In short, the trends defined by the Cape Granite Suite compositions appear to be quite sensitive to the addition of other minerals with Mg + Fe ratios to Ca, Si, and Al that are different from those defined by the stoichiometry of high-temperature garnet from aluminous metasedimentary sources.

The combined requirements of increasing A/CNK, Mg#, and Ca as a function of Mg + Fe, with a corresponding decrease in Si and K, appear to be met by only garnet addition to the melt (Fig. 1). Indeed, the major-element trends defined by the granites cannot be modeled effectively as the result of any simple process, other than garnet addition, once the starting point of a silicic melt has been defined (Fig. 1). Thus, the crux of the matter becomes the source of

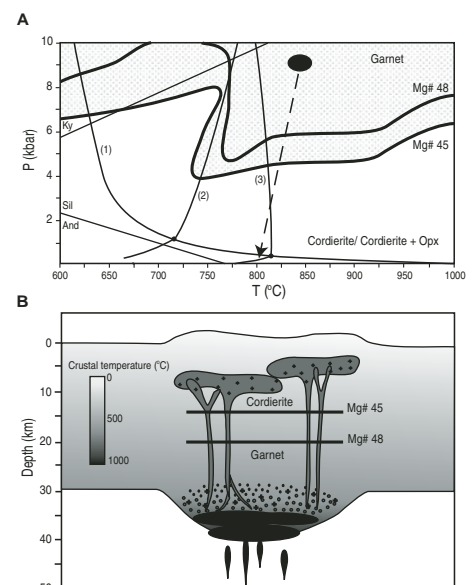
the garnet—does it represent an accumulation of a magmatic crystallization product, or does it represent a component preferentially entrained from the source? Three lines of evidence appear to argue against the former and for the latter. Firstly, the average Cape Granite Suite S-type granite is significantly more mafic than the average experimental melt, suggesting that the large volume of very silicic compositions that would be needed to counterbalance a large proportion of relatively mafic rocks produced by fractional crystallization from a relatively silicic melt is absent from the preserved rock record. Secondly, and perhaps most importantly, a strong positive correlation exists between Ti and Mg + Fe in the Cape Granite Suite S-type granites (Fig. 1F). This cannot represent biotite fractionation due to the negative correlations between K and Mg + Fe, and between K and Ti. Despite this, these correlations appear linked to the stoichiometric association of these elements within high-grade metasedimentary biotite. Thus, the trends on Figure 1F suggest that the silicic melt composition from which the Cape Granite Suite formed was characterized by low Ti (despite the relatively large range of Ti contents exhibited by the experimental glasses) and that the garnet and ilmenite produced by biotite incongruent melting were entrained into the melt with no fractionation of one phase over the other, but in variable proportions relative to the melt. Thirdly, there is a positive correlation between the heavy rare earth element (HREE) concentration in the granites and Mg + Fe (Fig. 1G), consistent with garnet as the source of Mg + Fe increase in the

magma, yet no strong HREE depletion in the most leucocratic granites, which show La/Yb values little different from those of the most mafic granites. However, the positive correlation that exists between Zr and Mg + Fe suggests that zircon, a common inclusion in biotite in high-grade metasediments, was a coentrained phase due to its proximity to the sites of melting and that the factors that controlled garnet entrainment also regulated the amount of zircon entrained. Monazite is probably also involved for similar reasons, complicating simple interpretations of the rare earth element (REE) patterns of the granites.

DISCUSSION AND SUMMARY

Rapid ascent of melts and magmas from the anatexic sources through fracturing and dike propagation processes is effectively geologically instantaneous (Clemens and Mawer, 1992; Petford et al., 1993). Thus, magmas initially emplaced into the shallow crust may be only slightly cooler, but at a much lower pressure than at the source (Fig. 2). Garnet breaks down to cordierite, or cordierite + orthopyroxene, at low pressures in a manner that is sensitive to bulk rock Mg# (Green, 1976). Importantly, higher Mg# equates with high-pressure (earlier) garnet destruction (Fig. 2). In S-type granites, higher Mg# equates with more Mg- and Fe-rich compositions and thus a higher entrained garnet fraction. Consequently, the system appears to be naturally ordered toward more effective garnet destruction in magmas that require the largest fractions of garnet addition. The magmatic

Figure 2. The model for the petrogenesis of S-type granite proposed in this study. A: Summary phase relations. Reaction 1 represents the wet granite solidus; reactions 2 and 3 represent the fluid-absent biotite incongruent melting equilibria in metapelites and metapsammites, respectively (Stevens et al., 1997). The dashed arrow represents a roughly adiabatic magma ascent path as appropriate for a high-temperature, water-undersaturated melt/magma generated by biotite fluid-absent melting at high pressures. The limits of garnet stability in two mafic granite compositions, CSS (Mg# = 0.45) and MBS (Mg# = 0.48), are superimposed on the melting reactions. The pseudosections constraining garnet stability were constructed via PERPLE_X (Connolly, 1990; Connolly and Pettrini, 2002) following the method of Connolly and Pettrini (2002) and using the thermodynamic data set of Holland and Powell (1998) (2.5 wt% H₂O and MnO-free). B: A simplified crustal section during granite genesis. Melting occurred within the garnet stability field, and the melting reactions progressed rapidly due to the high heat flux associated with intraplated or underplated mantle melts. The granitic magmas rapidly intruded to high levels in the crust via dike systems. The garnet-bearing magmas arrived at the low-pressure intrusive sites at a temperature only slightly cooler than at the melting sites. Garnet in both compositions is markedly out of equilibrium under these conditions, but garnet breakdown initiated earlier on the ascent path in the higher-Mg# magma. Ky—kyanite; Sil—Sillimanite; And—Andalusite.



nature of the products of garnet breakdown may create the textural impression of high Mg + Fe solubility in the melt, as well as garnet crystals equilibrated within the magmatic environment.

In summary, primary geochemical diversity in S-type granites is produced in the source. S-type granitic melt compositions will always be silicic, even at the highest temperatures possible for crustal anatexis, and melt compositions vary as a function of source chemistry, probably accounting for much of the compositional variability observed in leucocratic granite compositions. In contrast, mafic S-type granites cannot represent melts and must represent melt-crystal mixtures. The large-scale major-element geochemical trends defined by S-type granites appear to be the products of garnet addition to melts of different composition, with the most mafic compositions representing melt + ~20 wt% of the peritectic products of biotite breakdown. The peritectic garnet is likely to be preferentially entrained into the melt because it is abundant at the sites of melting, and because it may be texturally distinct (smaller in crystal size) from the earlier generations of regional metamorphic minerals.

ACKNOWLEDGMENTS

This research was supported by NRF funding to G.S. W. Collins, J.D. Clemens, and an anonymous reviewer provided excellent reviews. R. Scheepers provided the rock powders on which the REE analyses were based.

REFERENCES CITED

- Breaks, F.W., and Moore, J.M., 1992, The Ghost Lake batholith, Superior Province of northwestern Ontario—A fertile, S-type, peraluminous granite-rare-element pegmatite system: *Canadian Mineralogist*, v. 30, p. 835–875.
- Brown, M., and Pressley, R.A., 1999, Crustal melting in nature: Prosecuting source processes: *Physics and Chemistry of the Earth*, v. 24, p. 305–316, doi: 10.1016/S1464-1895(99)00034-4.
- Chappell, B.W., 1984, Source rocks of I- and S-type granites in the Lachlan Fold Belt, southeastern Australia: *Royal Society of London Philosophical Transactions*, ser. A, v. 310, p. 693–707.
- Chappell, B.W., 1996, Compositional variation within granite suites of the Lachlan Fold Belt: Its causes and implications for the physical state of granite magma: *Transactions of the Royal Society of Edinburgh*, v. 87, p. 159–170.
- Chappell, B.W., and White, A.J.R., 1974, Two contrasting granite types: *Pacific Geology*, v. 8, p. 173–174.
- Chappell, B.W., White, A.I.R., and Wyborn, D., 1987, The importance of residual source material (restitute) in granite petrogenesis: *Journal of Petrology*, v. 28, p. 1111–1138.
- Chappell, B.W., White, A.J.R., Williams, I.S., Wyborn, D., and Wyborn, L.A.I., 2000, Lachlan Fold Belt granites revisited: High- and low-temperature granites and their implications: *Australian Journal of Earth Sciences*, v. 47, p. 123–138, doi: 10.1046/j.1440-0952.2000.00766.x.
- Clemens, J.D., and Droop, G.T.R., 1998, Fluids, *P-T* paths and the fates of anatectic melts in the Earth's crust: *Lithos*, v. 44, p. 21–36, doi: 10.1016/S0024-4937(98)00020-6.
- Clemens, J.D., and Mawer, C.K., 1992, Granitic magma transport by fracture propagation: *Tectonophysics*, v. 204, p. 339–360, doi: 10.1016/0040-1951(92)90316-X.
- Clemens, J.D., and Watkins, J.M., 2001, The fluid regime of high-temperature metamorphism during granitoid magma genesis: *Contributions to Mineralogy and Petrology*, v. 140, p. 600–606.
- Collins, W.J., 1996, Lachlan Fold Belt granitoids: Products of three-component mixing: *Transactions of the Royal Society of Edinburgh*, v. 87, p. 171–181.
- Connolly, J.A.D., 1990, Multivariable phase diagrams: An algorithm based on generalized thermodynamics: *American Journal of Science*, v. 290, p. 666–718.
- Connolly, J.A.D., and Pettrini, K., 2002, An automated strategy for calculation of phase diagram sections and retrieval of rock properties as a function of physical conditions: *Journal of Metamorphic Geology*, v. 20, p. 697–708, doi: 10.1046/j.1525-1314.2002.00398.x.
- Foden, J.D., Elburg, M.A., Turner, S.P., Sandiford, M., O'Callaghan, J., and Mitchell, S., 2002, Granite production in the Delamerian orogen, South Australia: *Geological Society [London] Journal*, v. 159, p. 557–575.
- Gray, C.M., 1990, A strontium isotope traverse across the granitic rocks of southeastern Australia: Petrogenetic and tectonic implications: *Australian Journal of Earth Sciences*, v. 37, p. 331–349.
- Green, T.H., 1976, Experimental generation of cordierite or garnet bearing granitic liquids from a pelitic composition: *Geology*, v. 4, p. 85–88, doi: 10.1130/0091-7613(1976)4<85:EGOCGG>2.0.CO;2.
- Holland, T.J.B., and Powell, R., 1998, An internally consistent thermodynamic data set for phases of petrological interest: *Journal of Metamorphic Geology*, v. 16, p. 309–343, doi: 10.1111/j.1525-1314.1998.00140.x.
- Johnson, T.E., Hudson, N.F.C., and Droop, G.T.R., 2001, Partial melting of the Inzie Head gneisses: The role of water and a petrogenetic grid in KFMASH applicable to anatectic pelitic migmatites: *Journal of Metamorphic Geology*, v. 19, p. 99–118, doi: 10.1046/j.0263-4929.2000.00292.x.
- Miller, C.F., Watson, E.B., and Rapp, R.P., 1985, Experimental investigation of mafic mineral-felsic liquid equilibria: Preliminary results and petrogenetic implications: *Eos (Transactions, American Geophysical Union)*, v. 66, p. 1130.
- Montel, J.M., and Vielzeuf, D., 1997, Partial melting of metagreywackes, 2: Compositions of minerals and melts: *Contributions to Mineralogy and Petrology*, v. 128, p. 176–196, doi: 10.1007/s004100050302.
- Patiño Douce, A.E., and Beard, J.S., 1996, Effects of P, *f*(O₂) and Mg/Fe ratio on dehydration melting of model metagreywackes: *Journal of Petrology*, v. 37, p. 999–1024.
- Patiño Douce, A.E., and Harris, N., 1998, Experimental constraints on Himalayan anatexis: *Journal of Petrology*, v. 39, p. 689–710.
- Patiño Douce, A.E., and Johnston, A.D., 1991, Phase equilibria and melt productivity in the pelitic system: Implications for the origin of peraluminous granitoids and aluminous granites: *Contributions to Mineralogy and Petrology*, v. 107, p. 202–218.
- Petford, N., Kerr, R.C., and Lister, J.R., 1993, Dike transport of granitic magmas: *Geology*, v. 21, p. 845–847, doi: 10.1130/0091-7613(1993)021<0845:DTOGM>2.3.CO;2.
- Pickering, J.M., and Johnston, A.D., 1998, Fluid-absent melting behaviour of a two-mica metapelite: Experimental constraints on the origin of the Black Hills granite: *Journal of Petrology*, v. 39, p. 1787–1804, doi: 10.1093/petrology/39.10.1787.
- Sawyer, E.W., 1996, Melt segregation and magma flow in migmatites: Implications for the generation of granite magmas: *Transactions of the Royal Society of Edinburgh*, v. 87, p. 85–94.
- Scheepers, R., 1990, Magmatic association and radioelement geochemistry of selected Cape Granites with special reference to subalkaline and leucogranitic phases [Ph.D. thesis]: Stellenbosch, South Africa, University of Stellenbosch (in Afrikaans), 151 p.
- Scheepers, R., and Armstrong, R., 2002, New U-Pb zircon ages of the Cape Granite Suite: Implications for the magmatic evolution of the Saldania Belt: *South African Journal of Geology*, v. 105, p. 241–256, doi: 10.2113/1050241.
- Scheepers, R., and Poujol, M., 2002, U-Pb zircon age of Cape Granite Suite ignimbrites: Characteristics of the last phases of the Saldanian magmatism: *South African Journal of Geology*, v. 105, p. 163–178, doi: 10.2113/105.2.163.
- Spicer, E.M., Stevens, G., and Buick, I.S., 2004, The low-pressure partial-melting behaviour of natural metapelites from the Mt. Stafford area, central Australia, including the role of boron as a possible melt fluxing agent: *Contributions to Mineralogy and Petrology*, v. 148, p. 160–179, doi: 10.1007/s00410-004-0577-z.
- Stevens, G., and Clemens, J.D., 1993, Fluid-absent melting and the roles of fluids in the lithosphere: A slanted summary?: *Chemical Geology*, v. 108, p. 1–17, doi: 10.1016/0009-2541(93)90314-9.
- Stevens, G., Clemens, J.D., and Droop, G.T.R., 1997, Melt production during granulite-facies anatexis: Experimental data from “primitive” metasedimentary protoliths: *Contributions to Mineralogy and Petrology*, v. 128, p. 352–370, doi: 10.1007/s004100050314.
- Vielzeuf, D., and Montel, J.-M., 1994, Partial melting of metagreywackes, 1: Fluid-absent experiments and phase relationships: *Contributions to Mineralogy and Petrology*, v. 117, p. 375–393, doi: 10.1007/BF00307272.
- White, A.J.R., and Chappell, B.W., 1977, Ultrametamorphism and granitoid genesis: *Tectonophysics*, v. 43, p. 7–22, doi: 10.1016/0040-1951(77)90003-8.

Manuscript received 5 May 2006

Revised manuscript received 19 July 2006

Manuscript accepted 21 July 2006

Printed in USA

Chapter 5

Tracking S-type granite from source
to emplacement: Clues from garnet
in the Cape Granite Suite

Presentation of the publication

This paper ¹ published in *Lithos*, is first-authored by Arnaud Villaros. It aims to determine what happened to entrained peritectic phases in the S-type CGS. This paper, is a study of how garnet is preserved in S-type CGS, It establishes the conditions of stability of such garnet in the granite, and compares conditions of stability of garnet in granite with conditions recorded in xenoliths. Finally, it evaluates the effect of diffusion vs dissolution with respect to garnet in S-type magma. All calculations and data acquisitions were lead by Arnaud Villaros under the supervision of Gary Stevens and Ian Buick.

Arnaud Villaros^a

Gary Stevens, Gary^a

Ian S. Buick, Ian S ^{a,b}

a: Centre for Crustal Petrology

Department of Geology, Geography and Environmental Studies

Stellenbosch University Private bag X1

Matieland, South Africa

b: Research School of Earth Science

Australian National University

Canberra, Australia

¹Refer as: Villaros A., Stevens G. and Buick I.S., 2009. Tracking S-type granite from source to emplacement: Clues from garnet in the Cape Granite Suite. *Lithos* 112:217-235. doi:10.1016/j.lithos.2009.02.011



Tracking S-type granite from source to emplacement: Clues from garnet in the Cape Granite Suite

Arnaud Villaros*, Gary Stevens, Ian S. Buick

Centre for Crustal Petrology, Department of Geology, Geography and Environmental Studies, Stellenbosch University, Private bag X1, Matieland, South Africa

ARTICLE INFO

Article history:

Received 12 May 2008

Accepted 24 February 2009

Available online 12 March 2009

Keywords:

S-type granite petrogenesis

Pseudosection

Garnet

Thermobarometry

ABSTRACT

This study investigates, via a pseudosection approach, the conditions of formation of garnet in the leucogranitic to granodioritic S-type Cape Granite Suite (CGS), South Africa. Previous work has stressed the importance of peritectic garnet entrained from the anatexis source in the petrogenesis of these granites. In this study, garnet from S-type granites of the CGS, showing as little evidence for replacement as possible, was studied for major and trace element geochemistry. Surprisingly, the compositions of all the crystals investigated are essentially identical, despite significant differences in the composition of the host granite. The garnet major element compositions are characterised by homogeneous, unzoned core domains with a relatively Mg-rich composition ($\text{Alm}_{69-71}\text{Py}_{14-21}\text{Gro}_3\text{Sps}_{3-5}$) surrounded by a more Mn-rich rim, some 200 μm wide ($\text{Alm}_{70-76}\text{Py}_{5-12}\text{Gro}_3\text{Sps}_{6-12}$). Trace element compositions are similarly characterised by unzoned cores surrounded by thin rims of relative REE enrichment. Pseudosections calculated for compositions ranging from granite to granodiorite illustrate that garnet is a stable phase in all compositions at high temperatures. Garnet core compositions equilibrated under P – T conditions of 4 to 6.2 kbars and 740 to 760 °C, whilst the rims record conditions of 2.5 to 5 kbars and 690 to 730 °C. Rare granulite-facies metamafic xenoliths also may record the conditions in the source of the granite magma and provide estimated P – T condition above 10 ± 2 kbars and 810 ± 54 °C. This estimate overlaps with the P – T conditions required for fluid-absent biotite melting, the process believed to have produced the CGS magmas within the lower crust. The pseudosections show that garnet was present in the CGS magmas from the source down to near-solidus conditions, but that the composition of peritectic garnet entrained within the source is not preserved in the magma. Calculation of the time required to homogenise garnet compositions within the magma indicates that this cannot occur by diffusion within the garnet crystals, as this would require several orders of magnitude longer than the typical duration of felsic magmatic events. Thus, the findings of this study argue for 1) entrainment of peritectic garnet into melt at the source, 2) the subsequent re-equilibration of this garnet to lower pressure and temperature conditions within the magmatic environment through a dissolution precipitation mechanism, and 3) a near-solidus complete replacement of garnet in some compositions. Collectively, these three processes explain the chemical connectedness between granites and their sources, as well as why the details of the connection have remained so elusive.

© 2009 Elsevier B.V. All rights reserved.

1. Introduction

S-type granites result from the melting of aluminous metasediments (metapelites–metapsammities) and are typically strongly peraluminous (Chappell, 1984; Chappell and White, 1992; Chappell, 1999; Collins and Hobbs, 2001; Foden et al., 2002; Clemens, 2003). Some studies (e.g. Chappell et al., 1987; Barbero and Villaseca, 1992), see these granites as the source-contaminated consequence of relatively low temperature anatexis. However, such magmas would be close to water saturated and would remain in the neighbourhood of their source environments because of the shape of the water-saturated granite solidus (Cann, 1970). In addition, as discussed by Clemens and Droop (1998), the negative change in volume associated with melting of this

type makes it unlikely that such melts would escape their source. Consequently, granite magmas that intrude at a high level in the crust, or that erupt, are believed to be the products of incongruent fluid-absent melting of biotite in aluminous sources (Le Breton and Thompson, 1988; Clemens, 1992; Vielzeuf and Montel, 1994; Patino-Douce and Beard, 1995; Montel and Vielzeuf, 1997). These reactions always produce garnet and/or cordierite as a peritectic phase, depending principally on pressure and bulk-rock Mg# (e.g. Hensen, 1977). Higher pressures and lower Mg#s favour garnet. Thus most deep crustal melting in typical metapelitic compositions (relatively low Mg#s) produces melt in equilibrium with peritectic garnet. This is reflected in some S-type granites where magma formation appears to involve the selective entrainment of peritectic garnet in the source (Stevens et al., 2007). Melts formed from such sources are thus saturated with garnet in the source and even if they segregate efficiently are likely to be garnet-bearing just below the liquidus. Consequently, the garnet that is

* Corresponding author. Tel.: +27 21 808 3727; fax: +27 21 808 3129.
E-mail address: arnaudvillaros@gmail.com (A. Villaros).

relatively common in the more mafic varieties of S-type granite may be either magmatic or peritectic in origin. Another possibility is that the garnet is metamorphic and occurs as a restitic remnant from digested source material (Chappell et al., 1987) or from higher level xenoliths (Clarke, 2007; Erdmann et al., 2007). This potential uncertainty around the origin of garnet in S-type granites hampers its use as a tool for unravelling granite petrogenesis. This contrasts strongly with the enormous contribution that studies involving garnet have made toward understanding the petrogenesis of metamorphic rocks.

In metamorphic rocks, garnet has proven very useful in tracking pressure–temperature change in a number of different ways. Garnet is central to partitioning-based geothermometry and geobarometry (e.g. Ferry and Spear, 1978; Newton and Haselton, 1981; Hoisch, 1991). Patterns of garnet zonation are often interpreted to have metamorphic grade and *PT* path trajectory significance (e.g. Ferry and Spear, 1978; Lanzirotti, 1995; Escuder Viruete et al., 2000; Hwang et al., 2003). Assemblages containing garnet commonly have limited ranges of pressure–temperature stability when expressed on pseudosections (Hensen, 1977; Carrington and Harley, 1995; White and Powell, 2002). Such techniques have not commonly been applied to S-type magmatic rocks, possibly because the relatively short time scales of igneous events are considered insufficient to allow for appropriate degrees of equilibration, and possibly because of the difficulties in distinguishing between the different generations of garnet that may occur. The distinction between magmatic and xenocrystic crystals may be based on mineral shape and compositional zoning (Munksgaard, 1985; Dahlquist et al., 2007), or on the presence and the nature of inclusions (e.g. Roycroft, 1991). Thus, the fact that garnet in S-type granites is commonly characterised by flat or inverse bell-shaped Mn zonation patterns (e.g. Dahlquist et al., 2007); that metamorphic mineral inclusions are extremely rare (Clemens and Wall, 1984); and, that inclusions of magmatic crystals occur (Roedder, 1979), would appear to rule out a xenocrystic origin for most examples of garnet in such granites. However, the distinction between garnet of peritectic and magmatic origin is more difficult, as both varieties form in the presence of melt and will present similar characteristics, such as melt inclusions (Cesare et al., 1997). The main difference between peritectic and magmatic crystals lies in the *P–T* conditions of formation and the composition of the magmatic system from which the garnet grows. The peritectic generation forms at the discrete *P–T* conditions of the granite's source and within the source composition. In contrast, the magmatic generation forms at typically lower *P–T* conditions, although, as S-type melts formed by biotite breakdown are almost certainly garnet-saturated in the source (as discussed above), magmatic garnet could potentially form very early in the history of such magmas, and crystallise from the magma composition (e.g. McLaren et al., 2006). Recently, Dahlquist et al. (2007) used garnet zonation patterns to distinguish magmatic from xenocrystic metamorphic garnet in the S-type Peñon Rosado Granite in Argentina. This study successfully applied partitioning-based thermobarometry to determine the *P–T* conditions that applied during early stages of crystallization of the granite. Using such an approach, it may be possible to discriminate peritectic garnet from magmatic garnet if the *P–T* conditions within the source region are known and if the magmatic garnet crystallization occurred at a pressure sufficiently lower than that of the source to be resolvable.

The S-type granites of the Cape Granite Suite (CGS) in South Africa present an excellent opportunity to study the origin of garnet in such magmas. These granites commonly contain garnet and, in some discrete zones, are garnet-rich. Although the origin of garnet in these granites has not previously been studied, peritectic garnet has been implicated in the petrogenesis of the rocks. Stevens et al. (2007), arguing from the perspective of the major-element geochemistry of the granites compared to that of experimental melt compositions from appropriate sources, proposed that the more mafic CGS S-type granites represent mixtures of melt and up to 20% peritectic garnet (Fig. 1). As is typical for S-type granites, those of the CGS also contain a large population of

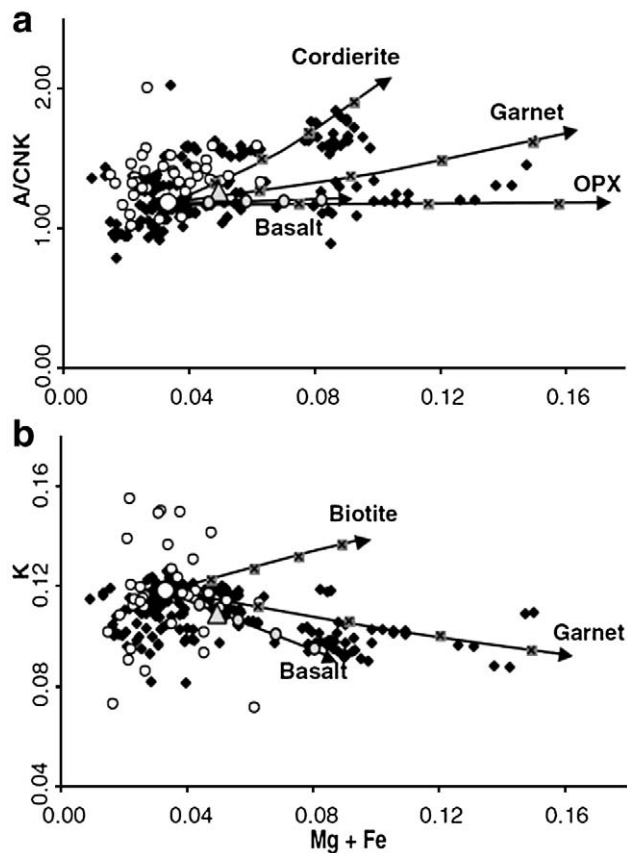


Fig. 1. A comparison of the compositions of experimental glasses (small white circles) and the compositions of Cape Granite Suite S-type rocks (black diamonds) from Scheepers (1990), Scheepers and Poujol (2002), and Scheepers and Armstrong (2002). The gray triangle represents the average of the Cape Granite Suite compositions. The evolution of this composition, as a function of the addition of the labelled mineral and basalt components in 5 wt.% increments, is shown by the evolution of the gray crossed squares away from this proposed melt composition (from Stevens et al., 2007).

xenoliths. Xenolith thermobarometry has been used to constrain the thermal structure of the crust through which granitic magmas have intruded (Hacker et al., 2000). Thus, xenoliths from the S-type CGS plutons may provide a minimum estimate of pressure conditions in the magma source area, assuming that peak metamorphic conditions recorded in the crust above the source reflects the metamorphic structure of the crust at the time of melting. The aim of this study is to investigate the origin of the garnet in the S-type granites of the CGS and to model the stability fields of the CGS garnet compositions on relevant pseudosections as a means to further developing our understanding of the petrogenesis of S-type granites. Information on the *P–T* conditions of equilibration of the xenoliths may form a useful backdrop to this exercise by potentially providing constraints on the conditions, particularly for pressure, in the magma source.

2. The garnet-bearing S-type granites of the Cape Granite Suite

The Pan-African Cape Granite Suite (CGS) in the Western Cape province of South Africa comprises mainly S-type (~560 Ma to 530 Ma), and I-type (540 to 520 Ma) plutons, in association with rare A-type intrusions (~515 to 510 Ma). Rare gabbros and late ignimbrites (515 Ma) form a minor component of the suite (Joordan et al., 1995; Armstrong et al., 1998; Scheepers and Nortje, 2000; Scheepers and Armstrong, 2002; Scheepers and Poujol, 2002). The CGS formed in response to the Saldanian Orogeny (~780 to 510 Ma, Rozendaal et al., 1999) which resulted from the convergence of the Kalahari and the Rio de la Plata cratons during Gondwana assembly (Fig. 2a). At the present level of

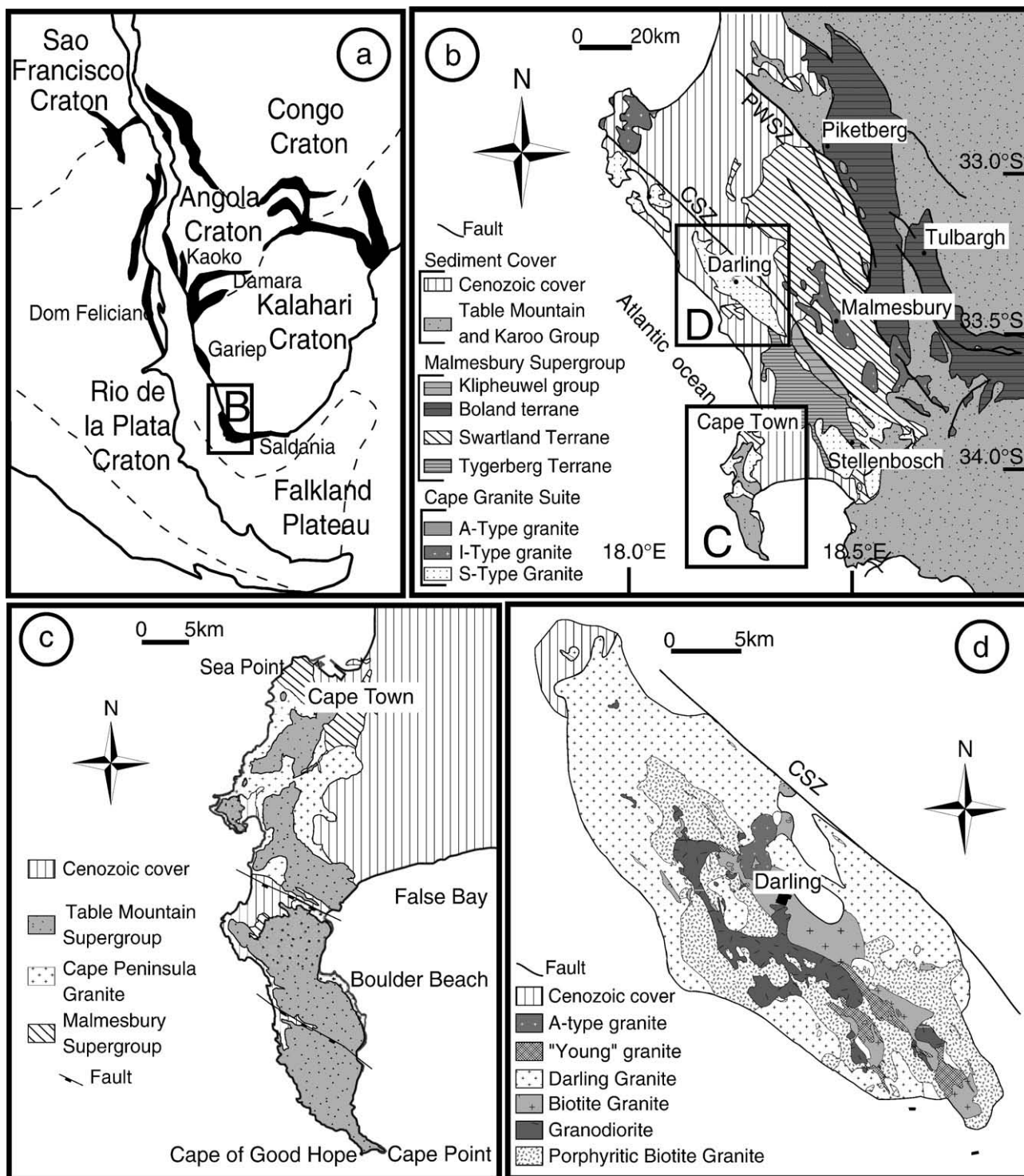
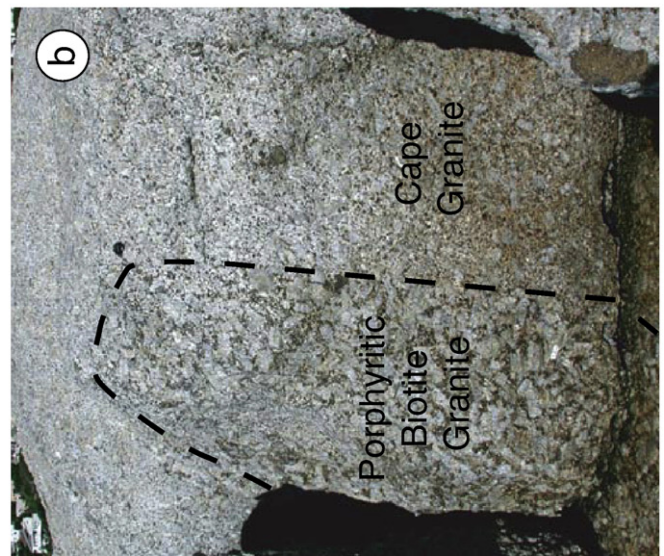
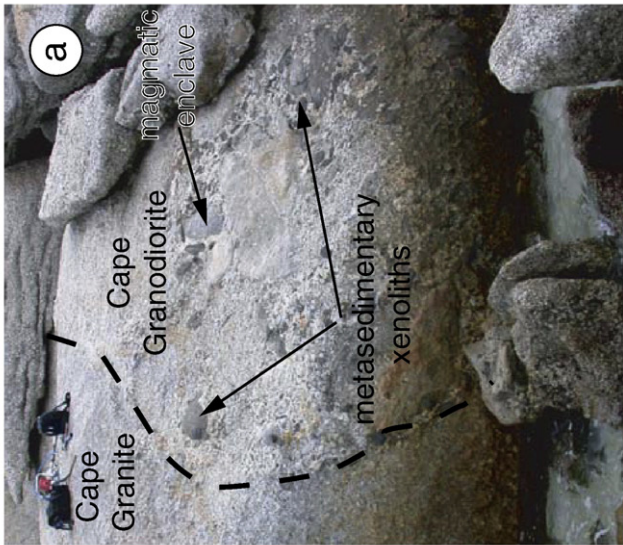
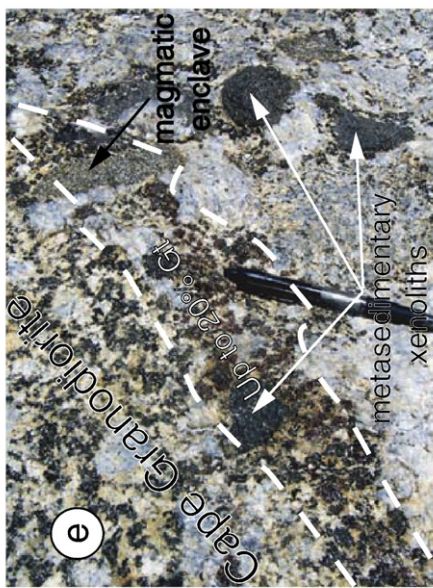
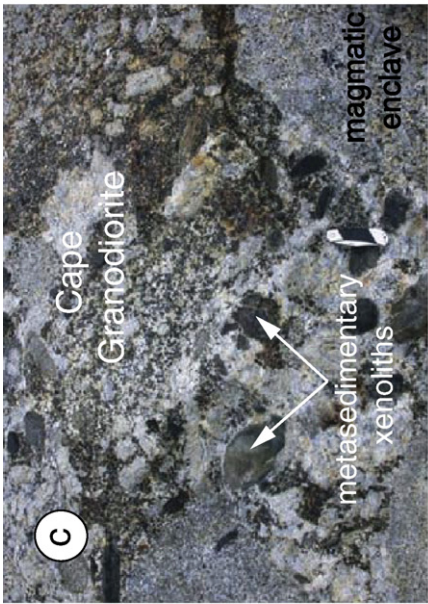
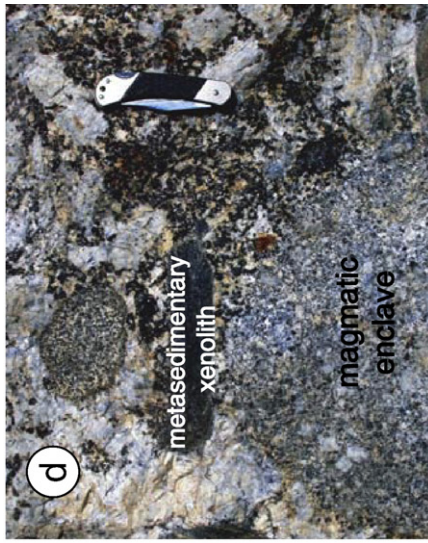


Fig. 2. a) A paleogeographic reconstruction showing the setting of the Saldanian Orogeny (Rozenaal et al., 1999); b) a geological map of the Cape Granite Suite (from Hartnady et al., 1974). CSZ = Colenzo Shear Zone, PWSZ = Piketberg-Wellington Shear Zone; c) the geology of the Peninsular Pluton (from Hartnady et al., 1974); and d) the geology of the Darling Batholith.

exposure, the Saldanian Orogeny produced a complex accretionary sedimentary mélangé, termed the Malmesbury Group (Hartnady et al., 1974; Belcher and Kisters, 2003). The CGS plutons intruded the Malmesbury Group at generally shallow crustal levels (Scheepers, 1995; Rozenaal et al., 1999; Belcher and Kisters, 2003), as shown by the lower greenschist-facies grade of the unit. The architecture of the orogeny at deeper crustal levels is unknown.

The CGS S-type granites do not normally contain high proportions of garnet in outcrop, with cordierite being the ubiquitous and abundant

ferromagnesian phase other than biotite. However, in certain localities described below garnet is abundant. In places, the S-type plutons also contain xenoliths and magmatic enclaves. Distinction between xenoliths and magmatic enclaves is simple as the latter are rounded, have mineral assemblages typical of granites, show igneous textures and generally exhibit the same overall compositional variation as the pluton in which they occur. Xenoliths are mainly metasedimentary rocks (metapelites and metapsammities). They are characterised by the preservation of sedimentary bedding in the lower metamorphic grade examples, and by



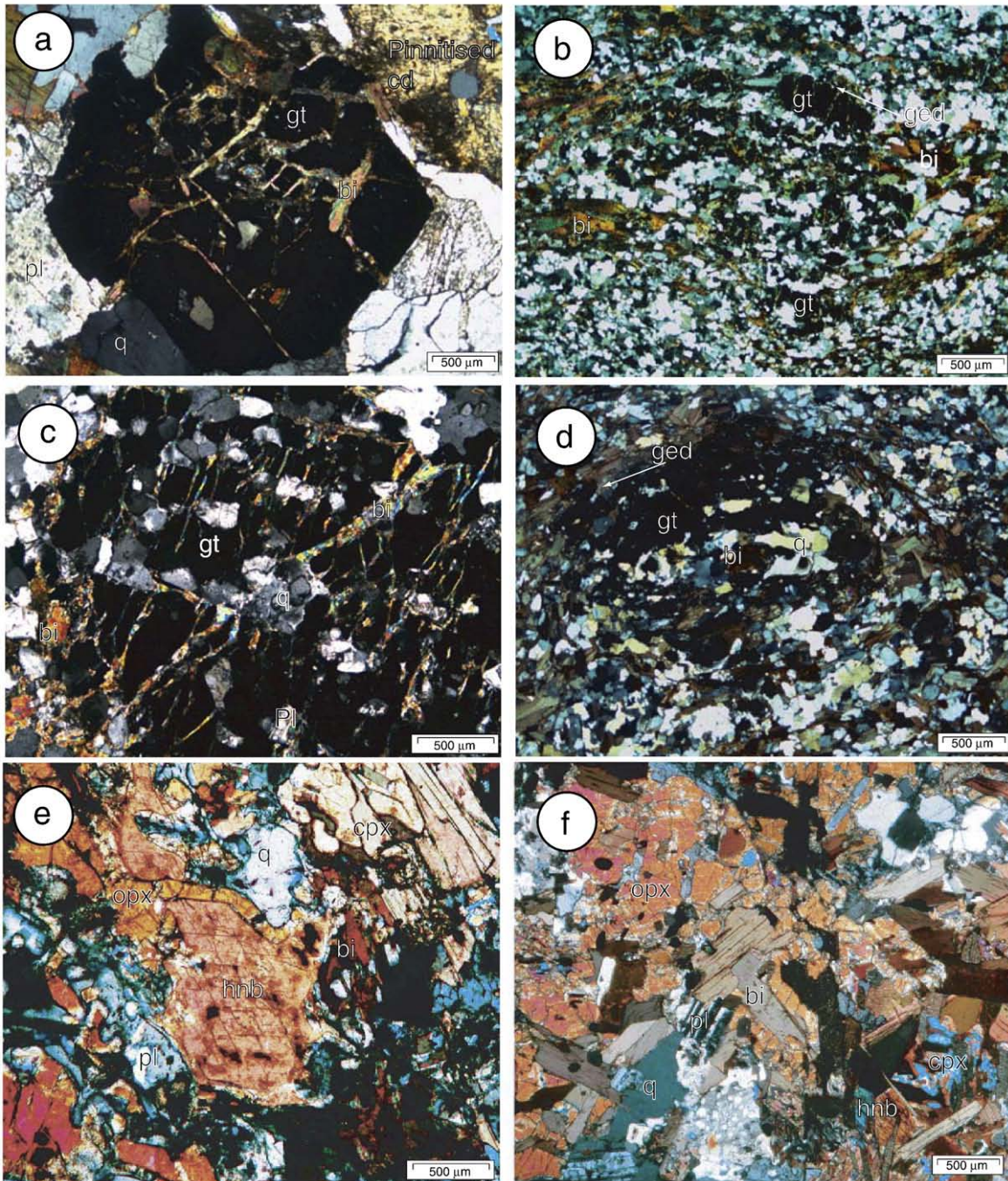


Fig. 4. Thin section image illustrating the textures of the garnet-bearing assemblages in the granites and in the metasedimentary xenoliths. – (a) garnet in S-type CGS. These crystals contain cracks filled with the matrix minerals biotite, plagioclase and quartz. – (b), (c) and (d) garnet in the metasedimentary xenoliths. Garnet in these rocks is wrapped by the biotite and orthoamphibole which define the foliation. Garnet contains large inclusions of plagioclase, quartz and biotite – (e) and (f) Mineral relationships in the metamafic xenolith. These images depict the different generations of biotite, as well as the intergrowths between cpx, opx and amphibole. Abbreviations : bi = biotite; gt = garnet; pl = plagioclase; kf = K feldspar; opx = orthopyroxene; cpx = clinopyroxene; cd = cordierite; q = quartz; ged = gedrite; hnb = hornblende.

well developed metamorphic fabrics, usually defined by biotite, in the higher metamorphic grade examples. Metamorphic mineral assemblages in the xenoliths range in grade from lower greenschist facies up to garnet-bearing amphibolite facies. The xenoliths are commonly considered to represent Malmesbury Group material (e.g. Schoch, 1975). In

the case of the lower grade xenoliths this is an obvious conclusion as the granites intrude essentially identical rocks. In the case of the high-grade xenoliths the relationship is not so obvious. However, a Malmesbury Group source for this material is supported by O and H stable isotopic evidence (Harris et al., 1997). Extremely rare metamafic xenoliths of

Fig. 3. Relevant field relationships from the Peninsular Pluton, where diversity in the granite is recorded on smaller scales than within the Darling Batholith. Images (a) and (b) show vertically orientated diffuse boundaries between different facies of the pluton (width of photographs are respectively 5 and 3 m). Images (c) to (e) show the magmatic enclave- and xenolith-rich character of zones within the pluton where garnet is commonly best preserved in significant proportions (up to 20% in some cases). However, there is textural evidence for the prior existence of garnet in almost all varieties of the plutons. This evidence constitutes rounded accumulations of biotite, and crystals of cordierite, interpreted to have formed by pseudomorphing after garnet. This interpretation appears to be substantiated by the existence of rare, partially replaced garnet (f to h) in most varieties of the granite.

Table 1
Average garnet major and trace elements compositions from garnet-bearing granites, as well as metamorphic mineral compositions from the xenoliths.

Garnet							
Rock type	S-type CGS		Metasedimentary xenolith				
	Core	Rim	Set 1	Set 2	Rim		
Analysis	n = 39	n = 31	n = 40	n = 41	n = 5		
SiO ₂	37.0 ± 0.7	36.2 ± 0.9	38.1 ± 0.1	38.5 ± 0.5	38.3 ± 1.9		
Al ₂ O ₃	20.7 ± 0.3	20.2 ± 0.2	21.2 ± 0.3	21.1 ± 0.3	21.1 ± 1.2		
FeO	34.7 ± 1.0	35.5 ± 1.2	27.9 ± 0.8	31.8 ± 0.9	32.3 ± 0.7		
MnO	3.6 ± 0.6	4.8 ± 1.6	4.7 ± 0.6	3.4 ± 1.0	4.8 ± 0.8		
MgO	2.9 ± 0.7	2.1 ± 0.9	3.5 ± 0.3	4.9 ± 0.6	4.1 ± 0.7		
CaO	1.1 ± 0.1	1.0 ± 0.1	4.5 ± 0.5	1.5 ± 0.2	1.3 ± 0.2		
Total	99.9 ± 0.6	99.8 ± 0.6	99.9 ± 0.1	101.2 ± 1.5	101.7 ± 3.8		
Si	6.0 ± 0.1	5.9 ± 0.1	6.0 ± 0.0	6.0 ± 0.1	6.0 ± 0.1		
AlIV	0.1 ± 0.1	0.1 ± 0.1	0.0 ± 0.0	0.0 ± 0.0	0.0 ± 0.0		
∑ T-site	6.0 ± 0.0	6.0 ± 0.0	6.1 ± 0.0	6.0 ± 0.1	6.0 ± 0.1		
AlVI	3.9 ± 0.1	3.8 ± 0.1	4.0 ± 0.0	3.9 ± 0.0	3.9 ± 0.1		
∑ M-site	3.9 ± 0.1	3.8 ± 0.1	4.0 ± 0.0	3.9 ± 0.0	3.9 ± 0.1		
Mg	1.1 ± 0.1	0.5 ± 0.2	0.8 ± 0.1	1.2 ± 0.1	1.0 ± 0.2		
Ca	0.2 ± 0.0	0.2 ± 0.0	0.8 ± 0.1	0.3 ± 0.0	0.2 ± 0.0		
Mn ²⁺	0.3 ± 0.1	0.7 ± 0.2	0.6 ± 0.1	0.5 ± 0.1	0.6 ± 0.1		
Fe ²⁺	4.5 ± 0.2	4.7 ± 0.2	3.7 ± 0.1	4.2 ± 0.1	4.3 ± 0.1		
∑ A-site	6.0 ± 0.1	6.0 ± 0.2	6.0 ± 0.0	6.0 ± 0.1	6.1 ± 0.2		
X _{pyr} (%)	17.3 ± 2.3	8.2 ± 3.6	14.0 ± 1.1	19.0 ± 2.4	15.71 ± 2.7		
X _{grs} (%)	3.0 ± 0.3	3.3 ± 2.0	12.9 ± 1.5	4.2 ± 0.5	3.604 ± 0.6		
X _{alm} (%)	70.3 ± 1.3	73.2 ± 1.7	62.4 ± 1.8	69.3 ± 1.6	70.19 ± 1.0		
X _{sps} (%)	4.4 ± 1.6	9.7 ± 2.4	10.7 ± 1.3	7.6 ± 2.2	10.49 ± 1.7		
(ppm)		n = 9		n = 11	n = 6		
Rb		1.7 ± 1.4		0.9 ± 0.0	11.0 ± 9.0		
Sr		0.2 ± 0.1		0.1 ± 0.0	1.3 ± 0.4		
Y		418.8 ± 20.9		1243.6 ± 87.4	454.1 ± 63.5		
Zr		7.6 ± 1.1		12.5 ± 1.3	29.9 ± 24.4		
Nb		0.1 ± 0.1		0.0 ± 0.0	0.5 ± 0.4		
Ba		0.3 ± 0.2		0.0 ± 0.0	14.8 ± 6.1		
La		0.1 ± 0.1		0.0 ± 0.0	0.2 ± 0.2		
Ce		0.1 ± 0.1		0.2 ± 0.2	0.5 ± 0.2		
Pr		0.1 ± 0.0		0.0 ± 0.0	0.2 ± 0.1		
Nd		0.3 ± 0.1		0.3 ± 0.1	1.6 ± 0.4		
Sm		0.6 ± 0.2		1.8 ± 0.2	3.8 ± 1.4		
Eu		0.1 ± 0.0		0.0 ± 0.0	0.7 ± 0.4		
Gd		4.5 ± 0.5		15.8 ± 0.7	14.6 ± 8.1		
Tb		2.7 ± 0.2		8.7 ± 0.6	5.0 ± 1.9		
Dy		44.0 ± 3.0		137.6 ± 8.1	58.3 ± 16.3		
Ho		15.8 ± 0.8		51.5 ± 2.9	16.0 ± 2.4		
Er		64.5 ± 4.4		216.2 ± 5.6	54.6 ± 5.2		
Tm		11.3 ± 1.1		38.0 ± 0.5	8.0 ± 1.4		
Yb		83.3 ± 9.9		266.2 ± 2.8	48.1 ± 11.6		
Lu		12.6 ± 2.2		37.7 ± 0.2	6.6 ± 2.1		
Hf		0.2 ± 0.0		0.3 ± 0.1	0.7 ± 0.7		
Eu/Eu*		0.155 ± 0.00		0.027 ± 0.01	0.292 ± 0.11		
Biotite				Plagioclases			
Rock type	Metasedimentary xenolith		Metabasite xenolith	Rock type	Metasedimentary xenolith		Metabasite xenolith
Analysis	Set 1	Set 2	n = 21	Analysis	Set 1	Set 2	n = 35
	n = 26	n = 25			n = 33	n = 38	
SiO ₂	36.5 ± 0.4	35.8 ± 1.3	37.9 ± 0.3	SiO ₂	55.9 ± 1.6	58.9 ± 1.3	46.5 ± 0.8
TiO ₂	3.2 ± 0.1	1.5 ± 1.1	5.2 ± 0.4	Al ₂ O ₃	27.4 ± 1.0	25.8 ± 0.2	34.8 ± 0.2
Al ₂ O ₃	16.4 ± 0.2	17.8 ± 1.0	14.0 ± 0.2	Fe ₂ O ₃	0.0 ± 0.0	1.2 ± 1.6	0.4 ± 0.1
FeO	19.6 ± 1.4	20.9 ± 2.0	15.9 ± 0.9	CaO	9.9 ± 1.2	6.8 ± 0.6	17.0 ± 0.8
MgO	10.1 ± 0.7	10.7 ± 0.6	13.5 ± 0.4	Na ₂ O	6.4 ± 0.6	7.4 ± 0.6	1.6 ± 0.3
MnO	0.2 ± 0.1	0.0 ± 0.0	0.0 ± 0.0	K ₂ O	0.5 ± 0.5	0.1 ± 0.1	0.0 ± 0.0
K ₂ O	10.2 ± 0.1	8.6 ± 1.6	9.5 ± 0.1	Total	100.0 ± 0.0	100.3 ± 0.8	100.2 ± 0.2
Total	96.2 ± 0.3	95.4 ± 0.8	96.0 ± 0.2	Si	2.5 ± 0.1	2.6 ± 0.0	2.1 ± 0.0
AlIV	2.5 ± 0.0	2.6 ± 0.12	2.4 ± 0.0	Al	1.5 ± 0.1	1.4 ± 0.0	1.9 ± 0.0
Si	5.5 ± 0.0	5.4 ± 0.12	5.6 ± 0.0	Fe ³⁺	0.0 ± 0.0	0.0 ± 0.0	0.0 ± 0.0
∑ T-site	8.0 ± 0.0	8.0 ± 0.00	8.0 ± 0.0	∑ T-site	4.0 ± 0.0	4.0 ± 0.0	4.0 ± 0.0
AlVI	0.5 ± 0.1	0.7 ± 0.03	0.1 ± 0.0	Na	0.5 ± 0.1	0.6 ± 0.0	0.1 ± 0.0
Mg	2.3 ± 0.1	2.5 ± 0.13	3.0 ± 0.1	K	0.0 ± 0.0	0.0 ± 0.0	0.0 ± 0.0
Ti	0.4 ± 0.0	0.1 ± 0.05	0.6 ± 0.0	Ca	0.4 ± 0.1	0.3 ± 0.0	0.8 ± 0.0
Fe ²⁺	2.5 ± 0.2	2.8 ± 0.11	2.0 ± 0.1	Fe ²⁺	0.0 ± 0.0	0.0 ± 0.0	0.0 ± 0.0
∑ M-site	6.0 ± 0.0	6.0 ± 0.02	5.6 ± 0.0	∑ A-site	1.0 ± 0.0	1.0 ± 0.0	1.0 ± 0.0
K	2.0 ± 0.0	2.0 ± 0.02	1.8 ± 0.0	xK [%Or]	2.7 ± 2.7	0.6 ± 0.4	0.0 ± 0.0

Table 1 (continued)

Biotite				Plagioclases			
Rock type	Metasedimentary xenolith		Metabasite xenolith	Rock type	Metasedimentary xenolith		Metabasite xenolith
Analysis	Set 1	Set 2	n = 21	Analysis	Set 1	Set 2	n = 35
∑ A-site	2.0 ± 0.0	2.0 ± 0.02	1.8 ± 0.0	xNa [%Ab]	52.4 ± 5.0	65.7 ± 3.9	14.4 ± 3.0
OHcalc	4.0 ± 0.0	4.0 ± 0.00	4.0 ± 0.0	xCa [%An]	44.9 ± 5.3	33.6 ± 3.7	85.6 ± 3.0
∑ OH-site	4.0 ± 0.0	4.0 ± 0.00	4.0 ± 0.0				
Mg#	47.9 ± 3.3	46.6 ± 0.9	60.2 ± 1.9				
Rock type	Orthopyroxene		Clinopyroxene	Amphiboles			
Analysis	Metabasite xenolith		n = 41	Rock type	Metabasite xenolith		
Analysis	n = 35		n = 41	Analysis	n = 31		
SiO ₂	51.9 ± 0.2		54.1 ± 0.5	SiO ₂	46.9 ± 0.4		
TiO ₂	0.0 ± 0.0		0.2 ± 0.0	TiO ₂	1.9 ± 0.2		
Al ₂ O ₃	0.8 ± 0.1		0.8 ± 0.5	Al ₂ O ₃	8.8 ± 0.7		
FeO	27.1 ± 0.7		10.5 ± 0.1	Cr ₂ O ₃	0.0 ± 0.1		
MgO	18.7 ± 0.3		13.7 ± 0.3	FeO	13.5 ± 0.6		
CaO	0.8 ± 0.0		20.7 ± 0.2	MgO	13.6 ± 0.3		
Total	99.8 ± 0.6		100.0 ± 0.5	MnO	0.1 ± 0.1		
AlIV	0.0 ± 0.0		0.0 ± 0.0	CaO	11.1 ± 0.3		
Si	2.0 ± 0.0		2.0 ± 0.0	Na ₂ O	1.0 ± 0.1		
∑ T-site	2.0 ± 0.0		2.0 ± 0.0	K ₂ O	1.0 ± 0.1		
Mg	1.1 ± 0.0		0.8 ± 0.0	Total	97.9 ± 0.6		
AlVI	0.0 ± 0.0		0.0 ± 0.0	AlIV	1.1 ± 0.1		
Ca	0.0 ± 0.0		0.8 ± 0.0	Si	6.9 ± 0.1		
Ti	0.0 ± 0.0		0.0 ± 0.0	∑ T-site	8.0 ± 0.0		
Fe	0.9 ± 0.0		0.3 ± 0.0	Mg	3.0 ± 0.1		
∑ M-sites	2.0 ± 0.0		2.0 ± 0.0	AlVI	0.4 ± 0.1		
Mg#	55.2 ± 1.0		70.0 ± 0.6	Ti	0.2 ± 0.0		
				Fe ²⁺	1.5 ± 0.1		
				∑ C-site	5.0 ± 0.0		
				Na	0.1 ± 0.0		
				Ca	1.7 ± 0.1		
				Mn ²⁺	0.0 ± 0.0		
				Fe ²⁺	0.2 ± 0.0		
				∑ B-site	2.0 ± 0.0		
				Na	0.2 ± 0.0		
				K	0.2 ± 0.0		
				∑ A-site	0.4 ± 0.0		
				OH	2.0 ± 0.0		
				∑ OH-site	2.0 ± 0.0		
				Mg#	64.3 ± 1.5		

Despite the low standard deviations, these compositions were obtained from 7 different samples, reflecting a significant bulk rock compositional range, from two different plutons. The garnet, biotite, plagioclase, pyroxene and amphibole structural formulae were calculated on the basis of 24, 22, 8, 6 and 23 Oxygens, respectively.

apparent granulite-facies grade have also been described (Schoch, 1975).

The composition of the S-type CGS rocks varies widely from leucogranite to granodiorite (Schoch et al., 1977; Scheepers, 1995; Scheepers, 2000; Scheepers and Nortje, 2000; Stevens et al., 2007). Stevens et al. (2007) related this variation, on major element geochemical grounds, to variable degrees of entrainment of the peritectic assemblage, principally garnet, into the typically leucocratic melt composition produced by the anatexis of metapelites at temperatures of 850 to 900 °C. The more mafic examples of the suite are estimated to contain more than 20% (by weight) of entrained peritectic garnet, with an approximate composition of Alm₆₂Py₂₈Gr₀Sps_{<1} (Stevens et al., 2007) (Fig. 1). Of the S-type CGS plutons, the Peninsula Pluton (Fig. 2c) and the Darling Batholith (Fig. 2d) are best exposed, providing good constraints on the spatial relationships between the different rock types that constitute the plutons. While the Peninsula Pluton is largely undeformed, the Darling Batholith, due to its proximity to the Colenso fault (Fig. 2b, c and d), is intensely deformed close to the fault. A previous study by Schoch (1975) described four different magmatic facies within the Darling Batholith; a porphyritic cordierite-rich leucogranite (the Cape Granite); a biotite-rich porphyritic granite (Porphyritic Biotite Granite); a fine grained, biotite-rich granite with rare K-feldspar phenocrysts (Biotite Granite); and, a fine grained biotite- and cordierite-rich granodiorite (Cape Granodiorite) (Fig. 2d). As a relative chronology cannot be established between the

different facies, and as contacts between the facies are commonly diffuse, they may relate to different injections of magma.

In the Peninsular Pluton, facies variation that is similar to that in the Darling Batholith is observed. Here, however, variation occurs on the scale of individual outcrops (typically metres) and cannot be mapped on a pluton scale (Fig. 3a and b). Contacts between different varieties are commonly very diffuse (Fig. 3a) but confined to narrow zones, indicating the existence of different magma types. In the exposed portions of the peninsular pluton, contacts between the different facies are generally steeply orientated. The Porphyritic Biotite Granite, Biotite Granite and Cape Granodiorite phases occur as diffuse dyke-like structures of steep but variable orientation and width (from 1 to several metres), or as pipe-like structures, typically between 1 and 2 m in diameter (Fig. 3a), within the Cape Granite. The interface between these zones is commonly the site of a concentration of enclaves of different types creating the impression of flow segregation (Fig. 3b).

3. Techniques for mineral analysis

In this study, minerals have been analysed using a Leo 1430VP Scanning Electron Microscope with an Oxford Instruments ED X-ray detector (133 KeV) and Inca Energy processor at Stellenbosch University. Beam conditions during the analyses were 20 KV accelerating voltage and 1.5 nA probe current, with a working distance of 13 mm. Natural

mineral standards were used for standardization and verification of the analyses. Pure Co, as well as Ti and Fe in ilmenite were used periodically to correct for detector drift. Spicer et al. (2004), Diener et al. (2005) and Moyen et al. (2006) provide an analysis of the analytical accuracy that can be achieved using this instrument. Trace element compositions were obtained using Laser Ablation-Inductively Coupled Plasma-Mass Spectrometry (LA-ICP-MS) at Stellenbosch University. In situ sampling on polished thin sections was performed with 80 μm or 100 μm diameter ablation spots generated by a New Wave 213 nm Nd-YAG Laser coupled to an Agilent 7500ce mass spectrometer with mixture of Ar-He as carrier gas. Operating conditions for the laser were 12 Hz frequency and 10 kJ energy. Data was reduced using a time resolved method (Longerich et al., 1996) which allowed potential contamination from mineral inclusions or fractures to be avoided. NIST-612 glass was used as an external standard (values from Pearce et al., 1997) and measured mineral (via EDS) SiO_2 contents were used as an internal standard. BHVO-1 glass (Flanagan, 1976) and an in-house garnet standard were used as secondary standards. Analysis of the BHVO-1 control standard established that the accuracy and reproducibility of multiple analyses (from secondary standards) for all elements included in the results were better than 5% relative.

4. Garnet in the CGS

Within the CGS, garnet is commonly partly, to almost completely, replaced by cordierite, particularly in portions of the plutons where garnet occurs as a dispersed phase. Garnet generally occurs as concentrations of relatively large, inclusion-free crystals (up to 10 mm in diameter) within the zones of xenolith and enclave accumulation discussed above (Fig. 3c, d and e). This garnet is commonly rounded to subhedral in shape, and is typically partially replaced by cordierite and/or biotite (Fig. 3f, g and h), the latter itself partially chloritised. Large pseudomorphs of cordierite after garnet indicate that some of the original garnet crystals were up to 30 mm in diameter (Fig. 3g). Garnet grains are commonly cracked. The cracks contain plagioclase, K-feldspar and biotite that is identical in composition to the matrix minerals in the granite. This indicates cracking of the crystals prior to the crystallization of the magma (Fig. 3a). Garnet crystals show no evidence of inclusions, with every mineral contained within the garnet being connected to the matrix by the cracks in the crystal (Fig. 4a).

Major element analysis of garnet from the granites (Table 1) indicates significant core-rim zonation (Fig. 5). The grains are Fe-rich and Ca-, Mn-poor with a composition very close to $\text{Alm}_{69-71}\text{Py}_{14-21}\text{Gro}_3\text{Sps}_{3-5}$, except for a narrow (100–200 μm -wide) rim, where they are more Fe- and Mn-

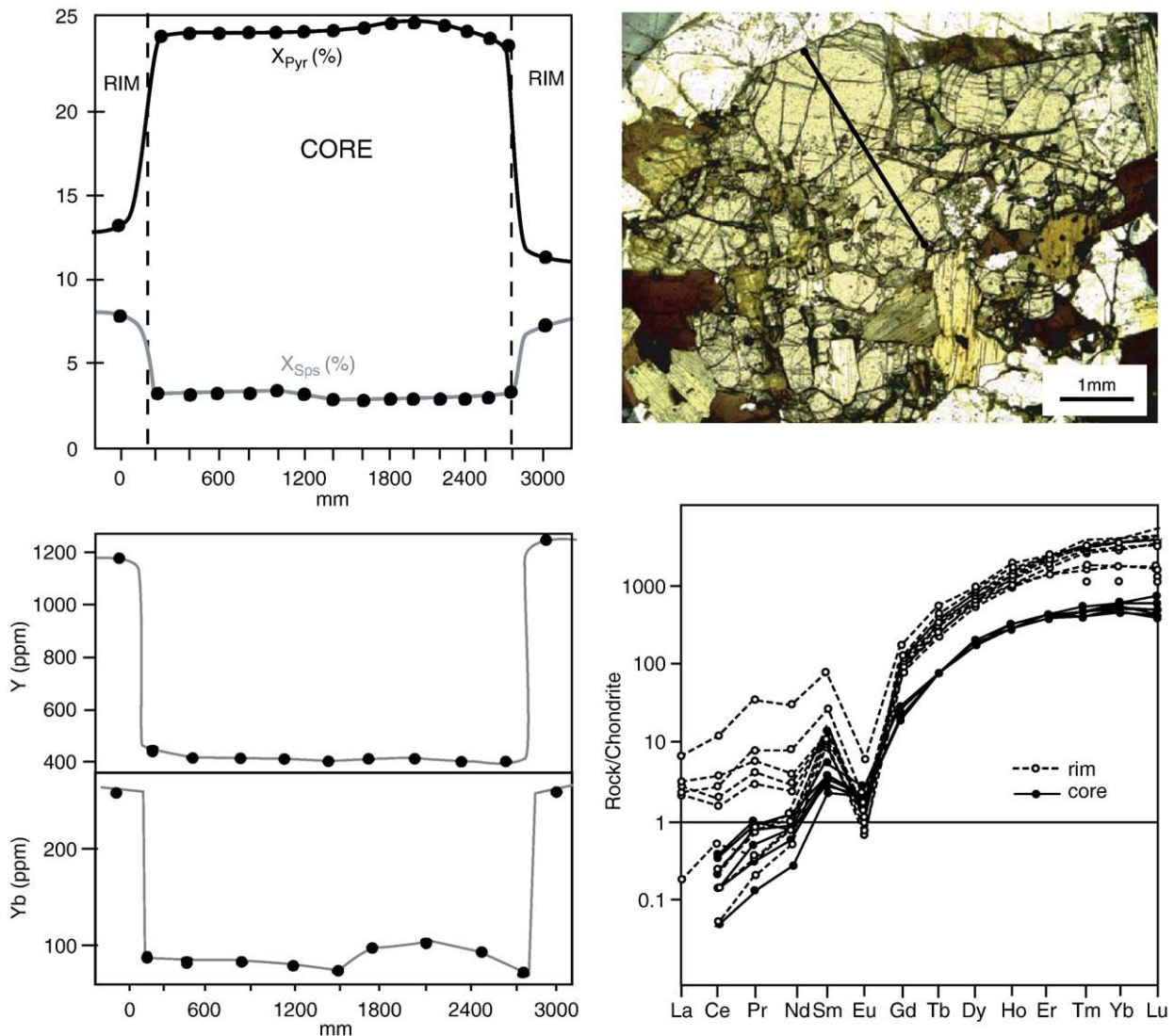


Fig. 5. Garnet in S-type CGS granitoids. The photograph illustrates the section analysed in the garnet. The diagrams below the photograph represent the rim to rim zonation patterns determined for the section through the crystal marked on the photograph. X_{Pyr} , X_{Sps} are plotted to reflect the major element zonation whilst Y and Yb concentrations in ppm are plotted as proxies for REE zonation. REE-chondrite normalised (Taylor and McLennan, 1985) spider plots showing different patterns for the core and rim zones of the garnet are included.

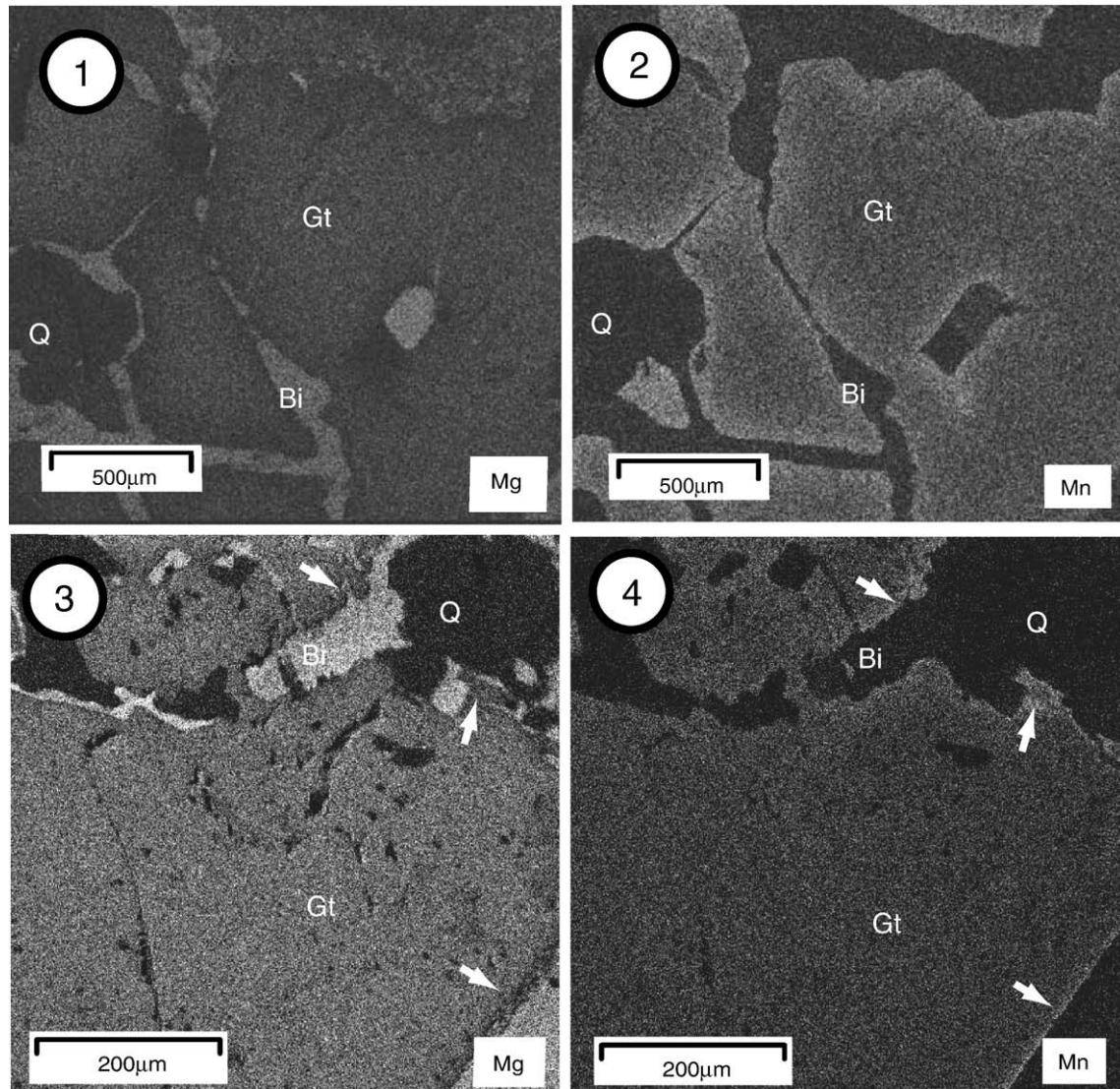


Fig. 6. Typical X-ray element maps of garnet from the granites and xenoliths. Images (1) and (2) represent Mg and Mn X-ray maps for garnet in a granodiorite. Images (3) and (4) represent Mg and Mn X-ray maps for garnet in a metasedimentary xenolith. The white arrows point at the 10 to 20 μm wide irregular Mn-rich rim of garnet in the xenolith.

rich, and Py-poor ($\text{Alm}_{70-76}\text{Py}_{5-12}\text{Gro}_3\text{Sps}_{6-12}$). Importantly, the compositions of both the unzoned interior and the narrow rim domains are constant throughout 12 samples selected from 5 different locations in the Peninsula Pluton and Darling Batholith. Element mapping using SEM-EDS (Fig. 6) illustrates the zonation pattern well and demonstrates that the 100 to 200 μm thick rim zone follows the pre-crystallization cracks in the garnet crystals described earlier. This zoning is also clearly shown by the concentration of trace elements (Fig. 5) in the garnet. Chondrite-normalised (Taylor and McLennan, 1985) REE patterns (Fig. 5) show preferential relative enrichment of HREE over the L-MREE. REE abundances are significantly higher in the narrow rims than in the broad cores; average Eu anomalies are also significantly more negative in the rims ($\text{Eu}/\text{Eu}^* = 0.027 \pm 0.012$) than in the cores ($\text{Eu}/\text{Eu}^* = 0.155 \pm 0.024$). Zonation patterns for Y and Yb across garnet from rim to rim, plotted as a proxy for HREE zonation in Fig. 5, show similar features to the major element zonation pattern, with a plateau-like core composition and a narrow rim zone of no more than 100 μm thickness.

5. Minerals in the xenoliths

Two different types of garnet-bearing metasedimentary xenoliths can be distinguished on the basis of petrography i.e. a biotite dominated-metapelite and a quartz and feldspar-dominated metapsammite. Both

xenolith types contain a well developed foliation defined by aligned biotite crystals and continuous quartzo-feldspathic layers with a metamorphic texture, both of which wrap the larger garnet crystals. Garnet in these rocks is texturally very different to the garnet in the granites (Fig. 4b, c and d) and is commonly smaller (~ 3 to 5 mm) and slightly elongated in the direction of the foliation (Fig. 4b and c). Mineral inclusions (mainly biotite, quartz and feldspars) define an internal foliation within the garnet that is in continuity with the rock foliation. Orthoamphibole, (Gedrite, after Leake et al., 1998), occasionally occurs within the external foliation wrapping garnet in both xenolith types.

Garnet, biotite, and plagioclase are characterised by distinctly different compositions in the different metasedimentary xenolith varieties (Table 1). The metapsammite xenoliths are characterised by relatively Ca- and Mn-rich garnet ($\text{Alm}_{60-65}\text{Py}_{12-15}\text{Gro}_{10-14}\text{Sps}_{9-12}$). In these rocks, biotite is characterised by high Ti (0.3 to 0.4 pfu) and low Al(IV) (0.4 to 0.5 pfu) contents, and contains traces of Mn (0.01 to 0.04 pfu). Plagioclase varies from An_{47} to An_{59} . In the metapelitic xenoliths, garnet has lower grossular and spessartine concentrations ($\text{Alm}_{67-72}\text{Py}_{16-21}\text{Gro}_4\text{Sps}_{5-9}$). In these rocks, biotite is relatively Ti poor (0.12 ± 0.05 pfu), relatively Al-rich (VI) (0.7 ± 0.04 pfu) and contains no detectable Mn. Plagioclase has a considerably lower anorthite content (An_{30} to An_{37}) than in the metapsammite xenoliths. X-ray mapping of garnet in the metapelitic xenoliths shows two

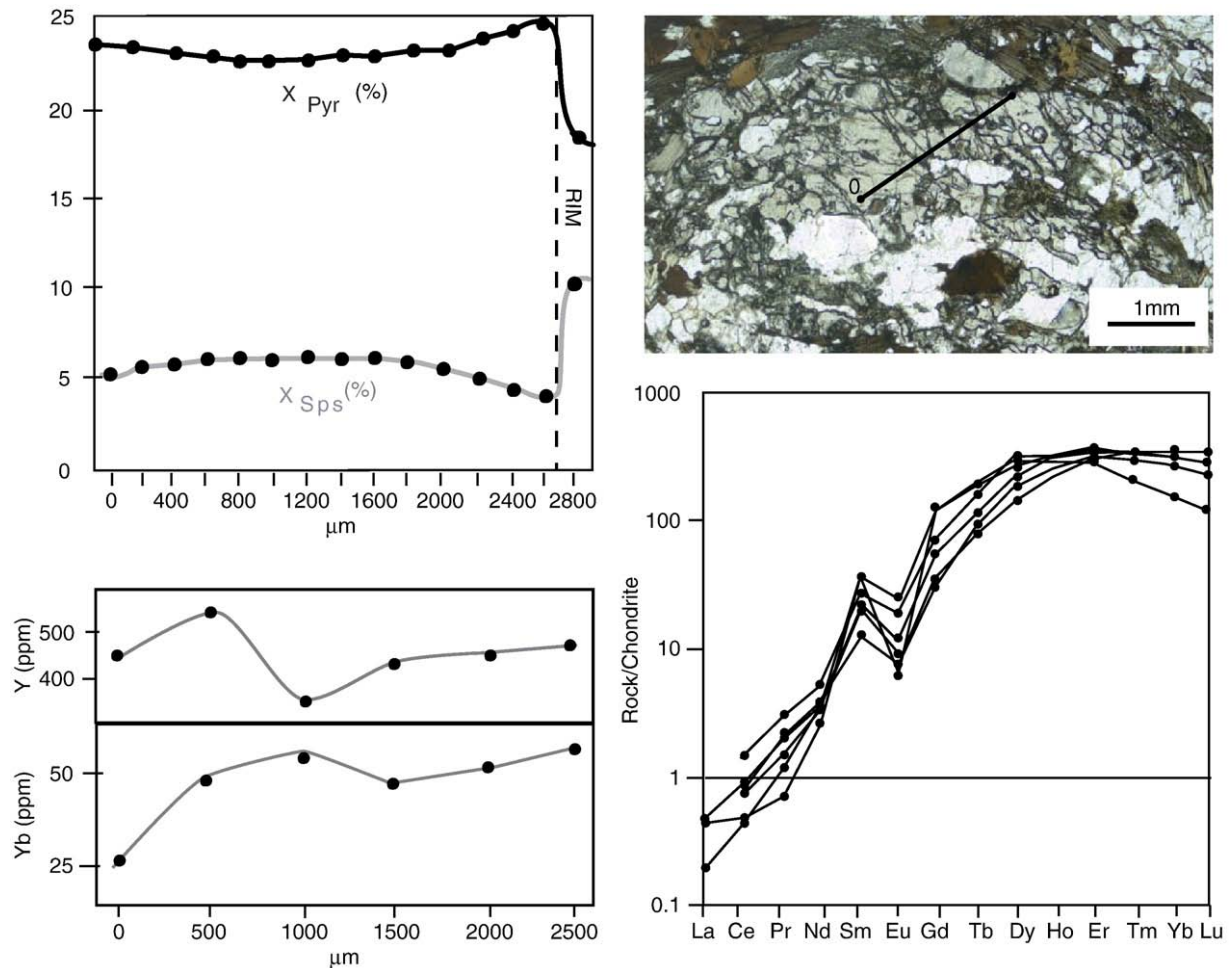


Fig. 7. Garnet in metasedimentary xenoliths: The photograph illustrates the section of garnet analysed for chemical zonation. The diagrams below the photograph illustrate the rim to rim zonation patterns for X_{Pyr} , X_{Sps} , as well as Y and Yb (in ppm). A REE chondrite-normalised (Taylor and McLennan, 1985) diagram is included below the zonation diagrams.

combined zonation effects. Firstly, the interiors of the crystals are characterised by a weak prograde pattern, with Mg content increasing from core to rim (typically from 1.1 pfu to 1.3 pfu). This is coupled with a slight decrease of the Mn content (from 0.4 pfu to 0.6 pfu). Secondly, a narrow retrograde rim exists that is no more than 20 μm wide (Figs. 6 and 7), and this is characterised by a more iron rich and Mn rich composition ($\text{Alm}_{69-71}\text{-Pyrr}_{12-17}\text{Gro}_{4}\text{Sp}_{10-13}$). Chondrite-normalised REE patterns (Fig. 7) obtained for this garnet do not show any meaningful zonation, although the rims are too narrow to be reliably analysed by LA-ICP-MS. The average Eu anomaly is quite variable ($\text{Eu}/\text{Eu}^* = 0.292 \pm 0.110$) but does not show consistent core-rim variation.

In both types of metasedimentary xenoliths, there is no significant variation in the composition of biotite or plagioclase, even where these minerals appear to occur as inclusions in the garnet. This may be because the garnet crystals are highly fractured and pokioblastic, making communication and chemical exchange with the matrix possible even for crystals that appear isolated within garnet. In both xenolith types, the relationship between garnet and the tectonic fabrics indicate that the growth of garnet was syntectonic. The major element zonation patterns of these garnets suggests core to rim prograde growth zoning combined with a thin, retrograde rim. In addition, the relatively flat chondrite-normalised HREE pattern (Fig. 7) in these crystals is typical for garnet crystallised under granulite-facies conditions (Ayles and Vance, 1997; Bea et al., 1997). This is at odds with the retention of a major element growth zoning pattern in the crystals; the existence of orthoamphibole as a peak metamorphic mineral, and the lack of anatexis phenomena. Garnet-biotite thermometry produces temperature estimates of 715 $^{\circ}\text{C}$ and 735 $^{\circ}\text{C}$ (± 25 $^{\circ}\text{C}$ from Holdaway, 2000) respectively for the

metapelitic and metapsammitic xenoliths. Collectively, these characteristics indicate that these assemblages recorded regional metamorphism close to lower granulite facies conditions and do not show any evidence for a discernable thermal overprint by the granite. This is in sharp contrast to the lower grade Malmesbury Group xenoliths and contact aureoles which show that clear contact metamorphic effects were intruded by the granites (Walker and Mathias, 1946).

As noted earlier, metamafic xenoliths have been described from the Darling Batholith. These rocks are very rare and this study yielded only one sample of this type. This rock contains an assemblage of biotite, orthopyroxene, plagioclase, quartz, clinopyroxene and hornblende (Fig. 4c and d). Two textural varieties of biotite exist. The first, earlier variety occurs as corroded remnants within orthopyroxene. A subsequent generation occurs as replacive rims on the same orthopyroxene crystals (Fig. 4, e and f). This, along with the weak foliation, is interpreted to confirm a metamorphic origin for this xenolith. Orthopyroxene and clinopyroxene are coarsely intergrown and appear to have formed from an original assemblage of biotite, hornblende, plagioclase and quartz. Despite the fact that two clearly different textural varieties of biotite exist, the minerals in this rock are unzoned and all biotite is of identical composition (Table 1). Orthopyroxene is characterised by $\text{Mg}\# = 54\text{--}56$, clinopyroxene has a $\text{Mg}\#$ of 70 ± 1 and a constant Ca content of 0.8 ± 0.01 pfu. Orthopyroxene is Al-poor (0.8 ± 0.1 wt.% of Al_2O_3). Hornblende has an Al(VI) content of 0.4 ± 0.1 pfu, while Na and Ca are 0.1 ± 0.05 and 1.74 ± 0.05 pfu respectively, and $\text{Mg}\#$ is very uniform (64 ± 1). Biotite has $\text{Mg}\#$ of 60.2 ± 2 and Ti of 0.6 ± 0.04 pfu. Plagioclase is calcic (An_{83} and An_{90}). Based on the occurrence of 2 co-existing pyroxenes this rock records a granulite-facies metamorphic assemblage.

6. Constraining pressure and temperature in the source

The only metamorphic rocks exposed in association with the CGS are the generally lower greenschist-facies grade metasediments of the Malmesbury Group that the granites intrude. As the xenoliths in the granite are considered to also represent parts of the Malmesbury Group (Schoch, 1975), and the ascending magma can only sample rocks above the level of magma generation, the P – T conditions of equilibration for these assemblages may have relevance for the level at which anatexis occurred within the Saldanian orogenic pile. As stated above, the metasedimentary xenoliths do not show any evidence for partial melting and must therefore record temperatures significantly lower than necessary for comprehensive fluid-absent melting. Thus, these rocks are unlikely to represent part of the source of the S-type CGS magmas, although they may be lower temperature equivalents. In contrast, the apparent granulite-facies conditions recorded by the metamafic xenolith are a reasonably good fit with possible source P – T conditions for the granites. Thus, this material may reflect mafic rock material intercalated

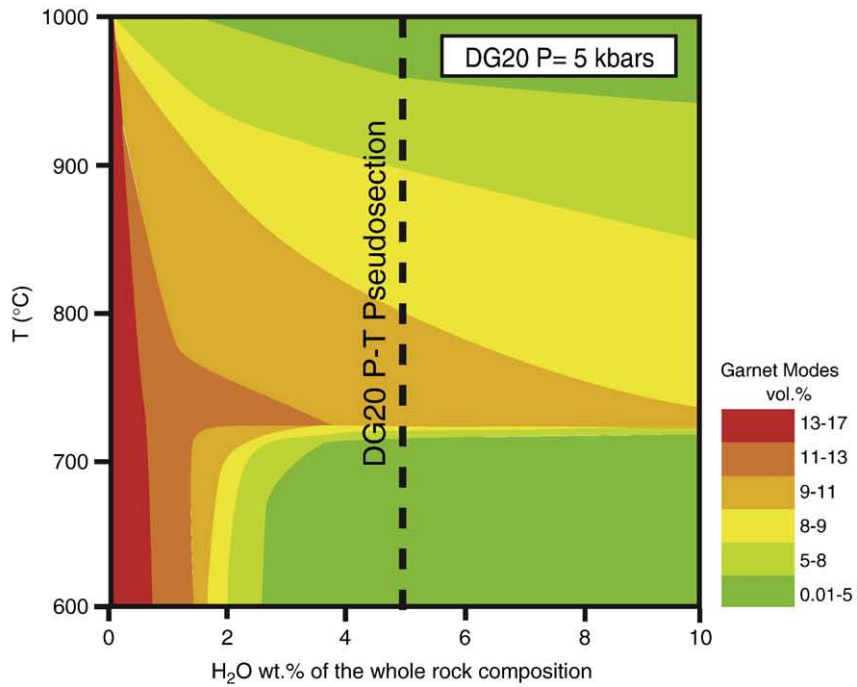
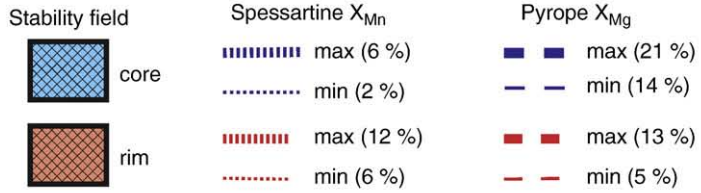
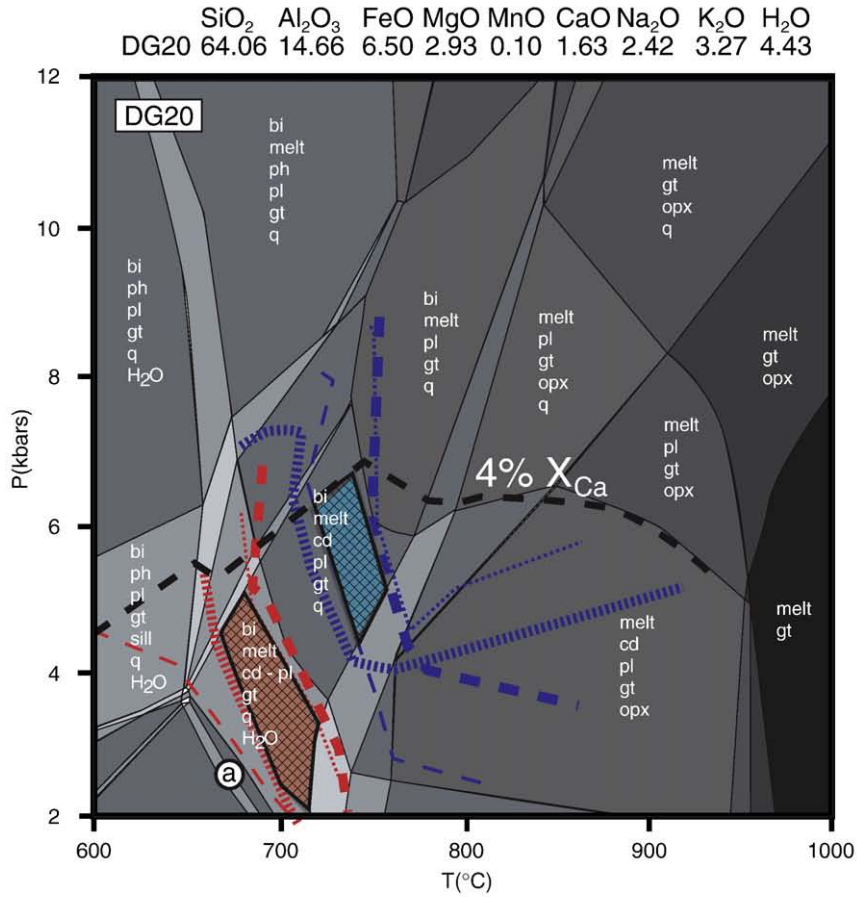
with the metasedimentary source, or possibly, the quenched heat source. However, the presence of metamorphic textures and fabrics may argue against the latter hypothesis. Average P and T estimates from the mineral assemblage (Table 2) in the metamafic xenolith were determined using the software package THERMOCALC (Powell and Holland, 1994; Holland and Powell, 2001). This method, based on an internally-consistent thermodynamic dataset (Holland and Powell, 1998), provides an optimal P – T estimate, that includes a statistical evaluation of the result (Powell and Holland, 1994). Mineral end-member activities were determined using the program a – x (Holland and Powell, 1998). Results of the calculations were optimised by using statistical parameters to exclude outlying end-members, thereby defining an independent reaction set that results in the best possible fit for a given mineral assemblage (Powell and Holland, 1994). Results and details of the equilibrium reaction sets and statistical parameters are given in Table 2. End members used were: orthoenstatite (en), orthoferrosilite (fs) and Mg-tschermakite (mgts) for opx; diopside (di), hedenbergite (hed) and Ca-tschermakite (cats) for cpx; anorthite (an), and albite (ab) for plagioclase; tremolite (tr), ferro-actinolite (fact),

Table 2

Results of the average P – T estimate calculations from the metamafic xenolith using THERMOCALC and different water activities ($a(\text{H}_2\text{O}) = 0.3$; $a(\text{H}_2\text{O}) = 0.5$; $a(\text{H}_2\text{O}) = 0.8$).

Activities of the endmembers			Average PT (for $a(\text{H}_2\text{O}) = 0.3$)						
a	$sd(a)/a$		Single endmembers diagnostic information						
			P (kbars)	T (°C)	cor	fit	e^*	hat	
en	0.2900	0.15	en	9.8 ± 1.5	742 ± 55	0.39	1.29	0.64	0.32
fs	0.2000	0.18	fs	9.8 ± 1.6	763 ± 46	0.45	1.32	–0.2	0
mgts	0.0150	0.67	mgts	10.0 ± 1.6	767 ± 47	0.48	1.31	–0.6	0.09
di	0.5600	0.10	di	10.0 ± 1.6	769 ± 48	0.47	1.31	–0.5	0.07
hed	0.3700	0.10	hed	9.8 ± 1.6	760 ± 47	0.46	1.32	0.4	0.03
cats	0.0780	0.26	cats	9.0 ± 1.9	749 ± 49	0.57	1.28	0.86	0.49
an	0.8700	0.05	an	10.1 ± 1.6	765 ± 46	0.45	1.31	0.38	0.05
ab	0.2400	0.17	ab	9.6 ± 1.6	776 ± 49	0.31	1.28	–0.7	0.19
tr	0.0480	0.37	tr	10.2 ± 1.7	773 ± 51	0.54	1.31	0.56	0.23
fact	0.0002	1.03	fact	9.7 ± 1.5	758 ± 45	0.45	1.27	–1.2	0.02
ts	0.0021	0.71	ts	10.1 ± 1.4	755 ± 42	0.42	1.2	–1.7	0.08
parg	0.0466	0.34	parg	10.0 ± 1.5	756 ± 46	0.41	1.29	–0.9	0.09
gl	0.0012	0.56	gl	9.4 ± 1.4	783 ± 42	0.36	1.14	1.77	0.21
phl	0.0990	0.28	phl	9.9 ± 1.6	762 ± 46	0.44	1.32	0.32	0.02
ann	0.0260	0.45	ann	9.9 ± 1.5	765 ± 46	0.45	1.3	0.72	0.01
east	0.0135	0.47	east	10.1 ± 1.5	764 ± 44	0.45	1.25	–1.3	0.05
			q	9.8 ± 1.6	763 ± 46	0.45	1.33	0.00	0.00
			H ₂ O	9.8 ± 1.6	763 ± 46	0.45	1.33	0.00	0.00
				T = 763 ± 46 °C		cor = 0.45			
				P = 9.8 ± 1.6 kbars		sigfit = 1.33			
Calculations for the independent set of reactions			Average PT (for $a(\text{H}_2\text{O}) = 0.5$)						
For 95% confidence fit sigfit < 1.39			Single endmembers diagnostic information						
			P (kbars)	T (°C)	cor	fit	e^*	hat	
en	9.9 ± 1.7	786 ± 64	0.39	1.35	0.68	0.32			
fs	10.0 ± 1.8	810 ± 54	0.45	1.39	–0.04	0.01			
mgts	10.2 ± 1.8	816 ± 55	0.48	1.37	–0.72	0.09			
di	10.0 ± 1.8	814 ± 56	0.47	1.39	–0.32	0.06			
hed	9.9 ± 1.8	807 ± 54	0.46	1.38	0.37	0.03			
cats	9.2 ± 2.2	797 ± 58	0.57	1.36	0.71	0.50			
an	10.3 ± 1.8	813 ± 53	0.45	1.37	0.44	0.05			
ab	9.6 ± 1.7	827 ± 56	0.31	1.34	–0.75	0.19			
tr	10.2 ± 1.9	818 ± 60	0.54	1.38	0.40	0.23			
fact	9.8 ± 1.7	803 ± 51	0.45	1.31	–1.47	0.02			
ts	10.3 ± 1.6	802 ± 49	0.42	1.26	–1.77	0.08			
parg	10.1 ± 1.7	802 ± 53	0.41	1.34	–1.02	0.09			
gl	9.4 ± 1.5	836 ± 47	0.35	1.15	2.04	0.22			
phl	10.0 ± 1.8	809 ± 54	0.44	1.38	0.33	0.02			
ann	10.0 ± 1.7	812 ± 53	0.45	1.37	0.66	0.01			
east	10.3 ± 1.7	812 ± 51	0.45	1.32	–1.24	0.04			
q	10.0 ± 1.8	810 ± 54	0.45	1.39	0.00	0.00			
H ₂ O	10.0 ± 1.8	810 ± 54	0.45	1.39	0.00	0.00			
	T = 810 ± 54 °C		cor = 0.45						
	P = 10 ± 1.7 kbars		sigfit = 1.39						
Average PT (for $a(\text{H}_2\text{O}) = 0.8$)			Single endmembers diagnostic information						
			P (kbars)	T (°C)	cor	fit	e^*	Hat	
en	10.0 ± 1.9	830 ± 75	0.38	1.47	0.71	0.32			
fs	10.1 ± 2.0	857 ± 63	0.44	1.51	0.13	0.01			
mgts	10.3 ± 2.0	865 ± 64	0.48	1.49	–0.82	0.09			
di	10.1 ± 2.0	859 ± 66	0.47	1.51	–0.13	0.06			
hed	10.0 ± 2.0	855 ± 64	0.46	1.51	0.33	0.03			
cats	9.4 ± 2.5	846 ± 68	0.57	1.49	0.58	0.50			
an	10.5 ± 2.1	861 ± 62	0.45	1.48	0.50	0.05			
ab	9.6 ± 2.0	877 ± 65	0.30	1.45	–0.84	0.19			
tr	10.2 ± 2.1	864 ± 70	0.54	1.51	0.27	0.23			
fact	9.9 ± 1.8	849 ± 59	0.45	1.41	–1.70	0.02			
ts	10.4 ± 1.8	848 ± 58	0.42	1.38	–1.84	0.09			
parg	10.2 ± 1.9	848 ± 61	0.41	1.45	–1.17	0.08			
gl	9.3 ± 1.6	890 ± 53	0.35	1.22	2.30	0.22			
phl	10.1 ± 2.0	857 ± 63	0.44	1.50	0.34	0.02			
ann	10.1 ± 1.9	860 ± 63	0.45	1.50	0.60	0.01			
east	10.3 ± 1.9	859 ± 61	0.44	1.45	–1.19	0.04			
q	10.0 ± 2.0	857 ± 63	0.45	1.51	0.00	0.00			
H ₂ O	10.0 ± 2.0	857 ± 63	0.45	1.51	0.00	0.00			
	T = 857 ± 63 °C		cor = 0.45						
	P = 10 ± 2 kbars		sigfit = 1.51						

Abbreviations: en = orthoenstatite, fs = orthoferrosilite and mgts = Mg-tschermakite for orthopyroxene; di = diopside, hed = hedenbergite and cats = Ca-tschermakite for clinopyroxene; an = anorthite, and ab = albite for plagioclase; tr = tremolite, (fact) = ferro-actinolite, (tsc) = tschermakite, parg = pargasite and gl = glaucophane for amphibole; phl = phlogopite, ann = annite and east = eastonite for biotite and q = quartz. End-members activities and default uncertainties are presented. Descriptions of the following statistical parameters: cor (correlation), fit (fitness), hat (degree of influence of the endmember) and e^* (residuals = observed minus of activity values; cutoff for $e^* > 2.5$) are given in Powell and Holland (1994).



tschermakite (tsc), pargasite (parg) and glaucophane (gl) for amphibole; phlogopite (phl), annite (ann) and eastonite (east) for biotite, and quartz (q). This assemblage of end members allows for the use of 10 different linearly independent reactions in constraining the P – T conditions of equilibrium. The average P – T estimates obtained from this set of reactions (Table 2) are only slightly sensitive to water activity. However, given the high-grade assemblage and the lack of macroscopic evidence of anatexis in the sample, an $a(\text{H}_2\text{O})$ value <1 can be assumed. Estimated P – T conditions of equilibration vary from 9.8 ± 1.6 kbars and 763 ± 46 °C (2σ) for $a(\text{H}_2\text{O}) = 0.3$ to 10.0 ± 1.7 kbars, 810 ± 54 °C for $a(\text{H}_2\text{O}) = 0.5$ (2σ) and 11.0 ± 1.7 kbars, 857 ± 63 °C (1σ) for $a(\text{H}_2\text{O}) = 0.8$. Thus, this rock records a metamorphic event at the base of the crust and at temperatures that are broadly consistent, within error, with those of biotite fluid-absent melting in metapelites (e.g. Vielzeuf and Schmidt, 2001).

7. Constraining the conditions of formation for garnet in the CGS

The role played by peritectic garnet entrainment in the CGS S-type rocks, combined with the fact that garnet is present in some rocks, indicates that it is likely that garnet has been present through most of the magmatic evolution of the more mafic varieties of granite. This garnet may be peritectic or magmatic. The unzoned interiors of the garnet crystals, as well as the fact that all garnet core domains within the CGS are essentially identical in composition, indicates that the garnet composition has been homogenised at some stage, most likely by equilibrating with the magma at high temperature. Thus, the magma compositions can be used to constrain the conditions of formation for the different zones of the garnet crystals.

Conventional partitioning-based thermobarometry would be difficult to apply to the assemblages in the CGS granites. The zoning pattern in the garnets suggests changes in conditions of formation between the relatively Mn-poor core and the narrow Mn-rich rim. Furthermore, garnet is almost ubiquitously partially replaced by cordierite and biotite. However, cordierite in this assemblage is generally severely pinnitised, making its original composition difficult to determine. The garnet rims may record equilibration during the relatively late growth of biotite and cordierite, but evaluating this is problematic due to the lack of information on the cordierite composition. Alternatively, the rims might record earlier equilibration, with subsequent reaction to form biotite and cordierite without the preservation of an equilibrated garnet composition. In addition, the core regions of the garnet crystals are devoid of higher-temperature mineral inclusions, so a thermobarometric approach to estimating conditions of formation of the cores would be impossible. Despite these limitations, using the rationale outlined above, a thermodynamic approach can still be taken towards modelling garnet stability in the high-temperature system through the use of pseudosections. This requires the assumption that the major element composition of the rock can be assumed to reflect the composition of the magmatic system in which garnet equilibrated. Clearly, mechanical segregation of garnet challenges this, as the resultant garnet-rich or garnet- and xenolith-rich domains may not accurately reflect the composition of the system from which garnet crystallised. Consequently, this study has chosen to model garnet stability in a spectrum of granite compositions considered to be representative of the entire S-type CGS. The bulk compositions used include some that now lack garnet. However, the deviation of the bulk compositions of these rocks from those of experimentally derived granitic melts formed through biotite fluid-

absent melting (Stevens et al., 2007) indicates that they originally contained garnet, which has since been replaced by other ferromagnesian minerals during magma ascent and crystallization. This is further supported by the common occurrence of rounded clots of biotite in these granites, which are interpreted as pseudomorphs after garnet.

Three granite compositions were used to model the P – T stability domains of the garnet compositions, with the results shown in Figs. 8 and 9. All three are peraluminous (A/CNK from 1.22 to 1.27) and comprise a granite and two granodiorites (SiO_2 from 64.06 to 69.93 wt.%). One of the samples used for modelling is a garnet-bearing granodiorite (DG20) and has a relatively high Mg# (45) and MnO content (0.1 wt.%). The other samples, BB08 (Cape Granite) and BB11 (Cape Granodiorite) are not garnet-bearing, have lower FeO + MgO (5.18 and 9.43 wt.% respectively), lower MnO (0.06 and 0.07 wt.%) and slightly lower Mg# (40 and 43 respectively). Thus, these rocks cover a substantial part of the range of compositions that exists within the S-type CGS (Schoch, 1975; Scheepers, 1995; Stevens et al., 2007). Garnet compositions for the core and rim zones are typically $\text{Alm}_{69-71}\text{Py}_{14-21}\text{Gr}_{0.3}\text{Sps}_{3-5}$ and $\text{Alm}_{70-76}\text{Py}_{5-12}\text{Gr}_{0.3}\text{Sps}_{6-12}$ respectively. The fields of P – T stability for these garnet compositions within the three whole-rock compositions discussed above were mapped onto pseudosections using the software program PERPLEX (Connolly, 1990; Connolly and Petrini, 2002; Connolly, 2005) which used an updated (2002, unpublished) version of the Holland and Powell (1998) thermodynamic dataset. The pseudosections were constructed between 2 to 12 kbar and from 600 to 1000 °C (Figs. 8 top and 9). The whole-rock H_2O content values used vary between 4.43 and 4.77 wt.% (Figs. 8 top and 9) and have been chosen such that the field of melt H_2O saturation is restricted to a relatively narrow band above the solidus and that the melts are H_2O under-saturated at the proposed high-pressure, high-temperature conditions in the source during partial melting. The width of the band of melt-water coexistence is typically 20 to 25 °C wide. Fig. 8 (bottom) includes a plot of garnet mode as a function of temperature and H_2O content of the system (from 0 to 10 wt.%) at 5 kbar. This diagram illustrates that garnet stability is relatively insensitive to H_2O content in the temperature interval from 720 to 900 °C, as within this range the modelled system always contains garnet. At the water contents selected for the calculation of pseudosections, the rock compositions modelled in this study consist predominantly of melt (60 to 64 wt.%) and garnet (14 to 23 wt.%) at a temperature typical for fluid absent biotite melting (850 °C) and at the maximum pressure recorded in the CGS xenoliths (10 kb) (Fig. 10).

Isopleth plots of the minimum and maximum X_{Mg} , X_{Mn} and X_{Ca} values measured in the core and rim zones of the CGS garnets are superimposed over the pseudosections (Figs. 8 and 9). Given the very high degree of chemical homogeneity in the garnet grains, these plots are considered to reliably reflect the conditions of equilibration of the two chemical domains within garnet in these magmas (Figs. 8 and 9). From the pseudosections it appears that garnet would have been stable in the granitic magma over almost all the P – T field above the solidus, in each of the 3 compositions. The only area where no garnet would coexist with melt is a region (up to 70 °C wide), extending from the solidus to higher temperature, at pressures below 4 kbar. In this area, cordierite and biotite are the only ferromagnesian minerals that co-exist with melt. The stability fields of the measured garnet compositions overlap with those of the assemblages that are inferred to have co-existed with garnet i.e. melt + biotite + plagioclase + quartz + cordierite. The upper and lower

Fig. 8. The pseudosection calculated for the DG20 granodiorite (Top) composition using Perplex (Connolly, 1990; Connolly and Petrini, 2002; Connolly, 2005). Solid solution models used to establish this pseudosection are: Bio(HP) and Pheng(HP) (Powell and Holland, 1999); Gt(HP) (Holland and Powell, 1998), Opx(HP), melt(HP) (Holland and Powell, 2001; White et al., 2001); hCrd; Ksp (Thompson and Hovis, 1979) and Pl(h) (Newton et al., 1980). Compositions used for modelling are given in wt.%. Garnet stability modelling is overlain on the pseudosections and represents the calculated P – T conditions of isopleths of garnet composition which bracket the measured core and rim compositions respectively for spessartine, grossular and pyrope. The plotted garnet stability fields include phase stability considerations and so are not propagated into the adjacent opx- and sillimanite-bearing fields, as these assemblages are not recorded in the granitoids. The TX section indicates the mode of garnet in composition DG20 as a function of temperature and water content. Note that within a temperature band which brackets likely biotite incongruent melting temperatures, garnet is always relatively abundant (>5%). Abbrev.: bi = biotite; gt = garnet; pl = plagioclase; kf = K feldspar; mu = muscovite; sill = sillimanite; opx = orthopyroxene; ky = kyanite; cd = cordierite; q = quartz. (a) represents near solidus K-feldspar-bearing assemblages.

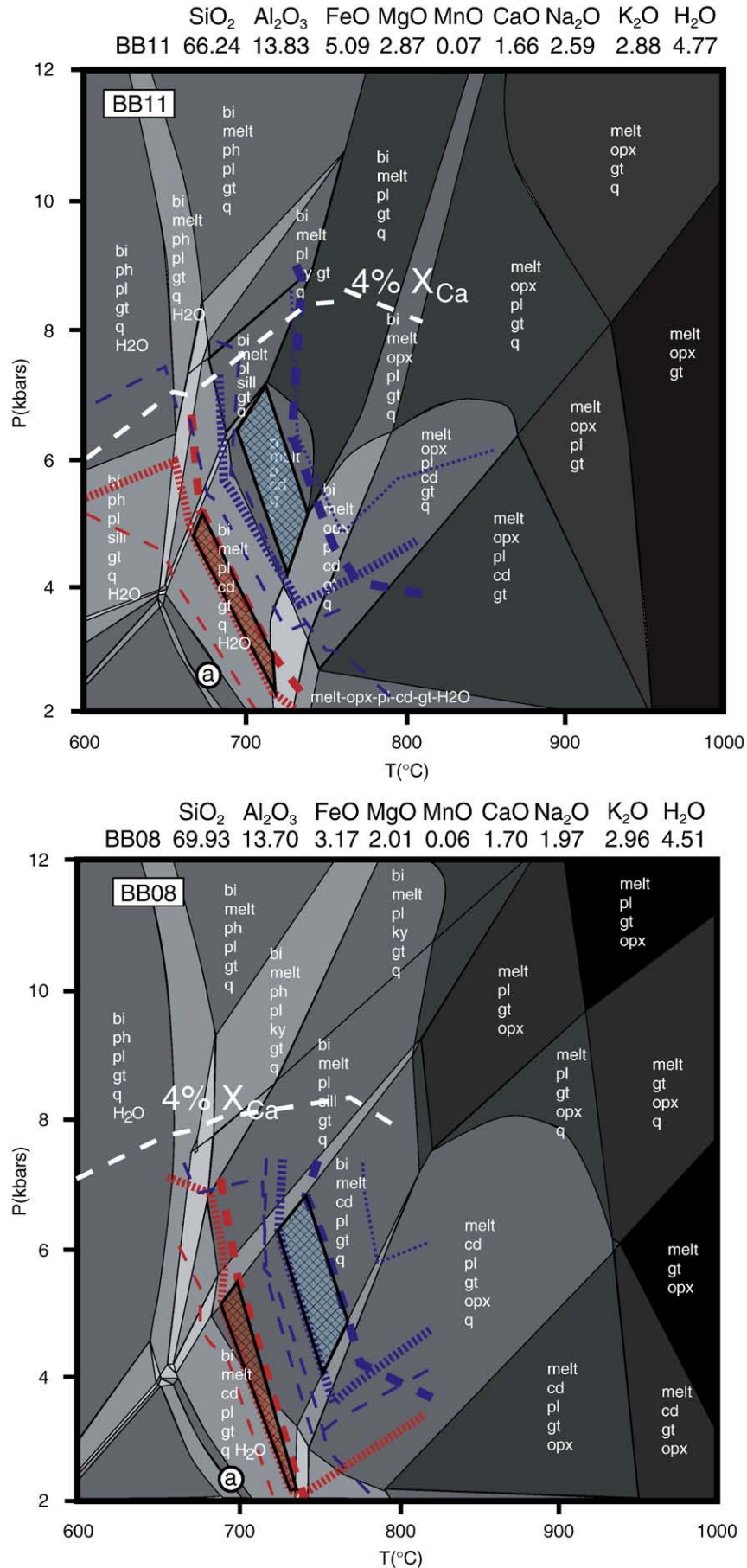


Fig. 9. The pseudosection calculated for the BB11 (top) and BB08 (bottom) granitoids compositions using Perplex. Legend and abbreviations are the same than in Fig. 8.

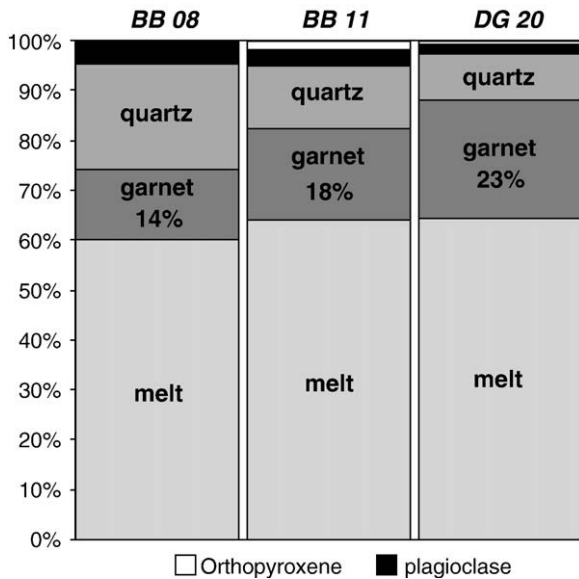


Fig. 10. Mineral proportions extracted from pseudosections calculated in Fig. 8 at 850 °C and 10 kbars.

pressure limits of both the core and rim fields of possible equilibration are restricted by sillimanite- and orthopyroxene-present fields, respectively. These minerals have not been observed in the CGS. Interestingly, major-element compositional variation, within the range exhibited by the CGS S-type granites, does not significantly affect the range of pressure and temperature stability of the observed garnet compositions. This is consistent with the extremely narrow range of compositions displayed by the natural garnets. The garnet-bearing sample (DG20, Fig. 8 top) gives conditions of equilibration for garnet cores from 740 to 760 °C and 3 to 5.2 kbars, with rim formation at 690 to 740 °C and 2.5 to 4.5 kbars. Samples BB08 and BB11 (Fig. 9) that do not contain garnet, but record textural evidence for its prior existence, provide similar estimates for the P – T stability fields represented by these garnet compositions i.e. from 4 to 6.5 kbars and 730 to 760 °C for the cores, and 3 to 5 kbars and 690 to 730 °C for the rims. In these compositions, where the more leucocratic character would have translated into a lower modal garnet abundance, garnet has been completely replaced by biotite and cordierite in the narrow band above the low-pressure solidus where garnet and melt do not coexist.

8. Origin of garnet in the granites

The pseudosections presented in Figs. 8 and 9 suggest that the CGS S-type granites contained garnet for (almost) all of their ascent history. Increasing the H_2O content of the system reduces the number of phases modelled as coexisting with melt in the high-temperature, high-pressure assemblages, reducing the modes of quartz, plagioclase and K-feldspar. However, this does not significantly reduce the mode of garnet. Thus, as suggested by Stevens et al. (2007) it appears that these commonly occurring granite compositions cannot represent pure melts and must, even at source conditions have been mixtures consisting predominantly of melt and garnet (Fig. 10). As garnet is likely to have been the dominant peritectic product of biotite incongruent melting, this finding appears to be compatible with the suggestion based on geochemistry of the CGS S-type suite, that the granites represent mixtures of melt and the peritectic assemblage (Stevens et al., 2007). The exact composition of the peritectic garnet relevant to the granites cannot be calculated because the specific source composition is unknown. Based on experimental evidence collated from other studies, Stevens et al. (2007) suggested a garnet composition of $Alm_{62}Py_{28}Gro_{9}Sps_{<1}$ as a proxy for CGS S-type peritectic garnet. The modelling in this study suggests that magmatic

garnet composition in the most mafic granite, following source separation but at the P – T conditions of the source would have been very different to $Alm_{48.2}Py_{43.1}Gro_{7.6}Sps_{1.1}$. However, whether the starting point for garnet compositional change should be regarded as the peritectic composition or the near-source magmatic composition is immaterial as both these compositions are very different from the relatively low-pressure garnet compositions present in the granites. Thus, the garnet observed in these granites has undergone significant chemical change to re-equilibrate with the magmatic environment during ascent. The possibility that this has occurred by self-diffusion can be tested using the Carlson (2006) diffusivity data for Fe, Mg, Ca and in garnet. Self-diffusion depends mainly on P , T and the initial garnet composition, with oxygen fugacity exerting a lesser influence. Considering the absence of Fe(III) in the garnet compositions measured in this study, we assume reducing conditions with fO_2 close to that imposed by the $C + O_2 = CO_2$ buffer. Assuming garnet to be a spherical body of defined size with no defects nor cracks, within an infinite reservoir of relevant chemical components (i.e. no matrix diffusion limitations), the time necessary to form the observed core compositions through self-diffusion from the peritectic composition proposed by Stevens et al. (2007) can be determined from the diffusion rates measured by Carlson (2006). The time (t) necessary for an element to diffuse through a distance (x) in a sphere of radius (r) can be determined using the equation of Crank (1975) ($t = x^2 \times t' / D$), where D is the diffusion rate (m^2/s) and t' is a dimensionless time parameter = 0.4 for a sphere ($x = r$) and $t' = 0.03$ for a hollow sphere ($x < r$). The radius of the garnets in the S-type CGS rocks varies from 2×10^{-3} to 1×10^{-2} m in diameter. Diffusivities for Fe, Mg, Ca and Mn differ by several orders of magnitude at a given temperature (Yardley, 1977; Schwandt et al., 1995). Thus, the time necessary to compositionally re-equilibrate garnet by self-diffusion is controlled by the time needed to re-equilibrate the cation with the lowest diffusivity. In this case, the slowest diffusing component is Ca which has to vary from the 9 mol% grossular in the proposed peritectic garnet down to 5 mol% grossular in the cores of the CGS garnet. Using the diffusivities

Table 3

Garnet self-diffusion modelling using the Fe, Mg, Ca and Mn diffusivities of Carlson (2006).

		$t' = 0.4$	X(Alm)	X(Pyrr)	X(Sps)	X(Gro)
Grt composition			0.62	0.28	0.01	0.09
850 °C/10 kbars	r (m)	Fe	Mg	Mn	Ca	
	0.001	1.07E+06	1.23E+06	1.04E+06	3.95E+06	
	0.002	4.29E+06	4.92E+06	4.16E+06	1.58E+07	
	0.005	2.68E+07	3.07E+07	2.60E+07	9.88E+07	
	0.01	1.07E+08	1.23E+08	1.04E+08	3.95E+08	
	0.02	4.29E+08	4.92E+08	4.16E+08	1.58E+09	
Grt composition		$t' = 0.4$	X(Alm)	X(Pyrr)	X(Sps)	X(Gro)
			0.62	0.28	0.01	0.09
750 °C/5 kbars	r (m)	Fe	Mg	Mn	Ca	
	0.001	1.70E+07	1.57E+07	1.64E+07	4.39E+07	
	0.002	6.78E+07	6.29E+07	6.57E+07	1.75E+08	
	0.005	4.24E+08	3.93E+08	4.11E+08	1.10E+09	
	0.01	1.70E+09	1.57E+09	1.64E+09	4.39E+09	
	0.02	6.78E+09	6.29E+09	6.57E+09	1.75E+10	
Grt composition		$t' = 0.003$	X(Alm)	X(Pyrr)	X(Sps)	X(Gro)
			0.70	0.20	0.05	0.05
750 °C/5 kbars	r (m)	Fe	Mg	Mn	Ca	
	0.001	6.26E+05	5.14E+05	6.06E+05	1.32E+06	
	0.002	2.50E+06	2.05E+06	2.42E+06	5.28E+06	
	0.005	1.56E+07	1.28E+07	1.51E+07	3.30E+07	
	0.01	6.26E+07	5.14E+07	6.06E+07	1.32E+08	
	0.02	2.50E+08	2.05E+08	2.42E+08	5.28E+08	

The first section of the table indicates the time in years for the measured core compositions to be established in a crystal of 1 cm radius from the experimentally constrained peritectic composition proposed by Stevens et al. (2007). The second section indicates the time taken for a rim of (100 μ m) thickness with the composition of the garnet rims measured in this study to be developed from the core composition.

the case of almandine garnet ($\sim 118 \text{ cm}^3/\text{mol}$ at 800°C , data from Skinner, 1956), dissolution of a 1 cm diameter garnet in a convecting magmatic system could be achieved within the time scale of days. Crystal growth rates in magmatic systems are also fast and are proposed to be of the order of 10^{-10} to $10^{-11} \text{ cm s}^{-1}$ (Hawkesworth et al., 2000) which means that a 1 cm crystal would take 10^2 and 10^3 years to grow, compatible with the duration of magmatic events discussed above. Consequently, a dissolution–precipitation process is proposed for the cycling of the garnet through the melt to keep it in equilibrium with the changing magmatic conditions. A partial dissolution–recrystallisation process has been proposed for garnet in the Violet Town volcanics of the Lachlan Fold Belt by Clemens and Wall (1984), who highlighted the coexistence of different garnet generations in the magmas. At some point in the crystallization sequence it is likely that decreasing melt volume and temperature will begin to impinge on the viability of this process, and the late rims on the CGS garnets may reflect this stage where the energy in the system became insufficient to propagate the process. The increase in Mn concentration within the garnet rim zones is probably indicative of garnet resorption, as the garnet mode decreases in accordance with conditions approaching the solidus. The higher HREE contents of the rim zones most likely also reflect this process. These domains have also a more pronounced Eu anomaly indicating an equilibration of garnet with the magma following the crystallisation of a significant proportion of plagioclase. Although the diffusion rates determined here are estimates that might be reduced by the presence of cracks or defects in the precursor garnet, the very substantial difference between the time necessary for garnet homogenisation by diffusion and the relatively short time proposed for magmatic processes argues strongly in favour of the proposed dissolution–precipitation mechanism. The fact that the garnets are devoid of true inclusions is in agreement with this.

9.3. Implications for S-type magma evolution

Average S-type CGS compositions are too mafic to represent melts (Stevens et al., 2007). The compositional trends defined by the suite are characterised by increasing A/CNK and decreasing K_2O as a function of $\text{FeO} + \text{MgO}$ content of the magmas. The major-element evolution trends of the suite, viewed as a function of the $\text{FeO} + \text{MgO}$ content of the magmas, follow trends consistent with the most leucocratic compositions (the first third of the dataset published by Stevens et al., 2007) representing melts, and the remainder representing mixtures of melt and peritectic garnet. The pseudosections presented in Figs. 8 and 9 support these findings. In these compositions, garnet will be present in the magma, even at very high temperatures, and clearly forms part of the magma segregated from the source. This even applies to compositions such as BB08 that are no less leucocratic than the majority of the CGS S-type rocks. Clemens and Wall (1984) highlighted the fact that H_2O -undersaturated magmas ascending along adiabatic paths have a high capacity to dissolve entrained material, principally due to the positive dP/dT slopes of mineral saturation boundaries. This is so if the entrained material can dissolve to produce roughly granitic liquid (some types of xenoliths for example). However, the modelling presented here indicates that this is unlikely to be the case for an individual restitic contaminant entrained in reasonably high volume. The fundamental reason for this is that the experimental melt compositions on which the melt models are based simply never become rich enough in the ferromagnesian component to digest the entrained phase. The net result is that the granites in question probably contained garnet throughout much of their magmatic history. However, as garnet composition is sensitive to P – T conditions, decompression via magma ascent must drive compositional change in garnet. In metamorphic rocks, where such change depends on solid-state or solid–fluid diffusion, high-pressure compositions are commonly “locked in”. In contrast, in the magmatic system, the dissolution–precipitation mechanism appears to have been extremely efficient in homogenising garnet compositions until shortly prior to crystallization. To some degree, this makes the debate on the origin of

garnet in S-type granites meaningless. If an efficient process exists to equilibrate any entrained garnet to the magmatic conditions, garnet of any origin would exhibit the same magmatic characteristics, despite the fact that the garnet fraction had never been completely dissolved in the melt.

This proposed dissolution–precipitation cycling of garnet through the magma, in order to achieve magmatic equilibrium, explains the fact that garnet with a peritectic geochemical signature and possibly metamorphic mineral inclusions is extremely rare in granites, even where a strong case can be made for the entrainment of garnet from the source. The results of this work are relevant to the petrogenesis of S-type granites, in general, in that they predict that components inherited from the source, but insoluble in the melt, will achieve equilibrium with the magmatic system within the relatively short time scales of magmatic events. This effectively masks the inheritance in such magmas. Additionally, the study highlights the usefulness of a compositionally appropriate phase stability modelling approach to understanding granite petrogenesis.

Granites have an obvious chemical connectedness with their sources (Clemens, 2003). In using the I and S nomenclature we work from this premise. Despite the reasonably general acceptance of this, the specific nature of connection has remained extremely elusive. This study proposes that collectively, the processes of peritectic phase entrainment, dissolution–crystallization re-equilibration and the later magmatic hydration of high-temperature ferromagnesian silicates in granites, as the solidus is approached, explain this connection as well as why the details of the process have remained so difficult to detect.

Acknowledgments

Dave Waters and an anonymous reviewer are thanked for their very helpful comments. The manuscript benefited from the discussions with J.-F. Moyen and John Clemens; the latter also provided a very helpful earlier informal manuscript review. This work forms part of a PhD study by AV. AV gratefully acknowledges an NRF PhD Bursary and support for the study via NRF grant funding to GS. ISB acknowledges the support from an ARC Australian Professorial Fellowship and Discovery Grant DP0342473.

References

- Armstrong, R.A., De Wit, M.J., Reid, D.L., York, D., Zattman, R., 1998. Table Mountain reveals rapid Pan-African uplift of its basement rocks. *Journal of African Earth Sciences* 27, 10–11.
- Ayres, M., Vance, D., 1997. A comparison study of diffusion profiles in Himalayan and Dalradian garnets: constraints on diffusion data and the relative duration of the metamorphic events. *Contributions to Mineralogy and Petrology* 128, 66–80.
- Ayres, M., Harris, N., Vance, D., 1997. Possible constraints on anatexis melt residence times from accessory mineral dissolution rates: an example from Himalayan leucogranites. *Mineralogical Magazine* 61, 29–36.
- Barbero, L., Villaseca, C., 1992. The Layos Granite, Hercynian Complex of Toledo (Spain) — an example of parautochthonous restite-rich granite in a granulitic area. *Transactions of the Royal Society of Edinburgh. Earth Sciences* 83, 127–138.
- Bea, F., Montero, P., Garuti, G., Zacharini, F., 1997. Pressure-dependence of rare earth element distribution in amphibolite- and granulite-grade garnets. A LA-ICP-MS study. *Geostandards Newsletter* 21, 253–270.
- Belcher, R.W., Kisters, A.F.M., 2003. Lithostratigraphic correlations in the western branch of the Pan-African Saldania Belt, South Africa: the Malmesbury Group revisited. *South African Journal of Geology* 106, 327–342.
- Cann, J.R., 1970. Upward movement of granitic magmas. *Geological Magazine* 43, 335–340.
- Carlson, W.D., 2006. Rates of Fe, Mg, Mn, and Ca diffusion in garnet. *American Mineralogist* 91, 1–11.
- Carrington, D.P., Harley, S.L., 1995. Partial melting and phase-relations in high-grade metapelites — an experimental petrogenetic grid in the KFMASH system. *Contributions to Mineralogy and Petrology* 120, 270–291.
- Cesare, B., Savioli Mariani, E., Venturelli, G., 1997. Crustal anatexis and melt extraction during deformation in the restitic xenoliths at El Joyazo (SE Spain). *Mineralogical Magazine* 61, 15–27.
- Chappell, B.W., 1984. Source rocks of I- and S-type granites in the Lachlan Fold Belt, southeastern Australia. *Philosophical Transactions of the Royal Society of London, Series A: Mathematical Physical and Engineering Sciences* 310, 693–707.
- Chappell, B.W., 1999. Aluminium saturation in I- and S-type granites and the characterization of fractionated haplogranites. *Lithos* 46, 535–551.
- Chappell, B.W., White, A.J.R., 1992. I-type and S-type granites in the Lachlan Fold Belt. *Transactions of the Royal Society of Edinburgh. Earth Sciences* 83, 1–26.

- Chappell, B.W., White, A.J.R., Wyborn, D., 1987. The importance of residual source material (restite). *Journal of Petrology* 28, 1111–1138.
- Clarke, D.B., 2007. Assimilation of xenocrysts in granitic magmas: principles, processes, proxies and problems. *Canadian Mineralogist* 45, 5–30.
- Clemens, J.D., 1992. Partial melting and granulite genesis — a partisan overview. *Precambrian Research* 55, 297–301.
- Clemens, J.D., 2003. S-type granitic magmas — petrogenetic issues, models and evidence. *Earth-Science Reviews* 61, 1–18.
- Clemens, J.D., Wall, V.J., 1981. Origin and crystallization of some peraluminous (S-type) granitic magmas. *Canadian Mineralogist* 19, 111–131.
- Clemens, J.D., Wall, V.J., 1984. Origin and evolution of a peraluminous silicic ignimbrite suite: the Violet Town volcanics. *Contributions to Mineralogy and Petrology* 88, 354–371.
- Clemens, J.D., Droop, G.T.R., 1998. Fluids, P-T paths and the fates of anatexic melts in the Earth's crust. *Lithos* 44, 21–36.
- Collins, W.J., Hobbs, B.E., 2001. What caused the Early Silurian change from mafic to silicic (S-type) magmatism in the eastern Lachlan Fold Belt? *Australian Journal of Earth Sciences* 48, 25–41.
- Connolly, J.A.D., 1990. Multivariable phase diagrams: an algorithm based on generalized thermodynamics. *American Journal of Science* 290, 666–718.
- Connolly, J.A.D., 2005. Computation of phase equilibria by linear programming: a tool for geodynamic modeling and its application to subduction zone decarbonation. *Earth and Planetary Sciences Letters* 236, 534–541.
- Connolly, J.A.D., Petrin, K., 2002. An automated strategy for calculation of phase diagram sections and retrieval of rock properties as a function of physical conditions. *Journal of Metamorphic Geology* 20, 697–708.
- Coulson, I.M., Villeneuve, M.E., Dipple, G.M., Duncan, R.A., Russell, J.K., Mortensen, J.K., 2002. Time-scales of assembly and thermal history of a composite felsic pluton: constraints from the Emerald Lake area, northern Canadian Cordillera, Yukon. *Journal of Volcanology and Geothermal Research* 114, 331–356.
- Crank, J., 1975. *The Mathematics of Diffusion*. Oxford University Press (Eds), Oxford, 414 pp.
- Dahlquist, J.A., Galindo, C., Pankhurst, R.J., Rapela, C.W., Alasino, P.H., Saavedra, J., Fanning, C.M., 2007. Magmatic evolution of the Penon Rosado Granite: petrogenesis of garnet-bearing granulites. *Lithos* 95, 177–207.
- Diener, J.F.A., Stevens, G., Kisters, A.F.M., Poujol, M., 2005. Metamorphism and exhumation of the basal parts of the Barberton greenstone belt, South Africa: constraining the rates of Mesoproterozoic tectonism. *Precambrian Research* 143, 87–112.
- Erdmann, S., London, D., Morgan, V.I., G.B., Clarke, D.B., 2007. The contamination of granitic magma by metasedimentary country-rock material: an experimental study. *Canadian Mineralogist* 45, 43–61.
- Escuder Viruete, J., Indares, A., Arenas, R., 2000. P-T paths derived from garnet growth zoning in an extensional setting: an example from the Tormes Gneiss Dome (Iberian Massif, Spain). *Journal of Petrology* 41, 1489–1515.
- Ferry, J.M., Spear, F.S., 1978. Experimental calibration of the partitioning of Fe and Mg between biotite and garnet. *Contributions to Mineralogy and Petrology* 66, 113–117.
- Flanagan, F.J., 1976. Descriptions and analysis of eight new USGS rock standards. United States Geological Survey Professional Paper 840, 192.
- Foden, J.D., Elburg, M.A., Turner, S.P., Sandiford, M., O'Callaghan, J., Mitchell, S., 2002. Granite production in the Delamerian Orogen, South Australia. *Journal of the Geological Society* 159, 557–575.
- Hacker, B.R., Gnos, E., Ratschbacher, L., Grove, M., McWilliams, M., Sobolev, S.V., Wan, J., Zhenhan, W., 2000. Hot and dry deep crustal xenoliths from Tibet. *Science* 287, 2463–2466.
- Harris, C., Faure, K., Diamond, R.E., Scheepers, R., 1997. Oxygen and hydrogen isotope geochemistry of S- and I- type granulites: the Cape Granite Suite, South Africa. *Chemical Geology* 143, 95–114.
- Harris, N., Vance, D., Ayres, M., 2000. From sediment to granite: timescales of anatexis in the upper crust. *Chemical Geology* 162, 155–167.
- Hartnady, C.J.H., Newton, A.R., Theron, J.N., 1974. The stratigraphy and structure of the Malmesbury Group in the southwestern Cape. *Bulletin of the Precambrian Research Unit* 15, 193–213.
- Hawkesworth, C.J., Blake, S., Evans, P., Hughes, R., Macdonald, R., Thomas, L.E., Turner, S.P., Zellmer, G., 2000. Time scales of crystal fractionation on magma chambers — integrating physical, isotopic and geochemical perspectives. *Journal of Petrology* 41, 991–1006.
- Hensen, B.J., 1977. Cordierite-garnet bearing assemblages as geothermometers and barometers in granulites facies terranes. *Tectonophysics* 43, 73–88.
- Hoisch, T.D., 1991. Equilibria with the mineral assemblage quartz + muscovite + biotite + garnet + plagioclase, and applications for the mixing properties of octahedrally-coordinated cations in muscovite and biotite. *Contributions to Mineralogy and Petrology* 108, 43–54.
- Holdaway, M.J., 2000. Application of new experimental and garnet Margules data to the garnet-biotite geothermometer. *American Mineralogist* 85, 881–892.
- Holland, T.J.B., Powell, R., 1998. An internally consistent thermodynamic data set for of petrological interest. *Journal of Metamorphic Geology* 16, 309–343.
- Holland, T., Powell, R., 2001. Calculation of phase relations involving haplogranitic melts using an internally consistent thermodynamic dataset. *Journal of Petrology* 42, 673–683.
- Hwang, S.L., Shen, P., Yui, T.F., Chu, H.T., 2003. On the mechanism of resorption zoning in metamorphic garnet. *Journal of Metamorphic Geology* 21, 761–769.
- Joordan, L.J., Scheepers, R., Barton, E.S., 1995. Geochemistry and isotopic composition of the mafic and intermediate igneous components of the Cape Granite Suite, South Africa. *Journal of African Earth Sciences* 21, 59–70.
- Kisters, A.F.M., et al., 2002. Timing and kinematics of the Colenso Fault: The Early Paleozoic shift from collisional to extensional tectonics in the Pan-African Saldania Belt, South Africa. *South African Journal of Geology* 105, 257–270.
- Lanzirotti, A., 1995. Yttrium zoning in metamorphic garnet. *Geochimica et Cosmochimica Acta* 59, 4105–4110.
- Le Breton, N., Thompson, A.B., 1988. Fluid-absent (dehydration) melting of biotite in metapelites in the early stages of crustal anatexis. *Contributions to Mineralogy and Petrology* 99, 226–237.
- Leake, B., Woolley, A.R., Arps, C.E.S., Birch, W.D., Gilbert, M.C., Grice, J.D., Hawthorne, F.C., Kato, A., Kisch, H.J., Krivovichev, V.G., Linthout, K., Laird, J., Mandarino, J.A., Maresch, W.V., Nickel, E.H., Rock, N.M.S., Schumacher, J.C., Smith, D.C., Stephenson, N.C.N., Ungaretti, L., Whittaker, E.J.W., Youzhi, G., 1998. Nomenclature of amphiboles: report of the Subcommittee on Amphiboles of the International Mineralogical Association, Commission on New Minerals and Mineral Names. *Canadian Mineralogist* 35, 219–246.
- Longerich, H.P., Jackson, S.E., Gunther, D., 1996. Laser ablation inductively coupled plasma mass spectrometric transient signal data acquisition and analyte concentration calculation. *Journal of Analytical Atomic Spectrometry* 11, 899–904.
- McLaren, S., Sandiford, M., Powell, R., Neumann, N., Woodhead, J., 2006. Palaeozoic intraplate crustal anatexis in the Mount Painter Province, South Australia: timing, thermal budgets and the role of crustal heat production. *Journal of Petrology* 47, 2281–2902.
- Montel, J.M., Vielzeuf, D., 1997. Partial melting of metagreywackes .2. Compositions of minerals and melts. *Contributions to Mineralogy and Petrology* 128, 176–196.
- Moyen, J.F., Stevens, G., Kisters, A., 2006. Record of mid-Archaean subduction from metamorphism in the Barberton terrain, South Africa. *Nature* 442, 559–562.
- Munksgaard, N.C., 1985. A non-magmatic origin for compositionally zoned euhedral garnet in silicic Neogene volcanics from SE Spain. *Neues Jahrbuch für Mineralogie Monatshefte* 73–82.
- Newton, R.C., Haselton, H.T., 1981. Thermodynamics of the garnet-plagioclase-Al₂SiO₅-quartz geobarometer. *Thermodynamics of Minerals and Melts*. Springer-Verlag.
- Newton, R.C., Charlu, T.V., Kleppa, O.J., 1980. Thermochemistry of the high structural state plagioclases. *Geochimica et Cosmochimica Acta* 44, 933–941.
- Patino-Douce, A.E., Beard, J.S., 1995. Dehydration-melting of biotite gneiss and quartz amphibolite from 3 to 15 kbar. *Journal of Petrology* 36, 707–738.
- Pearce, N.J.G., Perkins, W.T., Westgate, J.A., Gorton, M.P., Jackson, S.E., Mead, C.R., Chenery, S.P., 1997. A compilation of new and published major and trace element data for NIST SRM 610 and NIST SRM 612 glass reference materials. *Geostandards Newsletter* 21, 115–144.
- Petford, N., Cruden, A.R., McCaffrey, K.J.W., Vigneresse, J.L., 2000. Granite magma formation, transport and emplacement in the Earth's crust. *Nature* 408, 669–673.
- Powell, R., Holland, T.J.B., 1994. Optimal geothermometry and geobarometry. *American Mineralogist* 79, 120–133.
- Powell, R., Holland, T.J.B., 1999. Relating formulations of the thermodynamics of mineral solid solutions: activity modeling of pyroxenes, amphiboles, and micas. *American Mineralogist* 84, 1–14.
- Roedder, E., 1979. Origin and significance of magmatic inclusions. *Bulletin De Mineralogie* 109, 487–510.
- Roycroft, P.D., 1991. Magmatically zoned muscovite from the peraluminous two-mica granites of the Leinster batholith, southeast Ireland. *Geology* 19, 437–440.
- Rozendaal, A., Gresse, P.G., Scheepers, R., Le Roux, J.P., 1999. Neoproterozoic to early Cambrian crustal evolution of the Pan-African Saldania Belt, South Africa. *Precambrian Research* 97, 303–323.
- Scheepers, R., 1990. Magmatic association and radioelement geochemistry of selected Cape Granites with special reference to subalkaline and leucogranitic phases (In Afrikaans). Unpubl. Ph.D. dissertation, University of Stellenbosch, Stellenbosch, South Africa.
- Scheepers, R., 1995. Geology, geochemistry and petrogenesis of Late Precambrian S-, I- and A-type granulites in the Saldania Belt, Western Cape Province South Africa. *Journal of African Earth Sciences* 21, 35–58.
- Scheepers, R., 2000. Granites of the Saldania mobile belt, South Africa: radioelements and P as discriminators applied to metallogeny. *Journal of Geochemical Exploration* 68, 69–86.
- Scheepers, R., Nortje, A.N., 2000. Rhyolitic ignimbrites of the Cape Granite Suite, southwestern Cape Province, South Africa. *Journal of African Earth Sciences* 31, 647–656.
- Scheepers, R., Armstrong, R.A., 2002. New U-Pb SHRIMP zircon ages of the Cape Granite Suite: implications for the magmatic evolution of the Saldania Belt. *South African Journal of Geology* 105, 241–256.
- Scheepers, R., Poujol, M., 2002. U-Pb zircon age of Cape Granite Suite ignimbrites: characteristics of the last phases of the Saldanian magmatism. *South African Journal of Geology* 105, 163–178.
- Schoch, A.E., 1975. The Darling granite batholith. *Annals University Stellenbosch* A1, pp. 1–104.
- Schoch, A.E., Leterrier, J., De la Roche, H., 1977. Major element geochemical trends in the Cape granites. *Transactions of the Geological Society of South Africa* 80, 197–209.
- Schwandt, C.S., Cygan, R.T., Westrich, H.R., 1995. Mg self-diffusion in pyrope garnet. *American Mineralogist* 80, 483–490.
- Skinner, J., 1956. Physical properties of the garnet group. *American Mineralogist* 41, 428–436.
- Spicer, E.M., Stevens, G., Buick, I.S., 2004. The low-pressure partial-melting behaviour of natural boron-bearing metapelites from the Mt. Stafford area, central Australia. *Contributions to Mineralogy and Petrology* 148, 160–179.
- Stevens, G., Villaros, A., Moyen, J.F., 2007. Selective peritectic garnet entrainment as the origin of geochemical diversity in S-type granites. *Geology* 35, 9–12.
- Taylor, S.R., McLennan, S.M., 1985. *The continental crust: its composition and evolution*. Blackwell Scientific Pub., Palo Alto, CA, New York.
- Thompson, J.B., Hovis, G.L., 1979. Entropy of mixing in sanidine. *American Mineralogist* 64, 57–65.
- Vielzeuf, D., Montel, J.M., 1994. Partial melting of metagreywackes .1. Fluid-absent experiments and phase relationships. *Contributions to Mineralogy and Petrology* 117, 375–393.
- Vielzeuf, D., Schmidt, M.W., 2001. Melting relations in hydrous systems revisited: application to metapelites, metagreywackes and metabasalts. *Contributions to Mineralogy and Petrology* 141, 251–267.

- Walker, F., Mathias, M., 1946. The petrology of two granite-slate contacts at Cape Town, South Africa. *Quarterly Journal of the Geological Society* 102, 499–521.
- White, R.W., Powell, R., 2002. Melt loss and the preservation of granulite facies mineral assemblages. *Journal of Metamorphic Geology* 20 (7), 621–632.
- White, R.W., Powell, R., Holland, T.J.B., 2001. Calculation of partial melting equilibria in the system Na₂O–CaO–K₂O–FeO–MgO–Al₂O₃–SiO₂–H₂O (NCKFMASH). *Journal of Metamorphic Geology* 19, 139–153.
- Yardley, B.W.D., 1977. An empirical study of diffusion in garnet. *American Mineralogist* 62, 793–800.

Chapter 6

The trace element compositions of
S-type granites: Evidence for
disequilibrium melting and accessory
phases entrainment in the source

Presentation of the publication

This paper ¹, by Arnaud Villaros, has been published in Contributions to Mineralogy and Petrology. In this paper we studied the trace element variations in the Peninsular Pluton of the CGS. We explored these variations in the light of the entrainment of peritectic garnet. We modelled the composition of S-type melt and trace element variations have been modelled with the entrainment of accessory minerals in addition to garnet. Data acquisition and modelling were realised by Arnaud Villaros, data acquisition in collaboration with Gary Stevens and Ian Buick. Modelling was carried out by Arnaud Villaros in collaboration with J.-F. Moyen.

Arnaud Villaros

Gary Stevens

Jean-François Moyen

Ian S. Buick

Centre for Crustal Petrology

Department of Geology, Geography and Environmental Studies

Stellenbosch University, Private bag X1

Matieland, South Africa

¹Refer as: Villaros A., Stevens, G., Moyen, J.-F. and Buick I.S., 2009. The trace element compositions of S-type granites: Evidence for disequilibrium melting and accessory phase entrainment in the source. *Contrib. Mineral. Petrol.* 158:543-561, DOI : 10.1007/s00410-009-0396-3

The trace element compositions of S-type granites: evidence for disequilibrium melting and accessory phase entrainment in the source

Arnaud Villaros · Gary Stevens ·
Jean-François Moyen · Ian S. Buick

Received: 6 October 2008 / Accepted: 25 February 2009 / Published online: 24 March 2009
© Springer-Verlag 2009

Abstract Within individual plutons, the trace element concentrations in S-type granites generally increase with maficity (total iron and magnesium content and expressed as atomic Fe + Mg in this study); the degree of variability in trace element concentration also expands markedly with the same parameter. The strongly peraluminous, high-level S-type granites of the Peninsular Pluton (Cape Granite Suite, South Africa) are the product of biotite incongruent melting of a metasedimentary source near the base of the crust. Leucogranites within the suite represent close to pure melts from the anatectic source and more mafic varieties represent mixtures of melt and peritectic garnet and ilmenite. Trace elements such as Rb, Ba, Sr and Eu, that are concentrated in reactant minerals in the melting process, show considerable scatter within the granites. This is interpreted to reflect compositional variation in the source. In contrast, elements such as LREE, Zr and Hf, which are concentrated within refractory accessory phases (zircon and monazite), show well-defined negative correlations with increasing SiO₂ and increase linearly with increasing maficity. This is interpreted to reflect coupled co-entrainment of accessory minerals and peritectic phases to the melt: leucocratic rocks cannot have evolved from the more mafic compositions in the suite by a process of fractional crystallisation because in this case they

would have inherited the zircon-saturated character of this hypothetical earlier magma. Trace element behaviour of granites from the Peninsular Pluton has been modelled via both equilibrium and disequilibrium trace element melting. In the disequilibrium case, melts are modelled as leaving the source with variable proportions of entrained peritectic phases and accessory minerals, but before the melt has dissolved any accessory minerals. Thus, the trace element signature of the melt is largely inherited from the reactants in the melting reaction, with no contribution from zircon and monazite dissolution. In the equilibrium case, melt leaves the source with entrained crystals, after reaching zircon and monazite saturation. A significant proportion of the rocks of the Peninsular Pluton have trace element concentrations below those predicted by zircon and monazite saturation. In the case of the most leucocratic rocks all compositions are zircon undersaturated; whilst the majority of the most mafic compositions are zircon oversaturated. However, in both cases, zircon is commonly xenocrystic. Thus, the leucocratic rocks represent close to pure melts, which escaped their sources rapidly enough that some very closely match the trace element disequilibrium melting model applied in this study. Zircon dissolution rates allow the residency time for the melt in the source to be conservatively estimated at less than 500 years.

Communicated by T. L. Grove.

Electronic supplementary material The online version of this article (doi:10.1007/s00410-009-0396-3) contains supplementary material, which is available to authorized users.

A. Villaros (✉) · G. Stevens · J.-F. Moyen · I. S. Buick
Department of Geology, Geography and Environmental Studies,
Centre for Crustal Petrology, Stellenbosch University,
Private Bag X1, Matieland, South Africa
e-mail: arnaud.villaros@gmail.com

Keywords S-type granite · Trace element ·
Partial melting · Geochemical modelling ·
Accessory phases · Cape Granite Suite

Introduction

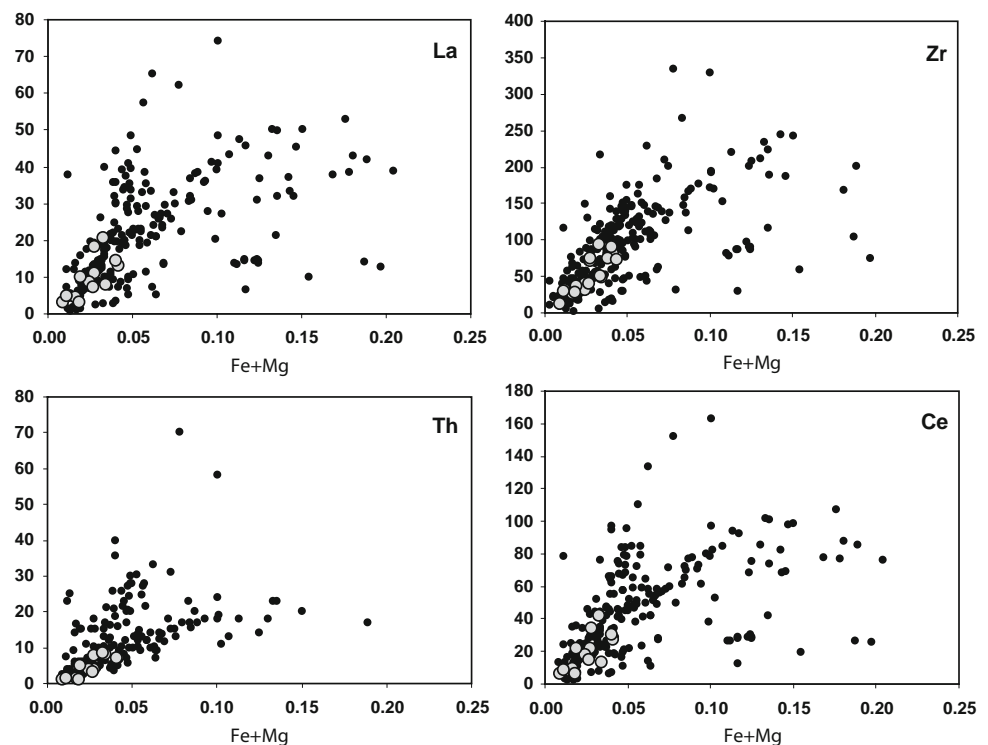
The relationship between S-type granites and their meta-sedimentary source rocks was established more than

30 years ago, principally on the basis of the major element compositions of the peraluminous granites of the Lachlan Fold Belt in eastern Australia (Chappell and White 1974; White and Chappell 1977; Chappell 1984). In these rocks, relatively high A/CNK ratios (>1.1), low sodium content ($\text{Na}_2\text{O} < 3.2$ wt%) and K/Na (molar) ratios in excess of 1, as well as Sr and O isotopic ratios consistent with their derivation from sediments were interpreted to reflect the melting of metasediments (S-type). Few studies have considered the relationship between S-type granites and their source rocks from the point of view of trace element compositions (e.g. Sylvester 1998). Where this approach has been followed, the studies have generally focused on small, near-source granitic bodies, where the anatectic zone can be observed and the trace element composition of the source is known (Sawyer 1991; Watt and Harley 1993; Harris et al. 1995; Bea 1996a; Jung et al. 1998; Johannes et al. 2003). Most trace elements display incompatible behaviour during magmatic processes (Rollinson 1993, p. 106). However, observations in the S-type leucogranites, and their source rocks referred to above, demonstrate that the granites are commonly depleted in REE and other “incompatible” elements such as Zr, Hf and Y, relative to what would be predicted from the source composition (Villaseca et al. 2007). Thus, these lower- to mid-crustal granites are interpreted to record trace element disequilibrium during partial melting that is related to the refractory behaviour of the accessory phases that constitute the dominant trace element reservoir in the source rock

(Nabelek and Glascock 1995; Bea 1996a, b; Ayres and Harris 1997; Bhadra et al. 2007; Villaseca et al. 2007): refractory minerals do not participate in the melting reactions and lock the largest part of the REE and HFSE budget in the source rock, such that the melting actually affects only the REE and HFSE-poor portion of the rock.

In contrast to some of the near-source granites discussed above, which may arise through low-temperature water-present melting (e.g. Ayres and Harris 1997), large volume S-type granites intruded at high levels in the crust, or their volcanic equivalents, are generally considered to be the product of fluid-absent melting of biotite-bearing assemblages in aluminous metasediments at temperatures of 850°C or higher (Vielzeuf and Holloway 1988; Patino-Douce and Johnston 1991; Vielzeuf and Montel 1994; Gardien et al. 1995; Clemens et al. 1997; Stevens et al. 1997). These granites commonly display a wide range of compositions from leucogranite to granodiorite (Chappell and White 1974; Chappell and White 1992; Collins and Hobbs 2001; Clemens 2003; Stevens et al. 2007). The trace element compositions of these rocks typically show a similarly wide range. However, trace element variation is coupled to the major element composition of the granites in two inter-related ways. First, for many elements, the scatter in concentration values increases as a function of maficity (Fig. 1). Secondly, most trace elements show a positive correlation with maficity (Fig. 1). This observation is supported by the findings of Elburg (1996), who observed that Zr in S-type granites increases as the granites become

Fig. 1 Atomic Fe + Mg versus trace element concentration (in ppm) diagram. *Black filled circles* represent samples from high level S-type plutons, *grey filled circles* represents the compositions of lower crustal leucogranites. The diagram represents a compilation of 397 published compositions from the following areas: Massif Central, France. (Downes et al. 1990; Williamson et al. 1996; Williamson et al. 1997; Solgadi et al. 2007), Brittany, France (Georget et al. 1986), Himalaya (Ayres and Harris 1997), central Spain (Bea et al. 2006), Lachlan Fold Belt, Australia (LFB Chappell and White 1992), Manitoba, Canada (Goad and Cerny 1981) and the Cape Granite Suite, South Africa (Scheepers 1995)



more mafic and Stevens et al. (2007), who noted a correlation between maficity and total HREE content in S-type granites of the Cape Granite Suite. The near-source leucogranites discussed earlier coincide in trace element composition with the most leucocratic and trace-element poor compositions of the high-level S-type suites.

Given the evidence presented above, it is interesting to consider the potential of trace element behaviour in S-type granites to provide information on the processes in the anatectic source. Several aspects of the granites appear to hold particular promise in this regard. In these rocks, some trace-elements are concentrated in minerals that commonly occur as xenocrysts. Zircon concentrates Zr, Hf and to a lesser degree Y and Yb, whilst xenocrystic monazite, which is reported in rare cases (e.g. Copeland et al. 1988; Parrish 1990) concentrates Ce and La. Other trace elements, such as Rb, Sr, Ba and Eu are concentrated within the minerals that are the major reactants in the melting reactions that produce the granites e.g. $Bt + Q + Pl + Sil = Grt + Melt$ (e.g. Vielzeuf and Montel 1994). Thus, some trace elements may be indicators of the melting reaction, whilst others may trace the degree of dissolution of accessory minerals in the source, as well as the entrainment of these minerals into the magma.

Experimental studies provide useful information on the melt compositions that are produced in the high-temperature fluid-absent anatectic sources of S-type granite magmas. They also provide information on the proportions and compositions of residual and peritectic phases produced during partial melting of likely source compositions. Stevens et al. (2007) used the melt compositions developed in such experiments, in combination with the range of natural rock compositions exhibited by the S-type magmas of the Cape Granite Suite to argue that the major element compositional variations in these granites can be accounted for by variable degrees of entrainment of peritectic phases into the melt. Thus, the general positive correlation between maficity and some trace elements may represent an alternative route to providing information about entrainment processes in the deep crustal source areas to granite magmas. However, the REE and HFSE concentrations of the melts that arise in these sources are not coupled to the stoichiometry of the melting reaction, but rather to the composition of the source and the degree of dissolution and entrainment of accessory minerals. These trace elements therefore present us with an opportunity to evaluate source processes independently from the major element approach. Importantly, as accessory phase dissolution is time dependent, there is possibly potential to constrain the time of residua-melt interaction.

In this study, we test these ideas by constructing a model for the trace element composition of the melts and magmas in the source area of the S-type granites of the Cape Granite Suite in South Africa. These high-level potassic granites

appear to have formed through fluid-absent biotite melting at a minimum of 850°C and 10 kbar (Stevens et al. 2007; Villaros et al. 2009). In this model, we consider two alternatives: (1) incongruent melting of biotite to produce a leucogranitic melt and a garnet-dominated peritectic assemblage where there is no equilibration of the melt with accessory phases prior to escaping the source [i.e. trace element disequilibrium melting (TEDM)]. In this case, all of the REE and HFSE remain trapped in accessory minerals; the melt itself is depleted in these elements. The composition of the resultant magmas are a function of the melt composition, the proportion of entrained peritectic assemblage (as per the model of Stevens et al. 2007) and the amounts and compositions of (un-reacted) zircon and monazite entrained to the magma. (2) An identical scenario, but with complete equilibration of the melt with the accessory mineral assemblage [trace element equilibrium melting (TEEM)] prior to segregation. In this case, the monazite and zircon dissolve, the melt is HFSE and REE richer, and the magma compositions are controlled by two parameters only, the melt composition and the entrained peritectic phases. The details of the modelling are presented below.

Geological setting of the Peninsular Pluton

The study focuses on the rocks of the Peninsular Pluton of the Cape Granite Suite of South Africa. The Cape Granite Suite (CGS) contains several plutons; the Peninsular Pluton is one of the least deformed and it contains co-magmatic varieties of granitoids ranging from granodiorite to leucogranite.

The Pan-African Cape Granite Suite was formed during the Saldanian Orogeny, as a consequence of the convergence of Rio de la Plata and Kalahari Cratons during Gondwana assembly (Fig. 2a). The plutons that form the suite intrude the greenschist-facies metasediments of the Malmesbury Group and consist of both S- and I-type granites (Scheepers 1995). The S-type plutons formed between 560 and 530 Ma (Da Silva et al. 2000; Scheepers and Armstrong 2002; Da Silva et al. 2005) and are slightly older than the I-type granites formed between 540 and 520 Ma (Da Silva et al. 2000; Scheepers and Armstrong 2002). The source of the S-type plutons of the CGS is commonly considered to be a higher grade equivalent of the Malmesbury Group metasediments (e.g. Harris et al. 1997) which the granites intrude and which occur as up to amphibolite-facies grade xenoliths within the granites. The S-type CGS consists of four major plutons (Darling, Saldanha, Stellenbosch and Peninsular), located to the south of the NW-SE trending Colenzo Fault (Fig. 2b). Of these plutons, the most southerly body, the Peninsular

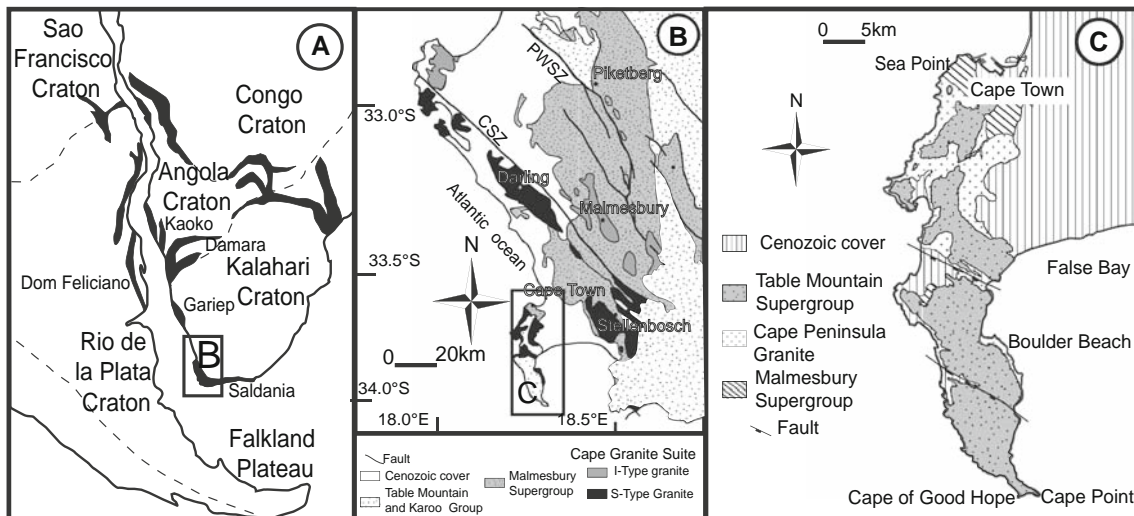


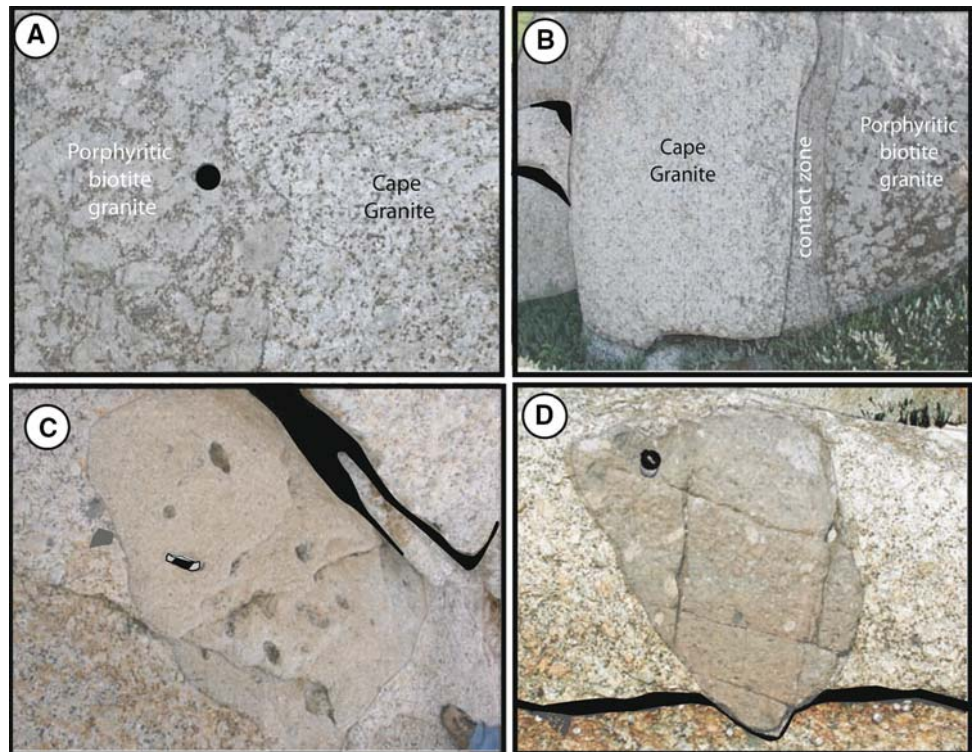
Fig. 2 a Palaeogeographic reconstitution of the Saldania orogen at 550 Ma (after Rozendaal et al. 1999). b Geological map illustrating the main plutons of the Cape Granite Suite (from Hartnady et al. 1974). c Geological map of the Peninsular Granite

Pluton is most suitable for this study in that it is essentially undeformed in the solid state, with very little alteration apart from very common pinitisation of cordierite. Furthermore, it contains rocks that record almost the full range of S-type CGS compositions, from leucogranitic to granodioritic. In this sense, apart from having a relatively high-K character, it could be considered to cover the major element compositional range that is typical for S-type granites. The Peninsular Pluton is generally cordierite rich, with rocks containing in excess of 10% cordierite being common. The cordierite is formed from the low-pressure conversion of high-P peritectic garnet entrained in the magma (Stevens et al. 2007; Villaros et al. 2009). Compositional variations are expressed in the proportions of biotite, cordierite, garnet and K-feldspar phenocrysts. Four main facies have been defined within the Peninsular Pluton (Schoch 1975; Schoch et al. 1977); a dominant leucocratic K-feldspar porphyritic granite (Cape Granite) and three minor, more mafic facies: a biotite-rich K-feldspar porphyritic granite (Biotite Porphyritic Granite), a biotite non-porphyritic granite (Biotite Granite) and a granodioritic facies (Cape Granodiorite). The contacts between the facies are generally steep to sub-vertical and diffuse over a 10–20 cm range (Fig. 3a, b). Within the peninsular pluton no sharp contacts have been observed between granite types other than between some magmatic enclaves and their hosts (Fig. 3c, d). There is no systematic layering within the pluton and boundaries between the facies cannot generally be followed for more than a few 10 s of metres. As a general observation, the Cape Granite constitutes the matrix of the Peninsular Pluton, within which the more mafic facies occur as domains elongated in the vertical dimension. The diffuse nature of the contacts between each

compositional facies emphasises the fact that the different components of the Peninsular Pluton are co-magmatic.

Stevens et al. (2007) investigated the origin of the major element geochemical diversity in the S-type CGS by using appropriate experimental melt compositions as a guide to the likely natural melt compositions. This study showed that melt compositions developed at temperatures less than 1,000°C from metapelitic and metapsammitic source rocks are always leucogranitic. Thus, this study proposed that the wide range in maficity observed in S-type granites is not the result of the evolution of melts of granodioritic or more mafic composition towards the leucocratic composition by fractionation. Similarly, it is not possible that moderately leucocratic “primitive” melt compositions produced the mafic rocks as crystal cumulates, with the most leucocratic granites then representing the residual liquids, as there is insufficient very leucocratic material to counterbalance the volume of relatively mafic granites. Consequently, Stevens et al. (2007) proposed that the granites left the source as a crystal contaminated magma and that the trends of increasing A/CNK, Ca, Mg# and Ti, and decreasing K and Si, as a function of total Fe + Mg, fit best with the mixing of melt and peritectic minerals (i.e. products of incongruent melting), together with the retention of the remaining un-melted mafic phases (“restites”) in the source region. In essence, this means that the granites represent mixtures of peritectic garnet, ilmenite and melt, with the addition of up to 20 wt% of the peritectic products being required as an adjunct in order to match the compositions of the most mafic S-type granites in the suite. Many of the granites proposed to have formed in this way no longer contain garnet due to the replacement of garnet by cordierite and biotite at higher levels within the magmatic system.

Fig. 3 Field relationships in the Peninsular Pluton. **a, b** illustrate the typically diffuse contacts between the different facies. **a** represents a plan view; **b** shows a vertical section through such a contact. The width of the field of view in **b** is about 3 m. **c, d** illustrate the sharp contacts displayed by magmatic enclaves as well as the texture of the microgranular magmatic enclave relative to the host Cape Granite



Villaros et al. (2009) have used a pseudosection modelling approach to investigate the origin of garnet in CGS S-type granites that are garnet-bearing, as well as the limits of garnet stability in garnet-free granites that are proposed to have contained garnet near the source. This study has demonstrated that all of the S-type CGS compositions investigated have garnet co-existing with melt at the pressure–temperature conditions of the source. The source conditions are estimated from rare granulite-facies metabasite xenoliths from the Darling batholith (Schoch 1975; Villaros et al. 2009), which record conditions of metamorphism of $P = 10 \pm 2$ kbar and $T = 850 \pm 56^\circ\text{C}$. These conditions are consistent with a biotite fluid-absent melting origin for the granite magmas, as proposed by Stevens et al. (2007). The study of Villaros et al. (2009) also demonstrated that garnet preserved within the CGS rocks has equilibrated, through a dissolution-precipitation process, at relatively low pressure within the magma chamber.

Geochemical data

Analytical methods

A suite of samples representative of compositional variation within the Peninsular Pluton was studied. These analysis have been supplemented by the existing database from Scheepers (1995) and Stevens et al. (2007), collectively this represents 43 rock compositions from within the Pluton.

Major element compositions have been obtained by XRF analysis on La-free glass beads (Phillip's PW1404w at Stellenbosch University), trace element compositions have been obtained from the same fused beads by applying the method described by Eggins (2003) and analysed using an Agilent 7500ce ICP-MS coupled with a Nd-YAG 223 nm New Wave LASER ablation (LA) system operating at a 12 Hz frequency with a mixed He-Ar carrier gas. Three analyses (each comprising a 30 s blank followed by data collection for 60 s) on each whole rock fused disc were obtained using a 100 μm diameter aperture, and the results averaged. After every three samples (i.e. every 10th analysis) a National Institute of Standards and Technology NIST612 (Pearce et al. 1997) glass bead was analysed as calibration standard, in addition to fused discs of Nim-G (granite) and BhVO-1 (basalt) as secondary standards. Data were collected in time-resolved mode and, were reduced using an Excel calculation spreadsheet using the SiO_2 content measured by XRF as the internal standard. For each element the reproducibility of replicate analyses of the samples, and deviation from the certified values of the secondary standards are better than 10%, and mostly below 5% relative.

Major element data

Major element compositional variation within the Peninsular Pluton is typical of K-rich peraluminous granitoids (Table S1) with SiO_2 content varying from 61.1 to

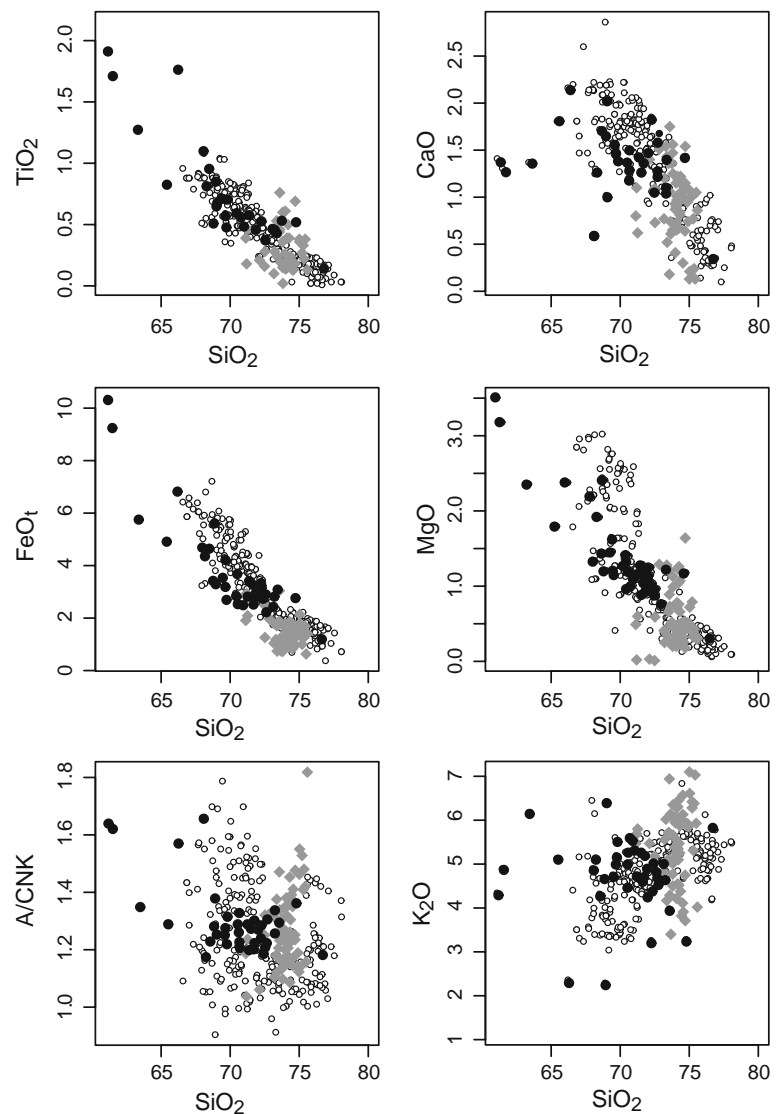
76.7 wt%; relatively high Al_2O_3 (12.9–17.1 wt%); and highly variable FeOt, MgO and TiO_2 (1.15–10.38, 0.32–3.5 and 0.14–1.91 wt%, respectively). A/CNK varies from 1.14 to 1.64 while X_{Mg} (molecular $\text{Mg}/(\text{Mg} + \text{Fe})$, all Fe as Fe^{2+}) values lie between 0.31 and 0.41. Figure 4 presents Harker diagrams for FeOt, MgO, CaO, TiO_2 , K_2O and A/CNK variation against SiO_2 in the S-type CGS. Experimental melt compositions are plotted for reference. FeOt, MgO, CaO and TiO_2 , show coherent trends as a function of SiO_2 content, while variations for K_2O and A/CNK show a larger scatter. The implications of these trends have been discussed in detail by Stevens et al. (2007), who interpreted these trends to reflect melt compositional variation due to a source compositional control, for parameters such as K and Na, and to reflect the entrainment of the ferromagnesian peritectic assemblage to produce the coherent evolution away from leucocratic melt compositions towards the compositions of the more mafic

granitoids. The major element composition of the granites is not interrogated further in this study.

Trace element data

The trace element compositions of the granites are variable. In particular, concentrated within monazite (e.g. LREE and Y) and zircon (high field strength elements (HFSE): Zr and Hf) show substantial variation, with maximum concentrations typically about 10 times those of the least enriched rocks. La varies from 10 to 103 ppm; Ce varies from 20 to 216 ppm; Zr values range from 67 to 632 ppm; Hf varies from 2 to 17 ppm and Y varies from 15 to 181 ppm. Some large ion lithophile elements (LILEs) are compatible within phases that are reactants in melting reactions (principally those elements in biotite and plagioclase) also show significant but smaller variations in concentration, a fourfold variation in concentration being

Fig. 4 Harker diagrams displaying compositional variation within the S-type CGS rocks. The black filled circles represent the different the Peninsular Pluton sampled in this study. The white filled circles represent a compilation of S-type CGS compositions (white filled circles from Scheepers 1995). The grey diamonds represent the compositions of experimental melts from both synthetic and natural metasediments at conditions comprised between 8 and 10 kbars and 800–900°C (Patino-Douce and Beard 1995; Stevens et al. 1997; Patino-Douce and Harris 1998; Pickering and Johnston 1998)



typical. For example Rb varies from 127 to 414 ppm, Sr from 32 to 148 ppm, Ba from 52 to 867 ppm and Eu from 0.4 to 1.8 ppm.

Figure 5 show the trends defined by trace elements as a function of maficity. The trends defined by the elements that are concentrated within zircon and monazite (La, Ce, Yb, Zr and Hf) are very similar to the variations displayed by FeO, MgO, TiO₂ and CaO, i.e. those elements proposed by Stevens et al. (2007) to be strongly controlled by peritectic phase entrainment (garnet and ilmenite). The Fe + Mg range of possible melt compositions plotted on the diagram gives an indication of which rocks may represent those close to pure melts, requiring no Fe + Mg enrichment mechanism to explain the major element chemistry of the rock. Note that in accordance with the observations in near-source granites, these leucogranitic compositions are generally defined by low abundances of the trace element associated with accessory phases relative to the more mafic rocks. In contrast, elements compatible in phases which are reactants during the incongruent melting of biotite (Rb, Ba, Sr and Eu) show a particularly large scatter for the range of rock Fe + Mg values corresponding those of likely melt. They also do not show the clear positive correlation with Fe + Mg defined by the other group. Variations in elements compatible in melting reaction reactant phases can be regarded as a consequence of the concentration of these elements within the reactant phases in the source rock, as well as the proportion of these phases consumed to form the melt or magma, and the degree of equilibration of the melt with residual biotite and feldspar. These elements appear to have peaks in concentration at intermediate (within the dataset) Fe + Mg contents. These are interpreted to represent the magma compositions formed by the highest degrees of biotite and plagioclase consumption relative to the amount of diluting entrained peritectic assemblage. The large degree of scatter at any given Fe + Mg content is interpreted to reflect variations in source mineralogy and trace element composition. These elements are not considered in more detail in this study. In contrast with the above behaviour, trace elements concentrated within monazite (La, Ce, Th) and zircon (Zr, Hf) show a reasonably well defined positive correlation with Fe + Mg.

As the variation of Fe + Mg, Ti, Ca, etc. is interpreted to reflect the degree of peritectic assemblage entrainment (garnet and ilmenite), the good correlation of the monazite and zircon controlled trace elements with these major element compositional parameters suggests the co-entrainment of these accessory phases and the peritectic assemblage. An alternative interpretation might be that the melts which have the greatest capacity to entrain peritectic crystals also have the greatest capacity to dissolve accessory minerals. However, the significant fraction of xenocrystic zircon in the more mafic granitoids argues for

co-entrainment. The model developed below sets out to investigate if considerations of zircon and monazite saturation in the melt provide information on the relative contributions of accessory phase dissolution and entrainment to the trace element budget of the rocks.

Modelling trace element behaviour during melting

Zircon and monazite play a negligible role in melting reactions which spawn granite magmas, yet in both the unmelted source and in the crystallised granite, they contain almost all the Zr, Hf, Th, Sm, Nd, Ce and La in the rock. Thus, these elements are related to the major element geochemistry of the rock through processes that control either the dissolution of zircon and monazite in the melt, or the entrainment of these minerals into the magma. As the S-type granite magmas of the CGS are interpreted to represent mixtures of melt and the peritectic assemblage, three possible trace element reservoirs need to be constrained in order to model trace element variations in the granites. These are: the melt; the entrained peritectic assemblage and the entrained accessory minerals. To do this the trace elements composition of the source needs to be defined. This study has used a biotite-quartz-plagioclase schist (BS4) from the proposed source (Malmesbury Group) as a proxy for the granite source composition (Table 1). This rock represents the highest grade non-xenolithic sample of the Malmesbury Group that is available and is derived from a single exposure of homogenous schist. It is assumed that the trace element composition of this rock is not meaningfully different from the trace element composition of the high-grade source of the granite. The trace element composition of BS4 was analysed using the same techniques described for the granites. Zircon in the rock is assumed to have the average composition of 12 inherited zircon cores from the Peninsular Pluton (LA-ICP-MS Villarros, unpublished). This material composition must reflect the actual zircon composition in the source. As sample BS4 is a low-grade metasediment, and monazite is typically not stable at these grades (Kingsbury et al. 1993), the monazite composition used is taken from monazite analysed from a granulite-facies metasediment by Montel (1993) (Table 1). Sample BS4 has Zr and Ce concentrations of 348 and 83 ppm, respectively. Zircon and monazite abundance in the source is calculated by assuming that all Zr and Ce in the source are contained within zircon and monazite, respectively. Thus, the Zr and Ce concentrations measured for BS4 translate to 0.075 wt% zircon and 0.028 wt% monazite in the source. This source composition is used in two forms in modelling the partial melting process. First, with the full complement of trace elements (the TEEM example discussed below), and secondly, with the much reduced trace element budget that would result from all

monazite and zircon being removed from the rock (the trace element disequilibrium example where melting and melt extraction is deemed to be so rapid that accessory phases do not have time to dissolve into the melt and contribute to its trace element composition). The two source compositions are presented in Table 1. The monazite and zircon compositions used in the modelling appear to be appropriate, as the modified source composition has all elements that concentrate strongly into the two minerals at very low values, yet none are strongly negative.

The assemblages that would form in the source during fluid-absent melting are predicted from a pseudosection calculated using PerpleX (Connolly 1990; Connolly and Pettrini 2002) for the BS4 composition (Table 1) with 2.5 wt% water (i.e. 6 mol%). This is the amount needed to just fluid-saturate mineral assemblages immediately below the wet solidus, yet have the system go fluid absent on the formation of a very low proportion melt evolved at the wet granite solidus. At the proposed PT conditions of melting for the CGS S-type granites (close to 850°C and 10 kbar) these proportions are 40 wt% leucogranitic melt coexisting with 60 wt% solid phases, with the latter comprising biotite, quartz, plagioclase and garnet in the proportions 10:31:29:30 (Table 2). These proportions are consistent with a large body of experiments on the melting of metapelites and metapsammities at 10 kbar (Patino-Douce 1996; Montel and Vielzeuf 1997; Stevens et al. 1997). Quartz, plagioclase and biotite are reactant phases which, under these conditions, persist in the source composition. Calculated melt and garnet compositions at 850°C and 10 kbar (similar to experimental compositions used by Stevens et al. 2007) are presented in Table 1 from the same pseudosection used to determine phase proportions.

Trace element equilibrium melting

The TEEM composition is generated by assuming that melting and melt extraction occur over a time period long enough such that zircon and monazite are allowed to dissolve in the melt until saturation is reached, or until the accessory phase is exhausted in the source. The composition is calculated using the BS4 source composition (Table 1); the mineral proportions from the pseudosection as determined above; a self-consistent set of partition coefficients ($Kd_n^i = \frac{C_n^i}{C_i^i}$ where C_n^i is the concentration of the element i in the mineral n and C_i^i the concentration of i in the melt) from Montel (1996; Table 1); and a batch melting equation (Eq. 1).

$$C_i^i = \frac{C_0^i}{[F + D^i \times (1 - F)]} \quad \text{and} \quad D^i = \sum_n (x_n \times Kd_n^i) \quad (1)$$

In Eq. 1, C_i^i is the concentration of i in the resulting melt and C_0^i the concentration of the element i in the source. F is the melt fraction, D^i is the distribution coefficient of the element i in the solid fraction of the partial melting reaction. Kd_n^i is the partition coefficient of i in mineral n , and x_n the proportion of mineral n . Zircon and monazite dissolution is controlled by Zr and LREE saturation, respectively, and can be determined from the major element composition of the melt and the saturation equations of Montel (1993) and Watson and Harrison (1983) at the temperature of partial melting (i.e. 850°C). The composition of the melt is expressed using the variable FM (Eq. 2, molar concentrations), defined as:

$$FM = \frac{\text{Na} + \text{K} + 2 \times (\text{Ca} + \text{Fe} + \text{Mg})}{\text{Al} \times \text{Si}} \quad (2)$$

The variable FM is preferred to the M parameter used by Watson and Harrison (1983), as it produces a better fit with natural rock data, as discussed in Baker et al. (2002) and Kelsey et al. (2008). Zircon and monazite saturation levels are calculated using the equations of Watson and Harrison (1983) and Montel (1993) modified from Baker et al. (2002) and Kelsey et al. (2008); Eqs. 3 and 4, respectively.

$$\ln\left(\frac{\text{Zr}_{\text{zircon}}}{\text{Zr}_{\text{melt}}}\right) = \frac{11,574}{T} - 0.679 \times FM - 1.7965 \quad (3)$$

$$\ln\left(\frac{\text{LREE}_{\text{monazite}}}{\text{LREE}_{\text{melt}}}\right) = -\frac{310}{T} - 1.324 \times FM - 7.5852 \quad (4)$$

where $\text{LREE} = \text{La} + \text{Ce} + \text{Pr} + \text{Nd} + \text{Sm} + \text{Gd}$.

At 850°C, the melt Zr saturation level is 199 ppm, whilst monazite saturation is reached at a total LREE concentration of 1,224 ppm. For the combination of melt proportion and melt and source rock compositions used in this study, monazite saturation is never attained (i.e. all of the monazite can dissolve in the melt). In contrast, zirconium saturation in the melt is readily achievable, with a significant fraction of zircon remaining undissolved. This indicates further that the source composition used in the modelling is potentially realistic as it is consistent with the general lack of observed monazite inheritance and the common observed zircon inheritance in S-type granites.

As the melt and peritectic phases form concurrently, the trace element composition of the peritectic phases is calculated as being in equilibrium with the melt, as predicted by the relevant Kd^i . As a consequence, the trace element composition of the melt produced in the TEEM scenario is rich in LREE due to monazite dissolution ($\text{Ce} = 108$ ppm). However, the HREE contents are relatively low because the HREE liberated by substantial zircon dissolution are largely partitioned into the peritectic garnet. Thus, the Yb concentration in TEEM melt composition is only 0.5 ppm and that

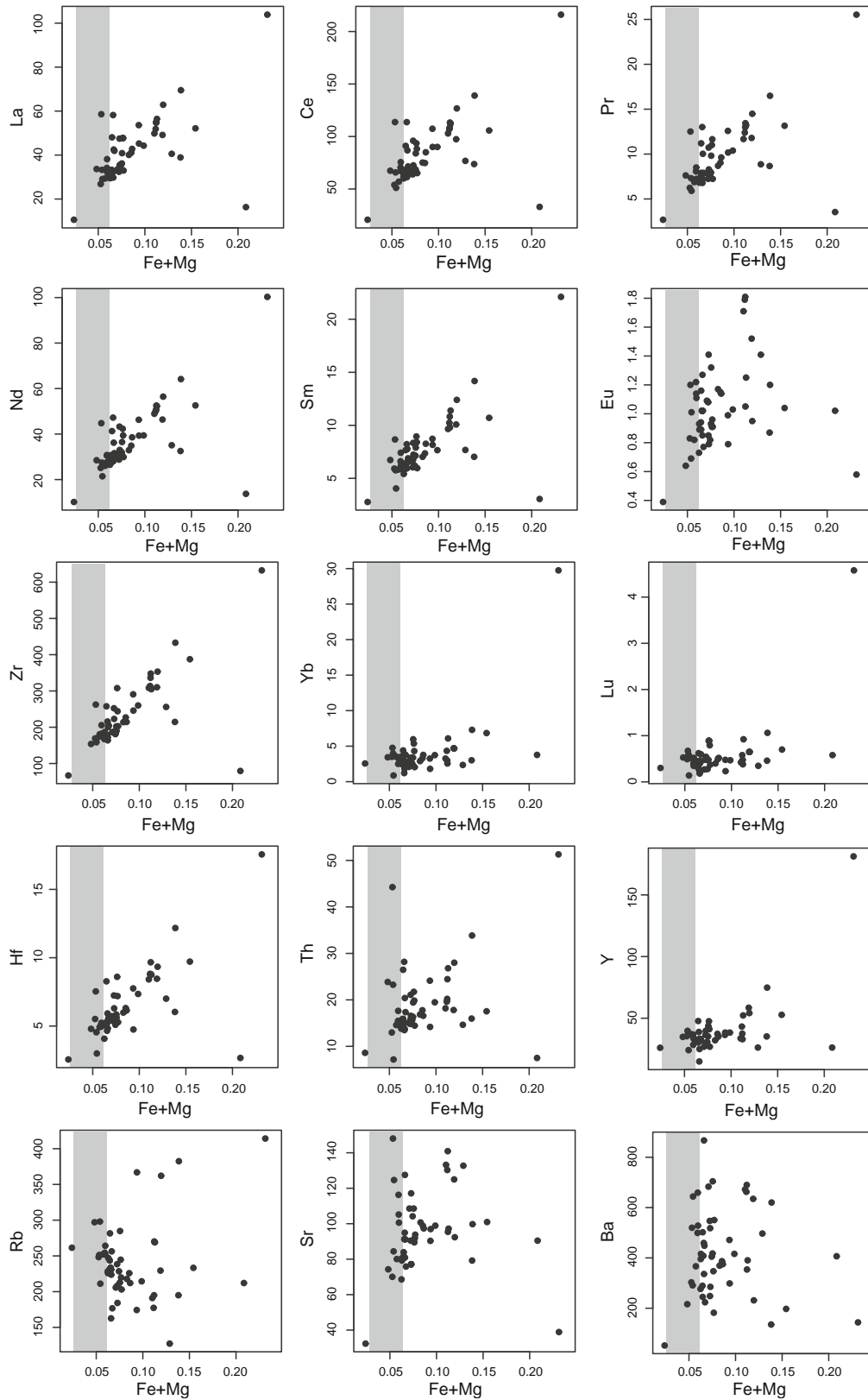


Fig. 5 Trace element versus Fe + Mg variation diagrams for the Peninsular Pluton. *Grey shaded areas* represent Fe + Mg range in experimental melt composition (as in Fig. 4)

Table 1 Trace element composition of monazite (mnz) and zircon (zrc); major and trace element of the source and the calculated zircon-and-monazite-free source

	zrc	mnz	Meta-sedimentary source	Zircon- and monazite-free source
SiO ₂	–	–	65.5	
TiO ₂	–	–	0.8	
Al ₂ O ₃	–	–	15.0	
FEOt	–	–	5.3	
MnO	–	–	0.1	
MgO	–	–	3.1	
CaO	–	–	1.5	
Na ₂ O	–	–	2.7	
K ₂ O	–	–	3.4	
Rb	–	–	106	106
Sr	1.4	–	79	79
Hf	10,350	–	9.3	1.6
Zr	461,051	–	348	2.5
Nb	1.75	–	13.5	13.5
Ba	–	–	389	389
La	1.9	147,859	40.6	2.5
Ce	10.1	359,411	83.4	4.1
Nd	7.0	154,036	38.9	13.9
Pr	1.02	375,28	9.7	1.1
Sm	7.1	21,024	7.7	4.2
Eu	0.6	134	1.2	1.1
Gd	34.9	6,569	7.0	6.9
Tb	12.2	314	1.0	0.9
Dy	154	630	6.5	6.2
Ho	55	82	1.3	1.2
Er	244	138	3.8	3.6
Tm	52	11	0.5	0.5
Yb	463	217	3.7	3.3
Y	1,602	1,946	34.3	32.6
Th	96	42,365	13.2	1.3
Eu*/Eu	0.03	0.01	0.16	0.20

of Hf is 11.4 ppm. The relevant calculated melt and mineral compositions are listed in Table 1. The REE patterns in Fig. 6b illustrate the composition of melt and peritectic phases produced during partial melting. These patterns also illustrate the negative Eu anomaly that exists in all the products of the partial melting reaction ($\text{Eu}/\text{Eu}^*_{\text{melt}} = 0.07$ and $\text{Eu}/\text{Eu}^*_{\text{garnet}} = 0.05$), owing to the partitioning of Eu into residual plagioclase.

Trace element disequilibrium melting

In case of TEDM, the trace element composition of the melt is calculated in an identical manner to that described above, but using the modified source composition created by hypothetically removing the trace element contribution of all monazite and zircon from composition BS4. This models the melt composition produced in situations where

melting and melt extraction is sufficiently rapid that no significant dissolution of accessory minerals can occur. As is predicted, the melt composition produced from this modified source is strongly depleted in the trace elements hosted in zircon and monazite (Table 1, Fig. 6b). This depletion is particularly marked for the LREE (e.g. La = 1.76 ppm and Ce = 9.09 ppm) as well as Zr and Hf (9 and 7.1 ppm, respectively). The HREE also have particularly low concentrations in the melt (e.g. Yb = 0.2 ppm), as a combination of them being trapped both in zircon and in residual garnet. In general, the melt formed by disequilibrium melting followed by rapid melt segregation from the residuum has lower trace element contents than that formed under the equilibrium case. Concentrations of LREE in the disequilibrium melt are at least ten times lower than in the equilibrium melting case. On the other hand, HREE concentrations are similar to

Table 2 Phase proportions determine at conditions of partial melting (i.e. 850°C and 10 kbar from Villaros et al. 2009) from Perple-X pseudosection calculation using BS4 major element composition in; partition coefficients (K_d 's) from Montel (1996) are preferred to other K_d 's in the literature as they constitute a consistent set for all of the mineral and trace elements of interest in this study

		Mineral modal proportion (%) for partial melting					
Retained from the source		Solid phases					Melt
		60					40
zrc	mnz	bi	pl	q	gt		
0.075	0.028	10	29	31	30		
		Reactants			Products		
		Mineral modal proportion (%) in the final magma (after extraction from the source)					
		zrc	mnz	gt	Melt		
TEDM		0.092	0.034	20	80		
TEEM		0.041	–				
		Partition coefficient (K_d)					
		bi	pl	q	gt		
Rb		5	0.1	0.012	0		
Sr		0.3	12	0.015	0		
Hf		0.5	0.06	0.018	0.2		
Zr		0.47	0.1	0.001	0.4		
Nb		1.3	0.02	0.007	0.1		
Ba		6	1.5	0.004	0		
La		0.76	0.3	0.012	0		
Ce		0.86	0.21	0.006	0.1		
Pr		0.07	4.22	0.001	0.9		
Nd		0.9	0.14	0.009	0.4		
Sm		1	0.11	0.008	0.9		
Eu		0.59	5	0.03	1.2		
Gd		0.6	0.1	0.007	4		
Tb		0.87	0.09	0.007	9		
Dy		0.5	0.07	0.01	26		
Ho		0.16	1	0.01	32		
Er		0.41	0.06	0.011	38		
Tm		0.22	1.63	0.01	45		
Yb		0.32	0.06	0.012	60		
Y		1	0.04	0.006	34		
Th		0.3	0.03	0.006	0.4		

These K_d are similar to those published for smaller sub-sets of minerals and trace elements of interest through natural-rock or experimental studies (Irving and Frey 1978; Nash and Crecraft 1985; Sisson and Bacon 1992; Ewart and Griffin 1994; Streck and Grunder 1997; Rubatto and Hermann 2007)

those of the TEEM composition, as they are primarily buffered by garnet, zircon playing a lesser role as even its high K_d 's for HREE do not offset the much higher abundance of garnet. LILEs, such as Eu, Rb, Sr or Ba, remain unchanged from the equilibrium case as their concentration in the accessory minerals is very low and their concentration in the melt depends only on the stoichiometry of the partial melting reaction and thus, the proportions of feldspar and biotite consumed. In a similar fashion to melt, peritectic phases in the disequilibrium case are generally depleted in trace elements compared to the equilibrium case. La and Ce in peritectic garnet have extremely low concentrations (0.04 and 0.91 ppm, respectively) while HREE show similar concentrations compared to the equilibrium case (Yb = 11.94 ppm). Thus, the REE patterns in

Fig. 6b for the disequilibrium case show a strong depletion in LREE for melt and peritectic phase. Compare to TEEM case, these compositions are notably different, thus the entrainment of peritectic phase in melt implies different trends particularly marked for LREE compositions, with lower contents LREE in the TEDM than in the TEEM case.

As for TEEM, the products of partial melting also show a negative Eu anomaly ($Eu/Eu^*_{melt} = 0.082$ and $Eu/Eu^*_{garnet} = 0.047$) inherited from the source composition and enhanced by the plagioclase-bearing residue. The white star in Fig. 7 illustrates the melt composition produced by TEDM case, while the grey star illustrates the melt composition produced by the TEEM case.

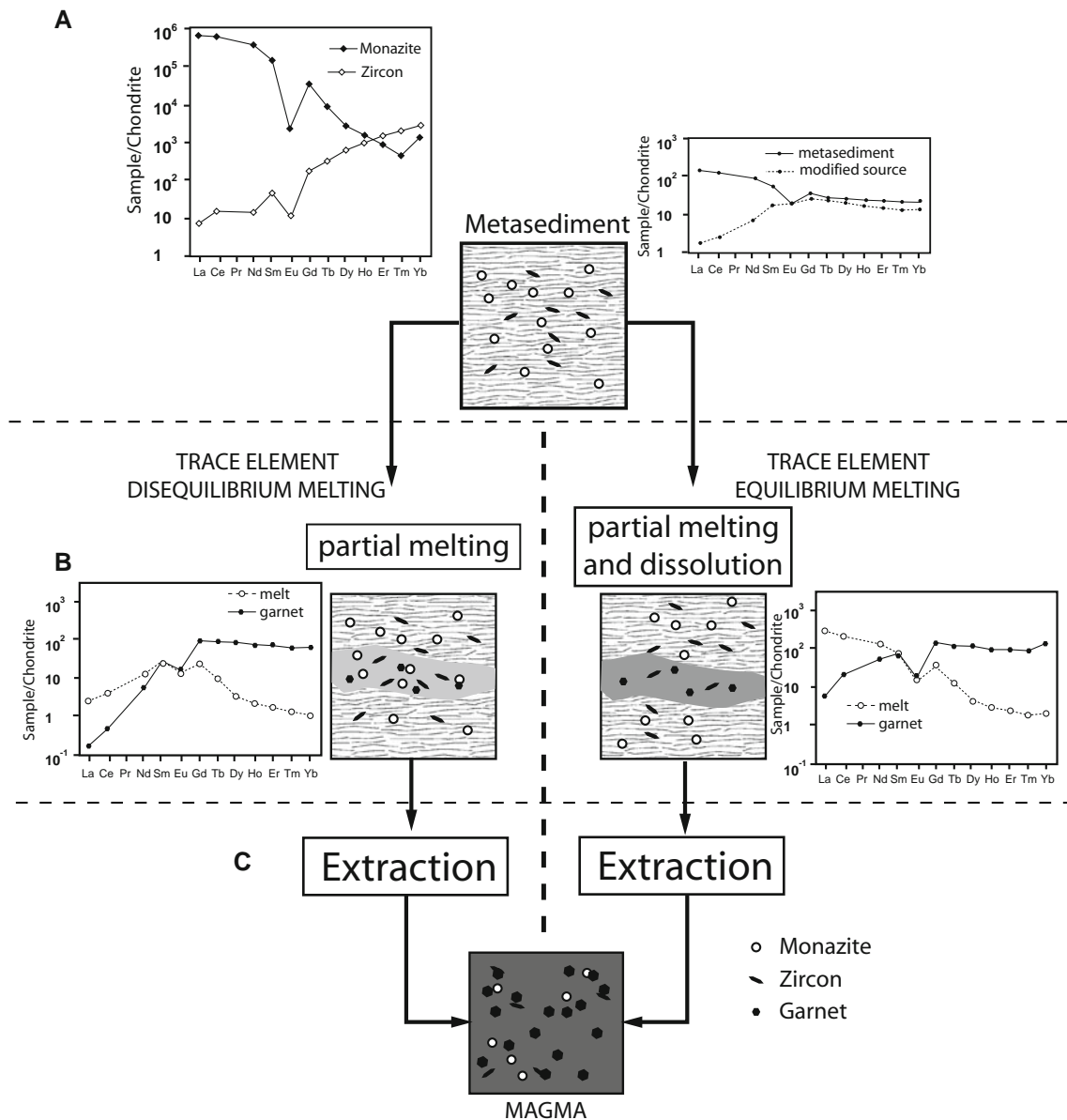


Fig. 6 A diagrammatic illustration of the principles underpinning the trace element modelling in this study. The trace element data are chondrite normalised (from Taylor and McLennan 1985). The top, **a** represents the metasedimentary source including the accessory minerals zircon and monazite. The plot to the left in **a** represents the composition of the accessory minerals. The plot to the right indicates the composition of the original metasediment (top line) and the effective composition of the source composition assuming that none of the accessory minerals are available for reaction (lower line). In the middle, **b** the two end-member cases for behaviour during partial melting in the source are illustrated. In the situation depicted in the pair of diagrams to the left, melting occurs without the dissolution of any accessory phases in the melt, although peritectic minerals are entrained. In this case, the segregated magma contains peritectic

phases and accessory minerals and the trace element budget of the magma is solely a function of the proportion of accessory minerals entrained. The pair of diagrams to the right illustrates the opposite scenario. Accessory minerals dissolve in the melt, until the elements that control accessory mineral stability (e.g. Zr in the case of zircon) are saturated in the melt. **c** represents the result, which in terms of concentrations can be identical. However, the path to the right will always produce trace element concentrations no lower than zircon and monazite saturation or than the complete dissolution of these phases in the source will produce, depending on the source composition relative to the saturation concentrations of the relevant elements in the melt at the conditions of anatexis. The path to the left will be characterised by trace element concentrations that can be as low as those of the pure melt that has not dissolved and zircon or monazite

Modelling phase entrapment

The consequences of the entrainment of both peritectic phases and accessory minerals for the magma composition

can be modelled using each of the two melt and two garnet (i.e. in TEEM and TEDM cases) compositions described above. The peritectic assemblage of garnet and ilmenite has been added to each of the melt compositions in five

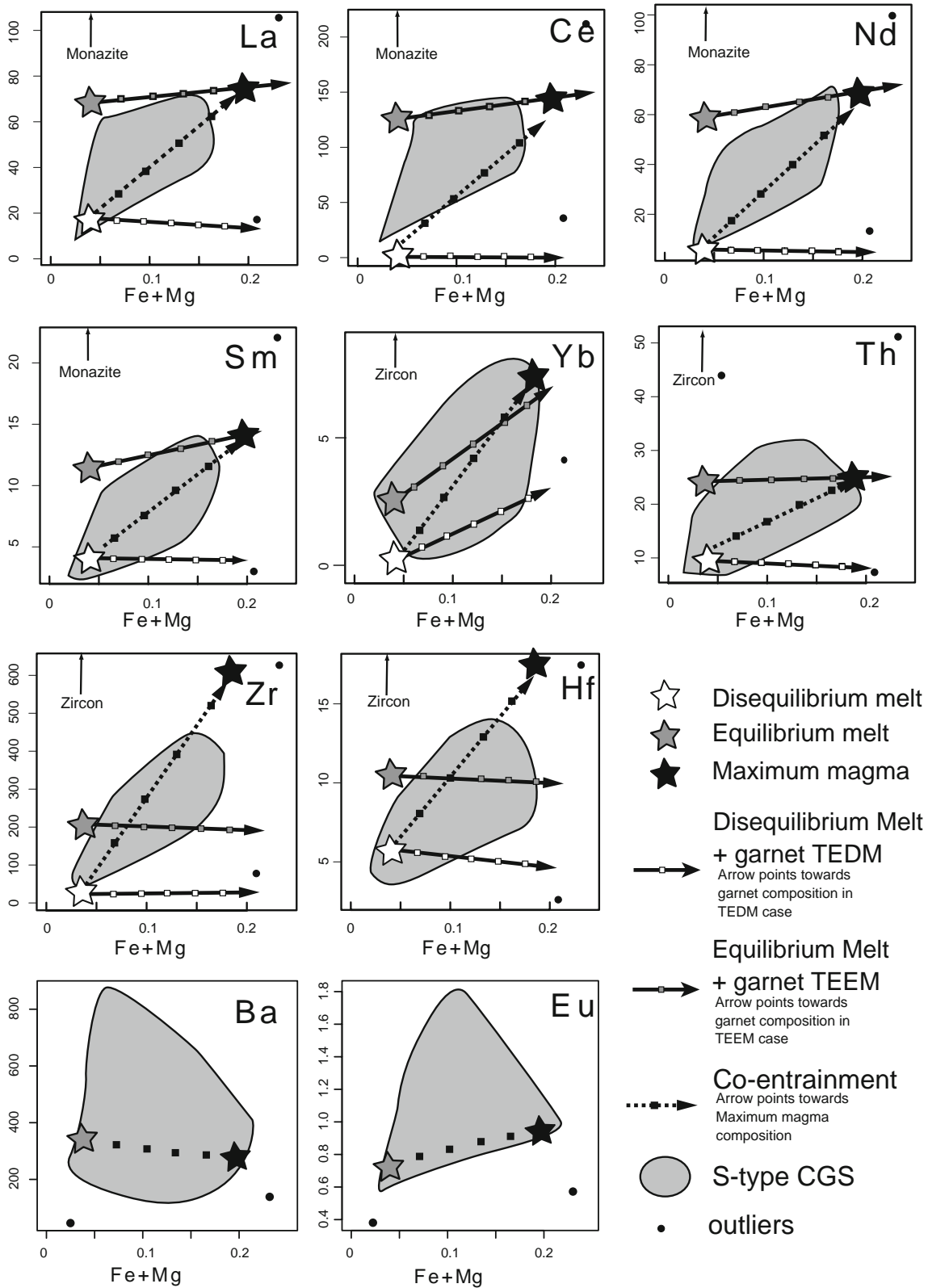


Fig. 7 Results of modelling compared to compositions of the S-type CGS described in Table S1. Diagrams show the variations of trace element concentrations versus atomic Fe + Mg. “Maximum magma”

is the addition of the totality of accessory minerals available, 20% of peritectic garnet to melt composition. Co-entrainment trend is an examples leading to the “maximum” composition of magma

increments of 4 wt%. As illustrated by Stevens et al. (2007), this produces the range of major element compositions exhibited by the Peninsular Pluton, from leucogranitic (pure melt) melt to the most FeO + MgO-rich granodiorite (melt plus 20 wt% peritectic assemblage). The vectors of compositional evolution away from the leucocratic model melt compositions that arise as a result of this are illustrated in Fig. 7.

As illustrated in Fig. 1, Zr in granites shows a positive correlation with maficity and in individual suites such as the CGS Zr commonly correlates quite tightly with maficity. Thus, if maficity is a function of peritectic phase entrainment, then co-entrainment of accessory and peritectic minerals commonly occurs. It is perhaps predictable that these functions are coupled, as circumstances that favour the entrainment of a greater proportion of peritectic phases may also favour the entrainment of more of the available accessory minerals. This coupled peritectic assemblage-accessory mineral co-entrainment has been modelled by allowing the entrainment of all of the available accessory minerals. As stated above, the amount of accessory minerals represents 0.075 wt% zircon and 0.028 wt% monazite in the source. After melt extraction, the maximum proportions of remaining minerals (i.e. not dissolved) in the resulting magma are 0.034 wt% monazite and 0.092 wt% zircon of the final magma in the TEDM case and only 0.041 wt% zircon in the TEEM (as all monazite is dissolved in the melt), concurrently with the maximum amount of peritectic phase entrainment (20 wt%). Thus, in modelling peritectic assemblage and accessory mineral co-entrainment, each 4 wt% increment of peritectic assemblage addition also involves the incorporation of 20% of the available accessory mineral assemblage. On Fig. 7 the resultant lines of compositional evolution for the magma follow the dashed arrows.

Results and discussion

Calculated melt compositions compared to the granites

For the trace elements contained within monazite and zircon, the lowest trace element concentrations recorded in the Peninsular Pluton are an identical to, or a very close match with, the modelled TEDM compositions. These compositions are recorded in the most leucocratic rocks, i.e. those compositions proposed by Stevens et al (2007) to most closely match pure melts. Within this least mafic portion of the population, elements that are markers for the behaviour of zircon (mainly Hf and Zr) have values significantly below melt saturation values. In contrast, the

highest concentrations of these elements are recorded in the most mafic portions of the granite. In a significant fraction of these most mafic rocks, Zr exceeds saturation values by a considerable margin (Fig. 7), consistent with the common xenocrystic zircons (e.g. Bea et al. 2007) in these rocks. Elements that reflect monazite behaviour (La, Ce, Pr, Sm, Nd and Th) show similar characteristics, with the concentrations of these elements closely matching the predicted TEDM compositions in the most leucocratic granites. In the most mafic granites, these elements are very close to saturation values, but generally do not exceed these limits. On plots comparing trace element concentration to maficity, much of the Peninsular Pluton dataset populates the compositional space located between the TEDM and the magma arising as mixtures of the TEEM, or the TEDM and the peritectic + accessory assemblage, for those elements concentrated in monazite (Fig. 7). Either melt is equally viable in this, as accessory phase dissolution and entrainment are compensatory processes. The elements concentrated in monazite never exceed monazite saturation limits in the magma. This is consistent with the common absence of xenocrystic monazite in S-type granites. It has to be noted that the calculated model matches efficiently the CGS data. Thus it clearly indicates that accessory mineral compositions used for modelling are probably not different than the actual compositions of zircon and monazite entrained in the S-type CGS (Table 3).

On similar plots elements such as Rb, Ba, Sr and Eu show completely different behaviour (Fig. 7). These elements are compatible with reactants of the partial melting reaction and as a result, both our models (TEEM and TEDM) give very similar results; the values resulting from an equilibrium trace element melting model are used here. This may be inappropriate, however, as it assumes equilibration of the residual fraction of these minerals with the melt prior to melt extraction. These elements reach their highest concentrations in granites of intermediate maficity. However, there is a difference in behaviour between elements that follow K and those which follow Ca. Elements such as Ba reach their maximum concentrations towards the more leucocratic side of the major element compositional range (Fig. 7). This is interpreted to reflect source differences, with the most K-rich rocks also being the most Ba-rich and melting to produce melts which leave the source with little entrained peritectic material. In contrast, Eu follows Ca and will partition into residual plagioclase during melting, only becoming liberated as plagioclase becomes exhausted by the melting reaction. Eu concentrations in the source are also likely to be higher in rocks with higher Ca (more plagioclase dominated and/or more calcic plagioclase).

Table 3 Results of calculation

Modelling results					
	Melt		gt		Magma
SiO ₂	73.3		39.7		66.5
TiO ₂	–		–		–
Al ₂ O ₃	15.0		22.4		16.5
FeOt	0.7		24.1		5.4
MnO	–		0.6		0.1
MgO	0.2		11.5		2.5
CaO	0.6		1.7		0.8
Na ₂ O	3.1		–		2.5
K ₂ O	7.1		–		5.7
	TEEM	TEDM	TEEM	TEDM	
Rb	183	183	1.8	1.8	183
Sr	23	23	0.5	0.5	23
Hf	11	7.1	2.3	1.4	21
Zr	200	9.0	80	3.6	622
Nb	6.8	6.8	2.8	2.8	57
Ba	366	367	3.7	3.7	366
La	51	1.8	1.0	0.0	51
Ce	108	9.1	11	0.9	108
Pr	11.2	0.7	10.1	0.7	11.2
Nd	72	42	30	17	72
Sm	13	9	12	8	13
Eu	0.6	0.6	0.8	0.7	0.6
Gd	5.5	5.5	22.1	22.0	5.5
Tb	0.5	0.4	4.2	3.2	0.5
Dy	1.1	0.9	29.8	22.5	1.3
Ho	0.2	0.1	6.0	4.4	0.2
Er	0.5	0.3	18.6	13.0	0.7
Tm	0.1	0.0	2.9	1.8	0.1
Yb	0.5	0.2	27.9	11.9	0.9
Y	4.8	3.5	163	118	6.3
Th	19.6	5.0	8.6	2.2	20
Eu*/Eu	0.07	0.08	0.05	0.05	0.07

TE-DM trace element disequilibrium melting, TE-EM trace element equilibrium melting

“Magma” represents the maximum composition calculated here i.e. melt + 20% garnet + all available zircon and monazite

Dissolution of accessory minerals and minimum residence time of melt in the source

A significant fraction of the most leucocratic granites have compositions that indicate that they have escaped their source prior to equilibration with monazite and zircon. In some granites, where zirconium concentrations are below magma saturation levels, the granites do contain xenocrystic zircon. Zircon dissolution rates can be used to constrain the duration of zircon residency in the magma (e.g. Bea et al. 2007). Using a similar approach, the

Peninsular Pluton granites with the lowest Zr concentrations can be used to constrain the maximum residence time of the melt in the source, as the source rocks to these granites are very likely to have contained at least some zircon and monazite and the trace element compositions of the rocks may also reflect entrainment of zircon and monazite. To do this, rates of zircon dissolution, as well as zircon abundance and size fraction in the source, need to be known.

The dissolution rate dr/dt (in cm/s) of zircon in peraluminous melt can be determined using Eq. 5 [from Eq. 17 in Watson (1996)]:

$$\frac{dr}{dt} = -(C_{Zr} - C_{Zr^*}) \left[\left(\frac{1.25 \times 10^{10}}{r} \right) \times e^{\left(-\frac{28,380}{T} \right)} + 7.24 \times 10^8 \times e^{\left(-\frac{23,280}{T} \right)} \right] \times 10^{-17} \quad (5)$$

where C_{Zr} is the original undersaturated concentration of Zr in the TEDM melt (Zr = 9.0 ppm in the case of these rocks), C_{Zr^*} is the saturation concentration of Zr in the melt (i.e. Zr = 199 ppm in the case of these rocks), r is the spherical radius of a hypothetical zircon and T the temperature (in K). Assuming dissolution of spherical zircons in a steady state environment and at constant temperature it is possible to determine the time necessary to reach a given concentration of Zr in the melt.

Figure 8 shows the result of this calculation for three different grain radii: 25, 50 and 75 μm . The minimum Zr content in the S-type CGS recorded in this study is 67.2 ppm. According to Eq. 5 this concentration would be attained in 337 years in the case of 25 μm radius, 1,330 years for 50 μm and finally 3,955 years for 75 μm . As a 75 μm radius would represent an uncommonly large zircon for a metasediment such as BS4, the 3,955 years given by the calculation provides a maximum estimate of the time of residence of melt within the source of the S-type CGS. The estimates of 337–1,330 years obtained for more reasonable size zircons (25 and 50 μm radii, respectively) are much more likely to represent a good bracket for residence time of melt within the source. Using the lower Zr concentration of 9 ppm obtained for TEDM, the dissolution times would be even lower (~ 30 years for 25 μm radius zircon). Harris et al. (2000) using the same method with a spherical radius of 15 μm and a temperature of 750°C, estimated a residence time of approximately 50 years to model the low Zr concentrations of Himalayan leucogranites. Considering the smaller size of zircons and the lower temperature, these two results agree quite well, and imply relatively a short time of residence of melt in the source of less than 500 years. A further important point to be considered when evaluating the meaning of this value is that the model is built around the incorrect assumption of a static state. Thus,

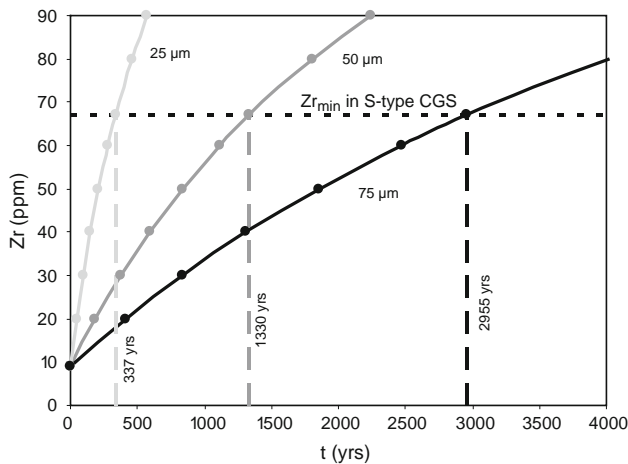


Fig. 8 Zr concentration versus time in a melt. The calculation assume a constant temperature and a complete dissolution of spherical zircons (from Eq. 17 of Watson 1996) Initial zircon radius of 25, 50 and 75 μm and initial undersaturation for Zr of 6.7 ppm (*Black Star*) corresponding to Zr concentration determine for TEDM in Table 1. Zr^* is the zirconium saturation at 850°C correspond to Zr concentration in TEEM of Table 1. *Dashed line* indicates temperature at which the minimum undersaturation in the S-type CGS is reached

zircon dissolution is controlled by the diffusion rate of zirconium in the melt and the melt is assumed to be static. Melt flow past the crystal will dramatically reduce the time by replacing Zr-saturated by -undersaturated melt, and melt flow must have occurred as the magma migrated out of the source. Importantly, it is only these leucocratic granites which are least contaminated by entrained phases that provide the possibility to establish this constraint. However, within the Peninsular Pluton there are no intrusive contacts between the various phases of the granite examined in this study. Thus, a very short source residence time is proposed for all of the rocks, with the more trace element enriched granites representing higher levels of entrainment of accessory minerals, not longer source residency times.

Co-entrainment of accessory minerals and peritectic phases

By allowing, for TEDM, rapid melt extraction from the source and coupled accessory mineral and peritectic assemblage entrainment, the model presented here appears to be able to account for the major and trace element geochemistry of the Peninsular Pluton. The reasons for the coupling are probably twofold. First, in high-grade metasediments zircon and monazite commonly occur as inclusions in biotite. Thus, they are liberated by biotite incongruent melting. Secondly, they are liberated in the sites most likely to also be characterised by the growth of peritectic minerals. Thus, physical circumstances favourable to

the entrainment of accessory minerals may also act to entrain peritectic crystals. Zircon and monazite are usually present in metasediments as small crystals. Thus, the coupled entrainment described above probably indicates that peritectic crystals entrain as small crystals, possibly with similar grain size distributions to those that characterise the accessory minerals. This process of co-entrainment would appear to not be constrained by degree of melting in the source. Biotite in high grade metasediments very commonly contains inclusions of monazite and zircon. Thus, these minerals are available where melt production is likely to occur. The peritectic minerals form with melt and low melt fractions, if they can efficiently mobilise out of the source, may carry entrained peritectic and accessory phases. At higher melt fractions, the abundance of accessory phases in the source may impinge on the ability of the process to deliver the Zr and LREE enriched compositions displayed by the more mafic granites. However, attaining these melt fractions would require the addition of water to the source and not the fluid absent process, as modelled here, that is commonly considered to account for high level granites (e.g. Stevens and Clemens 1993; Clemens 2006).

Conclusion

Modelling the major and trace element variation in the Peninsular Pluton of the CGS has revealed several important findings. The magmas that intruded at a high level in the crust to build the pluton formed via a TEDM process because the magmas did not spend sufficiently long in the source to establish equilibrium with the relatively refractory zircon and monazite residing there. Maximum magma residence time in the source was less than approximately 500 years and possibly very much less than 500 years, if melt flow and the dynamics of the system are considered. The rocks that appear saturated or close to saturated with regard to zircon and monazite achieved this state not as a result of a Zr or LREE rich melt, but rather by entraining these minerals from the source. In the case of monazite that is very far from saturation, there was sufficient time available in the magmatic environment for monazite equilibration with the melt, as evidenced by its complete dissolution. In the case of zircon, this was not the case as some rocks with zirconium contents lower than saturation values do still contain xenocrystic zircons.

The findings provide very important constraints on the petrogenesis of the different varieties of granite that make up the pluton. Bulk rock compositional ranges such as those in exhibited by the Peninsular Pluton are commonly interpreted to reflect fractional crystallisation (Schoch et al. 1977); or the unmixing of an entrained bulk restite component (Scheepers 1995). The findings of this study prove

that neither process is applicable to these rocks, nor possibly to other S-type rocks, which are all characterised by similar general features. In essence, the leucocratic portions of the pluton have not arisen through fractional crystallisation, or the unmixing of components from a homogenous magma representing more mafic or intermediate granite compositions. These more mafic magmas are typically saturated or close to saturated with regard to zircon and monazite. Consequently, evolution of residual melts via fractionation from these compositions would not be able to form strongly zircon and monazite undersaturated magmas.

Field observations in the Peninsular Pluton allow different phases of the granite to be identified, largely on the basis of different proportions of ferromagnesian minerals. This study shows that variations in major and trace element concentrations were closely correlated. This is interpreted to be a consequence of co-entrainment of peritectic products and accessory minerals from the source. Thus, the magmas which built up the Peninsular Pluton left the source as fundamentally different compositions. These magma batches contributed to pluton growth with sufficiently little mixing that their original chemical character is largely retained.

The fact that well-defined boundaries can be observed between the different Peninsular Pluton phases reflects this lack of mixing. The pluton is reasonably large (at least 40 km in length), yet the boundaries between different facies are generally steeply orientated. As these reflect different discrete magma batches, this orientation would seem to be most consistent with the pluton being fed by a number (perhaps many) smaller conduits, rather than few main feeders from which the pluton inflated. These proposed many conduits would also be consistent with the lack of mixing between magma batches and the tapping of different and discrete magma batches from the source.

Ultimately, this study has demonstrated that it is possible to establish a coherent model for the major and trace element geochemistry of S-type granites.

Acknowledgments The Authors want to thank J. Beard and an anonymous reviewer for their helpful comments that helped improving largely this paper. This work forms part of a PhD study by A. V. A. V. gratefully acknowledges an NRF PhD Bursary and support for the study via National Research Foundation grant funding to G. S. I. S. B. acknowledges support from an Australian Research Council Australian Professorial Fellowship and Discovery Grant No. DP0342473.

References

- Ayres M, Harris N (1997) REE fractionation and Nd-isotope disequilibrium during crustal anatexis: constraints from Himalayan leucogranites. *Chem Geol* 139:249–269. doi:10.1016/S0009-2541(97)00038-7
- Baker DR, Conte AM, Freda C, Ottolini L (2002) The effect of halogens on Zr diffusion and zircon dissolution in hydrous metaluminous granitic melts. *Contrib Mineral Petrol* 142:666–678
- Bea F (1996a) Residence of REE, Y, Th and U in granites and crustal protoliths: implications for the chemistry of crustal melts. *J Petrol* 37:521–552. doi:10.1093/ptrology/37.3.521
- Bea F (1996b) Controls on the trace element composition of crustal melts. *Trans R Soc Edinb Earth Sci* 87:33–41
- Bea F, Montero P, Ortega M (2006) A LA-ICP-MS evaluation of Zr reservoirs in common crustal rocks: implications for Zr and Hf geochemistry, and zircon-forming processes. *Can Mineral* 44:693–714. doi:10.2113/gscanmin.44.3.693
- Bea F, Montero P, Gonzalez-Lodeiro F, Talavera C (2007) Zircon inheritance reveals exceptionally fast crustal magma generation processes in central Iberia during the Cambro-Ordovician. *J Petrol* 48:2327–2339. doi:10.1093/ptrology/egm061
- Bhadra S, Das S, Bhattacharya A (2007) Shear zone-hosted migmatites (Eastern India): the role of dynamic melting in the generation of REE-depleted felsic melts, and implications for disequilibrium melting. *J Petrol* 48:435–457. doi:10.1093/ptrology/egl066
- Chappell BW (1984) Source rocks of I- and S-type granites in the Lachlan Fold Belt, southeastern Australia. *Philos Trans R Soc Lond A* 310:693–707
- Chappell BW, White AJR (1974) Two contracting granite types. *Pac Geol* 8:173–174
- Chappell BW, White AJR (1992) I-type and S-type granites in the Lachlan fold belt. *Trans R Soc Edinb Earth Sci* 83:1–26
- Clemens JD (2003) S-type granitic magmas—petrogenetic issues, models and evidence. *Earth Sci Rev* 61:1–18. doi:10.1016/S0012-8252(02)00107-1
- Clemens JD (2006) Melting of the continental crust: fluid regimes, melting reactions and source-rock fertility. In: Brown M, Rushmer T (eds) *Evolution and differentiation of the continental crust*. Cambridge University Press, UK, pp 297–331
- Clemens JD, Droop GTR, Stevens G (1997) High-grade metamorphism, dehydrations and crustal melting: a reinvestigation based on new experiments in the silica-saturated portion of the system KAlO₂-MgO-SiO₂-H₂O-CO₂ at P ≤ 1.5 GPa. *Contrib Mineral Petrol* 129:308–325. doi:10.1007/s004100050339
- Collins WJ, Hobbs BE (2001) What caused the early Silurian change from mafic to silicic (S-type) magmatism in the eastern Lachlan Fold Belt? *Aust J Earth Sci* 48:25–41. doi:10.1046/j.1440-0952.2001.00837.x
- Connolly JAD (1990) Multivariable phase diagrams: an algorithm based on generalized thermodynamics. *Am J Sci* 290:666–718
- Connolly JAD, Pettrini K (2002) An automated strategy for calculation of phase diagram sections and retrieval of rock properties as a function of physical conditions. *J Metab Geol* 20:697–708. doi:10.1046/j.1525-1314.2002.00398.x
- Copeland P, Parrish RR, Harrison TM (1988) Identification of inherited radiogenic Pb in monazite and its implications for U-Pb systematics. *Nature* 333:760–763. doi:10.1038/333760a0
- Da Silva LC, Gresse PG, Scheepers R, McNaughton NJ, Hartmann LA, Fletcher I (2000) U-Pb SHRIMP and Sm-Nd age constraints on the timing and sources of the Pan-African Cape Granite Suite, South Africa. *J Afr Earth Sci* 30:795–815. doi:10.1016/S0899-5362(00)00053-1
- Da Silva LC, McNaughton NJ, Armstrong RA, Hartmann LA, Fletcher IR (2005) The Neoproterozoic Mantiqueira Province and its African connection: a zircon based U-Pb geochronologic subdivision for the Brasiliano/Pan-African systems of orogens. *Precambrian Res* 136:203–240. doi:10.1016/j.precamres.2004.10.004

- Downes H, Dupuy C, Leyreloup A (1990) Crustal evolution of the Hercynian belt of Western Europe: evidence from lower crustal xenoliths (French Massif Central). *Chem Geol* 83:209–231. doi:10.1016/0009-2541(90)90281-B
- Eggs S (2003) Laser ablation ICP-MS analysis of geological materials prepared as lithium borate glasses. *Geostand Geoanal Res* 27:147–162. doi:10.1111/j.1751-908X.2003.tb00642.x
- Elburg MA (1996) U-Pb ages and morphologies of zircon in microgranitoid enclaves and peraluminous host granite: evidence for magma mingling. *Contrib Mineral Petrol* 123:177–189. doi:10.1007/s004100050149
- Ewart A, Griffin WL (1994) Application of proton-microprobe data to trace-element partitioning in volcanic-rocks. *Chem Geol* 117:251–284. doi:10.1016/0009-2541(94)90131-7
- Gardien V, Thompson AB, Gruzic D, Ulmer P (1995) Experimental melting of biotite + plagioclase + quartz ± muscovite assemblages and implications for crustal melting. *J Geophys Res Solid Earth* 100:15581–15591. doi:10.1029/95JB00916
- Georget Y, Martineau F, Capdevila R (1986) Age tardi-hercynien et origine crustale du granite de Brignogan (Finistère, France). Conséquences sur l'interprétation des granites Nord-armoricains = Late-hercynian radiometric age and crustal origin of Brignogan granite (Finistere, France). Consequences on the interpretation of the North-Armorican granites. *C R Acad Sci Série 2 Méc Phys Chim Sci Univ Sci Terre* 302:237–242
- Goad BE, Cerny P (1981) Peraluminous pegmatitic granites and their pegmatite aureoles in the Winnipeg River District, southeastern Manitoba. *Can Mineral* 19:177–194
- Harris N, Ayres M, Massey J (1995) Geochemistry of granitic melts produced during the incongruent melting of muscovite: implications for the extraction of himalayan leucogranite magmas. *J Geophys Res* 100:15767–15777. doi:10.1029/94JB02623
- Harris C, Faure K, Diamond RE, Scheepers R (1997) Oxygen and hydrogen isotope geochemistry of S- and I- type granitoids: the Cape Granite Suite, South Africa. *Chem Geol* 143:95–114. doi:10.1016/S0009-2541(97)00103-4
- Harris N, Vance D, Ayres M (2000) From sediment to granite: timescales of anatexis in the upper crust. *Chem Geol* 162:155–167. doi:10.1016/S0009-2541(99)00121-7
- Hartnady CJH, Newton AR, Theron JN (1974) The stratigraphy and structure of the Malmesbury Group in the southwestern Cape. *Bull Precamb Res Unit* 15:193–213
- Irving AJ, Frey FA (1978) Distribution of trace-elements between garnet megacrysts and host volcanic liquids of kimberlitic to rhyolitic composition. *Geochim Cosmochim Acta* 42:771–787. doi:10.1016/0016-7037(78)90092-3
- Johannes W, Ehlers C, Kriegsman LM, Mengel K (2003) The link between migmatites and S-type granites in the Turku area, southern Finland. *Lithos* 68:69–90. doi:10.1016/S0024-4937(03)00032-X
- Jung S, Mezger K, Masberg P, Hoffer E, Hoernes S (1998) Petrology of an intrusion-related high-grade migmatite: implications for partial melting of metasedimentary rocks and leucosome-forming processes. *J Metab Geol* 16:425–445. doi:10.1111/j.1525-1314.1998.00146.x
- Kelsey DE, Clark C, Hand M (2008) Thermobarometric modelling of zircon and monazite growth in melt-bearing systems: examples using model metapelitic and metapsammitic granulites. *J Metab Geol* 26:199–212. doi:10.1111/j.1525-1314.2007.00757.x
- Kingsbury JA, Miller CF, Wooden JL, Harrison TM (1993) Monazite paragenesis and U–Pb systematics in rocks of the eastern Mojave Desert, California: implications for thermochronometry. *Chem Geol* 110:147–168. doi:10.1016/0009-2541(93)90251-D
- Montel J-M (1993) A model for monazite melt equilibrium and application to the generation of granitic magmas. *Chem Geol* 110:127–146. doi:10.1016/0009-2541(93)90250-M
- Montel JM (1996) *Géochimie de la fusion de la croûte continentale*. University of Blaise Pascal, Clermont-Ferrand
- Montel JM, Vielzeuf D (1997) Partial melting of metagreywackes. 2. Compositions of minerals and melts. *Contrib Mineral Petrol* 128:176–196. doi:10.1007/s004100050302
- Nabelek PI, Glascock MD (1995) Rare earth element-depleted leucogranites Black Hills, South Dakota: a consequence of disequilibrium melting of monazite-bearing schists. *J Petrol* 36:1055–1071
- Nash WP, Crecraft HR (1985) Partition coefficients for trace elements in silicic magmas. *Geochim Cosmochim Acta* 49:2309–2322. doi:10.1016/0016-7037(85)90231-5
- Parrish RR (1990) U-Pb dating of monazite and its application to geological problems. *Can J Earth Sci* 27:1431–1450
- Patino-Douce AE (1996) Effect of pressure and H₂O content on the compositions of primary crustal melts. *Trans R Soc Edinb Earth Sci* 87:11–21
- Patino-Douce AE, Beard JS (1995) Dehydration-melting of biotite gneiss and quartz amphibolite from 3 to 15 Kbar. *J Petrol* 36:707–738
- Patino-Douce AE, Harris N (1998) Experimental constraints on Himalayan anatexis. *J Petrol* 39:689–710. doi:10.1093/petrology/39.4.689
- Patino-Douce AE, Johnston AD (1991) Phase equilibria and melt productivity in the pelitic system: implications for the origin of peraluminous granitoids and aluminous granulites. *Contrib Mineral Petrol* 107:202–218. doi:10.1007/BF00310707
- Pearce NJG, Perkins WT, Westgate JA, Gorton MP, Jackson SE, Meal CR, Chenery SP (1997) A compilation of new and published major and trace element data for NIST SRM 610 and NIST SRM 612 glass reference materials. *Geostand News* 21:115–144. doi:10.1111/j.1751-908X.1997.tb00538.x
- Pickering JM, Johnston AD (1998) Fluid-absent melting behaviour of a two-mica metapelite: experimental constraints on the origin of black hills granite. *J Petrol* 39(10):1787–1804. doi:10.1093/petrology/39.10.1787
- Rollinson H (1993) Using geochemical data: evaluation, presentation, interpretation. Edinburgh Gate, Edinburgh
- Rozendaal A, Grasse PG, Scheepers R, Le Roux JP (1999) Neoproterozoic to early Cambrian crustal evolution of the Pan-African Saldania Belt, South Africa. *Precambrian Res* 97:303–323. doi:10.1016/S0301-9268(99)00036-4
- Rubatto D, Hermann J (2007) Experimental zircon/melt and zircon/garnet trace element partitioning and implications for the geochronology of crustal rocks. *Chem Geol* 241:38–61. doi:10.1016/j.chemgeo.2007.01.027
- Sawyer EW (1991) Disequilibrium melting and the rate of melt residuum separation during migmatization of mafic rocks from the Grenville Front, Quebec. *J Petrol* 32:701–738
- Scheepers R (1995) Geology, geochemistry and petrogenesis of Late Precambrian S-, I- and A-type granitoids in the Saldania belt, Western Cape Province South Africa. *J Afr Earth Sci* 21:35–58. doi:10.1016/0899-5362(95)00087-A
- Scheepers R, Armstrong RA (2002) New U-Pb SHRIMP zircon ages of the Cape Granite Suite: implications for the magmatic evolution of the Saldania Belt. *S Afr J Geol* 105:241–256. doi:10.2113/1050241
- Schoch AE (1975) The darling granite batholith. *Ann Univ Stell* A1:1–104
- Schoch AE, Leterrier J, De la Roche H (1977) Major element geochemical trends in the Cape granites. *Trans Geol Soc S Afr* 80:197–209
- Sisson TW, Bacon CR (1992) Garnet high-silica rhyolite trace-element partition-coefficients measured by ion microprobe. *Geochim Cosmochim Acta* 56:2133–2136. doi:10.1016/0016-7037(92)90336-H

- Solgadi F, Moyen J-F, Vanderhaeghe O, Sawyer EW, Reisberg L (2007) The role of crustal anatexis and mantle derived magmas in the genesis of syn-orogenic hercynian granites of the Livradois Area, French Massif Central. *Can Mineral* 45:581–606. doi:[10.2113/gscanmin.45.3.581](https://doi.org/10.2113/gscanmin.45.3.581)
- Stevens G, Clemens JD (1993) Fluid absent melting and the roles of fluids in the lithosphere: a slanted summary? *Chem Geol* 108:1–17. doi:[10.1016/0009-2541\(93\)90314-9](https://doi.org/10.1016/0009-2541(93)90314-9)
- Stevens G, Clemens JD, Droop GTR (1997) Melt production during granulite-facies anatexis: experimental data from primitive metasedimentary protoliths. *Contrib Mineral Petrol* 128:352–370. doi:[10.1007/s004100050314](https://doi.org/10.1007/s004100050314)
- Stevens G, Villaros A, Moyen JF (2007) Selective peritectic garnet entrainment as the origin of geochemical diversity in S-type granites. *Geology* 35:9–12. doi:[10.1130/G22959A.1](https://doi.org/10.1130/G22959A.1)
- Streck MJ, Grunder AL (1997) Compositional gradients and gaps in high-silica rhyolites of the Rattlesnake Tuff, Oregon. *J Petrol* 38:133–163. doi:[10.1093/petrology/38.1.133](https://doi.org/10.1093/petrology/38.1.133)
- Sylvester P (1998) Post-collisional strongly peraluminous granites. *Lithos* 45:29–44. doi:[10.1016/S0024-4937\(98\)00024-3](https://doi.org/10.1016/S0024-4937(98)00024-3)
- Taylor SR, McLennan SM (1985) *The continental crust: its composition and evolution*. Blackwell, New York
- Vielzeuf D, Holloway JR (1988) Experimental determination of fluid absent melting relations in the pelitic system. *Contrib Mineral Petrol* 98:257–276. doi:[10.1007/BF00375178](https://doi.org/10.1007/BF00375178)
- Vielzeuf D, Montel JM (1994) Partial melting of Metagreywackes. 1. Fluid-absent experiments and phase-relationships. *Contrib Mineral Petrol* 117:375–393. doi:[10.1007/BF00307272](https://doi.org/10.1007/BF00307272)
- Villaros A, Stevens G, Buick IS (2009) Tracking S-type granite from source to emplacement: clues from garnet in the Cape Granite Suite. *Lithos* (in press)
- Villaseca C, Orejana D, Paterson BA (2007) Zr–LREE rich minerals in residual peraluminous granulites, another factor in the origin of low Zr–LREE granitic melts? *Lithos* 96:375–386. doi:[10.1016/j.lithos.2006.11.002](https://doi.org/10.1016/j.lithos.2006.11.002)
- Watson EB (1996) Dissolution, growth and survival of zircons during crustal fusion: kinetic principles, geological models and implications for isotopic inheritance. *Trans R Soc Edinb Earth Sci* 87:43–56
- Watson EB, Harrison TM (1983) Zircon saturation revisited—temperature and composition effects in a variety of crustal magma types. *Earth Planet Sci Lett* 64:295–304. doi:[10.1016/0012-821X\(83\)90211-X](https://doi.org/10.1016/0012-821X(83)90211-X)
- Watt GR, Harley SL (1993) Accessory mineral phase controls on the geochemistry of crustal melts and restites produced during water-undersaturated partial melting. *Contrib Mineral Petrol* 114:550–566. doi:[10.1007/BF00321759](https://doi.org/10.1007/BF00321759)
- White AJR, Chappell BW (1977) Ultrametamorphism and granitoid genesis. *Tectonophysics* 43:7–22. doi:[10.1016/0040-1951\(77\)90003-8](https://doi.org/10.1016/0040-1951(77)90003-8)
- Williamson BJ, Shaw A, Downes H, Thirlwall MF (1996) Geochemical constraints on the genesis of hercynian two-mica leucogranites from the Massif Central, France. *Chem Geol* 127:25–42. doi:[10.1016/0009-2541\(95\)00105-0](https://doi.org/10.1016/0009-2541(95)00105-0)
- Williamson BJ, Downes H, Thirlwall MF, Beard A (1997) Geochemical constraints on restite composition and unmixing in the Velay anatectic granite, French Massif Central. *Lithos* 40:295–319. doi:[10.1016/S0024-4937\(97\)00033-9](https://doi.org/10.1016/S0024-4937(97)00033-9)

Chapter 7

Synthesis and general conclusions

7.1 A comprehensive model for S-type granite petrogenesis

7.1.1 Peritectic phase entrainment in the petrogenesis of S-type granites

Experimental data from previous studies on the fluid-absent melting of metapelites (e.g. Vielzeuf and Montel 1994; Patiño Douce and Beard 1996) have demonstrated that the melts produced via the anatexis of metapelites and metagreywackes are limited to leucocratic granitic compositions, particularly if it is considered that temperatures within the metamorphic crust only rarely exceed 900°C (e.g. Harley 1998). This observation is important to our understanding of S-type granite petrogenesis, as none of the processes previously proposed to account for the origin of the more mafic S-type granites appears to be compatible with the requirement of exclusively leucocratic melt compositions, generated via fluid-absent anatexis. Each of the main models for S-type granite petrogenesis is discussed below, in light of these findings: The leucogranitic nature of the melts produced from the anatexis of metasediments requires mixing with a rather large component of mafic magma to produce the major element compositional variations observed in S-type granites. Typical mafic magma compositions that could mix with S-type melts range from basaltic to andesitic. Figure 7.1 shows that the addition of mafic magma to a typical metapelite-derived water-undersaturated leucogranitic S-type melt will increase the $Fe + Mg$ content, but will not change A/CNK values in a manner similar to the trend observed in the granites. Even the addition of high-K mafic magmas such as lamprophyre (e.g. Vaugnerite), do not match this variation. There are

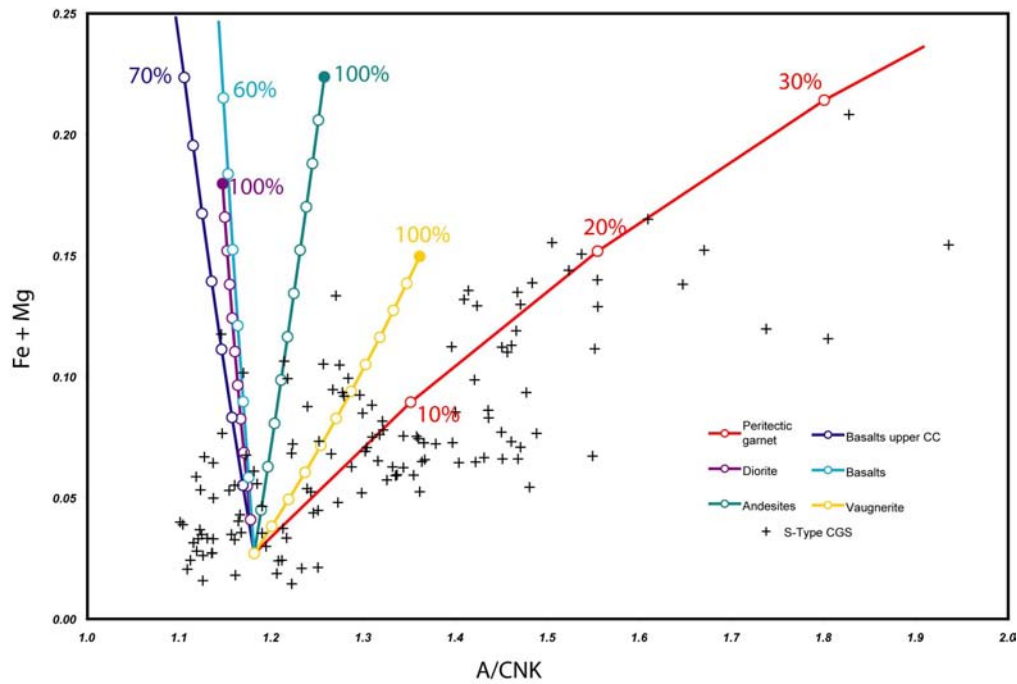


Figure 7.1: Fe+Mg vs. A/CNK diagrams showing the modelling of magma mixing. Average compositions from Condie *et al* 1993 (Andesites, Basalts upper CC, Basalts), Gao *et al* 1998 (Diorite) and Michon 1987 (Vaagnerite) Garnet composition is the same than in Stevens *et al* 2007.

significant challenges to fractional crystallisation in granitic systems, crystals are unlikely to segregate under gravity. Flow segregation (e.g. Weinberg *et al.* 2001) may be applicable (Pupier 2008), but may be of relatively local importance (Pons *et al.* 2006). On major element compositional grounds, fractional crystallization appears to be similarly unlikely in generating the compositional range exhibited by the granites, as the compositions of the more mafic granites are matched by mixtures of the leucogranitic melt composition and 20 wt% garnet cumulate. Typical experimental melt compositions produced at 900°C will crystallize only 4 wt% garnet. Thus, if the magma compositions that leave the source are similar to these

experimental melts, the more mafic granites would need to be balanced by the existence of substantially larger volumes (4 to 5 time more) of very leucocratic granites. For most S-type granitic complexes this volume of very leucocratic material is not present in the rock record. This is certainly the case for S-type CGS. One possibility to account for the absence of this material might be that it was vented through volcanoes. However, only a limited volume of peraluminous volcanic rocks are associated with the S-type granites of the CGS. The leucogranitic composition of these ignimbrites (Scheepers and Nortje 2000) is extremely close to composition of experimental melt composition and could correspond to such material. However, as there is no record of a sufficiently large quantity of this very leucogranitic residual magma in the case of most S-type granitoid suites, it is unlikely that the observed range in major element compositions has been produced only by fractional crystallisation. Assimilation of country rocks might have some potential to produce the compositions of the more mafic granites. However, high proportions of assimilated material are required. As shown in Figure 7.2, in the assimilation of pelites by magmas with the compositions of typical experimental melts, the more mafic granite compositions require the addition of $> 90\%$ pelite to a melt. Considering the low rates of assimilation of xenoliths (McLeod *et al.* 1998), the assimilation of a large number of xenoliths in a cooling magma is strongly challenged by the rather short time necessary for the formation of granite (100 kys from Hawkesworth *et al.* 2000) and thus assimilation of metasedimentary xenoliths is unlikely to be efficient to produce the observed compositional variation observed in S-type granites (Clarke 2007). The other major set of hypotheses for the origin of major element variation in granitic magmas revolves around restite entrainment and restite unmixing (e.g. Barbero *et al.* 1992). Restite is commonly defined as

residual source material. Sticking to this definition, restite entrainment can also produce some of the major element trends. However the quantity of restite material necessary to produce the observed variation is over 50% (Figure 7.2). However, according to Clemens (2003), the enclaves that are typically considered as restitic never show a typical melt-depleted composition. Still following the definition of Restite, there are four key arguments against restite entrainment and restite unmixing: 1) the essentially amphibolite-facies nature of restite as defined by Clemens and Watkins (2001) means that granites are the consequence of low-temperature, water-present melting. Obviously this is not the case for high-level granites. 2) Restite assimilation is a very similar process to country rock assimilation involving metapelites. The same arguments around heat budget that make this process unlikely also then apply to restite assimilation. 3) Restite entrainment should produce substantial scatter in the composition of mafic granites. This is contrary to the trends observed in suites which focus towards the mafic end of the compositional spectrum. 4) Restite unmixing is very much analogous to fractional crystallization. The same physical constraints to this process, insufficient density contrast between crystals and melt, melt too viscous etc. Also limit the applicability of restite unmixing. Beside these arguments, the restite model introduces a connection between source processes and composition of S-type granite with the notion that residual source material might affect the composition of magma and that might explain why the composition of S-type granite evolves from leucogranitic to granodioritic in the direction the composition of its source. In this case, we should see S-type suites evolving towards sedimentary compositions with the entire scatter inherent to typical shales and greywackes. Peritectic garnet entrainment is quite similar to restite entrainment. The main difference resides in the fact that in the first

case, the admixture is defined by a reaction stoichiometry and in the second, by the composition of the source. Observations made on the systematic of compositional variations in S-type CGS (Figure 2.1) show well developed trends. This observation is in agreement with the idea that the major element composition of the granite is not only controlled by the nature of the source but mainly controlled by the stoichiometry of the reaction of partial melting and that solid and liquid products of partial melting reaction are extracted from the source region to produce S-type granites. In comparison with the other models proposed for the formation of S-type granites the selective mineral entrainment model brings new insights to the understanding of the petrogenesis of S-type granite. Since S-type melt has a leucogranitic composition, peritectic phase entrainment is the only model that can produce the observed compositional variations using a reasonable amount of material. The addition of only 20 wt% of peritectic garnet is necessary, while a similar variation needs the addition more than 50 wt% of undifferentiated restitic material or more than 90 wt% of metasedimentary xenoliths. In this regard peritectic phase entrainment appears as a better option for creating the compositional range than restite models or assimilation and fractional crystallisation models. However, the lack of occurrences for peritectic phases in S-type granites constitutes a major obstacle for the peritectic phase entrainment model. Thus, in order to complete the model the fate of the entrained peritectic phase needs to be discussed.

7.1.2 The fate of the entrained peritectic phase

I have just made a case for peritectic phase entrainment (garnet) in the CGS. As in the case of restitic material, there is no clear field evidence for the entrainment

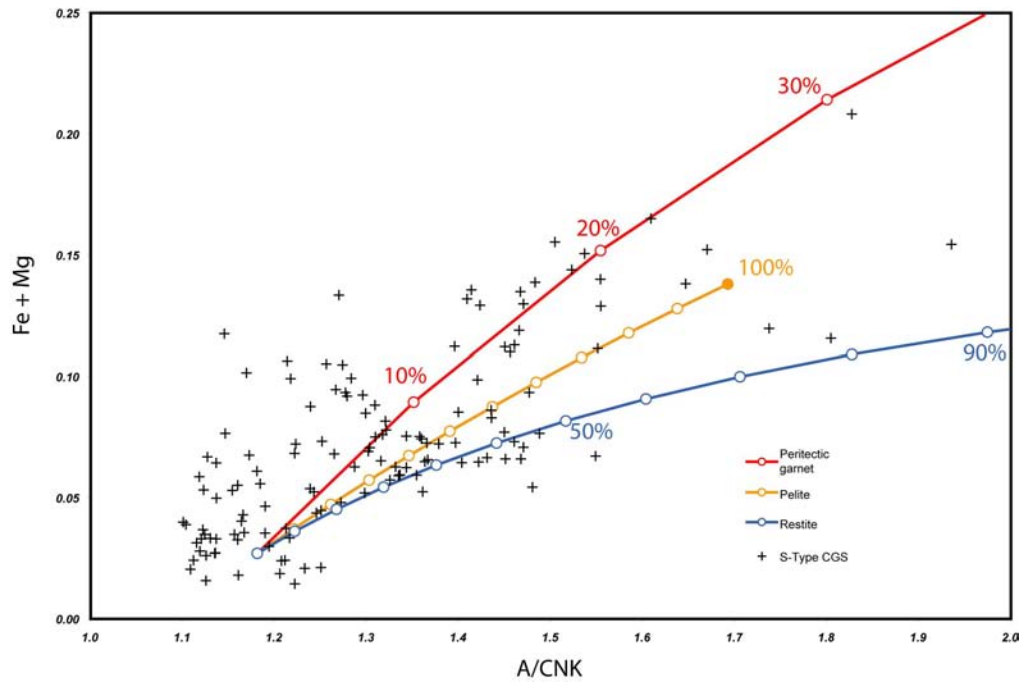


Figure 7.2: Fe+Mg vs. A/CNK diagrams showing the Modelling for contamination processes (restite, pelite). Average pelitic composition from Gao *et al.* 1998, Restite composition calculated from average pelitic composition (for 40% melt).

of peritectic garnet. Many S-type granites contain garnet, as do the CGS rocks. Is this the peritectic garnet? Garnet crystals in the CGS are cracked, pseudo-euhedral in-shape and only rarely contain mineral inclusions. They are characterised by a Mg-rich core of very homogeneous composition ($X_{pyr} = 15\%$ and $X_{Sps} = 4\%$) surrounded by a thin Mn-Rich rim ($\sim 100\mu m X_{pyr} = \sim 4\%$ and $X_{Sps} = \sim 12\%$). Pseudosections, calculated for different compositions of S-type CGS, help to understand the importance of garnet during the formation of S-type granites. At the suspected conditions of partial melting of the source (i.e. $> 850^{\circ}C$ and 10 kb) garnet is present as a solid phase in the magma in significant proportions (from 14 to 23 wt%, from composition used in Villaros *et al.* (2009a)). At lower temperatures and pressures, garnet remains present in the magma but with different composi-

tions. This is in agreement with the observation of local garnet-rich granites in the S-type CGS. However, the pseudo-euhedral shapes of the garnets and the homogeneous compositions of the cores indicate that they are likely to have a magmatic origin. Using the calculated pseudosections, compositions of garnet cores and rims show that garnet equilibrate in the magma at pressure and temperature conditions (5 kb and 750°C for the core; 3 kb and 720°C for the rim) much lower than those believed to represent the source of the magmas ($> 850^{\circ}\text{C}$ and 10 kb). Thus, garnets preserved in the S-type CGS plutons are unlikely to have a peritectic origin. So the chemistry of the rocks suggests peritectic garnet entrainment, and the rocks do contain garnet, but this garnet equilibrated at conditions below those of the source. So what does this garnet represent? Changes to pressure and temperature conditions during magma ascent must affect the stability of the entrained peritectic garnet. Typically garnet's composition in X_{Grs} and X_{Pyr} decreases with decreasing pressure and decreasing temperature. At pressure below 5 kb, X_{Spss} must increase considerably to ensure garnet stability (Spear *et al.* 1984). Thus, the entrained peritectic garnet becomes unstable with decreasing pressure and temperature but it cannot be simply dissolved in the melt as decreasing pressure and temperature reduces melt solubility for elements such as Ca, Fe and Mg. Interestingly, the behaviour of melt solubility indicates that none of the components of garnet can have been included in the melt. Considering the short time needed for the formation of large granitic bodies (< 100 ka), this replacement must have been relatively fast. On this time scale it is unlikely that peritectic garnet would re-equilibrate in the magma by a diffusional process on this time scale (Villaro *et al.* 2009a). Thus, the process leading to the disappearance of peritectic garnet must be sufficiently fast and does not imply a digestion of garnet by melt. Thus, the instability of entrained

peritectic garnet and the magmatic character of the few garnets preserved in granite imply that peritectic garnets were probably replaced by newly formed ferromagnesian phases such as garnet, but also biotite or cordierite. This transformation must occur as a particularly fast dissolution/precipitation reaction because melt can not absorb significant material from garnet. This replacement of entrained peritectic phases by apparent magmatic phases by dissolution/precipitation explains the absence of peritectic material in the granite.

7.1.3 Entrainment and the fate of accessory minerals

The strong positive correlation between maficity and Zr observed in S-type granite is fundamental in understanding the trace element composition of a granite. In a general way, the most mafic S-type granites have the highest concentrations of most of the trace elements. The behaviour of Zr, in regard to peritectic phase entrainment as an origin of the variation of maficity in S-type granite, suggests the entrainment of Zr-rich phases along with peritectic mineral in the melt. In this case zircon is an excellent candidate. In addition, the Zr-undersaturated nature of some of the leucogranites indicates that they cannot have been derived from the more mafic (and Zr-rich) granites by a process of magmatic evolution. This way, it is unlikely that compositional variations in S-type granite are due to fractional crystallization or to restite unmixing. In the same way, variation of trace element concentrations such as the LREE suggests the entrainment of monazite. The control of trace element concentration by accessory minerals and their importance during partial melting of the trace elements composition of melt have been long discussed (e.g. Bea 1996). The fact that a substantial fraction of the

more leucogranitic compositions are zircon-undersaturated, whilst the more mafic compositions are typically oversaturated suggests that the concentrations of most trace elements in S-type melts is particularly low. I shown that the variation of maficity in S-type granite is the result of the entrainment of peritectic phases in leucogranitic melt. Thus the correlation between Zr concentration and maficity of granite suggest a co-entrainment of zircon along with peritectic phases. Similarly, the positive correlation between LREE concentrations and maficity suggest the co-entrainment of monazite and S-type melt composition is likely to be undersaturated in LREE. This co-entrainment is nicely illustrated by the modelling undertaken by Villaros *et al.* (2009b). Evidence for the entrainment of zircon can be easily found in S-type granites as many studies have described the presence of inherited zircon cores commonly surrounded by thin magmatic zircon overgrowths (e.g. Williams 1995). In contrast, the inheritance of monazite in such granites has never been described. The mechanism for the entrainment of peritectic and accessory minerals in the melt finds a possible explanation in the fact that accessory minerals (commonly contained in biotite of metapelites) are released into the melt during partial melting reaction and the consumption of the biotite. Thus, zircons and monazite are entrained by the melt, as solid phases out of the source region, along with the peritectic products of the melting reaction. Whilst relicts of inherited zircons preserved in S-type granites suggest that entrained zircons have been partially dissolved, the magmatic overgrowth implies that the crystallisation of a new generation of zircon. The dissolution of zircon occurs within a Zr-undersaturated melt and the formation of magmatic overgrowth suggests that the magma from which they crystallise was Zr-oversaturated. The behaviour of zircon appear to be a consequence of the entrainment of zircons in a Zr-undersaturated leucogranitic

melt. At high temperature (relatively near the source) zircons are first dissolved until melt is saturated in zirconium. At lower temperature, as the solubility of Zr in peraluminous leucogranitic melt decreases, melt becomes oversaturated and magmatic zircon precipitates as overgrowths on relict zircons. The fate of monazite is likely to be very similar to zircon, except that entrained monazite is apparently entirely dissolved before LREE saturation of melt is reached. Thus only magmatic monazite, formed during granite crystallisation, is preserved.

7.2 Time of residence of melt in the source vs. time of building of large granitic bodies

The time of residence of melt in the source region of S-type CGS granites is less than 100 years (Villaros *et al.* 2009a), This contrasts with U-Pb dating of magmatic zircons in the S-type CGS which provides a 30 Ma range of S-type granite emplacement ages (Da Silva *et al.* 2000; Scheepers and Armstrong, 2002; Scheepers and Poujol 2002). This difference of time scale, between melt extraction and pluton construction, implies that plutons in the CGS are built from successive discrete magma batches that remain only a short time in the source before being extracted and quickly transported towards the crystallisation site. Several other studies suggest that the time of residence of melt in granite source regions is extremely short (e.g. Sawyer 1991; Bea 1996; Brown 2005; Bea *et al.* 2006), and that magma transport is nearly instantaneous on geological timescales (Clemens and Mawer 1992; Petford *et al.* 1993). In contrast, crystallisation ages recorded in plutons indicate a rather slow process that lasts for several millions years in certain cases (e.g. Annen

et al. 2006). This difference, between time of residence in the source and duration of granite emplacement and formation of large granitic bodies, is in agreement with the accumulation of successive magma batches, as proposed by several authors (e.g. Vigneresse and Bouchez 1997). Indeed, during partial melting, melt and peritectic phases reside briefly in the source before being transported quickly towards emplacement sites where magma crystallises. The accumulation of such batches with various proportions of peritectic and accessory minerals, helps to build very large volumes of granitic bodies.

7.3 General Conclusions

Taken together, the results of this study define a coherent model for the mechanisms of major and trace element compositional variation in S-type granites. The selective entrainment of peritectic phases and the coupled entrainment of accessory phases texturally associated with reactant biotite appears to present a reasonable explanation for both major and trace elements variations in S-type granites. This process shows that S-type magma compositional variation is inherited from the partial melting reactions of the metasedimentary source with no major addition of external material (juvenile magma or wall-rock). A subsequent re-equilibration of the entrained minerals within the magma occurs through a dissolution-recrystallisation process. The result of this process is that mineral textural and mineral chemical evidence for peritectic phase entrainment are almost entirely erased from the granites. This mechanism of entrainment, dissolution-precipitation is in agreement with short timescale inferred for the ascent and emplacement of granitic magma, and in agreement with a formation through successive pulses of magma with different

compositions extracted from the source. For the first time a petrogenetic model appears to answer satisfactorily the compositional and petrological requirements of S-type granite formation.

References

- Annen C., Scaillet B. and Sparks R.S.J., 2006. Thermal constraints on the emplacement route of a large intrusive complex: The Manaslu Leucogranite, Nepal Himalaya. *J. Petrol.* 47:71-95.
- Barbero L. and Villaseca C., 1992. The Layos Granite, Hercynian complex of Toledo (Spain) - an example of parautochthonous restite-Rich granite in a granulitic area. *Trans. Royal Soc. Edinburgh-Earth Sci.* 83:127-138.
- Bea F., 1996. Residence of REE, Y, Th and U in granites and crustal protoliths; Implications for the chemistry of crustal melts. *J. Petrol.* 37:521-552.
- Bea F., Montero P., and Ortega M., 2006. A LA-ICP-MS evaluation of Zr reservoirs in common crustal rocks: Implications for Zr and Hf geochemistry, and zircon-forming processes. *Can. Mineral.* 44:693-714.
- Brown M., 2005. The mechanism of melt extraction from lower continental crust of orogens. *Trans. Royal Soc. Edinburgh, Earth Sci.* 95:35-48.
- Clarke D.B., 2007. Assimilation of xenocrysts in granitic magmas: principles, processes, proxies and problems. *Can. Mineral.* 45:5-30.
- Clemens J.D. and Mawer C.K., 1992. Granitic magma transport by fracture propagation. *Tectonophysics* 204:339-360.
- Clemens J.D. and Watkins J.M., 2001. The fluid regime of high temperature metamorphism during granitoid magma genesis: *Contrib. Mineral. Petrol.* 140:600-606.
- Condie, K.C. 1993. Chemical composition and evolution of the upper continental crust: contrasting results from surface samples and shales. *Chem. Geol.* 104:1-37
- Da Silva L.C., Gresse P.G., Scheepers R., McNaughton N.J., Hartmann L.A. and Fletcher I., 2000. U-Pb SHRIMP and Sm-Nd age constraints on the timing and sources of the Pan-African Cape Granite Suite, South Africa. *J. Afr. Earth Sci.* 30:795-815.
- Gao S., Luo T.-C., Zhang B.-R., Zhang H.-F., Han Y.-W., Zhao Z.-D. and Hu Y.-K., 1998. Chemical composition of the continental crust as revealed by studies in East China. *Geochim. Cosmochim. Acta* 62:1959-1975.
- Harley S.L., 1998. On the occurrence and characterisation of ultrahigh temperature (UHT) crustal metamorphism. In: What Controls Metamorphism and Metamorphic Reactions? Treloar P.J. and O'Brien P. (eds), *Spec. Publ. Geol. Soc. London*, 138:75-101

- Hawkesworth C.J., Blake S., Evans P., Hughes R., Macdonald R., Thomas L. E., Turner S.P. and Zellmer G., 2000. Time scales of crystal fractionation on magma Chambers - integrating physical, isotopic and geochemical perspectives. *J. Petrol.* :41, 991-1006
- McLeod P., Stephen R. and Sparks J., 1998. The dynamics of xenolith assimilation. *Contrib. Mineral. Petrol.* 132:21-33.
- Michon G., 1987, Les vauugn erites de l'Est du Massif central fran ais: apport de l'analyse statistique multivari e   l' tude g ochimique des  l ments majeurs. *Bull. Soc.G ol. France* 3:591-600.
- Pati o Douce A.E. and Beard J.S., 1996. Effects of P, $f(O_2)$ and Mg/Fe ratio on dehydration melting of model metagreywackes: *J. Petrol.* 37:999-1024
- Petford N., Kerr R. C. and Lister J. R., 1993. Dike transport of granitic magmas. *Geology* 21: 843-845.
- Pons, J., Barbey, P., Nachit, H. and Burg, J. P. 2006. Development of igneous layering during growth of pluton: The Tarcouate Laccolith (Morocco). *Tectonophysics* 413:271-286.
- Pupier E., Barbey P., Toplis M. J. and Bussy F., 2008. Igneous layering, fractional crystallization and growth of granitic plutons: the Dolbel Batholith in SW Niger. *J. Petrol.* 49:1043-1068.
- Sawyer E. W., 1991. Disequilibrium melting and the rate of melt residuum separation during migmatization of mafic rocks from the Grenville Front, Quebec. *J. Petrol.* 32:701-738.
- Scheepers R. and Nortje A. N., 2000. Rhyolitic ignimbrites of the Cape Granite Suite, southwestern Cape Province, South Africa. *J. Afr. Earth Sci.* 31, 647-656
- Scheepers R. and Armstrong R. A., 2002. New U-Pb SHRIMP zircon ages of the Cape Granite Suite: implications for the magmatic evolution of the Saldania Belt. *S. Afr. J. Geol.* 105:241-256.
- Scheepers R. and Poujol M., 2002. U-Pb zircon age of Cape Granite Suite ignimbrites: characteristics of the last phases of the Saldaniaan magmatism. *S. Afr. J. Geol.* 105:163-178.
- Spear F.S., Selverstone J., Hickmott D., Crowley P. and Hodges K.V., 1984. P-T paths from garnet zoning: A new technique for deciphering tectonic processes in crystalline terranes. *Geology*, 12:87-90.
- Vielzeuf D. and Montel J.-M., 1994. Partial melting of metagreywackes, 1: Fluid-absent experiments and phase relationships: *Contrib. Mineral. Petrol.* 117:375-393

- Vignerresse J.-L. and Bouchez J.-L., 1997. Successive granitic magma batches during pluton emplacement: the case of Cabeza de Araya (Spain). *J. Petrol.* 38:1767-1776.
- Villaros A., Stevens G. and Buick I.S., 2009a. Tracking S-type granite from source to emplacement: Clues from garnet in the Cape Granite Suite, *Lithos* in press
- Villaros A., Stevens G., Moyen J.-F. and Buick I.S., 2009b. The trace element compositions of S-type granites: Evidence for disequilibrium melting and accessory phase entrainment in the source. *Contrib. Mineral. Petrol.* In press.
- Weinberg R.F., Sial A.N. and Pessoa R.R., 2001. Magma flow within the Tavares pluton, north-eastern Brazil: compositional and thermal convection. *Geol. Soc. Amer. Bull.* 113:508-520.
- Williams I.S., 1995. Zircon analysis by ion microprobe: the case of the eastern Australian granites, Leon T. Silver 70th Birthday Symposium and Celebration, *The California Institute of Technology*, 27-31

General references

- A -

- Acosta-Vigil A., London D. and Morgan G., 2006. Experiments on the kinetics of partial melting of a leucogranite at 200 MPa H_2O and 690 – 800°C: compositional variability of melts during the onset of H₂O-saturated crustal anatexis. *Contrib. Mineral. Petrol.* 151:539-557.
- Annen C., Scaillet B. and Sparks R.S.J., 2006. Thermal Constraints on the Emplacement Rate of a Large Intrusive Complex: The Manaslu Leucogranite, Nepal Himalaya. *J. Petrol.* 47:71-95.
- Armstrong R.A., De Wit M.J., Reid D.L., York D. and Zattman R., 1998. Table Mountain reveals rapid Pan African uplift of its basement rocks. *J. Afr. Earth. Sci.*, 27:10-11.
- Ayres M. and Harris N., 1997. REE fractionation and Nd-isotope disequilibrium during crustal anatexis: constraints from himalayan leucogranites. *Chem. Geol.* 139:249-269.
- Ayres M., Harris N. and Vance D., 1997. Possible constraints on anatexitic melt residence times from accessory mineral dissolution rates: an example from Himalayan leucogranites. *Mineral. Mag.*, 61:29-36.
- Ayres M. and Vance D., 1997. A comparison study of diffusion profiles in Himalayan and Dalradian garnets: constraints on diffusion data and the relative duration of the metamorphic events. *Contrib. Mineral. Petrol.* 128:66-80.

- B -

- Baker D.R., Conte A.M., Freda C., Ottolini L., 2002. The effect of halogens on Zr diffusion and zircon dissolution in hydrous metaluminous granitic melts. *Contrib. Mineral. Petrol.* 142:666-678
- Barbero L. and Villaseca C., 1992. The Layos Granite, Hercynian Complex of Toledo (Spain) - an Example of parautochthonous restite-rich granite in a granulitic area. *Trans. R. Soc. of Edinburgh-Earth Sci.*, 83:127-138.
- Bea F., 1996a. Residence of REE, Y, Th and U in granites and crustal protoliths; Implications for the chemistry of crustal melts. *J. Petrol.* 37:521-552
- Bea F., 1996b. Controls on the trace element composition of crustal melts. *Trans. Roy. Soc. of Edinburgh-Earth Sci.* 87:33-41

- Bea F., Pereira M.D. Corretge L.G. and Fershtater G.B., 1994. Differentiation of strongly peraluminous, perphosphorus granites - the Pedro Bernardo Pluton, Central Spain. *Geochim. Cosmochim. Acta* 58:2609-2627.
- Bea F., Pereira M.D. and Stroh A., 1994. Mineral leucosome trace-element partitioning in a peraluminous migmatite (a Laser Ablation-ICP-MS Study). *Chem. Geol.* 117:291-312.
- Bea F., Montero P., Garuti G. and Zacharini F., 1997. Pressure-dependence of rare earth element distribution in amphibolite- and granulite-grade garnets. A LA-ICP-MS study. *Geostand. Newsl. - J. Geostand. and Geoanal.*, 21:253-270.
- Bea F., Montero P., Ortega M., 2006. A LA-ICP-MS evaluation of Zr reservoirs in common crustal rocks: Implications for Zr and Hf geochemistry, and zircon-forming processes. *Can. Mineral.* 44:693-714
- Bea F., Montero P., Gonzalez-Lodeiro F., Talavera C., 2007. Zircon inheritance reveals exceptionally fast crustal magma generation processes in central Iberia during the Cambro-Ordovician. *J. Petrol.* 48:2327-2339
- Belcher R.W. and Kisters, A.F.M., 2003. Lithostratigraphic correlations in the western branch of the Pan-African Saldania Belt, South Africa: the Malmesbury Group revisited. *S. Afr. J. Geol.* 106:327-342.
- Bhadra S., Das S., Bhattacharya A., 2007, Shear zone-hosted migmatites (Eastern India): the role of dynamic melting in the generation of REE-depleted felsic melts, and implications for disequilibrium melting. *J. Petrol.* 48:435-457
- Bogaerts M. and Schmidt M.W., 2006. Experiments on silicate melt immiscibility in the system $Fe_2SiO_4 - KAlSi_3O_8 - SiO_2 - CaO - MgO - TiO_2 - P_2O_5$. *Contrib. Mineral. Petrol.* 152:257-274.
- Bohrson W.A. and Spera F.J., 2001. Energy-constrained open-system magmatic processes II: application of energy-constrained assimilation-fractional crystallization (EC-AFC) Model to Magmatic systems. *J. Petrol.* 42:1019-1041.
- Bourne J. and Danis D., 1987. A proposed model for the formation of reversely zoned plutons based on study of the Lacorne Complex, Superior Province, Quebec. *Can. J. Earth Sci.* 24:2506-2520.
- Breaks F. W. and Moore J. M., 1992. The Ghost Lake batholith, Superior Province of Northwestern Ontario - a fertile, S-type, peraluminous granite - rare-element pegmatite system. *Can. Mineral.* 30:835-875.
- Brown M., 1994. The generation, segregation, ascent and emplacement of granite magma - the migmatite-to-crustally-derived-granite connection in thickened orogens. *Earth-Science Rev.* 36:83-130.

- Brown M., 2001. Crustal melting and granite magmatism: Key issues. *Phys.Chem. Earth Part a-Solid Earth Geod.* 26:201-212.
- Brown M., 2005. The mechanism of melt extraction from lower continental crust of orogens. *Trans. Royal Soc. Edinburgh, Earth Sci.* 95:35-48.
- Brown M., Averkin Y.A., McLellan E.L. and Sawyer E.W., 1995. Melt segregation in migmatites. *J Geophys. Res.-Sol. Earth* 100:15655-15679.
- Brown M. and Pressley R.A., 1999. Crustal melting in nature: Prosecuting source processes. *Phys. Chem. Earth Part a-Sol. Earth and Geod.* 24:305-316.

- C -

- Cann J.R., 1970. Upward movement of granitic magmas. *Geol. Mag.*, 43:335-340.
- Carlson W.D., 2006. Rates of Fe, Mg, Mn, and Ca diffusion in garnet. *Am. Mineral.*, 91:1-11.
- Carrington, D.P. and Harley S.L. 1995. Partial melting and phase-relations in high-grade metapelites - an experimental petrogenetic grid in the KFMASH system. *Contrib. Mineral. Petrol.* 120:270-291.
- Cawthorn R.G., 1996. Layered Intrusions. Amsterdam, Elsevier. P. 531
- Cesare B., Savioli Mariani E. and Venturelli G., 1997. Crustal anatexis and melt extraction during deformation in the restitic xenoliths at El Joyazo (SE Spain). *Mineral. Mag.*, 61, 15-27.
- Chappell B.W., 1984. Source rocks of I- and S-type granites in the Lachlan Fold Belt, southeastern Australia. *Phil. Trans. Royal Soc. London Series a- Mathem. Phys. and Eng. Sci.* 310:693-707.
- Chappell B.W., 1996. Compositional variation within granite suites of the Lachlan Fold Belt: its causes and implications for the physical state of granite magma. *Trans. Royal Soc. Edinburgh: Earth Sci* 87:159-170.
- Chappell B.W., 1999. Aluminium saturation in I- and S-type granites and the characterization of fractionated haplogranites. *Lithos.* 46:535-551.
- Chappell B.W. and White A.J.R., 1974. Two contracting granite types. *Pac. Geol.* 8:173-174.

- Chappell B.W., White A.J.R. and Wiborn D., 1987. The importance of residual source material (Restite). *J. Petrol.* 28:1111-1138.
- Chappell B.W. and White A.J.R., 1992. I-Type and S-Type granites in the Lachlan Fold Belt. *Trans. Royal Soc. Edinburgh- Earth Sci.* 83:1-26.
- Chappell B.W., White A.J.R. and William I.S., 2000. Lachlan Fold Belt granites revisited: high- and low-temperature granites and their implications. *Austr. J. Earth Sci.* 47:123-138.
- Chappell B.W. and White A.J.R., 2001. Two contrasting granite types: 25 years later. *Austr. J. Earth Sci.* 48:489-499.
- Clarke D.B., 2007. Assimilation of xenocrysts in granitic magmas: principles, processes, proxies and problems. *Can. Mineral.* 45:5-30.
- Clarke D.B. and Carruzo S., 2007. Assimilation of country-rock ilmenite and rutile in the South Mountain batholith, Nova Scotia, Canada. *Can. Mineral.* 45:31-42.
- Clemens J.D., 1992. Partial melting and granulite genesis - a Partisan Overview. *Pre-camb. Res.* 55:297-301.
- Clemens J.D., 2003. S-type granitic magmas - petrogenetic issues, models and evidence. *Earth-Science Rev.* 61:1-18.
- Clemens J.D., 2006. Melting of the continental crust: fluid regimes, melting reactions and source-rock fertility, in Brown, M. and Rushmer, T. (eds) *Evolution and Differentiation of the Continental Crust*, Cambridge Univ. Press, 397-331.
- Clemens J.D. and Wall V.J., 1981. Origin and crystallization of some peraluminous (S-type) granitic magmas. *Can. Mineral.*, 19:111-131.
- Clemens J.D. and Mawer C.K., 1992. Granitic magma transport by fracture propagation. *Tectonophysics* 204:339-360.
- Clemens J.D., Droop G.T.R., and Stevens G., 1997. High-grade metamorphism, dehydrations and crustal melting: a reinvestigation based on new experiments in the silica-saturated portion of the system $KAlO_2 - MgO - SiO_2 - H_2O - CO_2$ at $P \leq 1.5GPa$. *Contrib. Mineral. Petrol.* 129:308-325.
- Clemens J.D. and Wall V.J., 1984. Origin and evolution of a peraluminous silicic ignimbrite suite: the Violet Town Volcanics. *Contrib. Mineral. and Petrol.* 88:354-371.
- Clemens J.D. and Droop G.T.R., 1998. Fluids, P-T paths and the fates of anatectic melts in the Earth's crust. *Lithos* 44:21-36.

- Clemens J.D. and Watkins J.M., 2001. The fluid regime of high-temperature metamorphism during granitoid magma genesis. *Contrib. Mineral. Petrol.* 140:600-606.
- Collins W.J., 1996. Lachlan Fold Belt granitoids: products of three-component mixing. *Trans. Royal Soc. of Edinburgh: Earth Sci.* 87:171-179.
- Collins W.J. and Hobbs B.E., 2001. What caused the Early Silurian change from mafic to silicic (S-type) magmatism in the eastern Lachlan Fold Belt? *Austr. J. of Earth Sci.* 48:25-41.
- Connolly J.A.D., 1990. Multivariable phase diagrams: an algorithm based on generalized thermodynamics. *Amer. J. Sci.* 290:666-718.
- Connolly J.A.D., 2005. Computation of phase equilibria by linear programming: a tool for geodynamic modeling and its application to subduction zone decarbonation. *Earth and Planet. Sci. Lett.* 236:534-541.
- Connolly J.A.D. and Petrini K., 2002. An automated strategy for calculation of phase diagram sections and retrieval of rock properties as a function of physical conditions. *J. Metam. Geol.* 20:697-708.
- Copeland P., Parrish R.R., Harrison T.M., 1988. Identification of inherited radiogenic Pb in monazite and its implications for U-Pb systematics. *Nature* 333:760-763
- Couch S., 2003. Experimental investigation of crystallization kinetics in a haplogranite system. *Amer. Mineral.* 88:1471-1485.
- Coulson I.M, Villeneuve M.E., Dipple G.M., Duncan R.A., Russel J.K. and Mortensen J.K., 2002. Time-scales of assembly and thermal history of a composite felsic pluton: constraints from the Emerald Lake area, northern Canadian Cordillera, Yukon. *J. Volc. Geotherm. Res.* 114:331-356.
- Crank J., 1975. *The mathematics of diffusion.* Oxford University Press, Oxford. P. 272

- D -

- Da Silva L.C., Gresse P.G., Scheepers R., McNaughton N.J., Hartmann L.A., Fletcher I., 2000. U-Pb SHRIMP and Sm-Nd age constraints on the timing and sources of the Pan-African Cape Granite Suite, South Africa. *J. Afr. Earth Sci.* 30:795-815
- Da Silva L.C., McNaughton N.J., Armstrong R.A., Hartmann L.A., Fletcher I.R., 2005. The Neoproterozoic Mantiqueira Province and its African connection: a zircon based U-Pb geochronologic subdivision for the Brasiliano/Pan-African systems of orogens. *Precamb. Res.* 136:203-240

- Davies G. R. and Tommasini S., (2000). Isotopic disequilibrium during rapid crustal anatexis: implications for petrogenetic studies of magmatic processes. *Chem. Geol.* 162: 169-191.
- Dahlquist J.A. Galindo C., Pankhurst R. J., Rapela C. W., Alasino P. H., Saavedra J. and Fanning C.M., 2007. Magmatic evolution of the Penon Rosado Granite: Petrogenesis of garnet-bearing granitoids. *Lithos* 95, 177-207.
- Day W.C. and Weiblen P.W., 1986. Origin of late Archean granite: geochemical evidence from the Vermilion Granitic Complex of northern Minnesota. *Contrib. Mineral. Petrol.* 93:283-296.
- De Paolo D. J., 1981. Trace element and isotopes effects of combined wallrock assimilation and fractional crystallization. *Earth Planet. Sci. Lett.* 53:189-202.
- Di Vincenzo G., Andriessen P.A.M. and Ghezzo C., 1996. Evidence of two different components in a Hercynian peraluminous cordierite-bearing granite: The San Basilio intrusion (Central Sardinia, Italy). *J. Petrol.* 37:1175-1206.
- Debon F. and Lefort P., 1982. A chemical-mineralogical classification of common plutonic rocks and associations. *Trans. Royal Soc. Edinburgh: Earth Sci.*, 73:135-139.
- Didier J., 1982. Mantle and crustal granites: Genetic classification of orogenic granites and the nature of their enclaves. *J. Volcanol. Geotherm. Res.* 14: 125-132.
- Didier J., 1984. The problem of enclaves in granitic rocks, a review of recent ideas on their origin. in *Geology of Granites and Their Metallogenic Relations*. K. T. Xu, G (Ed.). Beijing, Science Press: 137-144.
- Diener J.F.A., Stevens G., Kisters A.F.M. and Poujol M., 2005. Metamorphism and exhumation of the basal parts of the Barberton greenstone belt, South Africa: Constraining the rates of Mesoarchaean tectonism. *Precamb. Res.*, 143:87-112.
- Downes H., Dupuy C. Leyreloup A., 1990. Crustal evolution of the Hercynian belt of Western Europe: evidence from lower crustal xenoliths (French Massif Central). *Chem. Geol.* 83:209-231.
- Downes H. and Duthou J.-L., 1988. Isotopic and trace-element arguments for the lower-crustal origin of Hercynian granitoids and pre-Hercynian orthogneisses, Massif Central (France). *Chem. Geol.* 68:291-308.
- Droop G.T.R., Clemens J. D. 2003. Processes and Conditions During Contact Anatexis, Melt Escape and Restite Formation: the Huntly Gabbro Complex, NE Scotland. *J. Petrol.* 44:995-1029.
- Dunlevey J.N., 1988. Evolution of the Saldanian Orogeny and development of the Cape Granite Suite. *S. Afr. J. Sci.* 84:565-568.

- E -

- Eggins S., 2003. Laser ablation ICP-MS analysis of geological materials prepared as lithium borate Glasses. *Geostand. Geoanal. Res.* 27:147-162.
- Elburg M.A., 1996. U-Pb ages and morphologies of zircon in microgranitoid enclaves and peraluminous host granite: evidence for magma mingling. *Contrib. Mineral. Petrol.* 123:177-189.
- Ellis D.J. and Obata M., 1992. Migmatite and melt segregation at Cooma, New South Wales. *Trans. Royal Soc. Edinburgh, Earth Sci.* 83:95-106.
- Erdmann S., London D., Morgan Vi G.B. and Clarke D.B., 2007. the contamination of granitic magma by metasedimentary country-rock material: an experimental study. *Can. Mineral.* 45:43-61.
- Escuder Viruete J., Indares, A. and Arenas, R., 2000. P-T Paths derived from garnet growth zoning in an extensional Setting: an example from the Tormes Gneiss Dome (Iberian Massif, Spain). *J. Petrol.* 41:1489-1515.
- Ewart A., Griffin W. L., 1994. Application of proton-microprobe data to trace-element partitioning in volcanic-rocks. *Chem. Geol.* 117:251-284.

- F -

- Ferry J.M. and Spear F.S., 1978. Experimental calibration of the partitioning of Fe and Mg between biotite and garnet. *Contrib. Mineral. Petrol.*, 66, 113-117.
- Flanagan, F.J., 1976. Descriptions and analysis of eight new USGS rock standards. *U.S. Geol. Surv. Prof. Paper*, 840:192.
- Foden J.D., Elburg M.A., Turner S.P., Sandiford M., O'Callaghan J. and Mitchell S., 2002. Granite production in the Delamerian Orogen, South Australia. *J. Geol. Soc.* 159:557-575.

- G -

- Gardien V., Thompson A.B., Grujic D. and Ulmer P., 1995. Experimental melting of biotite + plagioclase + quartz \pm muscovite assemblages and implications for crustal

Melting. *J. Geophys. Res.-Solid Earth* 100:15581-15591

- Georget Y., Martineau F. and Capdevilla R., 1986. Age tardi-hercynien et origine crustale du granite de Brignogan (Finistère, France). Conséquences sur l'interprétation des granites Nord-armoricains: Late-hercynian radiometric age and crustal origin of Brignogan granite (Finistere, France). Consequences on the interpretation of the North-Armorican granites. *C. R. Acad. Sci. Série 2, Mécan. Phys., Chim., Sci. Univ, Sci. Terre* 302:237-242.
- Goad B.E. and Cerny P., 1981. Peraluminous pegmatitic granites and their pegmatite aureoles in the Winnipeg River District, southeastern Manitoba. *Can. Mineral.* 19:177-194.
- Gray C.M., 1990. A strontium isotope traverse across the granitic rocks of southeastern Australia: petrogenetic and tectonic implications. *Austr. J. Earth Sci.* 37: 331-349.
- Green T.H., 1976. Experimental generation of cordierite or garnet bearing granitic liquids from a pelitic composition. *Geology* 4:85-88.
- Gresse P.G., Theron J.N., Fitch F.J. and Miller J.A., 1992. Tectonic inversion and radiometric resetting of the basement in the Cape Fold Belt. In: De Wit M.J. and Ransome I.G.D. (Eds), *Inversion tectonics in the Cape Fold Belt, Karoo and Cretaceous basins of Southern Africa*. A.A. Balkema, Rotterdam, 217-228.
- Gresse P.G., Von Veh M.W. and Frimmel H.E., 2006. Namibian (Neoproterozoic) to early Cambrian successions. In Johnson M.R., Anhaeuser C.R. and Thomas R.J. (Eds) *The geology of South Africa*, Geological society of South Africa, Johannesburg and Council for Geoscience, Pretoria.

- H -

- Hacker B.R., Gnos E., Ratschbacher L., Grove M., McWilliams M., Sobolev S. V., Wan J. and Zhenhan W., 2000. Hot and Dry Deep Crustal Xenoliths from Tibet. *Science*, 287:2463-2466.
- Harley S. L., 1998. On the occurrence and characterisation of ultrahigh-temperature (UHT) crustal metamorphism. In: *What Controls Metamorphism and Metamorphic Reactions?* Treloar, P.J. and O'Brien, P. (eds), *Spec. Publ. Geolog. Soc. London*, 138:75-101
- Harris N., Ayres M., Massey J., 1995. Geochemistry of granitic melts produced during the incongruent melting of muscovite: Implications for the extraction of himalayan leucogranite magmas. *J. Geophys. Res.* 100:15767-15777.

- Harris C., Faure K., Diamond R.E. and Scheepers R., 1997. Oxygen and Hydrogen isotope geochemistry of S- and I- type granitoids: the Cape Granite Suite, South Africa. *Chem Geol.* 143:95-114.
- Harris N., Vance, D. and Ayres, M., 2000. From sediment to granite: timescales of anatexis in the upper crust. *Chem. Geol.* 162:155-167.
- Hartnady C.J.H., Newton, A.R. and Theron J.N., 1974. The stratigraphy and structure of the Malmesbury Group in the southwestern Cape. *Bull. Precamb. Res. Unit* 15: 193-213.
- Hartnady C.J.H., Joubert P. and Stowe C.W., 1985. Proterozoic crustal evolution of southwestern Africa. *Episodes*, 8:236-244.
- Hawkesworth, C.J., Blake S., Evans P., Hughes R., MacDonald R., Thomas L. E., Turner S. P. and Zellmer G., 2000. Time Scales of Crystal Fractionation on magma Chambers - integrating Physical, Isotopic and Geochemical Perspectives. *J. Petrol.* 41, 991-1006.
- Healy B., Collins and W.J. Richard S.W., 2004. A hybrid origin for Lachlan S-type granites: the Murrumbidgee Batholith example. *Lithos* 78:197-216.
- Hensen B.J., 1977. Cordierite-Garnet bearing assemblages as geothermometers and barometers in granulites facies terranes. *Tectonophysics* 43:73-88.
- Hoisch T.D., 1991. Equilibria with the mineral assemblage *quartz+muscovite+biotite+garnet + plagioclase*, and applications for the mixing propriety of octohedrally-coordinated cations in muscovite and biotite. *Contrib. Mineral. Petrol.* 108:43-54.
- Holdaway M.J., 2000. Application of new experimental and garnet Margules data to the garnet-biotite geothermometer. *Am. Mineral.*, 85:881-892.
- Holland T.J.B. and Powell R., 2001. Calculation of phase relations involving haplogranitic melts using an internally consistent thermodynamic dataset. *J. Petrol.* 42:673-683.
- Holland T.J.B. and Powell R., 1998. An internally consistent thermodynamic data set for of petrological interest. *J. Metam. Geol.* 16:309-343.
- Holtz F. and Johannes W., 1991. Genesis of Peraluminous Granites .1. Experimental Investigation of Melt Compositions at 3 and 5 Kb and Various H_2O Activities. *J. Petrol.* 32:935-958.
- Holtzman B.K. and Kohlstedt D.L., 2007. Stress-driven Melt Segregation and Strain Partitioning in Partially Molten Rocks: Effects of Stress and Strain. *J. Petrol.* 48:2379-2406.

Hwang S.L., Shen P., Yui T.F. and Chu H.T., 2003. On the mechanism of resorption zoning in metamorphic garnet. *J. Metam. Geol.* 21:761-769.

- I -

Icenhower J. and London D., 1996. Experimental partitioning of Rb, Cs, Sr, and Ba between alkali feldspar and peraluminous melt. *Amer. Mineral.* 81:719-734.

Inger S. and Harris N., 1993. Geochemical Constraints on Leukogranite Magmatism in the Langtang Valley, Nepal Himalaya. *J. Petrol.* 34:345-368.

Irving A.J. and Frey F.A., 1978. Distribution of trace-elements between garnet megacrysts and host volcanic liquids of kimberlitic to rhyolitic composition. *Geochim. Cosmochim. Acta* 42:771-787

- J -

Johannes W., 1985. The significance of experimental studies for the formation of migmatites. In Ashworth J. R. (Ed) *Migmatites*, Blackie, Glasgow, 36-85

Johannes W., 1988. What controls partial melting in migmatites? *J. Metam. Geol.* 6:451-465.

Johannes W., Ehlers C., Kriegsman L.M., Mengel K., 2003. The link between migmatites and S-type granites in the Turku area, southern Finland. *Lithos* 68:69-90

Johnson, T.E., Hudson N.F.C. and Droops G.T.R., 2001. Partial melting of the Inzie Head gneisses: The role of water and a petrogenetic grid in KFMASH applicable to anatectic pelitic migmatites. *J. Metam. Geol.* 19:99-118.

Jordaan L.J., 1990. The Geology and geochemistry of mafic and intermediate igneous rocks associated with the Cape Granites. M.Sc.Thesis (unpubl.), Univ. Stellenbosch.

Jordaan L.J., Scheepers R. and Barton E.S., 1995. Geochemistry and isotopic composition of the mafic and intermediate igneous components of the Cape Granite Suite, South Africa. *J. Afr. Earth Sci.* 21:59-70.

- Jung S., Mezger K., Masberg P., Hoffer E. and Hoernes S., 1998. Petrology of an intrusion-related high-grade migmatite: implications for partial melting of metasedimentary rocks and leucosome forming processes. *J. Metam. Geol.* 16:425-445.
- Jung S., Hoernes S., Masberg P. and Hoffer E., 1999. The petrogenesis of some migmatites and granites (central Damara Orogen, Namibia): Evidence for disequilibrium melting, wall-rock contamination and crystal fractionation. *J. Petrol.* 40:1241-1269.

- K -

- Keay S., Steele D. and Compston W., 1999. Identifying granite sources by SHRIMP U-Pb zircon geochronology: an application to the Lachlan fold belt. *Contrib. Mineral. Petrol.* 137:323-341.
- Kelsey D.E., Clark C., Hand M., 2008. Thermobarometric modelling of zircon and monazite growth in melt-bearing systems: examples using model metapelitic and metapsammitic granulites. *J. Metam. Geol.* 26:199-212
- Kingsbury J.A., Miller C.F., Wooden J.L., Harrison T.M., 1993. Monazite paragenesis and U-Pb systematics in rocks of the eastern Mojave Desert, California: implications for thermochronometry. *Chem. Geol.* 110:147-168
- Kisters A.F.M., Belcher R.W., Scheepers R., Rozendaal A., Jordaan L.S. and Armstrong R.A., 2002. Timing and kinematics of the Colenso Fault: The Early Paleozoic shift from collisional to extensional tectonics in the Pan-African Saldania Belt, South Africa. *S. Afr. J. Geol.* 105:257-270.
- Kriegsman L.M., 2001a. Partial melting, partial melt extraction and partial back reaction in anatectic migmatites. *Lithos* 56:75-96.
- Kriegsman L.M., 2001b. Quantitative field methods for estimating melt production and melt loss. *Phys. Chem. Earth, Part A: Sol. Earth Geod.* 26:247-253.

- L -

- Lanzirotti A., 1995. Yttrium zoning in metamorphic garnet. *Geochim. Cosmochim. Acta* 59:4105-4110.

- Le Breton N. and Thompson A.B., 1988. Fluid-absent (dehydration) melting of biotite in metapelites in the early stages of crustal anatexis. *Contrib. Mineral. Petrol.* 99:226-237.
- Leake B., Wooley A.R., Arps C.E.S., Birch W.D., Gilbert M.C., Grice J.D., Hawthorne F.C., Kato A., Kisch H.J., Krivovichev V.G., Linthout K., Laird J., Mandarino J.A., Maresch W.V., Nickel E.H., Rock N.M.S., Schumacher J.C., Smith D.C., Stephenson N.C.N., Ungaretti L., Whittaker E.J.W. and Youzhi G., 1998. Nomenclature of Amphiboles: Report of the Subcommittee on Amphiboles of the International Mineralogical Association, Commission on new minerals and minerals names. *Can. Mineral.* 35:219-246.
- Longerich H.P., Jackson S.E., and Gunther D., 1996. Laser ablation inductively coupled plasma mass spectrometric transient signal data acquisition and analyte concentration calculation. In: C. Royal Society of Chemistry, UK 1986 (Revue) (Editor), 1996 . *J. Analyt. At. Spectr.*, 899-904.

- M -

- Maas R., Nicholls I.A., Greig A. and Nemchin A., 2001. U-Pb zircon studies of mid-crustal metasedimentary enclaves from the S-type Deddick Granodiorite, Lachlan Fold Belt, SE Australia. *J. Petrol.* 42:1429-1448.
- Martin H. and Moyen J.-F., 2002. Secular changes in tonalite-trondhjemite-granodiorite composition as markers of the progressive cooling of Earth. *Geology* 30:319-322.
- McKenzie, D. and Onions R. K., 1991. Partial Melt Distributions from Inversion of Rare-Earth Element Concentrations. *J. Petrol.* 32:1021-1091.
- McLaren S., Sandiford, M., Powell R., Neumann N. and Woodhead J., 2006. Palaeozoic Intraplate Crustal Anatexis in the Mount Painter Province, South Australia: Timing, Thermal Budgets and the Role of Crustal Heat Production. *J. Petrol.*, 47:2281-2902.
- McLeod P., Stephen R. and Sparks J., 1998. The dynamics of xenolith assimilation. *Contrib. Mineral. Petrol.* 132(1): 21-33.
- Miller C. F., 1985. Are strongly peraluminous magmas derived from mature sedimentary (pelitic) sources? *J. Geol.* 93: 673-689.
- Montel J.-M., 1993 A model for monazite melt equilibrium and application to the generation of granitic magmas. *Chem. Geol.* 110:127-146

- Montel J.-M., 1996. Géochimie de la fusion de la croûte continentale. Univ. Blaise Pascal, Clermont-Ferrand. 186p.
- Montel J. M. and Vielzeuf D., 1997. Partial melting of metagreywackes .2. Compositions of minerals and melts. *Contrib. Mineral. Petrol.* 128:176-196.
- Moyen, J.F., Stevens, G. and Kisters, A., 2006. Record of mid-Archaean subduction from metamorphism in the Barberton terrain, South Africa. *Nature* 442:559-562.
- Munksgaard N.C., 1985. A non-magmatic origin for compositionally zoned euhedral garnet in silicic Neogene volcanics from SE Spain. *Neues Jahr. Mineral. Monatsh.* 73-82.

- N -

- Nabelek P.I. and Glascock M. D. 1995., Rare earth element-depleted leucogranites Black Hills, South Dakota: A consequence of disequilibrium melting of monazite-bearing schists. *J. Petrol.* 36: 1055-1071.
- Nabelek P.I., Russ-Nabelek C. and Haeussler G.T., 1992. Stable isotope evidence for the petrogenesis and fluid evolution in the Proterozoic, Harney Peak leucogranite, Black Hills, South Dakota. *Geochim. Cosmochim. Acta* 56: 403-417.
- Nash W.P. and Crecraft H.R., 1985. Partition coefficients for trace elements in silicic magmas. *Geochim. Cosmochim. Acta* 49:2309-2322
- Newton R.C., Charlu T.V. and Kleppa O.J., 1980. Thermochemistry of the high structural state plagioclases. *Geochim. Cosmochim. Acta*, 44:933-941.
- Newton R.C. and Haselton H.T., 1981. Thermodynamics of the *garnet – plagioclase – Al_2SiO_5 – quartz* geobarometer, in *Thermodynamics of Minerals and Melts Vol. 1.* 131-148, Springer-Verlag.

- P -

- Parrish R.R., 1990. U-Pb dating of monazite and its application to geological problems. *Can. J. Earth Sci.* 27:1431-1450
- Patiño-Douce A.E., 1996. Effect of pressure and H_2O content on the compositions of primary crustal melts. *Trans. R. Soc. of Edinburgh, Earth Sci.* 87:11-21

- Patiño-Douce A.E. and Johnston A.D., 1991. Phase equilibria and melt productivity in the pelitic system: implications for the origin of peraluminous granitoids and aluminous granulites. *Contrib. Mineral. Petrol.* 107:202-218
- Patiño-Douce A.E. and Beard J.S., 1995. Dehydration-Melting of Biotite Gneiss and Quartz Amphibolite from 3 to 15 Kbar. *J. Petrol.* 36:707-738.
- Patiño-Douce A.E. and Beard J.S., 1996. Effects of P, $f(O_2)$ and Mg/Fe ratio on dehydration melting of model metagreywackes. *J. Petrol.* 37:999-1024.
- Patiño-Douce A.E. and Harris N., 1998. Experimental constraints on Himalayan Anatexis. *J. Petrol.* 39:689-710.
- Patiño-Douce A.E. and Johnston A.D., 1991. Phase equilibria and melt productivity in the pelitic system: implications for the origin of peraluminous granitoids and aluminous granulites. *Contrib. Mineral. Petrol.* 107:202-218.
- Pearce N.J.G., Perkins W.T., Westgate J.A., Gorton M.P., Jackson S.E., Meal C.R. and Chenery S.P., 1997. A compilation of new and published major and trace element data for NIST SRM 610 and NIST-SRM-612 glass reference materials. *Geostand. Newslett.- J. Geostand. Geoanal.* 21:115-144.
- Petford N., Kerr R.C. and Lister J.R., 1993. Dike transport of granitic magmas. *Geology* 21:843-845.
- Petford N., Cruden A.R., McCaffrey K.J.W. and Vigneresse J.-L., 2000. Granite magma formation, transport and emplacement in the Earth's crust. *Nature* 408:669-673.
- Petford N., 2003. Rheology of granitic magmas during ascent and emplacement. *Ann. Rev. Earth Planet. Sci.* 31: 399-427.
- Pickering J.M. and Johnston A.D., 1998. Fluid-absent melting behavior of a two-mica metapelite: Experimental constraints on the origin of Black Hills granite. *J. Petrol.* 39:1787-1804.
- Pons J., Barbey P., Nachit H. and Burg J. P., 2006. Development of igneous layering during growth of pluton: the Tarcouate Laccolith (Morocco). *Tectonophysics* 413:271-286.
- Powell R. and Holland, T., 1994. Optimal geothermometry and geobarometry. *Amer. Mineral.* 79:120-133.
- Powell R. and Holland, T.J.B., 1999. Relating formulations of the thermodynamics of mineral solid solutions: Activity modeling of pyroxenes, amphiboles, and micas. *Amer. Mineral.* 84:1-14.

- Pupier E., Barbey P., Toplis M. J. and Bussy F., 2008. Igneous layering, fractional crystallization and growth of granitic plutons: the Dolbel Batholith in SW Niger. *J. Petrol.* 49:1043-1068.

- R -

- Reid J.B., Evans O.C. and Fates D.G., 1983. Magma mixing in granitic rocks of the central Sierra Nevada, California. *Earth Planet. Sci. Lett.* 66: 243-261.
- Roedder E., 1979. Origin and significance of magmatic inclusions. *Bull. Mineral.* 109:487-510.
- Rollinson H., 1993. *Using Geochemical Data: Evaluation, Presentation, Interpretation*, Edinburgh Gate, Edinburgh.
- Roycroft P.D., 1991. Magmatically zoned muscovite from the peraluminous two-mica granites of the Leinster batholith, southeast Ireland. *Geology* 19:437-440.
- Rozendaal A., Gresse P.G., Scheepers R. and De Beer C.H., 1994. Structural setting of the Riviera W-Mo deposit, Western Cape, South Africa. *Explor. Mining Geol.* 3:1747-1770.
- Rozendaal A., Gresse P.G., Scheepers R. and Le Roux J.P., 1999. Neoproterozoic to early cambrian Crustal Evolution of the Pan-African Saldania Belt, South Africa. *Precamb. Res.* 97:303-323.
- Rubatto D., Hermann J., 2007. Experimental zircon/melt and zircon/garnet trace element partitioning and implications for the geochronology of crustal rocks. *Chem. Geol.* 241:38-61.

- S -

- Sawyer E.W., 1991. Disequilibrium Melting and the Rate of Melt Residuum Separation During Migmatization of Mafic Rocks from the Grenville Front, Quebec. *J. Petrol.* 32:701-738.
- Sawyer E.W., 1994. Melt Segregation in the Continental-Crust. *Geology* 22:1019-1022.

- Sawyer E.W., 1996. Melt segregation and magma flow in migmatites: Implications for the generation of granite magmas. *Trans. Royal Soc. Edinburgh-Earth Sci.* 87:85-94.
- Sawyer E.W., 1998. Formation and evolution of granite magmas during crustal reworking: the significance of diatexites. *J. Petrol.* 39:1147-1167.
- Sawyer E.W., 2001. Melt segregation in the continental crust: distribution and movement of melt in anatectic rocks. *J. Metam. Geol.* 19:291-309.
- Scaillet B., France-Lanord C. and Le Fort P., 1990. Badrinath-Gangotri plutons (Garhwal, India): Petrological and geochemical evidence for fractionation process in a high himalayan leucogranite. *J. Volc. Geotherm. Res.* 44:163-188.
- Scaillet, B. and MacDonald R. 2001. Phase relations of peralkaline silicic magmas and petrogenetic implications. *J. Petrol.* 42:825-845.
- Scheepers R., 1990. Magmatic association and radioelement geochemistry of selected Cape Granites with special reference to subalkaline and leucogranitic phases (In Afrikaans). Ph.D. dissertation (Unpubl.) Univ. Stellenbosch.
- Scheepers R., 1995. Geology, Geochemistry and petrogenesis of Late Precambrian S-, I- and A-type granitoids in the saldania belt, Western Cape Province South Africa. *J. Afr. Earth Sci.* 21:35-58.
- Scheepers R., 2000. Granites of the Saldania mobile belt, South Africa: radioelements and P as discriminators applied to metallogeny. *J. Geochem. Expl.* 68:69-86.
- Scheepers R. and Nortje A. N., 2000. Rhyolitic ignimbrites of the Cape Granite Suite, southwestern Cape Province, South Africa. *J. Afr. Earth Sci.* 31:647-656.
- Scheepers R. and Armstrong R.A., 2002. New U-Pb SHRIMP zircon ages of the Cape Granite Suite: implications for the magmatic evolution of the Saldania Belt. *S. Afr. J. Geol.* 105:241-256.
- Scheepers, R. and Poujol M., 2002. U-Pb zircon age of Cape Granite Suite ignimbrites: characteristics of the last phases of the Saldaniaan magmatism. *S. Afr. J. Geol.* 105:163-178.
- Schoch A. E., 1975. The Darling granite Batholith. *Ann. Univ. Stellenbosch* A1:1-104.
- Schoch A. E. and Burger A.J., 1976. U-Pb ages of the Saldanha Quartz Porphyry. *Trans. Geol. Soc. S. Afr.* 79:239-241.
- Schoch A. E., Leterrier J. and De La Roche H., 1977. Major element geochemical trends in the Cape granites. *Trans. Geol. Soc. S. Afr.* 80:197-209.

- Schwandt C.S., Cygan R.T. and Westrich H.R., 1995. Mg Self-diffusion in Pyrope Garnet. *Amer. Mineral.* 80, 483-490.
- Skinner J., 1956. Physical properties of the garnet group. *Amer. Mineral.* 41:428-436.
- Sisson T.W., Bacon C.R., 1992. Garnet high-silica rhyolite trace-element partition-coefficients measured by ion microprobe. *Geochim. Cosmochim. Acta* 56:2133-2136
- Slabber N., 1995. *The geology and geochemistry of the Bridgetown Formation of the Malmesbury Group, Western Cape Province*. M.Sc thesis (unpubl.), Univ. Stellenbosch.
- Solar G.S. and Brown M., 2001. Petrogenesis of migmatites in Maine, USA: Possible source of peraluminous leucogranite in plutons? *J. Petrol.* 42:789-823.
- Solgadi F., Moyen J.-F., Vanderhaeghe O., Sawyer E.W. and Reisberg L., 2007. The role of crustal anatexis and mantle derived magmas in the genesis of syn-orogenic hercynian granites of the Livradois Area, French Massif Central. *Can. Mineral.* 45:581-606
- Spera F.J. and Bohron W.A., 2001. Energy-Constrained Open-System Magmatic processes I: General Model and Energy-Constrained Assimilation and Fractional Crystallization (EC-AFC) Formulation. *J. Petrol.* 42:999-1018.
- Spicer E.M., Stevens G. and Buick I.S., 2004. The low-pressure partial-melting behaviour of natural boron-bearing metapelites from the Mt. Stafford area, central Australia. *Contrib. Miner. Petrol.* 148:160-179.
- Stevens G. and Clemens J.D., 1993. Fluid absent melting and the roles of fluids in the lithosphere: A slanted summary? *Chem. Geol.* 108:1-17.
- Stevens G., Clemens J.D., Droop G.T.R., 1997. Melt production during granulite-facies anatexis: experimental data from primitive metasedimentary protoliths. *Contrib. Mineral. Petrol.* 128:352-370
- Stevens G., Villaros A., Moyen J.-F., 2007 Selective peritectic garnet entrainment as the origin of geochemical diversity in S-type granites. *Geology* 35:9-12
- Streck M.J., Grunder A.L., 1997. Compositional gradients and gaps in high-silica rhyolites of the Rattlesnake Tuff, Oregon. *J. Petrol.* 38:133-163
- Stump E., 1976. On the late Precambrian-early Palaeozoic metavolcanic and metasedimentary rocks of the Queen Maud Mountains, Antarctica and a comparison with rocks of a similar age of southern Africa. *Rep Inst. Polar Studies, Ohio State Univ.*, 62:212.
- Sylvester P., 1998. Post-collisional strongly peraluminous granites. *Lithos.* 45:29-44

- T -

- Taylor S.R. and McLennan, S.M., 1985. *The Continental Crust: Its Composition and Evolution*. Blackwell Scientific Pub., Palo Alto, CA, New York. P. 324
- Tankard A.J., Jackson M.P.A., Eriksson K.A., Hobday D. K., Hunter D.R. and Winter W. E. L., 1982. *Crustal evolution of Southern Africa: 3.8 billion years of Earth history*. Springer-Verlag, New York, 523p.
- Theron J.N., Gresse P.G., siegfried H.P. and Rogers J., 1992. The Geology of the Cape Town area. *Explan. Sheet 3318 Cape Town, Geol. Surv. S. Afr.*, 140.
- Thompson J.B. and Hovis G.L., 1979. Entropy of Mixing in Sanidine. *Amer. Mineral.* 64:57-65.

- V -

- Vernon R.H., 2007. Problems in identifying restite in S-type granites of southeastern Australia, with speculations on sources of magma and enclaves. *Can. Mineral.* 45: 147-178.
- Vielzeuf D., Holloway J.R., 1988. Experimental determination of fluid absent melting relations in the pelitic system. *Contrib. Mineral. Petrol.* 98: 257-276
- Vielzeuf, D. and Montel J. M., 1994. Partial Melting of Metagreywackes .1. Fluid-Absent Experiments and Phase-Relationships. *Contrib. Mineral. Petrol.* 117:375-393.
- Vielzeuf, D. and Schmidt M. W., 2001. Melting relations in hydrous systems revisited: application to metapelites, metagreywackes and metabasalts. *Contrib. Mineral. Petrol.* 141:251-267.
- Vignerresse J.-L. and Bouchez J.-L., 1997. Successive granitic magma batches during pluton emplacement: the case of Cabeza de Araya (Spain). *J. Petrol.* 38:1767-1776.
- Vignerresse, J.-L. and Burg J.-P., 2002. The paradoxical aspect of the Himalayan granites. *J. Virt. Expl.* 9:1-13.
- Villaros A., Stevens G. and Buick I.S., 2009. Tracking S-type granite from source to emplacement: Clues from garnet in the Cape Granite Suite. *Lithos* 112:217-235.

- Villaros A., Stevens, G., Moyon, J.-F. and Buick I.S., 2009. The trace element compositions of S-type granites: Evidence for disequilibrium melting and accessory phase entrainment in the source. *Contrib. Mineral. Petrol.* 158:543-561
- Villaseca C., Orejana D., Paterson B.A., 2007. Zr-LREE rich minerals in residual peraluminous granulites, another factor in the origin of low Zr-LREE granitic melts? *Lithos* 96:375-386
- Von Veh M. W., 1983. Aspects of sedimentation, structure and tectonic evolution in the Tygerberg terrane, southwestern Cape Province. *Bull. Precamb. Res. Unit, Univ. Cape Town* 32:88.

- W -

- Wager L. and Brown G., 1968. *Layered Igneous Rocks* Edinburgh, Oliver and Boyd. 588p.
- Walker F. and Mathias M., 1946. The petrology of two granite-slate contacts at Cape Town, South Africa. *Quart. J. Geol. Soc.* 102:499-521.
- Watson E. B., 1996. Dissolution, growth and survival of zircons during crustal fusion: kinetic principles, geological models and implications for isotopic inheritance. *Trans. Royal Soc. Edinburgh: Earth Sci.* 87:43-56.
- Watson E.B. and Harrison T.M., 1983 Zircon saturation revisited - temperature and composition effects in a variety of crustal magma types. *Earth Planet. Sci. Lett.* 64:295-304.
- Watt G.R. and Harley S.L., 1993. Accessory mineral phase controls on the geochemistry of crustal melts and restites produced during water-undersaturated partial melting. *Contrib. Mineral. Petrol.* 114:550-566
- White A.J.R. and Chappell B.W., 1977. Ultrametamorphism and granitoid genesis. *tectonophysics* 43:7-22.
- White A. J. R. and Chappell B.W., 1988. Some supracrustal (S-type) granites of the Lachlan Fold Belt. *Trans. Royal Soc. Edinburgh, Earth Sci.* 79:169-181.
- White R.W., Powell R. and Holland T., 2001. Calculations of partial melting equilibria in the system $Na_2O-CaO-K_2O-FeO-MgO-Al_2O_3-SiO_2-H_2O$ (NCKFMASH). *J. Metam. Geol.*, 19:139-153.
- White R.W. and Powell R., 2002. Melt loss and the preservation of granulite facies mineral assemblages. *J. Metam. Geol.*, 20:621-632.

Williamson B.J., Shaw A., Downes H. and Thirlwall M.F., 1996. Geochemical constraints on the genesis of hercynian two-mica leucogranites from the Massif Central, France. *Chem. Geol.* 127:25-42.

Williamson B.J., Downes H., Thirlwall M.F. and Beard A., 1997. Geochemical constraints on restite composition and unmixing in the Velay anatectic granite, French Massif Central. *Lithos* 40:295-319.

Weinberg R.F., Sial A.N. and Pessoa R.R., 2001. Magma flow within the Tavares pluton, northeastern Brazil: compositional and thermal convection. *Geol. Soc. Amer. Bull.* 113:508-520.

- Y -

Yardley B.W.D., 1977. An Empirical study of diffusion in garnet. *Amer. Mineral.* 62:793-800.

Appendices

.1 Compilation S-type granite composition

SAMPLE	kr4	hpgsc	darhbsc	darbisc	dar9c	dar9	dar8	DAR-5	dar4	dar3c	dar3	dar2	dar13	dar10	cpgsc77
<i>Pluton</i>	Stb-Kr-Grof	Hoedjiespunt	Hibr. Granod.	Darl. Biotiet.	Hibr. Granod.	Hibr. Granod.	Darl. Biotiet.	Darl. Biotiet.	Hibr. Granod.	Grofp. Bi. Gran	Skireiland				
<i>SiO₂</i>	71.93	70.02	66.86	67.79	69.22	68.56	69.04	69.17	67.34	68.07	67.96	67.03	69.94	68.92	70.38
<i>TiO₂</i>	0.39	0.67	0.88	0.88	0.82	0.82	0.80	0.85	0.79	0.88	0.89	0.88	0.71	0.74	0.43
<i>Al₂O₃</i>	14.14	14.90	15.64	14.83	14.17	14.39	14.49	13.82	14.53	14.44	14.39	14.84	13.95	14.35	15.34
<i>FeO</i>	2.82	3.73	5.86	5.22	5.52	5.77	4.59	6.07	6.16	5.54	5.88	6.58	5.24	5.48	2.95
<i>MnO</i>	0.07	0.07	0.11	0.08	0.07	0.09	0.07	0.09	0.09	0.07	0.09	0.10	0.08	0.10	0.05
<i>MgO</i>	0.88	1.20	2.85	2.28	2.55	2.56	1.43	2.67	2.81	2.21	2.17	2.96	2.30	2.36	1.13
<i>CaO</i>	0.96	1.81	1.81	2.14	1.75	1.70	2.11	1.49	2.60	2.22	2.15	1.65	1.72	1.61	1.52
<i>Na₂O</i>	2.92	2.74	2.32	2.34	2.29	2.51	2.88	2.57	2.24	2.39	2.45	2.45	2.51	2.52	2.79
<i>K₂O</i>	5.70	4.63	3.51	4.18	3.38	3.38	4.16	3.04	3.24	3.87	3.77	3.31	3.40	3.74	5.27
<i>P₂O₅</i>	0.20	0.22	0.16	0.25	0.22	0.21	0.43	0.22	0.20	0.31	0.25	0.19	0.15	0.17	0.14

SAMPLE	sbg	rg6	rg5	OLI-5	OLI-4*	OLI-3	OK-6	OK-5	ok4	OK-3	m7	lbgp	lbg	lbgg	KR-5
<i>Pluton</i>	Seeberg	Langeb. Gran.	Hoedjies punt	Seeberg	Seeberg	Seeberg	Seeberg	Seeberg	Langeb. Biot.	Seeberg	Langeb. Gran.	Langeb. Gran.	Langeb. Gran.	Langeb. Biot.	Stb-Kr-Grof
<i>SiO₂</i>	68.24	73.79	69.65	70.38	70.25	70.63	69.93	68.67	75.27	71.11	69.63	73.30	72.07	70.05	75.22
<i>TiO₂</i>	0.55	0.24	0.59	0.62	0.63	0.65	0.43	0.56	0.11	0.39	0.36	0.28	0.24	0.35	0.14
<i>Al₂O₃</i>	13.74	13.70	14.01	14.46	14.33	14.15	13.79	13.53	12.81	13.15	14.10	13.93	13.42	13.57	13.16
<i>FeO</i>	6.80	1.88	4.02	3.80	4.16	3.99	5.75	7.21	2.23	5.30	4.94	2.86	4.38	5.72	1.62
<i>MnO</i>	0.06	0.05	0.07	0.06	0.07	0.06	0.06	0.08	0.07	0.05	0.05	0.06	0.04	0.00	0.04
<i>MgO</i>	1.10	0.42	1.27	1.20	1.42	1.31	0.88	1.32	0.30	0.86	0.41	0.51	0.63	0.89	0.58
<i>CaO</i>	1.83	0.75	1.63	1.82	1.80	1.86	1.27	1.55	0.60	1.12	1.58	0.93	0.93	1.38	0.48
<i>Na₂O</i>	2.91	3.51	3.83	2.64	2.49	2.65	2.85	2.68	3.52	2.89	3.20	2.79	3.35	3.06	3.27
<i>K₂O</i>	4.56	5.49	4.69	4.78	4.61	4.47	4.83	4.17	4.85	4.86	5.60	5.22	4.80	4.79	5.33
<i>P₂O₅</i>	0.21	0.15	0.23	0.23	0.23	0.23	0.21	0.23	0.23	0.27	0.15	0.12	0.14	0.21	0.16

SAMPLE	dar7c	dar7	dar6c	dar6	cbsc	stksc77	stk2	stb2	stb1	sep3	sep2c	sep2	sep1c	sep1	sc77hb
<i>Pluton</i>	Contreberg	Contreberg	Contreberg	Contreberg	Contreberg	Stb-Kr-Grof	Stb-Kr-Med	Stb-Kr-Grof	Stb-Kr-Grof	Skierelland	Skierelland	Skierelland	Skierelland	Skierelland	Hibr. Granod.
<i>SiO₂</i>	73.53	72.17	73.50	73.10	72.59	74.07	70.62	73.51	72.31	71.24	70.75	70.56	67.95	68.16	66.86
<i>TiO₂</i>	0.26	0.24	0.22	0.22	0.30	0.33	0.57	0.34	0.40	0.42	0.49	0.49	0.51	0.50	0.88
<i>Al₂O₃</i>	14.01	13.96	14.27	14.31	14.68	13.16	14.33	13.49	14.00	14.35	14.83	15.00	16.12	16.20	15.64
<i>FeO</i>	1.91	2.03	1.72	1.75	2.20	1.95	3.17	2.28	2.56	2.75	3.33	3.35	3.24	3.32	5.86
<i>MnO</i>	0.03	0.41	0.03	0.30	0.06	0.04	0.03	0.05	0.05	0.06	0.04	0.06	0.05	0.05	0.11
<i>MgO</i>	0.41	0.41	0.36	0.38	0.86	0.50	0.92	0.73	0.79	0.82	1.16	1.27	1.09	1.10	2.85
<i>CaO</i>	1.64	1.57	1.40	1.33	1.48	1.16	2.02	1.11	1.34	1.95	1.35	1.27	1.35	1.25	1.81
<i>Na₂O</i>	2.70	3.06	3.04	3.42	2.64	3.12	3.39	3.01	2.93	3.45	2.75	2.93	2.95	3.05	2.32
<i>K₂O</i>	5.34	5.22	5.29	5.09	5.09	5.44	4.76	5.34	5.46	4.83	5.04	4.85	6.45	6.15	3.51
<i>P₂O₅</i>	0.17	0.92	0.17	0.10	0.10	0.23	0.20	0.14	0.16	0.12	0.26	0.22	0.28	0.23	0.16

SAMPLE	OLI-1	ok8	ok2	ok1	kr6	KR3*	kr3	KR2*	kr2	KR1*	kr1	KON4*	KON3*	KON2*	KON1*
<i>Pluton</i>	Olifantsk op	Olifantsko p	Olifantsk op	Olifantsk op	Stb-Kr-Fyn	Stb-Kr- Med	Stb-Kr-Fyn	Stb-Kr- Med	Stb-Kr-Fyn	Stb-Kr- Med	Stb-Kr- Fyn	Cuyper skraal	Cuyper skraal	Cuyper skraal	Cuyperskr aal
<i>SiO₂</i>	74.56	75.84	76.29	76.92	86.67	76.70	76.16	75.61	75.80	75.79	77.31	76.44	76.34	76.65	76.62
<i>TiO₂</i>	0.24	0.02	0.02	0.06	0.04	0.09	0.07	0.17	0.02	0.15	0.03	0.05	0.03	0.01	0.03
<i>Al₂O₃</i>	13.62	13.14	13.37	13.05	7.47	13.28	13.10	13.24	13.85	13.20	13.01	13.29	13.64	13.28	13.78
<i>FeO</i>	2.22	1.44	0.82	0.38	0.77	1.16	1.21	1.74	0.95	1.60	1.04	1.52	1.35	1.01	0.93
<i>MnO</i>	0.05	0.04	0.02	0.01	0.02	0.03	0.04	0.04	0.02	0.04	0.02	0.03	0.06	0.03	0.04
<i>MgO</i>	0.56	0.13	0.14	0.10	0.25	0.19	0.42	0.37	0.19	0.31	0.17	0.12	0.10	0.07	0.06
<i>CaO</i>	0.96	0.27	0.33	0.35	0.07	0.34	0.35	0.64	0.14	0.63	0.10	0.32	0.30	0.34	0.27
<i>Na₂O</i>	2.93	4.09	3.98	3.54	3.50	2.91	3.37	2.73	3.65	2.81	3.06	3.21	3.30	4.10	3.85
<i>K₂O</i>	4.68	4.87	4.86	5.43	1.12	5.13	5.11	5.26	5.20	5.30	5.11	4.85	4.68	4.21	4.19
<i>P₂O₅</i>	0.17	0.15	0.17	0.15	0.09	0.17	0.17	0.19	0.16	0.17	0.15	0.17	0.19	0.28	0.24

SAMPLE	dar11c	dar11	dar1	aeskarb	stkgsc77	stk1	stb6c	stb6	stb5c	stb5	stb4	sc77cb	rg8	OLI-6*	OLI-2*
<i>Pluton</i>	Grofp. Darl.	Grofp. Darl.	Grofp. Darl.	Karnberg	Stb-Kr-Fyn	Contreberg	Olifants kop	Olifants kop	Olifantsko p						
<i>SiO₂</i>	72.37	72.27	69.29	73.30	75.89	73.00	71.21	71.04	73.53	73.30	74.37	72.59	73.84	76.14	74.57
<i>TiO₂</i>	0.47	0.47	0.70	0.27	0.07	0.36	0.47	0.47	0.30	0.29	0.28	0.30	0.25	0.10	0.25
<i>Al₂O₃</i>	13.93	14.06	14.17	13.50	13.03	13.59	14.05	14.26	13.81	14.00	13.41	14.68	13.47	12.97	13.60
<i>FeO</i>	3.24	3.05	4.76	1.94	1.45	2.18	3.13	3.18	2.04	2.06	2.32	2.20	2.15	1.05	2.20
<i>MnO</i>	0.04	0.05	0.07	0.04	0.03	0.04	0.05	0.07	0.04	0.04	0.04	0.06	0.05	0.02	0.05
<i>MgO</i>	1.04	1.04	1.57	0.42	0.16	0.30	0.84	0.94	0.48	0.58	0.57	0.86	0.39	0.24	0.53
<i>CaO</i>	1.14	1.06	2.02	1.58	0.54	1.06	1.82	1.82	1.09	1.05	0.67	1.48	1.36	0.43	1.01
<i>Na₂O</i>	2.56	2.88	2.75	4.06	3.10	3.67	3.01	2.96	2.76	2.99	2.96	2.64	3.40	2.77	2.90
<i>K₂O</i>	4.91	4.88	4.43	4.84	5.53	5.72	5.19	5.09	5.74	5.54	5.23	5.09	5.02	6.13	4.71
<i>P₂O₅</i>	0.31	0.25	0.23	0.06	0.19	0.07	0.22	0.16	0.20	0.14	0.14	0.10	0.07	0.16	0.17

SAMPLE	kn17c	kn17	kn15	kn14	kn13	kn12	kn11	KN-10	KN-1	darSc77	darSc	DAR-B1	dar1c	dar12c	dar12
<i>Pluton</i>	Karnberg	Karnberg	Karnberg	Trekoskr aal	Karnberg	Karnber g	Karnberg	Karnberg	Karnberg	Grofp. Darl.	Grofp. Darl.	Grofp. Darl.	Grofp. Darl.	Grofp. Darl.	Grofp. Darl.
<i>SiO₂</i>	76.88	76.27	75.03	66.57	74.70	75.59	75.11	75.30	77.07	71.88	71.88	68.71	69.36	70.64	70.41
<i>TiO₂</i>	0.17	0.18	0.21	0.96	0.24	0.19	0.21	0.20	0.14	0.45	0.45	0.69	0.73	0.68	0.66
<i>Al₂O₃</i>	12.20	12.19	13.25	14.55	13.07	12.84	13.40	12.68	11.95	13.99	13.99	14.06	14.12	13.93	13.97
<i>FeO</i>	1.66	1.68	2.07	6.41	2.02	1.77	1.87	1.89	1.59	3.31	3.31	4.09	4.58	4.11	4.36
<i>MnO</i>	0.02	0.04	0.03	0.10	0.03	0.03	0.02	0.04	0.03	0.05	0.05	0.07	0.07	0.07	0.07
<i>MgO</i>	0.16	0.28	0.28	1.79	0.44	0.34	0.38	0.35	0.31	0.90	0.90	2.44	1.65	1.40	1.37
<i>CaO</i>	0.69	0.64	0.51	2.20	0.76	0.54	0.48	0.78	0.65	1.51	1.51	2.01	2.09	1.86	1.79
<i>Na₂O</i>	2.29	2.90	2.79	2.78	3.00	2.87	2.86	3.02	2.87	2.88	2.88	3.44	2.53	2.53	2.71
<i>K₂O</i>	5.78	5.66	5.70	4.40	5.63	5.65	5.55	5.62	5.27	4.81	4.81	4.28	4.54	4.56	4.45
<i>P₂O₅</i>	0.15	0.15	0.13	0.24	0.12	0.17	0.12	0.12	0.11	0.22	0.22	0.20	0.32	0.23	0.20

SAMPLE	1.74/12	kn9	kn8c	kn8	kn6c	kn6	kn5c	kn5	kn3c	kn3	kn2c	kn21	KN-20	kn2	kn19
<i>Pluton</i>	Grofp. Darl.	Karnberg	Trekosk raal	Karnberg	Karnberg	Trekosk raal	Karnberg								
<i>SiO₂</i>	70.28	75.60	74.38	74.45	74.99	74.77	74.62	74.29	76.68	76.51	68.52	71.44	75.87	68.03	75.53
<i>TiO₂</i>	0.57	0.18	0.25	0.23	0.17	0.18	0.22	0.21	0.17	0.17	0.76	0.40	0.18	0.74	0.20
<i>Al₂O₃</i>	14.21	12.51	13.42	13.19	13.22	13.34	13.23	12.91	12.35	12.49	14.57	14.31	12.69	14.64	12.86
<i>FeO</i>	3.87	1.73	2.07	1.95	1.67	1.72	1.99	1.96	1.61	1.66	4.69	2.83	1.81	5.02	1.89
<i>MnO</i>	0.06	0.02	0.03	0.03	0.02	0.04	0.03	0.03	0.02	0.03	0.06	0.05	0.03	0.08	0.03
<i>MgO</i>	1.37	0.36	0.25	0.52	0.19	0.37	0.22	0.92	0.15	0.39	1.37	0.56	0.25	1.47	0.34
<i>CaO</i>	2.11	0.78	0.83	0.72	1.07	1.02	0.95	0.84	0.76	0.70	2.19	1.49	0.65	2.14	0.57
<i>Na₂O</i>	2.69	2.97	2.60	3.04	2.71	2.76	2.61	3.06	2.54	2.56	2.91	3.17	2.81	2.97	2.95
<i>K₂O</i>	4.62	5.70	5.97	5.73	5.79	5.68	5.94	5.64	5.54	5.37	4.68	5.58	5.58	4.71	5.49
<i>P₂O₅</i>	0.22	0.15	0.20	0.14	0.16	0.11	0.17	0.13	0.17	0.12	0.25	0.17	0.12	0.20	0.14

SAMPLE	D214	D14	D213	D13	D11	D211	D210	D10	D21	treksc77	trek1	MAM-3	MAM-2	MAM-1	I.karb
<i>Pluton</i>	ukn	Trekoskr aal	Trekosk raal	Grofp. Darl.	Grofp. Darl.	Grofp. Darl.	Karnberg								
<i>SiO₂</i>	68.13	68.70	69.20	69.32	69.70	69.04	69.99	69.88	70.23	72.77	68.91	70.81	70.82	70.60	74.56
<i>TiO₂</i>	0.88	0.89	0.82	0.83	0.77	0.78	0.84	0.85	0.83	0.44	0.59	0.64	0.62	0.69	0.26
<i>Al₂O₃</i>	14.95	14.88	14.56	14.68	14.46	14.29	14.40	14.42	14.82	13.69	14.65	14.10	14.26	13.97	13.67
<i>FeO</i>	5.91	5.94	5.37	5.46	5.12	5.15	5.56	5.54	4.81	2.80	3.81	3.96	3.81	4.17	1.73
<i>MnO</i>	0.10	0.09	0.08	0.08	0.08	0.08	0.08	0.09	0.07	0.06	0.07	0.05	0.05	0.05	0.04
<i>MgO</i>	3.01	3.02	2.69	2.75	2.39	2.35	2.57	2.51	2.03	0.68	0.91	1.33	1.29	1.39	0.54
<i>CaO</i>	1.80	1.83	1.81	1.77	1.98	2.02	1.98	1.99	2.22	1.28	2.86	1.78	1.78	1.73	0.88
<i>Na₂O</i>	1.63	1.06	1.98	1.59	2.06	2.79	1.05	1.25	1.15	2.76	4.05	2.40	2.64	2.37	2.59
<i>K₂O</i>	3.40	3.41	3.35	3.36	3.33	3.38	3.43	3.38	3.62	5.30	4.01	4.72	4.53	4.81	5.63
<i>P₂O₅</i>	0.19	0.18	0.15	0.16	0.10	0.13	0.09	0.09	0.23	0.22	0.15	0.22	0.22	0.23	0.10

SAMPLE	D6	D224	D4	D223(B)	D3(B)	D222	D2	D218	D18	D217(A)	D17(A)	D216	D16	D215	D15
<i>Pluton</i>	ukn	ukn	ukn	ukn	ukn	ukn	ukn	ukn	ukn	ukn	ukn	ukn	ukn	ukn	ukn
<i>SiO₂</i>	71.23	68.97	68.99	71.13	71.33	68.75	68.68	70.77	70.94	70.03	69.86	69.79	70.01	70.78	70.64
<i>TiO₂</i>	0.74	0.88	0.89	0.76	0.75	0.88	0.90	0.80	0.81	0.79	0.77	0.75	0.77	0.75	0.75
<i>Al₂O₃</i>	14.58	14.89	14.92	14.59	14.54	15.05	15.28	14.06	14.17	14.58	14.64	14.24	14.38	14.41	14.30
<i>FeO</i>	4.47	5.40	5.44	4.42	4.38	5.57	5.54	5.18	5.20	5.28	5.28	5.04	5.12	4.97	4.96
<i>MnO</i>	0.08	0.09	0.09	0.07	0.06	0.09	0.09	0.07	0.07	0.08	0.09	0.08	0.08	0.07	0.08
<i>MgO</i>	1.99	2.20	2.17	1.83	1.83	2.26	2.30	2.48	2.59	2.63	2.57	2.50	2.61	2.36	2.41
<i>CaO</i>	1.58	2.19	2.19	2.06	2.03	2.09	2.09	1.71	1.70	1.70	1.72	1.69	1.68	1.88	1.86
<i>Na₂O</i>	1.17	1.30	1.21	1.16	1.11	1.24	1.04	1.28	0.90	1.16	1.34	2.24	1.71	1.35	1.51
<i>K₂O</i>	4.01	3.82	3.83	3.75	3.74	3.81	3.84	3.50	3.49	3.56	3.56	3.51	3.50	3.30	3.33
<i>P₂O₅</i>	0.15	0.25	0.25	0.23	0.23	0.25	0.24	0.15	0.13	0.18	0.19	0.16	0.15	0.15	0.15

SAMPLE	HL18*	HL17*	HL16*	HL14*	HL12*	HL11*	HL-10	HL1*	D229	D9	D228	D8	D227	D7	D226
<i>Pluton</i>	Haelkraal	ukn													
<i>SiO₂</i>	75.68	76.04	76.68	73.71	76.13	75.82	76.39	76.47	67.72	67.68	70.86	70.91	69.08	69.42	71.20
<i>TiO₂</i>	0.18	0.11	0.05	0.17	0.12	0.13	0.11	0.08	0.91	0.92	0.78	0.80	0.80	0.81	0.72
<i>Al₂O₃</i>	13.26	13.63	13.27	14.66	13.63	13.47	13.24	13.56	15.29	15.27	14.55	14.57	14.82	14.85	14.43
<i>FeO</i>	1.85	1.46	0.94	1.62	1.33	1.53	1.47	1.15	6.05	6.05	4.40	4.51	5.82	5.79	4.47
<i>MnO</i>	0.02	0.04	0.01	0.02	0.02	0.03	0.03	0.01	0.10	0.09	0.06	0.06	0.10	0.10	0.08
<i>MgO</i>	0.38	0.23	0.19	0.33	0.26	0.26	0.22	0.20	2.96	2.98	1.53	1.57	2.82	2.76	1.96
<i>CaO</i>	0.59	0.42	0.30	0.36	0.43	0.48	0.34	0.32	2.14	2.11	2.06	2.03	1.57	1.53	1.57
<i>Na₂O</i>	2.62	2.85	2.92	2.81	2.76	2.84	2.78	3.02	1.22	1.25	1.32	1.11	1.18	0.93	1.36
<i>K₂O</i>	5.22	4.99	5.46	6.13	5.13	5.26	5.20	4.97	3.53	3.57	4.19	4.19	3.67	3.69	4.05
<i>P₂O₅</i>	0.19	0.24	0.17	0.19	0.19	0.19	0.21	0.21	0.09	0.09	0.25	0.25	0.13	0.13	0.15

SAMPLE	HPT-4(B)	HPT-14(A)	HPT-4(A)	HPT-13	HPT-3	HPT-11	HPT-1	HL9*	HL8*	HL7*	HL6*	HL5*	HL-4	HL3*	HL2*
<i>Pluton</i>	ukn	ukn	ukn	ukn	ukn	ukn	ukn	Haelkraal							
<i>SiO₂</i>	70.70	71.16	71.11	69.59	70.32	71.85	71.82	75.55	76.35	76.16	75.99	77.54	76.75	76.06	76.52
<i>TiO₂</i>	0.65	0.63	0.64	0.76	0.75	0.61	0.60	0.10	0.07	0.11	0.11	0.09	0.11	0.10	0.07
<i>Al₂O₃</i>	15.10	14.99	15.02	15.44	15.18	15.01	14.91	13.59	13.40	13.46	13.83	12.34	12.89	13.51	13.29
<i>FeO</i>	3.99	4.05	4.07	4.31	4.30	3.86	3.85	1.58	1.14	1.46	1.42	1.43	1.53	1.39	1.24
<i>MnO</i>	0.07	0.07	0.07	0.08	0.06	0.07	0.07	0.03	0.02	0.02	0.02	0.02	0.02	0.01	0.02
<i>MgO</i>	1.21	1.23	1.23	1.27	1.19	1.11	1.17	0.20	0.15	0.28	0.25	0.20	0.23	0.21	0.20
<i>CaO</i>	1.79	1.79	1.78	1.88	1.86	1.66	1.70	0.42	0.33	0.36	0.32	0.25	0.28	0.31	0.33
<i>Na₂O</i>	1.65	1.39	1.37	2.12	1.74	1.09	1.17	2.94	2.90	2.77	2.97	2.51	2.66	3.00	2.96
<i>K₂O</i>	4.58	4.43	4.46	4.26	4.30	4.49	4.45	5.40	5.40	5.20	4.89	5.44	5.33	5.19	5.16
<i>P₂O₅</i>	0.27	0.26	0.26	0.31	0.30	0.25	0.25	0.18	0.24	0.18	0.20	0.17	0.19	0.21	0.21

SAMPLE	LPG-1	KAN-3	KAN-2	KAN-1	HPT-18	HPT-8	HPT-17(B)	HPT-7(B)	HPT-17(A)	HPT-7(A)	HPT16	HPT-6	HPT-15	HPT-5	HPT-14(B)
<i>Pluton</i>	ukn	Darl. Biotiet.	Darl. Biotiet.	Darl. Biotiet.	ukn	ukn	ukn	ukn	ukn	ukn	ukn	ukn	ukn	ukn	ukn
<i>SiO₂</i>	75.61	69.80	70.30	69.97	71.94	71.85	69.88	70.00	71.53	71.22	72.17	72.29	71.28	71.46	70.51
<i>TiO₂</i>	0.23	0.66	0.64	0.70	0.56	0.55	0.58	0.57	0.58	0.58	0.54	0.53	0.62	0.61	0.64
<i>Al₂O₃</i>	14.00	14.43	14.34	14.40	14.80	14.78	15.70	15.59	14.95	14.84	14.95	14.95	15.13	15.04	15.29
<i>FeO</i>	1.98	4.14	4.14	4.10	3.46	3.48	3.97	3.90	3.74	3.72	3.55	3.45	3.95	3.91	3.96
<i>MnO</i>	0.07	0.06	0.06	0.06	0.07	0.07	0.06	0.07	0.06	0.06	0.06	0.06	0.06	0.06	0.06
<i>MgO</i>	0.48	1.64	1.63	1.64	0.95	1.00	1.20	1.14	1.15	1.12	1.05	1.05	1.19	1.23	1.19
<i>CaO</i>	0.89	1.75	1.66	1.79	1.76	1.81	1.65	1.64	1.64	1.67	1.64	1.65	1.77	1.80	1.81
<i>Na₂O</i>	1.92	2.56	2.42	2.53	1.35	1.32	1.72	1.77	1.46	1.96	1.32	1.32	1.34	1.27	1.65
<i>K₂O</i>	4.63	4.75	4.59	4.60	4.87	4.90	4.94	5.00	4.63	4.55	4.46	4.44	4.41	4.36	4.62
<i>P₂O₅</i>	0.18	0.22	0.22	0.22	0.24	0.24	0.31	0.31	0.25	0.27	0.25	0.25	0.26	0.26	0.28

SAMPLE	RON-6	RON-5*	RON-4*	RON-3*	RON-2*	RON-11*	RON-10*	RON-1	LPG-17	LPG-7	LPG-16	LPG-6	LPG-12	LPG-2	LPG-11
<i>Pluton</i>	Darl. Biotiet.	ukn	ukn	ukn	ukn	ukn	ukn	ukn							
<i>SiO₂</i>	73.15	74.17	74.47	73.55	72.84	72.86	72.48	73.44	77.12	76.58	76.26	76.16	75.50	75.60	75.81
<i>TiO₂</i>	0.38	0.20	0.03	0.28	0.38	0.37	0.39	0.30	0.17	0.17	0.23	0.23	0.24	0.24	0.23
<i>Al₂O₃</i>	13.78	14.39	14.86	13.95	14.03	14.04	13.96	14.29	13.24	13.62	13.71	13.76	14.05	14.11	13.93
<i>FeO</i>	2.41	1.58	0.69	2.19	2.39	2.43	2.66	2.06	1.61	1.63	1.89	1.88	1.82	1.88	1.94
<i>MnO</i>	0.04	0.07	0.09	0.09	0.04	0.04	0.04	0.05	0.06	0.06	0.07	0.07	0.05	0.05	0.07
<i>MgO</i>	0.71	0.41	0.13	0.56	0.72	0.74	0.79	0.58	0.31	0.34	0.44	0.43	0.39	0.41	0.47
<i>CaO</i>	1.29	0.86	0.68	1.10	1.33	1.32	1.32	1.10	0.74	0.75	0.98	0.94	0.90	0.89	0.92
<i>Na₂O</i>	2.59	3.27	1.90	2.61	2.60	2.52	2.70	2.60	1.70	1.75	1.61	1.76	1.78	1.53	1.78
<i>K₂O</i>	5.49	4.85	6.84	5.51	5.51	5.51	5.50	5.39	4.88	4.94	4.66	4.62	5.13	5.15	4.67
<i>P₂O₅</i>	0.15	0.20	0.31	0.16	0.16	0.16	0.15	0.19	0.16	0.16	0.16	0.16	0.15	0.15	0.17

SAMPLE	sqpsc	SEE-18	SEE-8	SEE-15	SEE-5	SEE-14	SEE-4	SEE-13	SEE-3	SEE-12	SEE-2	SEE-11	SEE-1	RON-9	RON-7*
<i>Pluton</i>	Saldanha Qporf.	ukn	ukn	Darl. Biotiet.	Darl. Biotiet.										
<i>SiO₂</i>	76.53	72.12	72.35	71.68	71.50	71.41	71.34	71.56	71.54	78.04	78.07	67.63	67.02	73.04	73.37
<i>TiO₂</i>	0.20	0.53	0.52	0.59	0.58	0.61	0.62	0.64	0.63	0.03	0.03	0.89	0.88	0.37	0.35
<i>Al₂O₃</i>	12.41	14.80	14.76	14.64	14.80	14.85	14.78	14.64	14.68	13.27	13.08	14.63	14.70	14.04	13.94
<i>FeO</i>	1.72	3.48	3.45	3.63	3.60	3.70	3.70	3.94	3.96	0.71	0.71	6.39	6.33	2.38	2.36
<i>MnO</i>	0.03	0.06	0.06	0.06	0.06	0.06	0.06	0.07	0.07	0.02	0.02	0.12	0.13	0.05	0.04
<i>MgO</i>	0.26	1.11	1.04	1.14	1.09	1.17	1.17	1.20	1.22	0.09	0.09	2.13	2.06	0.72	0.69
<i>CaO</i>	1.02	1.48	1.51	1.94	1.95	1.88	1.83	1.80	1.79	0.46	0.48	1.47	1.47	1.24	1.20
<i>Na₂O</i>	2.43	1.59	1.51	1.51	1.55	1.43	1.63	1.61	1.50	1.75	1.91	1.27	1.93	2.52	2.69
<i>K₂O</i>	5.25	4.59	4.57	4.60	4.63	4.66	4.64	4.32	4.38	5.51	5.48	5.18	5.16	5.46	5.17
<i>P₂O₅</i>	0.15	0.25	0.24	0.23	0.23	0.22	0.22	0.23	0.23	0.12	0.13	0.30	0.32	0.17	0.19

.2 Compilations of experimental melt compositions

Sample	PDB4	PDB3	PDB2	PDB1	M40	M39	M36	M33	M32	M30
Ref	Patino-Douce and Beard ((1996))	Montel and Vielzeuf (1997)								
What	SFAG	SFAG	SFAG	SFAG	CEVG	CEVP	CEVG	CEVG	CEVP	CEVG
Nature	Synthetic	Synthetic	Synthetic	Synthetic	Natural	Natural	Natural	Natural	Natural	Natural
Run n°	-	-	-	-	PC92-20	PC92-20	A113A	A113B	A113B	A104
Startmat	-	-	-	-	G	P	G	G	P	G
Apparatus	IH	IH	IH	IH	-	-	-	-	-	-
added H ₂ O	0	0	0	0	0	0	0	0	0	0
P(kb)	3	3	3	3	10	10	10	10	10	8
T(°C)	925	900	875	840	1000	1000	874	858	858	1040
SiO ₂	73.3	73.1	72.8	71.2	69.64	67.63	68.44	69.82	66.46	69.31
TiO ₂	0.36	0.19	0.12	0.16	0.45	0.37	0.26	0.1	0.18	0.37
Al ₂ O ₃	13.8	13.9	14.2	15.1	15.47	15.25	15.3	15.37	14.34	14.79
FeO	1.92	2.01	2.11	1.63	2.04	1.82	1.19	0.99	0.84	2.28
MnO	0.2	0.16	0.26	0.26	0.04	0.03	0.1	0.15	0.04	0.14
MgO	0.1	0.1	0.09	0.1	0.59	0.47	0.56	0.39	0.32	0.88
CaO	0.93	0.94	0.88	1.06	0.61	0.76	0.69	0.73	0.58	1.59
Na ₂ O	1.98	2.06	2.01	2.04	3.21	3.55	3.29	3.26	3.18	3.55
K ₂ O	5.85	6.02	6.06	5.75	5.67	5.2	4.54	4.61	3.79	3.16
P ₂ O ₅	-	-	-	-	-	-	-	-	-	-
H ₂ O	-	-	-	-	4.37	3.93	3.73	8.36	3.3	1.74
F	1.5	1.5	1.45	2.63	-	-	-	-	-	-

Sample	PDB14	PDB13	PDB12	PDB11	PDB10	PDB9	PDB8	PDB7	PDB6	PDB5
Ref	Patino-Douce and Beard ((1996))									
What	SFAG									
Nature	Synthetic									
Run n°	-	-	-	-	-	-	-	-	-	-
Startmat	-	-	-	-	-	-	-	-	-	-
Apparatus	PC	PC	PC	PC	IH	IH	IH	IH	PC	IH
added H ₂ O	0	0	0	0	0	0	0	0	0	0
P(kb)	10	7	7	7	5	5	5	5	5	5
T(°C)	850	900	875	850	950	925	900	875	850	840
SiO ₂	70.3	71.1	72.7	71.1	71.9	72.2	70.9	69.6	71.8	70.6
TiO ₂	0.16	0.21	0.14	0.07	0.3	0.2	0.23	0.18	0.12	0.16
Al ₂ O ₃	-	14.6	13.8	14.7	14.7	14.3	14.4	15.1	14.3	15.7
FeO	2.64	2.67	2.45	2.66	2.92	2.54	2.09	1.97	2.68	1.79
MnO	0.04	0.1	0.03	0.03	0.28	0.24	0.23	0.21	0.07	0.19
MgO	0.01	0.04	0.01	0.01	0.11	0.11	0.08	0.08	0.03	0.07
CaO	1.02	1.67	1.28	1.2	1.48	1.31	1.06	1.13	1.34	1.48
Na ₂ O	3.9	3.18	3.27	3.25	2.59		2.85	2.81	2.81	1.92
K ₂ O	5.07	5.21	5.26	5.42	5.71	5.64	6.37	6.43	5.61	5.17
P ₂ O ₅	-	-	-	-	-	-	-	-	-	-
H ₂ O	-	-	-	-	-	-	-	-	-	-
F	1.64	1.19	1.07	1.52	-	1.4	1.79	2.48	1.23	2.91

Sample	PDB24	PDB23	PDB22	PDB21	PDB20	PDB19	PDB18	PDB17	PDB16	PDB15
Ref	Patino-Douce and Beard ((1996))									
What	SMAG									
Nature	Synthetic									
Run n°	-	-	-	-	-	-	-	-	-	-
Startmat	-	-	-	-	-	-	-	-	-	-
Apparatus	-	IH	IH	IH	-	PC	PC	PC	PC	PC
added H ₂ O	0	0	0	0	0	0	0	0	0	0
P(kb)	5	3	3	3	3	15	15	10	10	10
T(°C)	840	925	900	875	840	950	900	950	925	900
SiO ₂	76.7	76.1	75.4	76.6	76.6	70.6	70.2	70.2	70.9	71.2
TiO ₂	0.41	0.39	0.36	0.33	0.3	0.25	0.2	0.18	0.21	0.16
Al ₂ O ₃	14.4	13.6	13.6	13.4	14.5	14.3	15.5	14.8	14.3	15.3
FeO	1.5	1.56	1.65	1.87	1.55	2.72	2.12	2.9	2.91	2.45
MnO	0.11	0.13	0.1	0.14	0.14	0.07	0.02	0.03	0.06	0.03
MgO	0.56	0.55	0.44	0.45	0.31	0.06	0.02	0.02	0.03	0.01
CaO	0.83	0.73	1.04	0.92	1.32	0.87	0.75	1.08	1.38	1.07
Na ₂ O	1.38	1.94	1.9	1.63	1.7	3.86	4.12	3.79	3.14	2.91
K ₂ O	4.09	4.84	5.17	4.42	3.41	5.75	5.14	5.61	5.38	5.09
P ₂ O ₅	-	-	-	-	-	-	-	-	-	-
H ₂ O	-	-	-	-	-	-	-	-	-	-
F	0.04	0.17	0.27	0.24	0.14	1.54	1.95	1.43	1.66	1.78

Sample	PDB34	PDB33	PDB32	PDB31	PDB30	PDB29	PDB28	PDB27	PDB26	PDB25
Ref	Patino-Douce and Beard ((1996))									
What	SMAG									
Nature	Synthetic									
Run n°	-	-	-	-	-	-	-	-	-	-
Startmat	-	-	-	-	-	-	-	-	-	-
Apparatus	PC	PC	PC	PC	PC	IH	IH	IH	IH	PC
added H ₂ O	0	0	0	0	0	0	0	0	0	0
P(kb)	10	10	7	7	7	5	5	5	5	5
T(°C)	900	850	900	875	850	950	925	900	875	850
SiO ₂	74.6	74.3	73.3	75.2	74.1	73.8	75.1	74.6	76.3	74.8
TiO ₂	0.18	0.24	0.45	0.16	0.25	0.47	0.39	0.37	0.28	0.22
Al ₂ O ₃	14.5	15.1	13.9	14	14.5	14.3	14	14.3	13.9	13.9
FeO	1.71	1.6	2.19	1.73	1.76	2.34	2.26	1.89	1.54	2.12
MnO	0.05	0.04	0.04	0.02	0.03	0.12	0.06	0.11	0.07	0.05
MgO	0.18	0.22	0.32	0.16	0.21	0.64	0.56	0.54	0.39	0.21
CaO	1.15	1.22	1.09	1.28	1.49	1.35	1.05	1.12	0.9	1.09
Na ₂ O	2.75	2.81	2.61	2.6	2.79	2.41	1.67	2.06	1.85	2.4
K ₂ O	4.74	4.38	5.88	4.71	4.57	4.56	4.73	4.72	4.56	5.09
P ₂ O ₅	-	-	-	-	-	-	-	-	-	-
H ₂ O	-	-	-	-	-	-	-	-	-	-
F	0.1	0.1	0.17	0.19	0.32		0.19	0.2	0.2	0.13

Sample	Ref	PDH7	PDH6	PDH5	PDH4	PDH3	PDB39	PDB38	PDB37	PDB36	PDB35
		Patino-Douce and Harris (1998)	Patino-Douce and Beard ((1996))								
What	MS	MS	MS	MS	MS	MS	SMAG	SMAG	SMAG	SMAG	SMAG
Nature	Natural	Natural	Natural	Natural	Natural	Natural	Synthetic	Synthetic	Synthetic	Synthetic	Synthetic
Run n°	-	-	-	-	-	-	-	-	-	-	-
Startmat	-	-	-	-	-	-	-	-	-	-	-
Apparatus	-	-	-	-	-	-	PC	PC	PC	PC	PC
added H ₂ O	0	2	0	2	1	1	0	0	0	0	0
P(kb)	6	6	6	6	6	6	15	15	15	10	10
T(°C)	800	775	775	750	750	750	950	900	860	950	925
SiO ₂	74.09	74.65	75.43	74.7	74.95	74.95	73.8	73.4	75.7	73.1	73.5
TiO ₂	0.15	0.11	0.17	0.1	0.14	0.14	0.32	0.31	0.16	0.28	0.36
Al ₂ O ₃	15.86	15.55	15.04	15.99	15.73	15.73	14.3	14.7	14.8	14.6	14.3
FeO	1	0.76	0.76	0.87	1.01	1.01	1.63	1.4	0.92	1.79	1.72
MnO	0.05	0.06	0.04	0.04	0.04	0.04	0.04	0.03	0.05	0.02	
MgO	0.21	0.26	0.18	0.35	0.34	0.34	0.21	0.19	0.14	0.25	0.25
CaO	0.49	0.61	0.52	0.77	0.56	0.56	0.88	0.86	0.99	1.2	1.46
Na ₂ O	3.22	3.79	3.57	4.18	4.53	4.53	3.63	3.74	2.82	3.06	3.02
K ₂ O	4.91	4.2	4.29	3.01	2.7	2.7	4.98	5.29	4.49	5.55	4.99
P ₂ O ₅	-	-	-	-	-	-	-	-	-	-	-
H ₂ O	-	-	-	-	-	-	-	-	-	-	-
F	-	-	-	-	-	-	0.18	0.06	0.02	0.12	0.35

Sample	PDJ12	PDJ11	PDJ10	PDJ9	PDJ8	PDJ7	PDJ6	PDJ5	PDJ4	PDJ3
Ref	Patino-Douce and Johnston (1991)									
What	HQ-36									
Nature	Natural									
Run n°	-	-	-	-	-	-	-	-	-	-
Startmat	-	-	-	-	-	-	-	-	-	-
Apparatus	-	-	-	-	-	-	-	-	-	-
added H ₂ O	0	0	0	0	0	0	0	0	0	0
P(kb)	10	10	10	10	7	7	7	7	7	7
T(°C)	900	875	850	825	1075	1000	975	950	900	875
SiO ₂	71.54	70.39	70.86	69.36	72.95	70.21	70.79	71.41	70.85	69.72
TiO ₂	0.21	0.17	0.13	0.02	0.61	0.61	0.51	0.28	0.38	0.13
Al ₂ O ₃	13.46	13.65	14.25	13.55	12.9	13.25	13.14	13.84	13.72	14.85
FeO	1.61	1.62	1.7	1.62	2.01	2.14	1.99	1.78	1.72	1.65
MnO	0.03	0.01	0.05	0.01	0.13	0.1	0.15	0.03	0.02	-
MgO	0.41	0.37	0.41	0.45	0.88	0.66	0.87	0.39	0.35	0.35
CaO	0.23	0.28	0.39	0.6	0.38	0.39	0.39	0.15	0.24	0.35
Na ₂ O	1.29	1.65	2.24	2.89	0.82	0.89	0.85	0.87	1.32	1.77
K ₂ O	6.06	6.2	5.69	5.32	6.23	6.72	6.38	6.52	5.31	5.61
P ₂ O ₅	0.1	0.09	0.05	0.14	0.07	0.09	0.07	0.06	0.05	0.05
H ₂ O	3.47	4.72	4.33	4.67	2.9	3.13	2.98	3.06	3.33	4.09
F	0.08	0.11	0.1	-	0.14	0.17	0.11	0.16	0.11	0.01

Sample	P1	PDJ21	PDJ20	PDJ19	PDJ18	PDJ17	PDJ16	PDJ15	PDJ14	PDJ13
Ref	Pickering and Johnston (1998)	Patino-Douce and Johnston (1991)								
<i>What</i>	HP-60	HQ-36								
<i>Nature</i>	Natural	Natural	Natural	Natural	Natural	Natural	Natural	Natural	Natural	Natural
<i>Run n°</i>	-	-	-	-	-	-	-	-	-	-
<i>Startmat</i>	-	-	-	-	-	-	-	-	-	-
<i>Apparatus</i>	-	-	-	-	-	-	-	-	-	-
<i>added H₂O</i>	0	0	0	0	0	0	0	0	0	0
<i>P(kb)</i>	10	13	13	10	10	10	10	10	10	10
<i>T(°C)</i>	812	950	900	1075	1025	1000	975	975	950	925
<i>SiO₂</i>	70.81	68.46	68.15	69.44	70.62	72.63	70.86	73.13	73.66	71.85
<i>TiO₂</i>	0.12	0.26	0.28	0.73	0.65	0.35	0.42	0.37	0.37	0.26
<i>Al₂O₃</i>	14.95	13.51	14.14	13.64	13.4	13.48	13.37	13.62	13.46	13.8
<i>FeO</i>	1.31	1.4	1.51	3.04	3.26	2.07	2.93	1.74	1.65	1.6
<i>MnO</i>	-	0.04	0.02	0.08	0.11	0.04	0.04	0.03	0.05	0.02
<i>MgO</i>	0.28	0.34	0.41	1.09	1.04	0.7	0.86	0.49	0.33	0.37
<i>CaO</i>	0.81	0.1	0.21	0.28	0.26	0.2	0.17	0.13	0.13	0.21
<i>Na₂O</i>	1.63	1.21	1.79	0.84	0.79	0.85	0.93	0.97	1.1	1.22
<i>K₂O</i>	3.77	7.72	5.92	6.05	5.98	6.4	6.69	6.92	6.86	6.13
<i>P₂O₅</i>	-	0.09	0.05	0.06	0.11	0.08	0.06	0.1	0.04	0.07
<i>H₂O</i>	5.9	5.33	7.14	2.95	2.79	3	3.38	3.49	3.55	3.23
<i>F</i>	-	0.12	0.11	0.17	0.1	0.12	0.15	0.15	0.08	0.08

Sample	S80	S79	S78	S77	S76	S75
Ref	Stevens (1995)					
What	C	C	C	C	B	B
Nature	Synthetic	Synthetic	Synthetic	Synthetic	Synthetic	Synthetic
Run n°	-	-	-	-	-	-
Startmat	-	-	-	-	-	-
Apparatus	-	-	-	-	-	-
added H ₂ O	0	0	0	0	0	0
P(kb)	10	10	10	10	10	10
T(°C)	1000	950	900	875	1000	950
SiO ₂	73.75	75.22	74.51	75.5	73.5	74.06
TiO ₂	-	-	-	-	-	-
Al ₂ O ₃	14.86	13.7	14.62	14.19	14.73	14.33
FeO	0.99	1	0.83	0.63	1.86	1.69
MnO	-	-	-	-	-	-
MgO	0.52	0.79	0.51	0.31	0.66	0.47
CaO	1.36	1.01	1.07	1.05	1.36	1.15
Na ₂ O	2.46	2.01	2.48	2.39	2.16	2.22
K ₂ O	6.07	6.28	5.98	5.93	5.72	6.09
P ₂ O ₅	-	-	-	-	-	-
H ₂ O	-	-	-	-	-	-
F	-	-	-	-	-	-

.3 Mineral compositions and Structural Formulae

PYROXENE

Sample	DG6B a7	DG6B a6	DG6B a5	DG6B a4	DG6B a3	DG6B a2	DG6B a1	DG6B B37	DG6B B34	DG6B B30	DG6B B29	DG6B B27	DG6B B24	DG6B B22	DG6B B19	DG6B B31	DG6B B27	DG6B B23	DG6B B20	DG6B B19
An.																				
SiO ₂	66.3	51.8	52.1	52.3	52.2	51.9	51.7	50.6	52.0	52.2	50.9	54.1	54.0	53.6	66.3	51.3	53.6	53.6	52.7	53.3
Al ₂ O ₃	3.4	0.8	1.0	0.8	0.8	0.7	0.8	1.8	0.9	1.0	0.9	1.1	1.1	0.9	3.4	1.2	0.0	0.0	1.5	0.0
FeO	7.9	28.0	27.8	26.5	27.4	26.5	26.2	29.6	27.3	26.8	29.5	10.4	10.6	10.5	7.9	25.9	26.3	26.5	25.9	26.3
MgO	20.9	18.3	18.5	19.2	18.8	19.0	18.8	17.1	18.6	19.0	17.7	13.8	13.5	13.5	20.9	18.7	19.7	19.8	19.5	19.6
CaO	0.2	0.8	1.0	0.9	0.8	0.9	0.8	0.9	0.8	0.9	0.9	20.5	20.9	20.7	0.2	0.9	0.9	0.8	0.9	0.9
Total	98.7	99.7	100.3	99.8	99.9	99.0	98.3	100.0	99.6	99.8	99.9	99.9	100.1	99.1	98.7	97.9	100.5	100.7	100.4	100.1

Normalisation: Generalised Pyroxene formula: (M2)(M1)T2O6

Numbers of ions based on 6 oxygens, equivalent to 12 negative charges

Si	2.3	2.0	2.0	2.0	2.0	2.0	2.0	2.0	2.0	2.0	2.0	2.0	2.0	2.0	2.3	2.0	2.0	2.0	2.0	2.0
Al _{IV}	0.0	0.0	0.0	0.0	0.0	0.0	0.0	0.0	0.0	0.0	0.0	0.0	0.0	0.0	0.0	0.0	0.0	0.0	0.0	0.0
Σ T-sit	2.3	2.0	2.3	2.0	2.0	2.0	2.0	2.0												
Mg	1.1	1.0	1.0	1.1	1.1	1.1	1.1	1.0	1.1	1.1	1.0	0.8	0.7	0.8	1.1	1.1	1.1	1.1	1.1	1.1
Al _{VI}	0.1	0.0	0.0	0.0	0.0	0.0	0.0	0.0	0.0	0.0	0.0	0.0	0.0	0.0	0.1	0.0	0.0	0.0	0.0	0.0
Ca	0.0	0.0	0.0	0.0	0.0	0.0	0.0	0.0	0.0	0.0	0.0	0.0	0.0	0.0	0.0	0.0	0.0	0.0	0.0	0.0
Fe ²⁺	0.2	0.9	0.9	0.8	0.9	0.9	0.8	1.0	0.9	0.9	1.0	0.3	0.3	0.3	0.2	0.8	0.8	0.8	0.8	0.8
Σ M-sit	1.4	2.0	1.4	2.0	2.0	2.0	2.0	2.0												

Feldspars in metabasite

Sample	Dg6b	Dg6b	Dg6b	Dg6b	Dg6b	Dg6b	Dg6b	Dg6b										
An.	b32	b17	b15	b12	90	80	60	39	33	30	25	13	5	2	10			
SiO ₂	46.6	47.3	46.6	45.3	47.0	47.2	46.9	47.6	46.6	75.3	46.7	45.1	45.3	45.2	44.9			
Al ₂ O ₃	34.9	34.5	34.9	34.8	36.2	36.6	35.8	33.6	35.2	16.9	34.8	34.6	34.7	33.3	33.6			
Fe ₂ O ₃	0.5	0.4	0.2	0.5	0.2	0.3	0.2	2.3	0.5	0.3	0.3	0.6	0.0	0.5	1.4			
CaO	16.5	16.5	16.8	18.2	17.5	17.5	17.2	14.9	16.5	8.2	16.6	18.1	18.1	17.3	17.3			
Na ₂ O	1.6	1.9	1.7	1.1	1.3	1.3	1.5	1.7	1.5	0.8	1.6	1.1	1.3	1.5	1.3			
K ₂ O	0.0	0.0	0.0	0.0	0.0	0.2	0.0	0.1	0.2	0.0	0.0	0.0	0.0	0.0	0.0			
Total	100.2	100.5	100.2	100.0	102.2	103.0	101.6	101.5	100.4	101.5	100.0	99.5	99.4	97.8	99.6			

Normalisation: Generalised Feldspar formula: Or: K[AlSi₃O₈] - Ab: Na[AlSi₃O₈] - An: Ca[Al₂Si₂O₈]

Numbers of ions based on 16 oxygens, equivalent to 32 negative charges

Si	4.3	4.3	4.3	4.2	4.2	4.2	4.2	4.3	4.3	6.3	4.3	4.2	4.2	4.3	4.2			
Al	3.8	3.7	3.8	3.8	3.8	3.8	3.8	3.6	3.8	1.7	3.8	3.8	3.8	3.7	3.7			
Fe ³⁺	0.0	0.0	0.0	0.0	0.0	0.0	0.0	0.1	0.0	0.0	0.0	0.0	0.0	0.0	0.1			
Ti	0.0	0.0	0.0	0.0	0.0	0.0	0.0	0.0	0.0	0.0	0.0	0.0	0.0	0.0	0.0			
Σ T-site	8.0	8.0	8.0	8.0	8.0	8.1	8.0											
Na	0.3	0.3	0.3	0.2	0.2	0.2	0.3	0.3	0.3	0.1	0.3	0.2	0.2	0.3	0.2			
K	0.0	0.0	0.0	0.0	0.0	0.0	0.0	0.0	0.0	0.0	0.0	0.0	0.0	0.0	0.0			
Ca	1.6	1.6	1.7	1.8	1.7	1.7	1.7	1.4	1.6	0.7	1.6	1.8	1.8	1.7	1.7			
Mg	0.0	0.0	0.0	0.0	0.0	0.0	0.0	0.2	0.0	0.0	0.0	0.0	0.0	0.0	0.1			
Fe ²⁺	0.0	0.0	0.0	0.0	0.0	0.0	0.0	0.0	0.0	0.0	0.0	0.0	0.0	0.0	0.0			
Σ A-site	1.9	2.0	2.0	2.0	1.9	1.9	1.9	2.0	1.9	0.9	1.9	2.0	2.0	2.0	2.1			

xK [Or]	0.0	0.0	0.0	0.0	0.0	0.0	0.0	0.0	0.0	0.0	0.0	0.0	0.0	0.0	0.0			
xNa [Ab]	0.1	0.2	0.2	0.1	0.1	0.1	0.1	0.2	0.1	0.1	0.1	0.1	0.1	0.1	0.1			
xCa [An]	0.9	0.8	0.8	0.9	0.9	0.9	0.9	0.8	0.8	0.9	0.9	0.9	0.9	0.9	0.9			

**.4 Relative standard deviation obtained using
Stellenbosch ICP-MS**

BHVO 1					
	Std	Av n=23	sd	Rsd%	Rsd to std
Rb	9.19	9.86	0.79	8.02	7.26
Sr	396	396.99	17.99	4.53	0.25
Y	26	26.37	1.25	4.73	1.41
Zr	174	170.99	7.83	4.58	1.73
Nb	18.6	17.78	0.80	4.52	4.41
Ba	133	126.72	7.55	5.96	4.72
La	15.5	16.97	1.13	6.63	9.47
Ce	38.1	37.52	2.05	5.47	1.52
Nd	24.7	24.18	1.43	5.90	2.11
Sm	6.12	5.96	0.65	10.90	2.56
Eu	2.09	2.06	0.29	14.11	1.26
Gd	6.33	6.47	0.76	11.78	2.26
Tb	0.96	0.98	0.08	8.31	1.61
Dy	5.31	5.54	0.54	9.81	4.31
Ho	0.98	1.03	0.12	11.28	5.32
Er	2.55	2.65	0.24	8.99	3.99
Tm	0.33	0.32	0.04	10.77	1.52

NIM-G					
	Std	av n=12	stdev	%rsd	Rsd to std
Rb	321.25	297.23	21.97	7.65	7.48
Sr	9.73	8.90	1.76	20.74	8.52
Y	137.00	127.33	2.80	2.28	7.06
Zr	293.24	265.19	2.43	0.91	9.57
Nb	59.59	53.66	3.09	6.14	9.96
Ba	113.00	102.17	2.83	2.77	9.58
La	111.93	104.71	0.50	0.48	6.44
Ce	201.75	189.84	8.86	4.67	5.90
Nd	70.48	64.85	2.61	4.02	7.98
Sm	14.80	13.56	1.23	9.09	8.32
Eu	0.35	0.35	0.04	10.40	0.66
Gd	14.55	15.12	0.39	3.41	3.93
Tb	2.77	2.66	0.13	4.96	3.82
Dy	17.90	16.20	0.32	1.98	9.51
Ho	4.31	3.97	0.16	4.10	7.85
Er	13.47	12.22	0.45	3.69	9.27
Tm	2.07	1.93	0.17	9.41	6.57

.5 Partition coefficient used for modelling

	bi	pl	gt	q
Rb	5.000	0.100	0.010	0.012
Sr	0.300	12.000	0.020	0.015
Hf	0.500	0.060	0.200	0.018
Zr	0.470	0.100	0.400	0.001
Nb	1.300	0.020	0.050	0.007
Ba	6.000	1.500	0.010	0.004
La	0.760	0.300	0.020	0.012
Ce	0.860	0.210	0.100	0.006
Pr	0.070	4.220	0.900	0.001
Nd	0.900	0.140	0.410	0.009
Sm	1.000	0.110	0.900	0.008
Eu	0.590	5.000	1.200	0.030
Gd	0.600	0.100	4.000	0.007
Tb	0.870	0.090	9.000	0.007
Dy	0.500	0.070	26.000	0.010
Ho	0.160	1.000	32.000	0.010
Er	0.410	0.060	38.000	0.011
Tm	0.220	1.630	45.000	0.010
Yb	0.320	0.060	60.000	0.012
Y	1.000	0.040	34.000	0.006
Th	0.300	0.030	0.440	0.006

Abstract to international Conferences

.6 Goldschmidt conference - Melbourne - 2006



Please ensure that your abstract fits into one column on one page and complies with the Instructions to Authors available from the Abstract Submission web page.

Origins of the S-type Cape Granites (South Africa)

A. VILLAROS¹, G. STEVENS¹ AND I.S. BUICK²

¹ Department of Geology, University of Stellenbosch, South Africa, arnaud@sun.ac.za; gs@sun.ac.za

² School of Geosciences, Monash University, Melbourne, Australia, ian.buick@sci.monash.edu.au

Abstract:

The Pan-African Cape Granite (CG) Suite, South Africa, consists of S- (~ 560 – 540 Ma), I- (~ 540 – 515 Ma) and A-type (~ 515 – 510 Ma) plutons and extrusive rocks. They intruded the low-grade (greenschist-facies) Malmesbury Supergroup (~ 750 – 610 Ma) during and after the Saldanian orogeny (~ 580 – 545 Ma). The syn- to late-tectonic S-type CG vary in composition from granodioritic to leucogranitic and contain biotite, cordierite and occasionally garnet. These granites host fine-grained granitic enclaves, metasedimentary xenoliths (predominantly amphibolite-facies) and rare metamafic xenoliths.

The Sm-Nd and Rb-Sr geochemistry of the S-type granites indicates that all have a purely crustal origin. The narrow range of Nd-isotope compositions ($\epsilon_{\text{Nd}}(550\text{Ma}) = -4.0$ to -4.7) matches those of the Malmesbury Group and the metasedimentary xenoliths ($\epsilon_{\text{Nd}}(550\text{Ma}) = -4.3$ to -10.2 ; mostly -4.3 to -5.1) this suggests that the Malmesbury Group is the source of S-type CGs. The ϵ_{Nd} values of the magmatic enclaves are typically very similar to those of the granites (-4 to -5), although some with ϵ_{Nd} as high as -2.3 at 550 Ma, possibly indicate a second source.

Thermobarometry using the mineral assemblage (Cpx-Amp-Pl-Bt-Qtz) from a metamafic xenolith result in a peak P - T estimate of 10 ± 1 kb and 850 ± 50 °C. This is interpreted to reflect the metamorphic conditions in the magma source region. Similarly, the highest grade, but non-restitic, metasedimentary xenoliths (Grt-Bt-Pl-Qtz) result in P - T estimates of ~ 750 °C and ~ 7 kb, possibly representing conditions in the metamorphic terrain overlying the melting zone. Zoned garnet within the plutons varies in composition from $\sim \text{Alm}_{70}\text{Pyr}_{25}\text{Grs}_2\text{Sps}_3$ in the interiors to rim overgrowths of $\text{Alm}_{70}\text{Pyr}_{10}\text{Grs}_2\text{Sps}_{18}$. Both differ from the $\text{Alm}_{60}\text{Pyr}_{15}\text{Grs}_{15}\text{Sps}_{10}$ garnet cores in the metasedimentary xenoliths. The two garnet generations in the granites are interpreted to record different stages of the P - T evolution of the magma. Modelling of the phase stabilities in these compositions suggests that the cores record pressures of 5 to 7 kb (at ~ 750 °C), while the rims formed at 3 to 4 kb and a temperature close to the solidus (~ 650 °C).

Collectively, these results suggest that the S-type CG magmas resulted solely from biotite fluid-absent partial melting of tectonically thickened (≥ 35 km) Malmesbury Group like metasediments along a convergent continental margin

.7 Hutton conference - Stellenbosch - 2007

Zircon U-Pb-Hf isotope and trace element geochemistry as constraints on the petrogenesis of S-type granites of the Cape Granite Suite.

A. Villaros¹, I.S Buick², G. Stevens¹

¹ Department of Geology, Geography and Environmental Studies, University of Stellenbosch, South Africa arnaud@sun.ac.za, gs@sun.ac.za

² Research School of Earth Sciences, Australian National University, Acton, 0200 ACT, Australia, ian.buick@anu.edu.au

Zircons as refractory accessory minerals are useful tracers of both source-related (inheritance, partial melting) and magmatic evolution aspects of granite petrogenesis. The Pan-African S-type granites of the Cape Granite Suite (CGS) were produced during the Saldanian Orogeny, which resulted from collision between the Rio de la Plata and Kalahari Cratons. Petrogenetic models for the origin of S-type granite are diverse in detail, but commonly agree on an aluminous metasedimentary source. S-type granites are characterised by a large variation from granodiorite to leucogranite. Several models have been proposed to explain such variations e.g. magma mixing, source component entrainment, fractional crystallisation. In the case of the CGS S-type granites, a particular type of source component contamination has been proposed (Stevens et al 2007) i.e. that the observed compositional variation results from differing degrees of contamination of the melt by the garnet produced as a product of biotite incongruent melting. In order to better understand the petrogenesis of S-type CGS, zircon from a range of plutonic compositions from the Darling Batholith, the Peninsular Pluton and from granitoid enclaves within these rocks, has been subjected to radiogenic isotope and trace elements analysis.

LA-ICP-MS ²⁰⁶Pb-²³⁸U ages obtained for zircon representative of Saldanian magmatic event yield an identical emplacement age of ~530Ma for both the Peninsula pluton and Darling Batholith. Similar zircon from a magmatic enclave has a ²⁰⁶Pb-²³⁸U age of ~545 Ma. This is identical, within error, to the oldest magmatic age documented within the CGS (SHRIMP U-Pb age of 546±3 Ma for an older phase of the Darling Batholith,).

Along with these Pan-African magmatic ages, some inherited cores and whole grains reveal a scatter of concordant ages from ~1200 to ~600Ma. The inherited zircons from each sample show principal age clusters at ~1100 Ma, ~850 Ma and ~660 Ma.

Interestingly, all zircons examined in this study show typically magmatic REE patterns (i.e. large negative Eu anomalies $Eu/Eu^* = 0.016-0.42$, large positive Ce anomalies $Ce/Ce^* = 1.28-47.5$ and low $(La/Lu)_N = 7.10^{-6} - 0.015$). This fits with the fact that these rocks have relatively low proportion of inherited zircon (typically 15%), indicating a significant capability of the initial magma to dissolve zircon. This would imply a high magma temperature, and may account for the lack of metamorphic rims on any of the inherited zircons. The lack of metamorphic zircon is also consistent with the fact that there is little evidence in the granites for contamination by metamorphic country rock during magma cooling.

The Ti-in-zircon geothermometer, corrected for ilmenite saturation, indicates a temperature variation of 730 to 920°C for the Saldanian (~530 Ma) age zircons in the granodiorites, and from 700 to 870°C in the granite. In a recent study, Lowery-Claiborne et al. (2006) showed that the Hf content of magmatic zircon increases with decreasing temperature as crystallization proceeds. In the present study, CGS Saldanian-age zircon shows a negative correlation between Ti-in-zircon temperature and Hf content (Figure 1). This indicates that the temperatures recorded by the magmatic CGS zircon may record different stages of the crystallization of these granites and that the maximum and minimum temperatures recorded have petrogenetic



significance. This suggests the granodioritic magmas originated at a higher temperature (920°C) than granite (870°C).

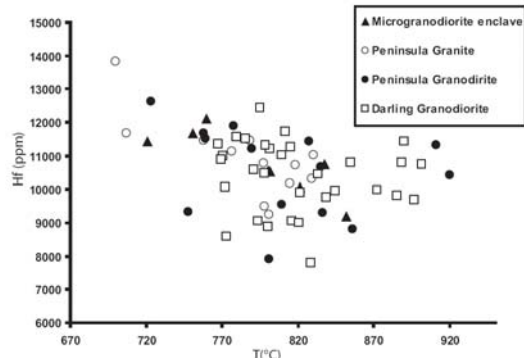


Figure 1: Hf vs. T°C (Ti-in-Zircons) in magmatic ~530 Ma zircons from the CGS

The hafnium isotope composition (LA-MC-ICP-MS) of magmatic and inherited zircons from the CGS reveal the following features: 1) at the time of emplacement, magmatic zircons show a wide range of ϵ_{Hf} values (~-18 to ~-1) and a relatively narrow range of depleted mantle Hf model ages (TDM=1.15-1.52Ga); 2) inherited zircons yield a similar range of depleted mantle Hf model ages to those of latest magmatic zircons ($T_{\text{DM}} = 1.12-1.86\text{Ga}$) regardless of their crystallisation ages; 3) the oldest and most primitive inherited grains still have depleted mantle Hf model ages ~300 Ma older than their crystallisation ages; all other inherited zircons have even more evolved Hf isotope compositions; and 4) the Hf isotopic heterogeneity in Saldanian S-type magmatic zircons is almost completely bracketed by the ϵ_{Hf} v. time trends for inherited zircons, suggesting that S-type magmatism involved little or no involvement (<5%) of juvenile material.

In combination, these results bring some clarity to our understanding of S-type CGS petrogenesis. The U-Pb magmatic ages indicate intrusion of the main plutons at around 530Ma, and confirm previous findings in this regard. The age obtained on

the magmatic enclave indicates S-type magmatic activity in the area of the Peninsular and Darling batholiths, or the plumbing systems to those batholiths, some 10 Ma prior to the main pulse of magmatic activity.

The similarity in age distributions of inherited zircon suites for the three rock types would be compatible with their derivation from the same or similar sources. The Hf isotopes indicate a composite source for the magmas, comprising material from uniquely evolved continental crust of different ages. The inherited zircon ages from this source match the ages of major Gondwanian orogenic events (Namaqua-Natal, Brasiliano) in southern Africa and Southern America, indicating the recycling of the crust that formed the source to the CGS S-type granites through successive active continental margins. The highest temperatures obtained from Ti in zircon geothermometry (~ 920°C) match with the temperature of fluid-absent biotite incongruent melting in the deep crust (820 to 950°C). As magmas of this type are typically always saturated with Zr, and Zr solubility decreases as a function of temperature, this information suggests that the magma arose through fluid-absent anatexis of biotite in a metasedimentary source and that the zircon Ti temperatures track cooling of the magma from the initial temperature (~ 920°C) to the solidus, which appears to have been located at ~ 700°C for these rocks. As these rocks contain tourmaline enriched nodules and patches that appear to indicate fluid saturation during the final stages of crystallization, it may well be that this final crystallization temperature has pressure significance. A pressure of ~ 1.5 kbar would be implied by the magma intersecting the water saturated granite solidus at 700°C to 730°C.

References

- Stevens, G., Villaros A. and Moyon J.F. 2007, Selective peritectic garnet entrainment as the origin of geochemical diversity in S-type granites, *Geology*, vol. 35(1) pp 9-12
- Lowery Claiborne L., Miller C. F., Walker B. A., Wooden, J. L., Mazdab F. K. and Bea F. (2006). Tracking magmatic processes through Zr/Hf ratios in rocks and Hf and Ti zoning in zircons: An example from the Spirit Mountain batholith, Nevada, *Mineralogical Magazine*, Vol. 70(5), pp. 517–543



**.8 Abstract: AGU - Fall meeting - San Francisco -
2007**

The role and fate of peritectic garnet in S-type granite Petrogenesis: The example of the Cape Granite Suite (South Africa)

The 560-530 Ma S-type components of the Cape Granite Suite (CGS) vary in composition from granodiorite to leucogranite. In places these rocks contain an abundance of xenoliths, including rare granulite facies metasediments and metamafic rocks. Thermobarometry applied to these assemblages gives consistent results of 850 ± 45 °C and 9 ± 1 kbar. These conditions are interpreted to reflect those of the source area at the time of magma genesis and lie within the experimentally determined interval for biotite fluid-absent melting, which, under these conditions, produces garnet as the dominant peritectic phase. Entrainment of different proportions of this garnet (up to 20wt%) of this generation of garnet into the experimentally determined leucocratic melt compositions produces magma compositions that match well with the major element bulk composition of the CGS S-type granites. Zr and Fe + Mg are strongly positively correlated in the CGS S-types, and in many rocks occur in concentrations exceeding those possible in pure melts. This indicates the co-entrapment of peritectic garnet, derived from biotite breakdown, and, and zircon, typically hosted as an inclusion within biotite prior to anatexis. A model for the trace element composition of the granites, that is a near perfect fit with the natural rocks, can be created by applying a partial disequilibrium melting model. In this model, elements contained within pre-existing metamorphic garnet and the refractory fraction of zircon are not available for sequestration into the melt and melt trace element abundance is a function of the trace element composition of the accessible portion of the source, the fraction of zircon that dissolves and partitioning between melt and the peritectic garnet and other residual minerals. Magma trace element compositions are a function of the melt composition and the compositions of the entrained garnet, zircon and other accessory minerals such as monazite. Ce concentration in the granites over that which occurs in the compositions identified as close to pure melts is taken to be a proxy for monazite entrainment. Garnet in the CGS rocks is strongly zoned from relatively homogenous Mn-poor interiors to Mn-enriched rims some 200 μm in width. Pseudosections created for the more mafic varieties of S-type granite indicate that the garnet interiors equilibrated at close to 750 °C and 5 kbar and the rims at 730 °C and 3 kbar. This is interpreted to reflect re-equilibration and then partial re-equilibration of the entrained peritectic garnet during the ascent of the magma.